TRANSIENT FLOW IN WATER DISTRIBUTION SYSTEM

by

Hyuk Jae Kwon

A Dissertation Presented to the
FACULTY OF THE GRADUATE SCHOOL
UNIVERSITY OF SOUTHERN CALIFORNIA
In Partial Fulfillment of the
Requirements for the Degree
DOCTOR OF PHILOSOPHY
(CIVIL ENGINEERING)

May 2005

INFORMATION TO USERS

The quality of this reproduction is dependent upon the quality of the copy submitted. Broken or indistinct print, colored or poor quality illustrations and photographs, print bleed-through, substandard margins, and improper alignment can adversely affect reproduction.

In the unlikely event that the author did not send a complete manuscript and there are missing pages, these will be noted. Also, if unauthorized copyright material had to be removed, a note will indicate the deletion.

ProQuest Information and Learning Company
300 North Zeeb Road
P.O. Box 1346
Ann Arbor, MI 48106-1346

ACKNOWLEDGEMENTS

I sincerely express my gratitude to my advisor, Professor Jiin-Jen Lee, for his assistance, guidance, encouragement, and supervision of all investigations during the progress of this study.

I would like to thank members of my thesis committee, Professor Landon C. Wellford, Professor Sami F. Masri, Professor Hung L. Wong, and Professor Julian A. Domaradzki for their willingness to review the manuscript and to offer suggestions throughout this study. I would also like to thank Hyoung Jin Kim for his assistance in the experimental part of this study. I would like to thank my sister, my younger brother, and my wife, for their encouragement and support during my graduate study.

Finally, it is my deepest pride to thank my mother and my father for their endless support and inspiration. This dissertation is dedicated to my parents.

TABLE OF CONTENTS

LIST OF TABLES

LIST OF FIGURES

ABSTRACT

Transient flow in a piping network was studied using both experimental and computer models. In the present study, three different numerical methods, the method of characteristics, the two-dimensional method, and the implicit method, are presented and discussed. Experiments for transient flow in a piping system has also been conducted to verify the computer model.

The method of characteristics was developed using two traditional governing equations namely the continuity and the dynamic equation. The two-dimensional method was developed using cylindrical coordinates with transient computation employing an explicit scheme. Logarithmic velocity profiles are used in the cross section of a pipe and the hydraulic head as a function of space and time are computed. The implicit method was also developed using the same governing equations as that used in the method of characteristics with the implicit scheme for the finite difference analysis. Experimental investigations were conducted in order to measure the pressure time history for transient flow. Both frictional head loss and various minor losses in the piping system were measured experimentally. The equivalent head loss coefficient C_L has been introduced in this study for both the method of characteristics and the implicit method. After conducting several experiments, the equivalent head loss coefficient C_L for the experimental piping system in the present study was determined. All of the numerical methods were compared with the experimental data. The results of different methods of computation developed in the present study agree well with the experimental data. Six cases of numerical simulation for transient flow in distribution system were considered to demonstrate the transient effects in a distribution system. These

cases are the simple looped network, small city model, small city model with backflow prevention assembly, small city with surge tank, medium sized city model, and the large sized city model. Each case was simulated with specified scenarios.

The numerical methods developed in this study have been found to be a promising simulation tools for the solution of transient flow in a distribution system. These numerical methods can be used for the design of distribution system subject to transient flow. Moreover, it can be used as operational tools to protect the distribution system from the excessively high pressure, column separation due to excessive negative pressure, or any undesirable incidents in a distribution system.

CHAPTER 1

INTRODUCTION

1.1 Background

One of the most significant hydraulic engineering accomplishments has been the development of the potable water distribution systems. Through engineered distribution systems, potable water can be delivered to users at relatively high elevations such as occupants within tall buildings or to hillside residents. A wide variation in ground elevation causes pressure existing in distribution system to vary markedly. Variable water demands and water usage patterns can also produce significant variation of system pressure, especially when the changes are sudden such as when main breaks occur in the distribution system or during fire fighting activities. The system response to these sudden changes in water demand can create transient flow that could induce many undesirable consequences such as excessive negative pressure, backflows or back siphonage. Thus, it is important for engineers to explore various transient flow phenomena and to develop emergency response strategies in order to minimize the negative impacts.

A piping network system is typically designed for certain normal operating conditions and should be operated by operating guidelines. Failure to do so can cause significant property damage, tragic accidents or tremendous economic loss. To design such systems, various parameters and network geometry are defined and analyzed for transients caused by certain scenarios. If a system's response such as exceeding the limits of maximum and minimum pressures is unacceptable, then parameters or network geometry of the system has to be changed and the analysis should be performed again. Therefore, analysis of transient flow in distribution system is an important undertaking.

For the present study, numerical analysis for transient flow in distribution system has been performed. The method of characteristics, the two-dimensional method, and the implicit method have been developed for the numerical analysis of transient flow. Experiments for transient flow in a piping system have also been conducted. Results of the computer models are compared with the experimental data. Numerical simulations for distribution system with the different scenarios have also been performed in the present study.

1.2 Review of Previous Studies

The water hammer phenomenon has been noticed for hundreds of years. Along with broad applications of computer modeling, the method of characteristics has been refined in the last two decades. There are several methods suitable for the numerical analysis of piping systems. These are two-dimensional model, the implicit method, graphical analysis, the explicit finite-difference method, and the finite element method. Both the explicit method and the fully implicit method have stability problems or running time problems. Even though significant advances in the analytical study of transient flow have been made, it was still a formidable task to simulate transient flow in large distribution system because of the large computation time required, as well as proper specifications of boundary conditions for various hydraulic devices, and system parameters.

Chaudhry (1979) provided a comprehensive and systematic discussion of hydraulic transients and presented methods of transient analysis suitable for digital computer solution. He developed computer model using the method of characteristics. Chaudhry also discussed practical applications to pump stations, nuclear power plants, and industrial piping systems.

Silver-Araya and Chaudhry (1997) developed a new model for the computation of unsteady friction loss in transient flow. He showed the energy dissipation in transient flow could be estimated from the instantaneous velocity profiles. The instantaneous velocity profile through the cross section was used to estimate the unsteady energy dissipation of one-dimensional model. Silver-Araya and Chaudhry's the energy dissipation factor can be used in combination with the method of characteristics to model unsteady frictional loss in transient flow. That was a major advantage for practical applications. Silver-Araya and Chaudhry showed the results of computation only in duration of 0.4 second because of computational time and memory requirements of computer. Time duration of computation should be long enough to observe the energy decay. Computation using a new model underestimated the energy dissipation when compared with experimental data in duration of 0.4 second.

Watters (1979) provided a general treatment on water hammer in the piping systems. He specified boundary conditions associated with different hydraulic devices in the distribution system under transient flow conditions. He provided computational results using the method of characteristics for the transient flow in a single pipe. However, computational results he presented were too limited to allow a detail comparison. Moreover, the time increment Δt he used appeared to be too large. Watters used Darcy-Weisbach frictional coefficient for the head loss term. Comparing with experimental data, this steady state friction term using Darcy-Weisbach frictional coefficient underestimated the head loss in transient flow analysis.

Wylie (1983) presented transient flow analysis in distribution systems using microcomputers. His analysis includes the concepts for system data handling. He also introduced ideas to realize computational efficiencies when using the method of

characteristics. Alternatives to the method of specified time intervals, algebraic treatment and boundary condition for series connection were discussed. Wylie suggested that $\frac{f\Delta xQ}{4DAa}$ should be much less than unity to achieve a stable solution ($\frac{f\Delta xQ}{4DAa} \leq 1$). Valuable information for the computation was given in this paper. However, a simple improved modification in the friction term was not well documented in this literature. When the method of characteristics was used for the analysis of transient flow, further investigation in the energy decay under a large time domain is needed.

Karney (1990) developed an alternative interpretation of transient conditions in a pipeline and simplified the presentation of transient information. He also discussed the importance of energy relations, the proper expression of internal energy, energy transformations, and compressibility. Karney (1992) showed the results of simulation for transient flow in simple pipe networks. The method of characteristics was used for this simulation and a few simple hydraulic devices and boundary conditions are simplified. In 1995, Karney discussed the relatively unexplored area of transients in complex pipe networks. The behavior predicted by a network transient model was compared with the results of field-testing. The computer model was generally in agreement with the trend of the field data but the computer model poorly represented the long-term decay of transient flow. Karney discussed several reasons for the larger energy dissipation than the results predicted by the computer models. In this analysis, many pipelines are neglected for the simplicity and a lot of minor losses and hydraulic devices are neglected as well. He was suggesting an "artificial damper", but it wasn't sufficient to explain the differences in the results. Karney used Darcy-Weisbach frictional coefficient for the head loss term. This steady friction term in his model also underestimated the actual head losses.

Vardy et al (1993) computed unsteady friction using "weighting function model" in turbulent flow. This model was used in a conventional one-dimensional computer program to predict the pressure time history. The agreement between the experimental and predicted pressure time histories was quite good. However, Vardy et al showed the results of computation only in duration of 0.32 second. Energy decay in transient flow cannot be observed in such short time duration of computation. Furthermore, this model is valid only for very low Reynolds number.

Brunone (1995) discussed the rapid damping of pressure peak in a water hammer phenomenon after the sudden valve closure. Brunone pointed out one-dimensional model (i.e. the method of characteristics) underestimates the energy decay and suggested unsteady friction term for a two-dimensional flow field. In his study, the computation was performed for a single pipe and the results of the numerical analysis with the two-dimensional unsteady friction term are compared with those of one-dimensional model. Comparison showed that pressure wave of two-dimensional model damped out faster than that of one-dimensional model since the steady friction term in one-dimensional model underestimates the head loss. However, complex pipe networks cannot be easily simulated because the boundary conditions were not defined and the long computation time was required for his two-dimensional model. Later on, Brunone's approach was further extended by Pezzinga (1999) for the analysis of transient flow in actual pipe networks.

Pezzinga (1999) explained that one-dimensional models in which the energy dissipation is computed by a relation between energy slope and mean velocity valid for the method of characteristics underestimate the friction forces and overestimate the persistence of oscillations. Pezzinga suggested a "stress model" as a quasi-2D model for unsteady flow in pipe networks using both explicit method and implicit method at the same time. Pezzinga

used the implicit method for the momentum equation and the explicit method for the continuity equation because of the stability problems. This model assumed that pressure gradient in the radial direction can be ignored and that the longitudinal velocity was a function of radial direction, longitudinal distance, and time. In his literature, a quasi-unsteady-1D model and quasi-2D model were compared. However the quasi-2D model was quite time consuming, calculation time required 35 times more than that required for 1D model. The results obtained by the quasi-2D model were in good agreement with experimental data. The comparisons showed that the average error on maximum oscillations is 19.1 % by 1-D model and 8.6 % by quasi-2D model. Pezzinga used Darcy-Weisbach frictional coefficient for the head loss term in 1-D model. However, he computed only first 4 seconds of simulation. To observe the energy decay for a large time, computation should be performed for longer time period than his results. Furthermore, damping coefficient κ in his model should be carefully calibrated. Motivated by these shortcomings, the present study is conducted to simulate transient flows for a large time as well as comparing the results with corresponding experiments.

1.3 Objective and Scope of Present Study

The main objective of this study is to numerically solve the problem of transient flow in distribution system that incorporates the effect of various hydraulic devices. The relationships between the system responses and the operational parameters of the system are investigated to develop guidelines for the optimal design and the operation of the system.

The final goal of this analysis is to achieve system safety. As part of this goal, a guideline is provided for designing and for operating the distribution system. In addition, it is sought to develop a numerical model for transient flow in the system, and to define the

relationships between flow parameters and the system parameters. To accomplish this objective, both steady and unsteady analyses are studied. For steady state analysis, the nodal point method is selected. Results of the steady state analysis are used as input data for the unsteady flow analysis. For the unsteady state analysis, the method of characteristics, the two-dimensional method, and the implicit method are used. Experiments for transient flow were also conducted to verify the accuracy of the numerical methods and to confirm the parameters of the governing equations with the numerical model.

In the present study, computational programs for simulating transient flow in distribution system have been developed. Additionally, various boundary conditions associated with hydraulic devices such as series junctions, branching junctions, constant head reservoirs, check valves, backflow prevention assemblies, and surge tanks are discussed and are considered within the numerical model. Numerical simulations for transient flow in a distribution system are performed under various scenarios.

CHAPTER 2

NUMERICAL MODELS FOR HYDRAULIC TRANSIENT ANALYSIS

Numerical analysis for transient flow in distribution system will be discussed in this chapter. Numerical solutions of the equations governing unsteady flow in pipelines are developed in the present study. For the computer model, the method of characteristics, the two-dimensional method, and the implicit method have been used in the present study. They will be presented with the specified boundary conditions in this chapter.

2.1 Mathematical Formulations for the Hydraulic Transient Analysis

Applicable fluid mechanics principles and the governing equations for the computer simulation used in this study will be briefly outlined below:

2.1.1 Steady State Calculation

One of the major tasks in the flow analysis of a piping network under steady state condition is computing the frictional head loss. There are two well-known formulas for calculating the frictional head loss for the steady flow computations:

(1) Darcy-Weisbach equation

$$h_f = f\frac{L}{D}\frac{V^2}{2g} \tag{2.1}$$

h_f : Head loss due to friction

L : Pipe length

f : Friction factor as a function of Reynolds number and relative roughness

D : Pipe diameter

V : Average velocity in the pipe

g : Gravitational acceleration

(2) Hazen-Williams formula

$$V = 0.85 C_H R^{0.63} s^{0.54} \tag{2.2}$$

C_H : Hazen-Williams roughness coefficient

R : Hydraulic radius ($\frac{A}{P} = \frac{d}{4}$)

s : Energy loss per meter of pipe ($\frac{h_f}{L}$)

If the flow is a fully developed turbulent flow, the Hazen-Williams roughness coefficient is only a function of the pipe characteristics and not the flow characteristics. Therefore, Hazen-Williams formula is used for many engineering application.

2.1.2 Steady State Calculation for Distribution System

Two methods are commonly employed to analyze steady state flow in a pipe distribution system: the Hardy-Cross Method and the Nodal Point Method. If the system comprises large number of pipes and hydraulic devices, Hardy-Cross Method is not as efficient. The Nodal Point Method can easily be programmed using a digital computer and has been proven to be very efficient. The basic concept of the Nodal Point Method is the evaluation of correction for the hydraulic heads at each junction. For the Nodal Point Method, the hydraulic grade

line at each junction in a distribution system is assumed. Corrections are calculated and iterated until steady state relations are satisfied throughout the distribution system. This procedure starts with the assumed hydraulic head at each junction in the system. External boundary conditions such as the flow take off at the junctions, pump characteristic curve, or reservoir elevation must be defined. A linearized form of the pipe flow equation is then applied to each pipe at a junction.

The equations for steady state calculations are summarized below:

All the energy loss equations are expressed in the following form.

$h = kQ^n$

where k is a function of pipe geometry and fluid viscosity.

In the case of SI units, if the Darcy-Weisbach equation is used, n = 2 and $k = \frac{fL}{2gDA^2}$

where f is the friction factor, L is the pipe length, D is the pipe diameter, and A is the cross sectional area of the pipe.

If the Hazen-Williams formula is used, n = 1.85 and $k = \frac{L}{(0.85C_H R^{0.63} A)^{1.85}}$, where C_H is the Hazen-Williams roughness coefficient and R is the hydraulic radius.

Energy loss equation $h = kQ^n$ is rewritten in the form:

$$Q = Wh^N \tag{2.3}$$

where $N = 1.0/n$ and $W = 1.0/k^N$.

This equation can be written for each pipe at a node as follows:

$$Q_i = W(H_j - H_i)^N \tag{2.4}$$

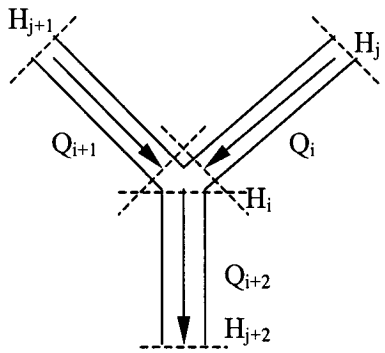

Figure 2.1 Node point for the steady state analysis

Subscript i indicates the node (junction) for which the equation is written, and subscript j indicates the node at the opposite end of a given pipe segment. Therefore, H_i indicates the hydraulic head at i^{th} node while H_j indicates the hydraulic head at j^{th} node. If the initially assumed values of H were correct, the sum of Q would be zero at each node. Since this is not the case, for the initial trial solution a correction factor α is introduced. This equation should satisfy continuity at each node.

Introducing correction factor α, Eq. 2.4 becomes

$$Q_i = W\{H_j - (H_i + \alpha)\}^N \tag{2.5}$$

Expanding right-hand side term using Taylor series expansion:

$$\gamma(x_0 + \Delta x) = \gamma(x_0) + \gamma'(x_0)\Delta x + \gamma''(x_0)\frac{\Delta x^2}{2!} \cdots\cdots$$

Non-linear head loss terms in Eq. 2.5 are linearized using the first two terms in the Taylor series. Eq. 2.5 can then be rewritten as follows:

$$Q_i = W\{(H_j - H_i)^N - N \cdot (H_j - H_i)^{N-1}\alpha\} \tag{2.6}$$

Rearranging the right hand side of Eq. 2.6, one obtains the following equation:

$$Q_i = A - \alpha C$$

Where A and C are defined as follows:

$$A = W(H_j - H_i)^N$$

$$C = W \cdot N(H_j - H_i)^{N-1}$$

Continuity condition requires that the sum of all inflows to the junction must be zero.

$$\sum Q = \sum A - \alpha \cdot \sum C = 0 \tag{2.7}$$

The adjustment to the hydraulic grade line is given by

$$\alpha = \frac{\sum A}{\sum C}$$

After calculating the correction factor α, α must be put into Eq. 2.6 again. This iterating computation should be repeated until value of correction factor α is small enough. Convergence to the final results is slower than the Hardy-Cross Method. But Nodal Point Method is much better suited for the computer solution. Results of the steady state analysis are used as the input data for the unsteady state analysis.

2.1.3 Unsteady State Calculation

For the transient condition, when changes of flow are rapid, the fluid compressibility has to be taken into consideration. As a result, the flow changes are not experienced instantaneously throughout the system. The resulting pressure waves move back and forth in the piping system with a rapid velocity.

Using the momentum theorem, the change in hydraulic head ΔH can be related to the change in velocity ΔV by the following equation:

$$\Delta H = \frac{c}{g}\Delta V \tag{2.8}$$

Where H : Hydraulic head

c : Wave speed

g : Gravitational acceleration

V : Flow velocity

For the transient analysis of a piping network, we need to satisfy all the equations describing these flows. Certain assumptions are needed for the analysis: The fluid is assumed slightly compressible, the walls of the conduit are linearly elastic and are slightly deformable, and the head losses during the transient state may be computed using the Darcy-Weisbach equation in terms of the instantaneous flow velocity in the pipe.

The governing continuity equation for transient flow analysis is:

$$\frac{\partial P}{\partial t} + V\frac{\partial P}{\partial x} + \rho c^2 \frac{\partial V}{\partial x} = 0 \tag{2.9}$$

Where P : Pressure

V : Average velocity in pipe

ρ : Fluid density

c : Wave speed

x : Spatial variable in longitudinal direction

t : Time variable

The governing momentum equation for transient flow analysis is:

$$\frac{\partial V}{\partial t} + V\frac{\partial V}{\partial x} + \frac{1}{\rho}\frac{\partial P}{\partial x} + f\frac{V|V|}{2D} = 0 \tag{2.10}$$

Where V : Average velocity in pipe

D : Pipe diameter

P : Pressure

ρ : Fluid density

f : Darcy-Weisbach friction factor

$|V|$: Absolute value of the velocity

Eqs. 2.9 and 2.10 can be further simplified by eliminating the non-linear terms $V\frac{\partial V}{\partial x}$ and $V\frac{\partial P}{\partial x}$, because these terms are small when compared to other terms. By substituting the pressure term with the hydraulic head ($P = \rho g H$), we obtain the simplified governing equations for transient flow analysis as follows:

$$\frac{\partial H}{\partial t} + \frac{c^2}{gA}\frac{\partial Q}{\partial x} = 0 \tag{2.11}$$

$$\frac{\partial Q}{\partial t} + gA\frac{\partial H}{\partial x} + \frac{f}{2DA}Q|Q| = 0 \tag{2.12}$$

Where H : Hydraulic head

Q : Flow rate

c : Wave speed

A : Cross-sectional area

D : Diameter of the pipe

g : Gravitational acceleration

$|Q|$: Absolute value of the flow rate

2.2 The Method of Characteristics

The solution for the unsteady flow in pipelines and pipe networks requires that pressure and velocity should be determined as a function of time at any point in the system. The two independent, one-dimensional, partial differential equations used to solve for velocity and pressure are the dynamic equation and the continuity equation. Three methods are used to solve the governing equations in the present study. The first is the method of characteristics to be presented in this section. The second is the two-dimensional method to be presented in the next section. The third is the implicit method to be presented in one after the next section. The method of characteristics is very compatible with numerical solution of the distribution system. Comparisons of the computational results and the experimental data will be presented and discussed in Chapter 4.

2.2.1 Governing Equations

Dynamic and Continuity equations presented in previous section are summarized again as follows:

$$\frac{\partial Q}{\partial t} + gA\frac{\partial H}{\partial x} + \frac{f}{2DA}Q|Q| = 0 \quad \text{Dynamic Equation} \tag{2.13}$$

$$\frac{c^2}{gA}\frac{\partial Q}{\partial x} + \frac{\partial H}{\partial t} = 0 \quad \text{Continuity Equation} \tag{2.14}$$

These two equations could be rewritten as follows:

$$L_1 = \frac{\partial Q}{\partial t} + gA\frac{\partial H}{\partial x} + \frac{f}{2DA}Q|Q| = 0 \tag{2.15}$$

$$L_2 = c^2\frac{\partial Q}{\partial x} + gA\frac{\partial H}{\partial t} = 0 \tag{2.16}$$

Now, let's consider a linear combination of equations of $L = L_1 + \lambda L_2$ (Where λ is a unknown multiplier).

$$\left(\frac{\partial Q}{\partial t} + \lambda c^2 \frac{\partial Q}{\partial x}\right) + \lambda g A\left(\frac{\partial H}{\partial t} + \frac{1}{\lambda}\frac{\partial H}{\partial x}\right) + \frac{f}{2DA} Q|Q| = 0 \tag{2.17}$$

It is noted that $H = H(x,t)$, $Q = Q(x,t)$, thus the total derivatives may be written by chain rule as:

$$\frac{dQ}{dt} = \frac{\partial Q}{\partial t} + \frac{\partial Q}{\partial x}\frac{dx}{dt} \tag{2.18}$$

$$\frac{dH}{dt} = \frac{\partial H}{\partial t} + \frac{\partial H}{\partial x}\frac{dx}{dt} \tag{2.19}$$

The unknown multiplier can be defined by comparing Eq. 2.17 and Eqs. 2.18 and 2.19.

$$\frac{1}{\lambda} = \frac{dx}{dt} = \lambda c^2 \tag{2.20}$$

$$\lambda = \pm\frac{1}{c} \tag{2.21}$$

By using Eqs. 2.18, and 2.19, Eq. 2.17 can be rewritten as

$$\frac{dQ}{dt} + \frac{gA}{c}\frac{dH}{dt} + \frac{f}{2DA} Q|Q| = 0 \tag{2.22}$$

$$\text{If } \frac{dx}{dt} = c \tag{2.23}$$

$$\frac{dQ}{dt} - \frac{gA}{c}\frac{dH}{dt} + \frac{f}{2DA} Q|Q| = 0 \tag{2.24}$$

$$\text{If } \frac{dx}{dt} = -c \tag{2.25}$$

Eq. 2.22 is valid if Eq. 2.23 is satisfied. And Eq. 2.24 is valid if Eq. 2.25 is satisfied. Fig. 2.2 shows the characteristic lines when the method of characteristics is used for the computation.

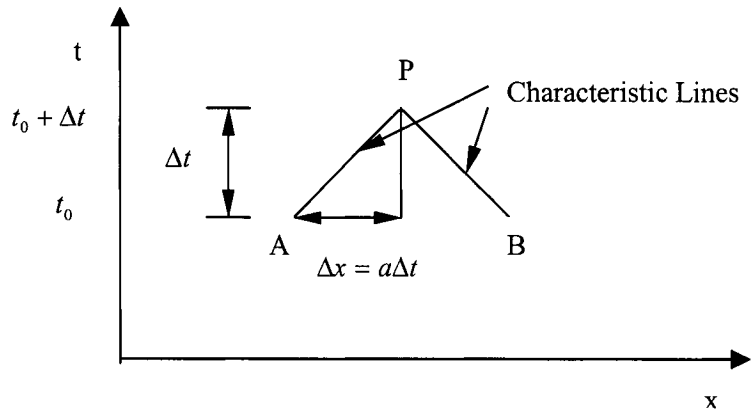

Figure 2.2 Characteristic lines

Using Eqs. 2.23 and 2.25, Eqs. 2.13 and 2.14 could be converted to ordinary differential equation with the independent variable t. In x-t plane, Eq. 2.23 and Eq. 2.25 represent straight lines having slope $\pm 1/c$. These lines are called characteristic lines.

Subscript P represents unknown variable.

We can write equations along the positive characteristic line AP

$$dQ = Q_P - Q_A \tag{2.26}$$

$$dH = H_P - H_A \tag{2.27}$$

We can also write equations along the negative characteristic line BP

$$dQ = Q_P - Q_B \tag{2.28}$$

$$dH = H_P - H_B \tag{2.29}$$

The subscripts in Eqs. 2.26, 2.27, 2.28, and 2.29 refer to the locations in the x-t plane.

$$(Q_P - Q_A) + \frac{gA}{c}(H_P - H_A) + \frac{f\Delta t}{2DA} Q_A |Q_A| = 0 \tag{2.30}$$

$$(Q_P - Q_B) - \frac{gA}{c}(H_P - H_B) + \frac{f\Delta t}{2DA} Q_B |Q_B| = 0 \tag{2.31}$$

Substituting Eqs. 2.26 and 2.27 into 2.30 and Eq. 2.28 and 2.29 into 2.31, computing the friction term at the points A and B and multiplying Δt, one obtains the following equations:

$$Q_P = C_p - C_a H_P \tag{2.32}$$

$$Q_P = C_n + C_a H_P \tag{2.33}$$

$$C_a = \frac{gA}{c} \tag{2.34}$$

$$C_p = Q_A + \frac{gA}{c} H_A - \frac{f\Delta t}{2DA} Q_A |Q_A| \tag{2.35}$$

$$C_n = Q_B - \frac{gA}{c} H_B - \frac{f\Delta t}{2DA} Q_B |Q_B| \tag{2.36}$$

Finally, we could simply get this relation $Q_P = 0.5(C_P + C_n)$.

The well-known stability and convergence condition must be satisfied:

$$\frac{\Delta t}{\Delta x} \leq \frac{1}{c} \tag{2.37}$$

To achieve reasonable accuracy in most transient pipeline problems, this time step-distance interval relationship specified by the "Courant condition" is a requirement.

2.2.2 Boundary Conditions

Boundary conditions representing different devices in the piping network will be identified one by one in the following subsections:

2.2.2.1 Pipe Outlet

At the pipe outlet as shown in sketch Fig. 2.3, the continuity condition at the downstream end requires that $Q_P = Q_{out}$.

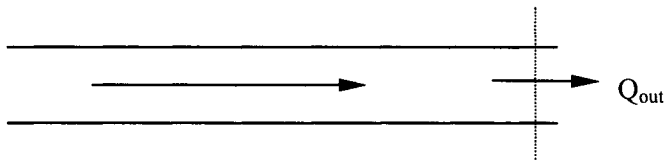

Figure 2.3 Pipe outlet

From the positive characteristic equation, it follows that

$$H_P = \frac{C_P - Q_{out}}{C_a} \tag{2.38}$$

2.2.2.2 Series Junction

In the preceding discussion, we considered only one conduit, and the boundary condition was specified at the downstream end. However, if the boundary is at the junction of two or more conduits, then the variables at different sections of different conduits have to be specified. A simple junction connecting two pipes is shown in Fig. 2.4.

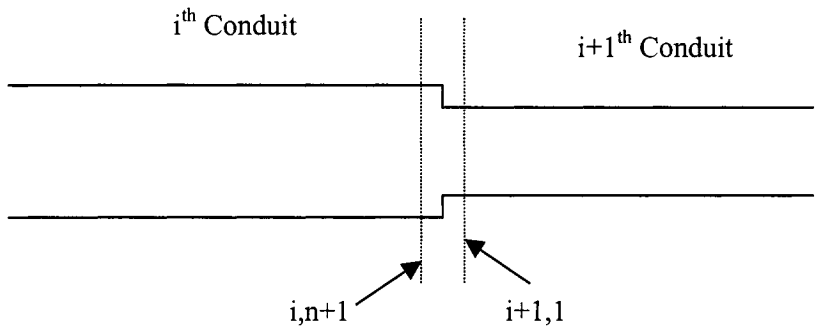

Figure 2.4 Series junction

The continuing condition requires:

$$H_{P_{i,n+1}} = H_{P_{i+1,1}} \tag{2.39}$$

Eq. 2.39 is valid if the difference between section $(i, n+1)$ and $(i+1,1)$ and pressure head loss at the junction can be negligible.

$$Q_{P_{i,n+1}} = C_{p_i} - C_{a_i} H_{P_{i,n+1}} \tag{2.40}$$

$$Q_{P_{i+1,1}} = C_{n_{i+1}} + C_{a_{i+1}} H_{P_{i+1,1}} \tag{2.41}$$

Continuity equation at the junction is

$$Q_{P_{i,n+1}} = Q_{P_{i+1,1}} \tag{2.42}$$

Thus, the hydraulic head can be obtained as follows:

$$H_{P_{i,n+1}} = \frac{C_{p_i} - C_{n_{i+1}}}{C_{a_i} + C_{a_{i+1}}} \tag{2.43}$$

Now $H_{P_{i+1,1}}$, $Q_{P_{i,n+1}}$, and $Q_{P_{i+1,1}}$ can be determined.

2.2.2.3 Branching Junction

A junction containing branching pipes is shown in Fig. 2.5.

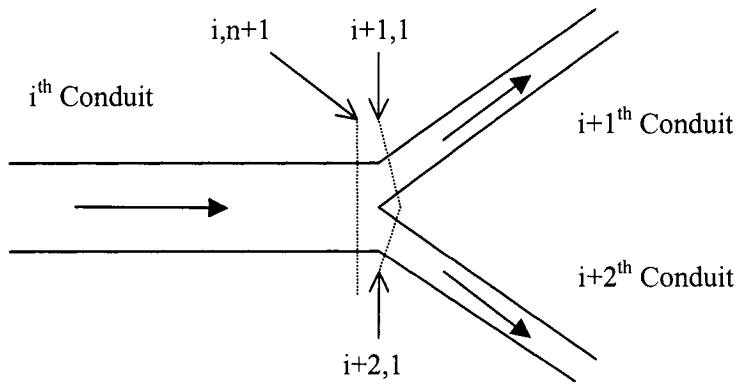

Figure 2.5 Branching junction

At the branching junction, continuity condition must be satisfied:

$$Q_{P_{i,n+1}} = Q_{P_{i+1,1}} + Q_{P_{i+2,1}} \tag{2.44}$$

The flow rate in each pipe at the branching junction is written in the form of characteristic equations:

$$Q_{P_{i,n+1}} = C_{P_i} - C_{a_i} H_{P_{i,n+1}} \tag{2.45}$$

$$Q_{P_{i+1,1}} = C_{n_{i+1}} + C_{a_{i+1}} H_{P_{i+1,1}} \tag{2.46}$$

$$Q_{P_{i+2,1}} = C_{n_{i+2}} + C_{a_{i+2}} H_{P_{i+2,1}} \tag{2.47}$$

Continuity condition at the branching junction requires:

$$H_{P_{i,n+1}} = H_{P_{i+1,1}} = H_{P_{i+2,1}} \tag{2.48}$$

In Eq. 2.48, the head losses at the junction are neglected.

2.2.2.4 Constant Head Reservoir

For a constant head reservoir as shown in the sketch in Fig. 2.6, the constant head is maintained for all time.

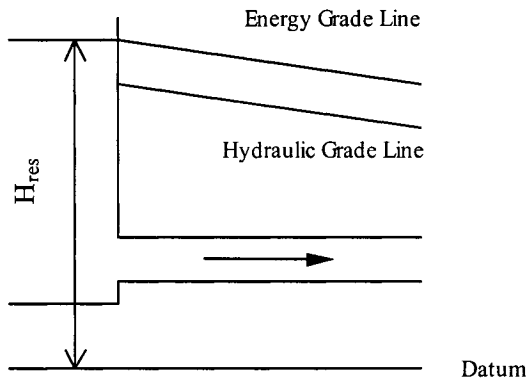

Figure 2.6 Constant-level downstream reservoir

Again, the continuity equation requires that

$$H_P = H_{res} \tag{2.49}$$

where, H_{res} is the height of water surface level above the datum.

Eq. 2.49 is valid if entrance head loss can be neglected.

$$Q_P = C_n + C_a H_{res} \tag{2.50}$$

where, H_P and Q_P is for the upper end of the pipe.

2.2.2.5 Check Valve

Piping network is often equipped with check valves for system control or system repair, this is shown in Fig. 2.7.

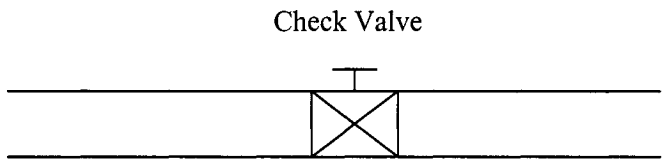

Figure 2.7 Check Valve

The equations for the junction node with a valve are specified below:

$$Q_{P_{i,n+1}} = C_{P_i} - C_{a_i} H_{P_{i,n+1}}$$

$$Q_{P_{i+1,1}} = C_{n_{i+1}} + C_{a_{i+1}} H_{P_{i+1,1}}$$

$$Q_{P_{i,n+1}} = Q_{P_{i+1,1}}$$

$$H_{P_{i,n+1}} = H_{P_{i+1,1}} + K_L \left(\frac{Q_{P_{i+1,1}}^{\ 2}}{2gA_{i+1}^{\ 2}} \right) \tag{2.51}$$

where, K_L is related to the time history of valve closure. For illustration purpose, if we assume

$$C_{a_i} = C_{a_{i+1}} = C_a$$

these equations can be rearranged to become:

$$C_a K_L \left(\frac{Q_{P_{i+1,1}}^{\ 2}}{2gA_{i+1}^{\ 2}} \right) + 2Q_{P_{i+1,1}} - C_{P_i} - C_{n_{i+1}} = 0 \tag{2.52}$$

$$Q_{P_{i+1,1}} = \frac{-b + \sqrt{b^2 - 4ac}}{2a} \tag{2.53}$$

where, $a = \frac{C_a K_L}{2gA_{i+1}^{\ 2}}$, $b = 2$, $c = -(C_{P_i} + C_{n_{i+1}})$

in which K_L has a specific function in time.

After complete closing of valve, B.C. should be $Q_{P_{i,n+1}} = 0$, $Q_{P_{i+1,1}} = 0$

2.2.2.6 Backflow Prevention Assembly

A piping network may be equipped with backflow prevention assembly. This is shown in Fig. 2.8.

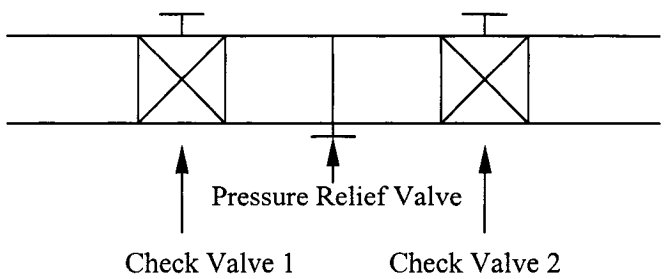

Figure 2.8 Reduced pressure principle backflow prevention assembly (RP)

There are several types of cross-connection control assembly. Shown in Fig. 2.8 is a RP device which consists two independently acting check valves and a relief valve in the middle. Backflow prevention assembly may be introduced wherever a water user may generate contaminants or any hazard into the piping network. Cross-Connection means any unprotected connection between a consumer's potable water system and any other source wherever it is possible to introduce any contaminated water, industrial fluid or harmful substance into the potable system. Backflow prevention assembly means any effective assembly used to prevent backflow into a potable water system. Commonly used backflow prevention assemblies can be grouped into the following categories:

(1) Atmospheric Vacuum Breaker Backsiphonage Prevention Assembly (AVB)

(2) Double Check Valve Backflow Prevention Assembly (DC)

(3) Double Check-Detector Backflow Prevention Assembly (DCDA)

(4) Pressure Vacuum Breaker Backsiphonage Prevention Assembly (PVB)

(5) Reduced Pressure Principle Backflow Prevention Assembly (RP)

(6) Reduced Pressure Principle-Detector Backflow Prevention Assembly (RPDA)

(7) Spill-Resistant Pressure Vacuum Breaker Backsiphonage Prevention Assembly (SVB)

Two of the most widely used backflow prevention assemblies are double check valve backflow prevention assembly (DC) and reduced pressure principle backflow prevention assembly (RP). Double check valve backflow prevention assembly (DC) is composed of two independently acting valves. Reduced pressure principle backflow prevention assembly (RP) contains two independently acting check valves with an independent pressure relief valve located between the two check valves. If the first and second check valve were working properly (closing completely), then the boundary conditions can be specified as:

$$Q_{P_{i,n+1}} = 0 \ , \ H_{P_{i,n+1}} = \frac{C_{P_i}}{C_{a_i}} \tag{2.54}$$

$$Q_{P_{i+1,1}} = 0 \ , \ H_{P_{i+1,1}} = \frac{-C_{n_{i+1}}}{C_{a_{i+1}}} \tag{2.55}$$

If first check valve is working but second check valve is not. Then pressure release valve is working. The boundary conditions would be specified as follows:

$$H_{P_{i,n+1}} = \frac{C_{P_i}}{C_{a_i}} \tag{2.56}$$

while, $Q_{P_{i,n+1}} = 0$

$$H_{P_{i+1,1}} = \frac{(-C_{n_{i+1}} - Q_{out})}{C_{a_{i+1}}} \tag{2.57}$$

while, $Q_{P_{i+1,1}} = C_{n_{i+1}} + C_{a_{i+1}} H_{P_{i+1,1}}$

2.2.2.7 Surge Tank

A piping network sometimes is equipped with a surge tank to minimize the pressure surge in transient conditions. This is shown in Fig. 2.9. A surge tank is usually an open standpipe or a shaft connected to the conduit of hydroelectric power plant or to the pipeline of a piping system. Surge tank is used to prevent excessively high or low pressure in the distribution system whenever there is a rapid change in flow condition.

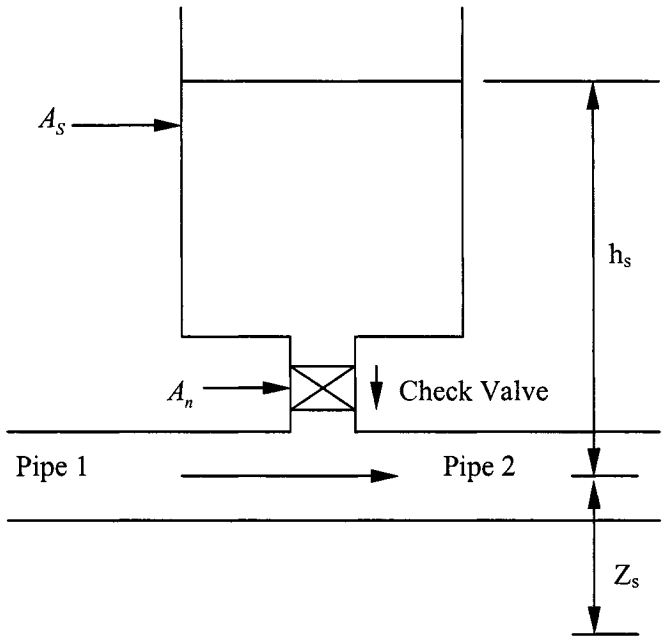

Figure 2.9 One-Way Surge Tank

In Fig. 2.9, A_s is the area of Surge Tank, A_n is the area of the pipe connecting the surge tank to the pipeline, and h_S is the height of water in the surge tank.

The main functions of the surge tank are:

(1) It reduces the fluctuation of excessive fluctuations by reflecting the incoming pressure waves.

(2) A surge tank acts as storage for excessive water and also it provides water during power failure in a pumping system.

There are several types of surge tanks like simple, orifice, one-way, and two-way surge tank. An one-way or two-way surge tanks are widely used for the distribution system. One-way surge tanks are used primarily in connection with pumping system, it is usually designed to avoid column separation. One-way surge tanks are often used to prevent low pressures in the

pipelines. A two-way surge tanks are used when hydraulic grade line (HGL) is located too far above the pipeline. One-Way Surge Tank provides water to the pipeline when HGL for the pipeline drops below the water level in the surge tank. Under normal situation, the HGL is located above the water level in the surge tank. Surge tank is isolated from the pipeline with a check valve.

When $(h_S + Z_S - H_P)$ is positive, where Z_s is the elevation of the centerline of the pipe, then the surge tank is in operation.

The boundary conditions can be specified as follows:

$$Q_{P_{i,n+1}} = C_{P_i} - C_{a_i} H_{P_{i,n+1}}$$

$$Q_{P_{i+1,1}} = C_{n_{i+1}} + C_{a_{i+1}} H_{P_{i+1,1}}$$

$$H_{P_{i,n+1}} = H_{P_{i+1,1}} = H_P$$

$$Q_{P_{i,n+1}} + Q_S = Q_{P_{i+1,1}} \tag{2.58}$$

where Q_S is the discharge from surge tank.

Q_S can be computed from the available head as:

$$Q_S = C_0 A_n \sqrt{2g(h_S + Z_S - H_P)} \tag{2.59}$$

$$\text{New } h_S = h_S - \frac{\Delta t}{A_S} Q_S \tag{2.60}$$

After combining these equations,

$$H_P{}^2 + (2K + 2L^2 g) H_P + K^2 - 2L^2 g(h_S + Z_S) = 0 \tag{2.61}$$

where, $K = \dfrac{C_{n_{i+1}} - C_{P_i}}{C_{a_i} + C_{a_{i+1}}}$, $L = \dfrac{C_0 A_n}{C_{a_i} + C_{a_{i+1}}}$

$$H_P = \frac{-b + \sqrt{b^2 - 4c}}{2} \quad , \; b = 2K + 2L^2 g \; , \; c = K^2 - 2L^2 g(h_S + Z_S)$$

When Two-Way Surge Tanks is used, we need one additional boundary condition.

If $(h_S + Z_S - H_P)$ is negative, then:

$$Q_{P_{i,n+1}} = C_{P_i} - C_{a_i} H_{P_{i,n+1}}$$

$$Q_{P_{i+1,1}} = C_{n_{i+1}} + C_{a_{i+1}} H_{P_{i+1,1}}$$

$$H_{P_{i,n+1}} = H_{P_{i+1,1}} = H_P$$

$$Q_{P_{i,n+1}} - Q_S = Q_{P_{i+1,1}} \tag{2.62}$$

$$Q_S = C_0 A_n \sqrt{2g(H_P - h_S - Z_S)} \tag{2.63}$$

$$\text{New } h_S = h_S + \frac{\Delta t}{A_S} Q_S \tag{2.64}$$

$$H_P{}^2 + (2K - 2L^2 g)H_P + M^2 + 2L^2 g(h_S + Z_S) = 0 \tag{2.65}$$

Where, $K = \dfrac{C_{n_{i+1}} - C_{P_i}}{C_{a_i} + C_{a_{i+1}}}$, $L = \dfrac{C_0 A_n}{C_{a_i} + C_{a_{i+1}}}$, $M = \dfrac{C_{P_i} - C_{n_{i+1}}}{C_{a_i} + C_{a_{i+1}}}$

$$H_P = \frac{-b - \sqrt{b^2 - 4c}}{2},$$

Where, $b = 2K - 2L^2 g$, $c = M^2 + 2L^2 g(h_S + Z_S)$

2.3 Two-Dimensional Method

In the previous section, frictional loss is estimated by using steady state formula. Such procedure has been known, as quasi-steady approximation. In essence this means that the energy loss during the transient condition can be obtained in the same manner as the steady state condition.

In the transient condition, the shear stress at the wall is not associated with the mean velocity. The velocity profile in transient flow could be different from the fully developed flow profile. Therefore, frictional losses computed by using steady state friction coefficient might be inaccurate in transient flow. Unsteady flow in distribution system is commonly analyzed by the one-dimensional model such as the method of characteristics presented in the previous section. For the method of characteristics, energy dissipation term is evaluated by Darcy-Weisbach approximation from a steady state analysis. Therefore, friction coefficient is assumed to be constant. Comparing with experiment data, this steady state friction term appears to be underestimating the actual head losses.

The unsteady flow could also be modeled by means of two-dimensional method by considering the velocity profile in the cross section. Approaches used for this method will be presented in the following. The results of the two-dimensional method will be compared with the experimental data and presented in Chapter 4 (Section 4.4).

2.3.1 Governing Equations

The quasi 2-D method is based on the continuity and the momentum equations for an elastic pipe with a circular cross section. Defining the cylindrical coordinates and the grid system as shown in Fig. 2.10 and 2.11, the continuity and the momentum equations in cylindrical coordinates can be written as:

$$\frac{\partial \rho}{\partial t} + \frac{\partial(\rho u)}{\partial x} + \frac{1}{r}\frac{\partial(\rho r v)}{\partial r} = 0 \tag{2.66}$$

$$\frac{\partial u}{\partial t} + u\frac{\partial u}{\partial x} + v\frac{\partial u}{\partial r} = -g\frac{\partial H}{\partial x} - \frac{1}{\rho}\frac{\partial \sigma_x}{\partial x} - \frac{1}{\rho r}\frac{\partial(r\tau)}{\partial r} \tag{2.67}$$

$$\frac{\partial v}{\partial t} + u\frac{\partial v}{\partial x} + v\frac{\partial v}{\partial r} = -g\frac{\partial H}{\partial r} - \frac{1}{\rho}\frac{\partial \tau}{\partial x} - \frac{1}{\rho r}\frac{\partial(r\sigma_r)}{\partial r} + \frac{\sigma_\theta}{\rho r} \tag{2.68}$$

x : Distance along the pipe

r : Distance in radial direction

t : Time variable

H : Pressure head

u, v : Velocity components in the longitudinal and radial direction, respectively

ρ : Density of the fluid

g : Gravitational acceleration

$\sigma_x, \sigma_r, and \sigma_\theta$: Normal stresses from pressure in longitudinal, radial, and angular direction

The velocity component v can be neglected in momentum equations, Eqs. 2.67 and 2.68. The convective term will be neglected in the momentum equation and it is further assumed that

$$\frac{\partial H}{\partial r} = 0 \tag{2.69}$$

Therefore, single value of the pressure head exists at each section, u is a function of r, x and t while H is a function of x and t only.

With additional simplifications such as those used in the method of characteristics, Eqs. 2.66 and 2.67 can be simplified as follows:

$$\frac{\partial H}{\partial t} + \frac{c^2}{gA_0}\frac{\partial Q}{\partial x} = 0 \tag{2.70}$$

$$\frac{\partial U}{\partial t} + g\frac{\partial H}{\partial x} + \frac{1}{\rho r}\frac{\partial (r\tau)}{\partial r} = 0 \tag{2.71}$$

Where A_0 : Cross sectional area of pipe

c : Wave speed

Q : Discharge

Using $dA = 2\pi r dr$, Eq. 2.71 can be written as

$$\frac{\partial U}{\partial t} + g\frac{\partial H}{\partial x} + \frac{2\pi}{\rho}\frac{\partial (r\tau)}{\partial A} = 0 \tag{2.72}$$

For the shear stress, Prandtl mixing length approximation can be used.

$$\tau = -\rho\nu\frac{\partial u}{\partial r} - \rho l^2 \left|\frac{\partial u}{\partial r}\right| \frac{\partial u}{\partial r} \tag{2.73}$$

where ν is the kinematic viscosity and l is the mixing length.

Following the study of Marchi (1961), the mixing length l is assumed as following:

$$\frac{l}{R} = \kappa \frac{y}{R} e^{-(y/R)} \tag{2.74}$$

κ is to be determined by experimental data.

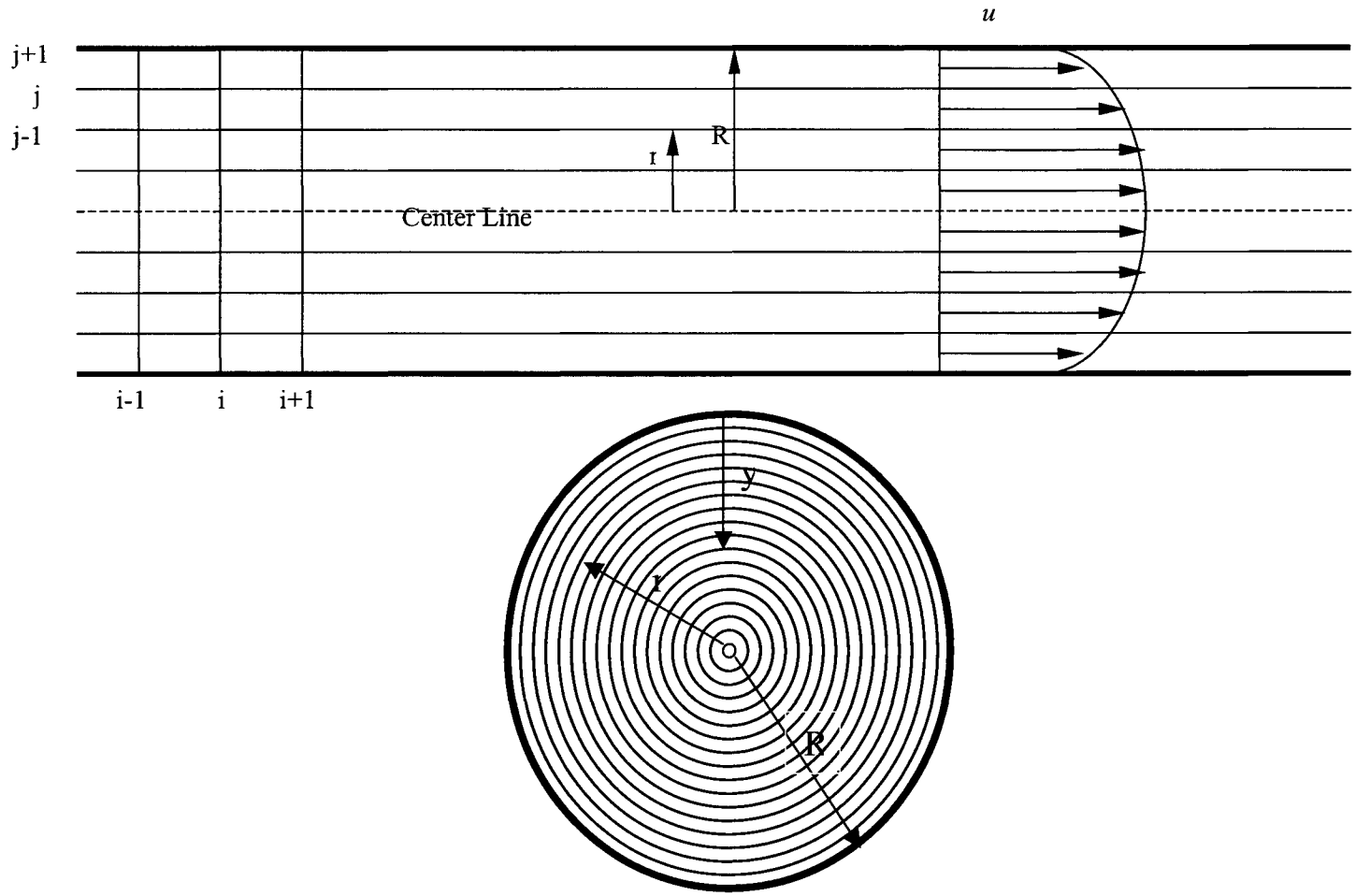

Figure 2.10 Cylindrical coordinates and grid

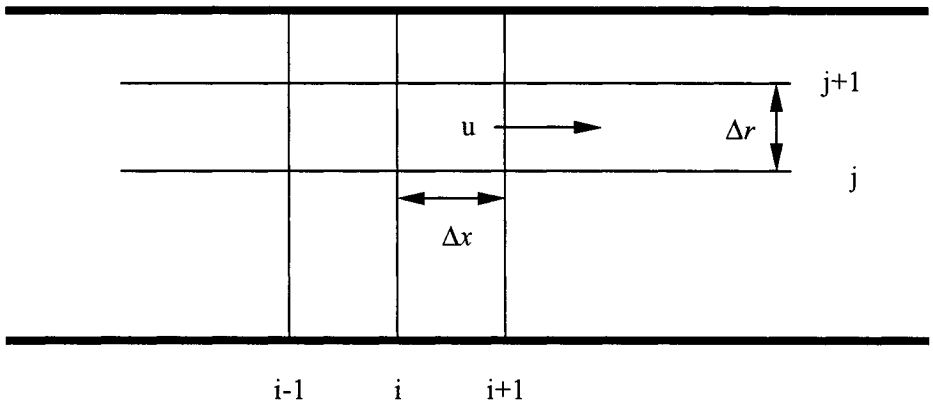

Figure 2.11 Descriptions of grid

2.3.2 Numerical Scheme

Eqs. 2.70 and 2.71 can be solved by finite difference method. The grid size Δx will have constant length in longitudinal direction and constant area ΔA in radial direction. The Courant condition $\Delta t = \frac{\Delta x}{c}$ will be maintained such as that used in the method of characteristics as presented in the previous section. The velocity profile will be defined at each radial grid for each longitudinal grid section. And the pressure head will be defined at each longitudinal section.

Applying the explicit scheme to the continuity and momentum equations, the finite-difference equations can be written as:

$$\frac{H_i^{n+1} - H_i^n}{\Delta t} + \frac{c^2}{gA_0}\frac{Q_{i+1}^n - Q_i^n}{\Delta x} = 0 \qquad (2.75)$$

The subscript i is numbered along x-direction and the subscript n represents the time step.

$$\frac{U_{i,j}^{n+1}-U_{i,j}^{n}}{\Delta t}+g\frac{H_{i}^{n+1}-H_{i-1}^{n+1}}{\Delta x}+\frac{2\pi}{\rho}\frac{(r_{j+1}\tau_{i,j+1}^{n}-r_{j}\tau_{i,j}^{n})}{\Delta A}=0 \tag{2.76}$$

The second j represents the r direction.

Pressure head can be calculated directly from Eq. 2.75 and it will be used to calculate the velocity in Eq. 2.76.

The stress term is computed from the finite-difference form of Eq. 2.73 as follows:

$$\tau_{i,j}^{n+1}=-\rho\nu\left[\frac{u_{i,j+1}^{n}-u_{i,j}^{n}}{\Delta r}\right]-\rho l^{2}\left|\frac{u_{i,j+1}^{n}-u_{i,j}^{n}}{\Delta r}\right|\left[\frac{u_{i,j+1}^{n}-u_{i,j}^{n}}{\Delta r}\right] \tag{2.77}$$

2.3.3 Boundary Conditions

Boundary conditions used for the two-dimensional method will be specified in the following subsections.

2.3.3.1 Pipe Outlet

Fig. 2.12 presents a sketch for the pipe outlet. The boundary condition at the pipe outlet can be simply specified as:

$$H_{k,N+1}^{n+1}=H_{k,N+1}^{n}+\frac{c^{2}\Delta t}{g\Delta x}\left(\frac{Q_{k,N+1}^{n}-Q_{out}}{A_{k}}\right) \tag{2.78}$$

Eq. 2.78 is valid if sudden exit head loss can be neglected.

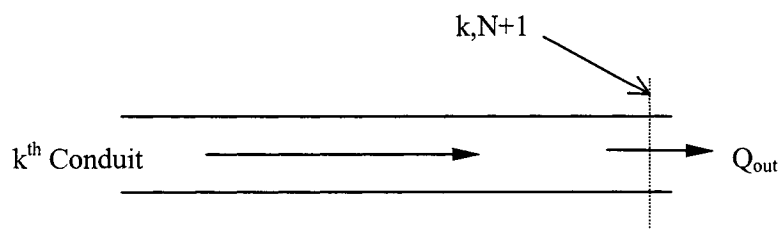

Figure 2.12 Pipe outlet

2.3.3.2 Constant Head Reservoir

For a constant head reservoir as shown in the sketch in Fig. 2.13, the constant head is maintained for all time as follows:

$$H_{k,1}^{n+1} = H_{res} \tag{2.79}$$

Where H_{res} is the height of water surface level above the datum. Eq. 2.79 is valid if entrance head loss can be neglected.

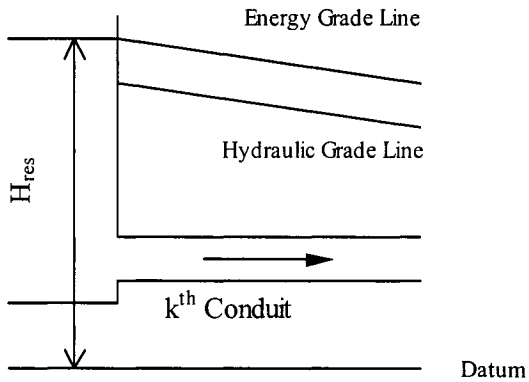

Figure 2.13 Constant head reservoir

2.4 Implicit Method

In the previous two sections, the method of characteristics and the two-dimensional method have been discussed. These two numerical schemes are explicit method of finite difference analysis. The implicit method can also be considered as a solution for the transient flow. The model using the implicit method has also been developed in this study. This method can be combined with the method of characteristics while analyzing certain piping system. Let's consider a piping system in which i^{th} conduit is to be analyzed using the

implicit method. For this method, centered implicit finite difference scheme will be used to solve the continuity and the dynamic equations Eq.2.2 and 2.1.

2.4.1 Governing Equations

Dynamic and Continuity equations presented earlier are summarized again as follows:

$$\frac{\partial Q}{\partial t} + gA\frac{\partial H}{\partial x} + \frac{f}{2DA}Q|Q| = 0 \quad \text{Dynamic Equation} \tag{2.80}$$

$$\frac{c^2}{gA}\frac{\partial Q}{\partial x} + \frac{\partial H}{\partial t} = 0 \quad \text{Continuity Equation} \tag{2.81}$$

2.4.2 Numerical Scheme

For the numerical approximation, centered finite difference method will be used as below.

$$\frac{\partial H}{\partial x} = \frac{(Hp_{i+1} + H_{i+1}) - (Hp_i + H_i)}{2\Delta x} \tag{2.82}$$

$$\frac{\partial H}{\partial t} = \frac{(Hp_{i+1} + Hp_i) - (H_{i+1} + H_i)}{2\Delta t} \tag{2.83}$$

$$\frac{\partial Q}{\partial x} = \frac{(Qp_{i+1} + Q_{i+1}) - (Qp_i + Q_i)}{2\Delta x} \tag{2.84}$$

$$\frac{\partial Q}{\partial t} = \frac{(Qp_{i+1} + Qp_i) - (Q_{i+1} + Q_i)}{2\Delta t} \tag{2.85}$$

$$Q = (Q_{i+1} + Q_i)/2 \tag{2.86}$$

After simplification of the equations, Eqs. 2.82 to 2.86 can be used in representing the governing dynamic and continuity equation Eqs. 2.80 and 2.81.

$$\frac{(Qp_{i+1} + Qp_i) - (Q_{i+1} + Q_i)}{2\Delta t} + gA\frac{(Hp_{i+1} + H_{i+1}) - (Hp_i + H_i)}{2\Delta x} + \frac{f}{2DA}Q|Q| = 0 \tag{2.87}$$

$$c^2 \frac{(Qp_{i+1} + Q_{i+1}) - (Qp_i + Q_i)}{2\Delta x} + gA \frac{(Hp_{i+1} + Hp_i) - (H_{i+1} + H_i)}{2\Delta t} = 0 \tag{2.88}$$

These two equations are simplified as:

$$Qp_i + Qp_{i+1} - B_1 Hp_i + B_1 Hp_{i+1} + B_2 = 0 \tag{2.89}$$

$$-Qp_i + Qp_{i+1} + B_3 Hp_i + B_3 Hp_{i+1} + B_4 = 0 \tag{2.90}$$

Where $$B_1 = \frac{gA\Delta t}{\Delta x} \tag{2.91}$$

$$B_2 = B_1(H_{i+1} - H_i) - (Q_i + Q_{i+1}) + \frac{f\Delta t}{4DA}(Q_i + Q_{i+1})|Q_i + Q_{i+1}| \tag{2.92}$$

$$B_3 = \frac{gA\Delta x}{c^2 \Delta t} \tag{2.93}$$

$$B_4 = Q_{i+1} - Q_i - B_3(H_i + H_{i+1}) \tag{2.94}$$

There are four unknowns in Eqs. 2.89 and 2.90, Qp_i, Qp_{i+1}, Hp_i, and Hp_{i+1}. In order to obtain unique solution of the four parameters, four equations are needed. Two additional equations can be provided by the boundary conditions. The grid system for the x-t plane used in the implicit method is shown in Fig. 2.14.

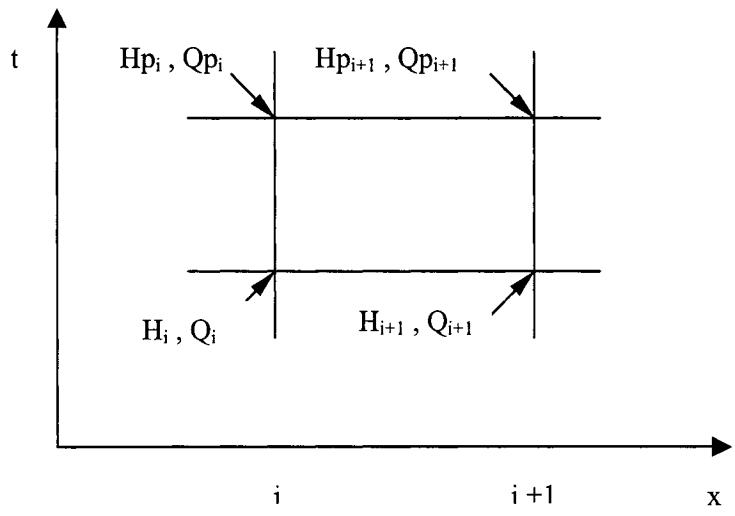

Figure 2.14 Grids for Implicit Method

2.4.3 Boundary Conditions

Boundary conditions used for the implicit method are briefly summarized in the following subsections.

2.4.3.1 Pipe Outlet

At the pipe outlet as shown in sketch Fig. 2.15, the continuity condition at the downstream end requires that $Q_P = Q_{out}$.

From the positive characteristic equation presented in Section 2.2, it follows that

$$H_P = \frac{C_P - Q_{out}}{C_a}$$

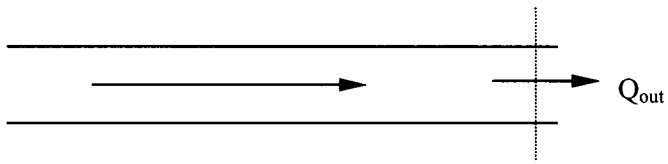

Figure 2.15 Pipe outlet

2.4.3.2 Dead End at Downstream

For a dead end at the downstream as shown in the sketch Fig. 2.16, the discharge $Q_P = 0$.

From the positive characteristic equation, the pressure head can be computed as follows:

$$H_P = \frac{C_P}{C_a} \tag{2.95}$$

This boundary condition could be applied when shut off valve is completely closed.

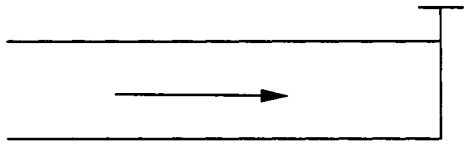

Figure 2.16 Dead end at downstream

2.4.3.3 Constant Head Reservoir

As shown in sketch Fig. 2.17, the head and discharge at the constant head reservoir are specified as follows:

$$H_P = H_{res}$$

$$Q_P = C_n + C_a H_{res}$$

These two equations, same as Section 2.2, may be considered in the analysis only if the entrance losses are small and negligible. C_P and C_a are defined in Section 2.2.

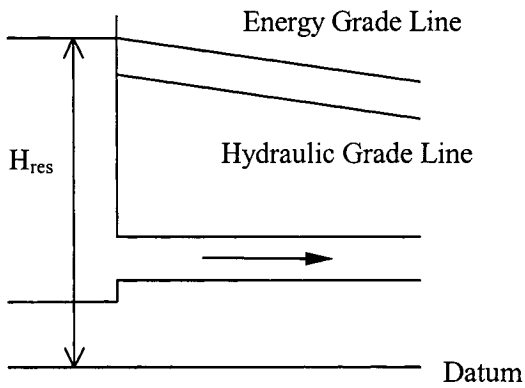

Figure 2.17 Constant head reservoir

CHAPTER 3

EXPERIMENTS

In order to investigate the transient flow in distributions system, experiments simulating water hammer are conducted. For a complete experimental investigation, large amount of experiments would have to be performed in complex distribution system with many branches and hydraulic devices. However, in the present study, a simple pipeline has been constructed in the laboratory.

The data collected from the experiments will be used to compare with the numerical simulations in an effort to determine the experimentally generated coefficient used in the model. These experiments are also used to determine the values of the speed of pressure wave, energy losses, etc. All of the experiments have been performed at the laboratory of Foundation for Cross Connection Control and Hydraulic Research (FCCCHR) at the University of Southern California. In this chapter, the experimental facilities and procedures will first be described followed by the presentation of experimental results.

3.1 Experimental Setup

For measuring the pressure wave associated with the water hammer phenomena generated by sudden closure of control valves, a pipeline consisting 278 ft long galvanized iron pipe was installed as shown in Fig. 3.1. Table 3.1 shows the information of fluid and experiment setup.

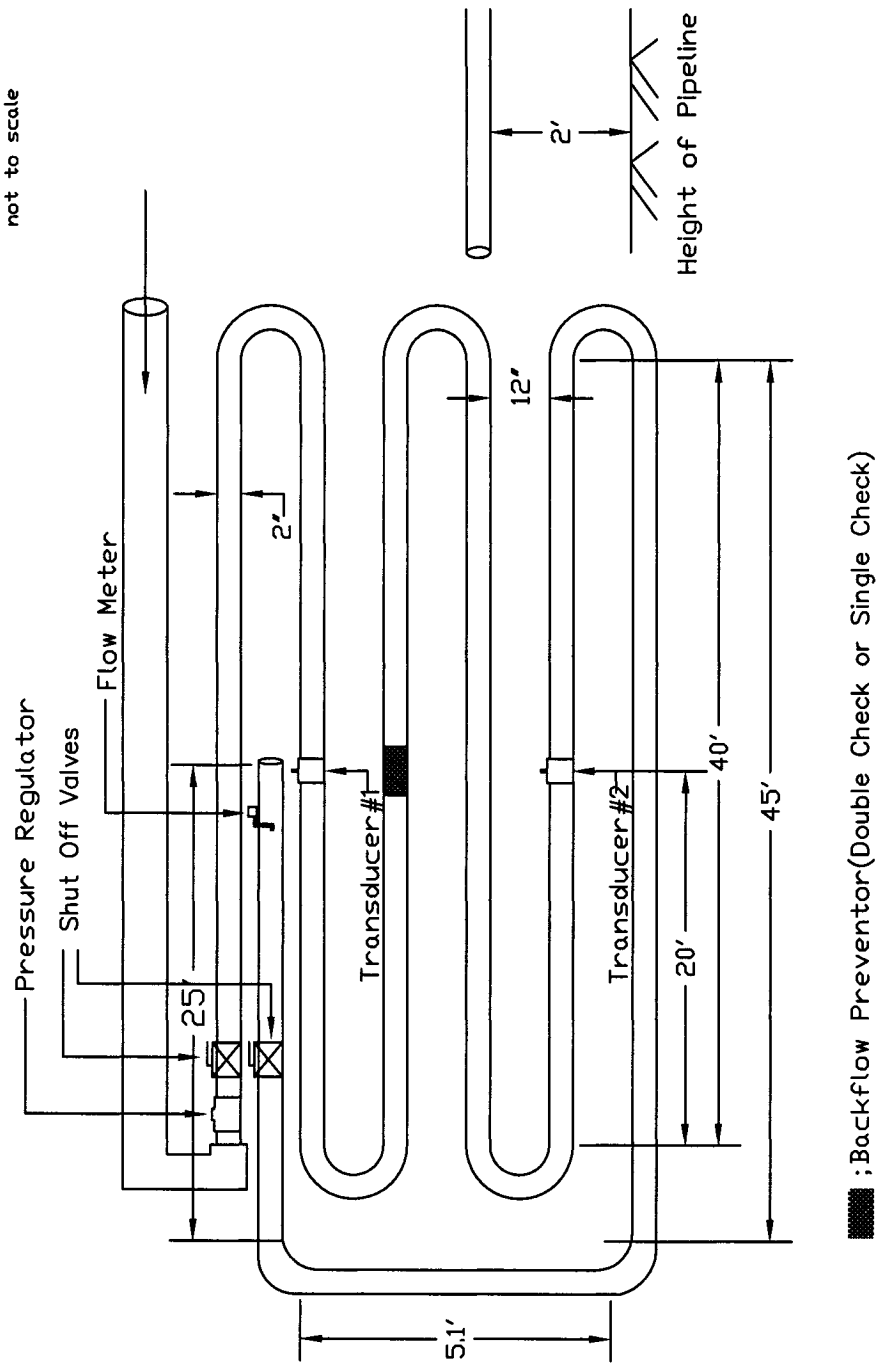

Figure 3.1 Plan view of experiment setup

Table 3.1 Information of fluid and experiment setup

Length of Pipe (ft)	278
Diameter (in)	2
Area (ft^2)	0.021825
Temperature of Fluid (^oF)	58
Kinematic Viscosity (ft^2/sec)	1.22×10^{-5}

As shown in Table 3.1, total length of pipeline is 278feet with pipe diameter at 2 inches. At the moment of performing experiment, temperature of water was 58 ^oF and the kinematic viscosity is 1.22×10^{-5} ft^2/sec. The distance between the shut-off valve no.1 to the upstream pressure transducer is 66.8ft and the distance from the shut-off valve no.1 to the downstream pressure transducer is 208ft.

3.2 Experimental Apparatus

For the experimental investigation, the water pressure at the upstream of the experimental piping system can be maintained up to 150psi in the steady state condition. A backflow prevention assembly is located in the middle of the pipeline. The backflow prevention assembly is removed first in order to measure the transient flow induced pressure wave. For some experiment, the backflow prevention assembly is placed in order to determine the effect of transient flow on backflow prevention assembly. The upstream and downstream shut-off valves (2" diameter) are located at both ends of the pipeline to close the system. When these two shut-off valves are suddenly closed, it creates a pressure wave which is observed to travel back and forth within the piping system.

The pressure time histories are measured by pressure transducers. The transducers have a range of 0 to maximum 11,250psi. The sample rate of the pressure transducer is 500kHz but the signal from the transducer was sampled as 4000Hz for these experiments. The strain gauge input module was used for the signal conditioning. Data acquisition system used in this study can transfer at 1.25million data per second.

To control the line pressure at the steady state, pressure-reducing valve was used. It was installed at the upstream of the pipeline. Line pressure could be changed using this valve. Therefore, different line pressures are produced with this pressure-reducing valve. For the measurement of the flow rate, a flow meter was used. Flow meter has two parts. One is sensor that has five rotors with accuracy of ± 1% error over the full measuring range. The other part is an analog flow indicator with range of 0 to 100 GPM.

As shown in Fig. 3.1, water for the piping system is fed from upstream and the pressure-reducing valve controls the specific line pressure. After maintaining the predetermined steady state line pressure, two shut-off valves at upstream and downstream ends are closed simultaneously. Two transducers are installed at 66.8ft (upstream pressure transducer) from the upstream end and at 208ft (downstream pressure transducer) from the upstream end of the 278ft-long pipeline. These two transducers are collecting the pressure time history and transfer the signal to the data acquisition system digitally.

3.3 Head Losses at the System

Head losses at the piping system have been measured as a part of present study. As shown in Table 3.2, various items are included in this piping system. For the major head loss, the frictional loss and the minor losses were measured.

Table 3.2 Various items in piping system

No.	Item in the system	Quantity
1	2" Ball Valve (SOV)	2
2	2" Ball Valve (Fully Opened)	2
3	90° Elbow	12
4	T-fitting	2
5	Small Ball Valve for the T-fitting	2
6	Union	2
7	Coupling	9

Eq. 3.1 is the well known Darcy-Weisbach equation for the frictional loss. For the minor losses, Eq. 3.2 is used.

$$h_f = f\frac{L}{D}\frac{V^2}{2g} \tag{3.1}$$

$$h_m = k\frac{V^2}{2g} \tag{3.2}$$

Coefficients f and k are determined by the experiments.

Eq. 3.3 shows total head loss at the piping system:

$$h_{total} = (f\frac{L}{D} + k_1 + k_2 + k_3 + \cdots\cdots)\frac{V^2}{2g} \tag{3.3}$$

This shows that the total head loss is the sum of the frictional loss and the minor losses for the various items contained in a piping system.

Now a new coefficient for the summation of friction and minor losses of the various items in a piping system is introduced:

$$M = (f\frac{L}{D} + k_1 + k_2 + k_3 + \cdots\cdots) \tag{3.4}$$

Where M is the new coefficient for the total head loss. Fig. 3.2 presents the value of M as a function of the Reynolds number of the piping system covered by the present experiments.

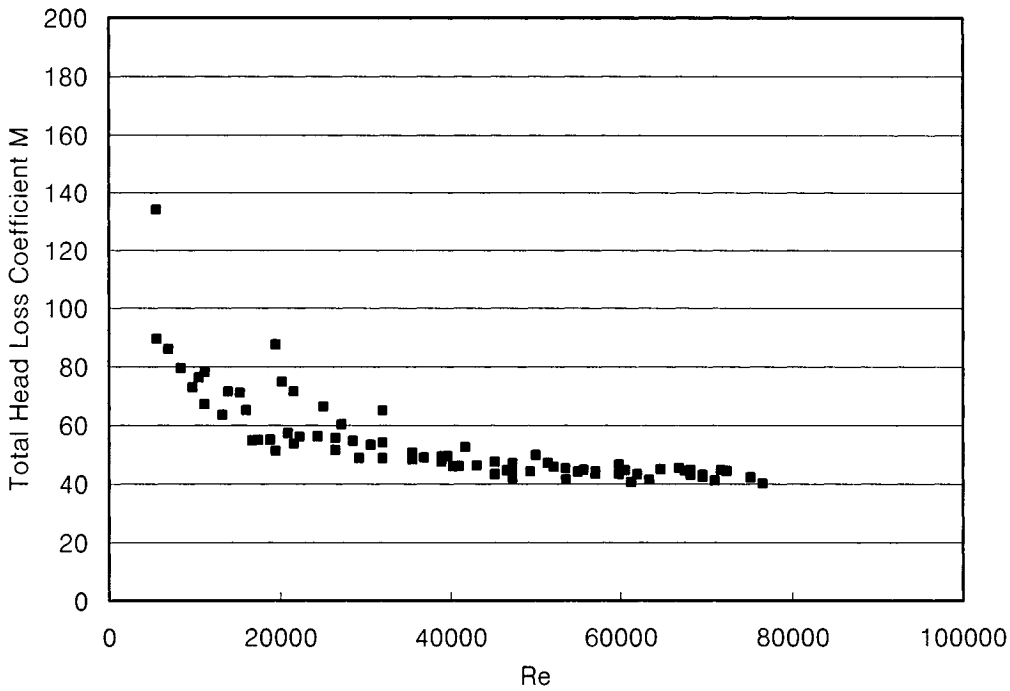

Figure 3.2 Coefficient M for the total head loss vs. Reynolds number

In an attempt to determine the relative importance of M and f(L/D). The value of f(L/D) is plotted in Fig. 3.3 along with the value of M in the range of Reynolds number covered.

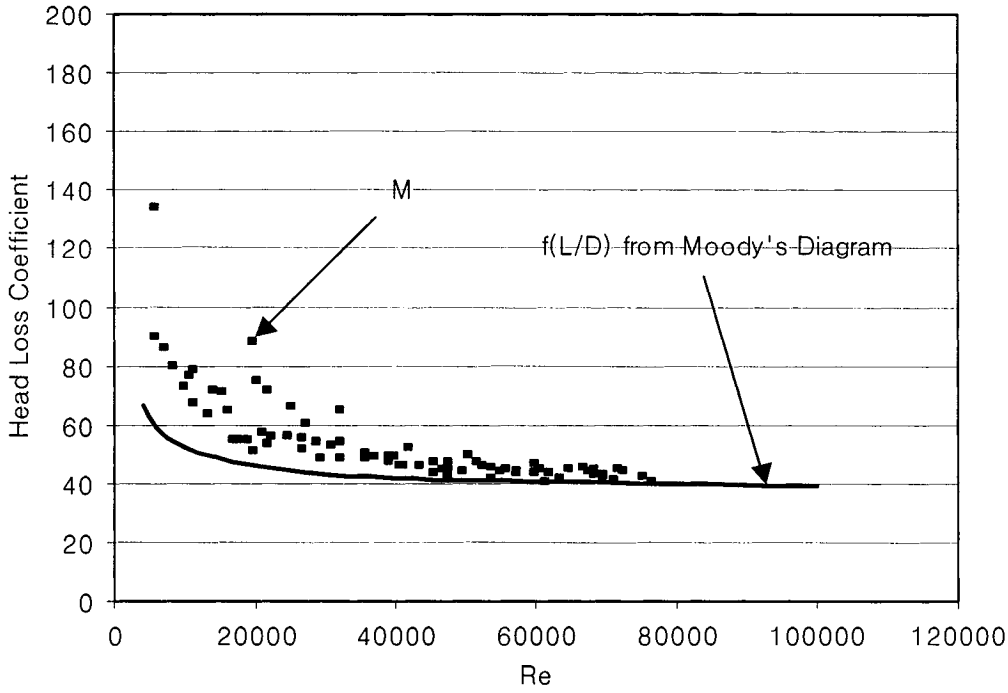

Figure 3.3 Comparison of M and f(L/D)

Frictional coefficient "f" is collected from the Moody's Diagram. In this case, relative roughness $\frac{k_x}{D}$ is 0.025 with galvanized iron pipe. It shows that the values of M are bigger than f(L/D) because M contains all the minor losses and the frictional losses. The effect of minor loss is significant for experimental system used in the present study as shown in Fig. 3.3. From Fig. 3.3, it is clearly seen that the effect of the minor losses is significant in the region of lower Reynolds number. Minor loss term is certainly not minor in the range of Reynolds number between 4,000 and 40,000 used in the present experiment.

3.4 Head Loss at Ball Valve

Head loss at the ball valve was also measured experimentally in this study. Ball valve can cause significant head losses. When ball valve is used as a shut-off valve, head loss at ball valve is strongly dependent on the opening area of the valve. It is very difficult to determine the exact opening area of ball valve as it opens or closes. Obviously, the rate of opening or closing area of ball valve is not linear with the time. In addition as the flow passes through the ball valve, flow separation and turbulence are introduced.

From Eq. 3.2,

$$k_{Ball} = \frac{2g\Delta h}{V^2} \tag{3.5}$$

Head loss coefficient k_{Ball} for ball valve is determined using the experimental data. Fig. 3.4 shows the assumption that rate of closed area of ball valve is linear with the angle of handle of ball valve. For example, if the angle from the centerline of a pipe to the handle of ball valve is equal to 45^{o} as shown in Fig. 3.5, then 50 % of the area of ball valve is closed. And when angle is zero, then ball valve is fully opened. And when angle is 90^{o}, then angle is completely closed.

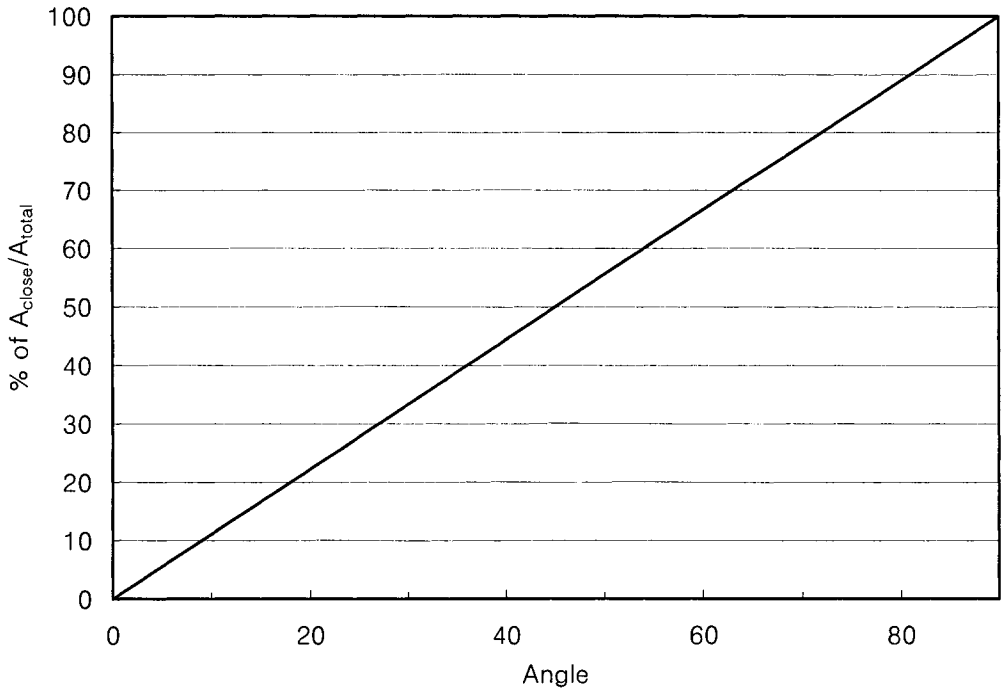

Figure 3.4 Ratio of closed area as a function of ball valve angle

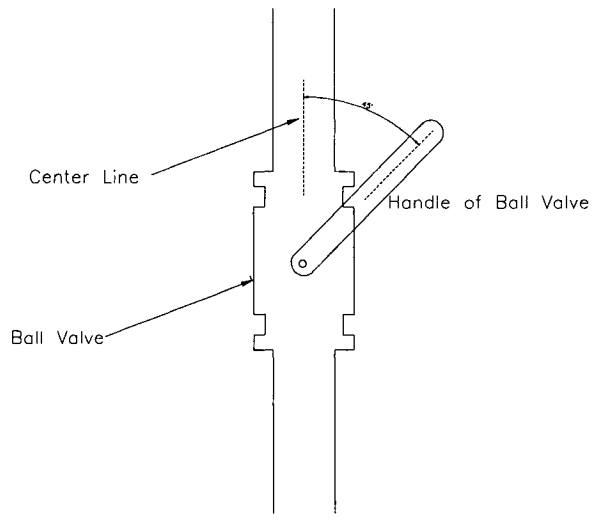

Figure 3.5 Angle measurement of a ball valve

Fig. 3.6 shows the pressure loss versus the angles of the 2-inch ball valve for different flow rates. As it is expected, when the flow rate is small, the curve tends to be at the right hand side. For large flow rate, it is difficult to measure the pressure loss at the beginning of opening the ball valve because head loss is huge and the line pressure at the place of ball valve has been found to have large fluctuations. As expected at the same angle of handle of ball valve, pressure loss at the high flow rate is bigger than that at the low flow rate as shown in Fig. 3.6.

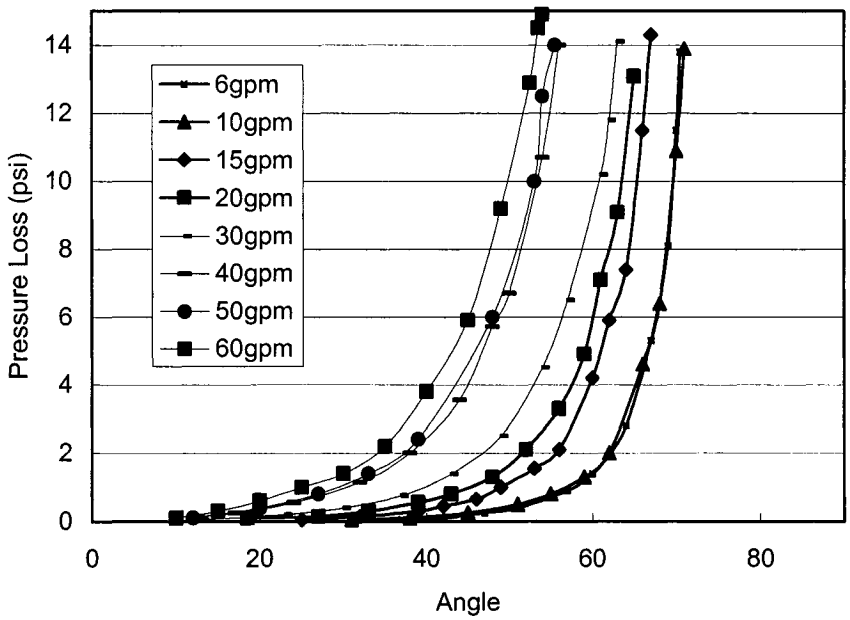

Figure 3.6 Pressure losses at 2-inch ball valve with various angles

Fig. 3.7 shows head loss coefficient k_{Ball} with different flow rates such as 10, 15, and 20gpm at different closing angles for 2-inch ball valve. As we can see, k_{Ball} can not be a constant in the minor loss equation as shown in Eq. 3.2 because its range is too wide and it varies with the angles of the handle of ball valve. Most importantly, head loss at a ball valve is not minor rather it is a major head loss when the ball valve is closing or opening.

Therefore, both the frictional head loss and the head loss at ball valve could all be the major factors to damp out the oscillations of transient flow in the experimental system used in the present study.

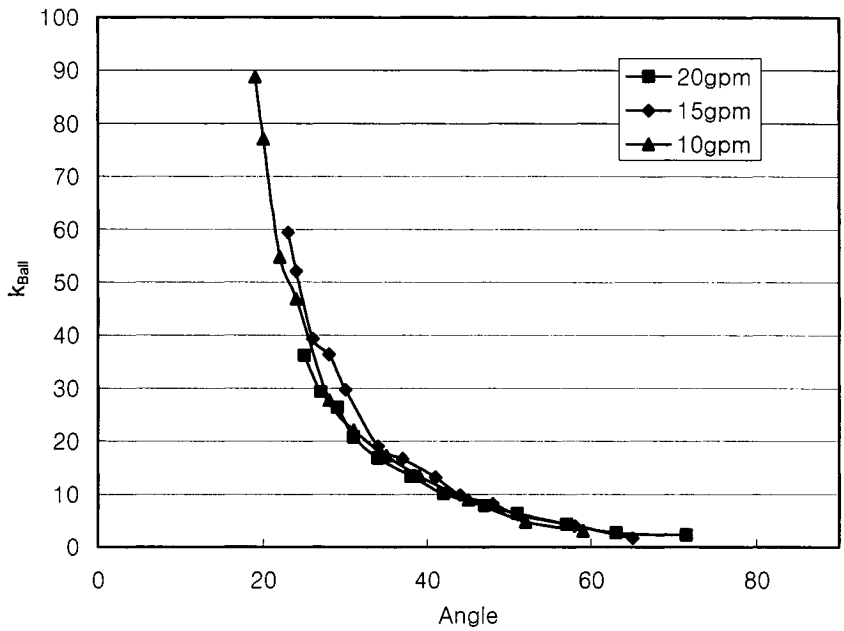

Figure 3.7 Head loss coefficient k_{Ball} for 2-inch ball valve vs. angle of ball valve

3.5 Head Loss at Backflow Prevention Assembly

Head loss at the backflow prevention assembly in piping system has been measured. Backflow prevention assembly produces significant head loss in piping system. In the present study, head losses at backflow prevention assembly were measured for both single check and the double check valve. The head loss coefficient for backflow prevention assembly can be expressed as:

$$k_{DC} = \frac{2g\Delta h}{V^2} \tag{3.6}$$

Fig. 3.8 shows the head loss at the single check and the double check valve backflow prevention assembly. As shown in Fig. 3.8, rectangular dots show the pressure loss when only one check disc was installed in the backflow prevention assembly. Triangular dots show the pressure loss when two check discs were installed in the backflow prevention assembly.

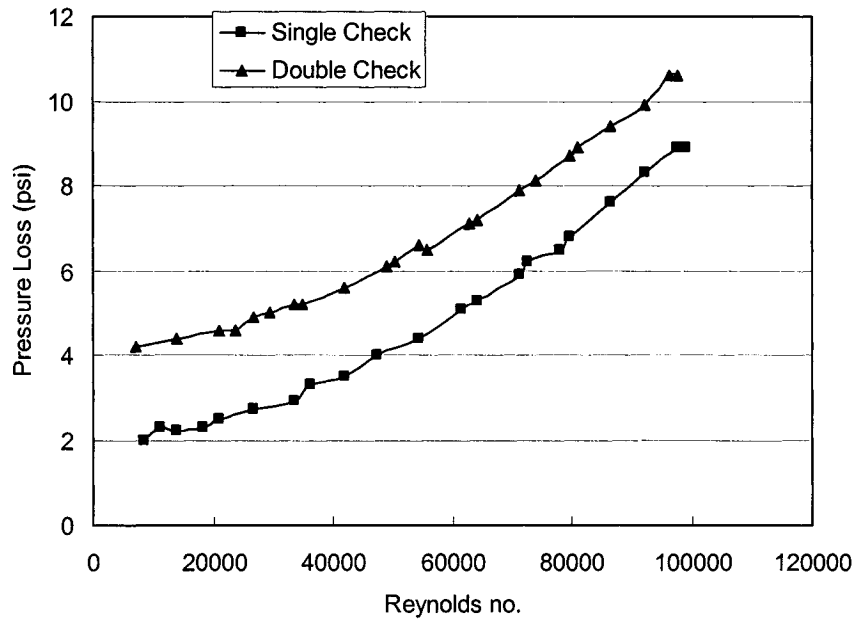

Figure 3.8 Pressure losses at backflow prevention assembly

Fig. 3.9 shows the head loss coefficient for the single check and the double check valve. Rectangular dots show the head loss coefficient when the one check disc is installed in backflow prevention assembly. Triangular dots show the head loss coefficient when the two check discs are installed in backflow prevention assembly. In the range of Reynolds number between 4,000-40,000, the head loss coefficient k_{DC} is very significant as shown in Fig. 3.9.

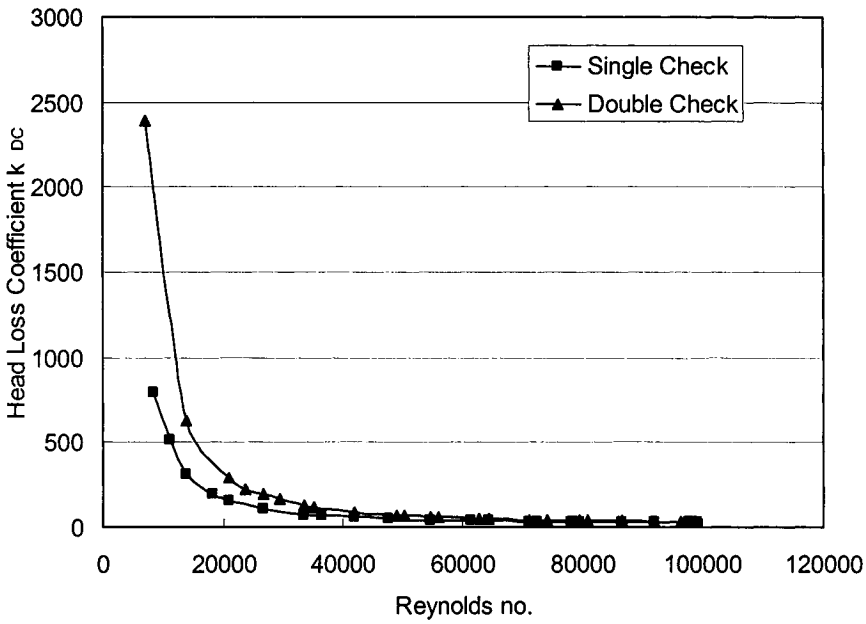

Figure 3.9 Head loss coefficient k_{DC} for 2-inch backflow prevention assembly

CHAPTER 4

RESULTS AND DISCUSSION

The numerical simulation procedures and experimental set up were discussed and presented in Chapter 2 and Chapter 3. The computer model results using three different numerical methods, i.e. the method of characteristics, the two-dimensional method, and the implicit method will be presented in this chapter. Experimental data will be compared and discussed along with results of the numerical simulations. Furthermore, several scenarios of simulation for the transient flow problem will also be presented in this chapter.

4.1 A Brief Discussion of Pressure Waves (Water Hammer) Caused by Sudden Valve Closure

Fig. 4.1 shows an example of water hammer in single pipeline depicting the sequence of pressure wave of water hammer after instantaneous valve closure. After a valve is completely closed, the sequence of events for $0 < t < \frac{4L}{c}$ (where L is the total length of pipe and c is the wave speed of water hammer) is shown in four major stages in Fig. 4.1. Once a pressure wave is produced in a pipeline, it propagates back and forth in the pipeline until it is dissipated by friction. This wave is reflected and transmitted at different boundaries.

Let L = Pipe length, c = Wave speed, H_0 = Initial piezometric head, and V_0 = Flow velocity.

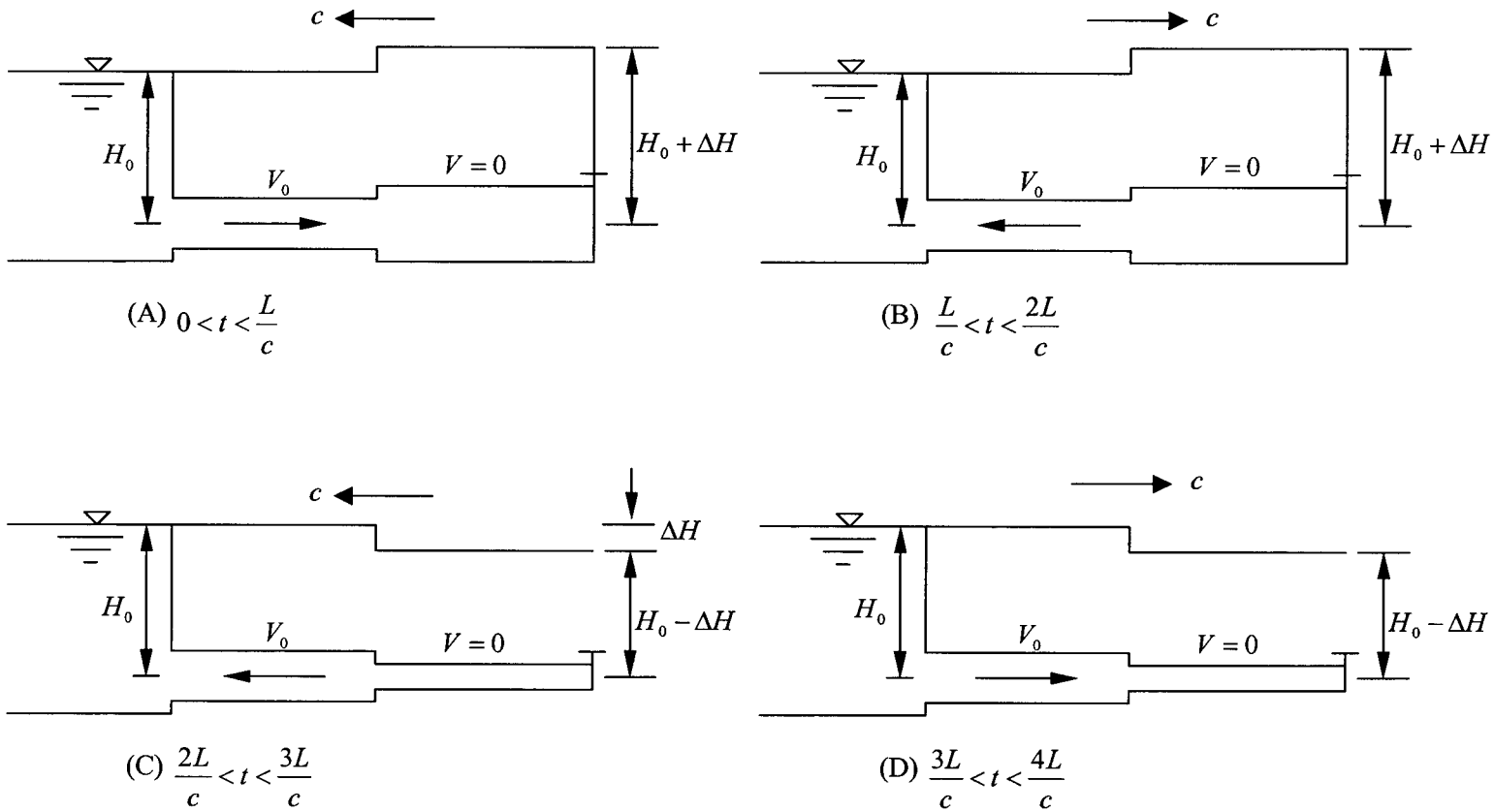

Figure 4.1 Propagation of pressure wave caused by closing the shut-off valve at the downstream end

(A) Pressure wave propagation toward the reservoir ($0 < t < \frac{L}{c}$)

The pressure wave will reach the upstream reservoir in $\frac{L}{c}$ seconds. For anytime less than $\frac{L}{c}$, the pressure wave will be between the valve and the reservoir. On the reservoir side of the wave, flow velocity will be V_0, the piezometric head will be H_0 (assume $\frac{V_0^2}{2g}$ is negligible compared to H_0) and the pipe diameter will be the same as during the initial steady-state condition.

On the valve side of the wave front (behind the wave) the flow velocity will be zero. Piezometric head will be $H_0 + \Delta H$, the pipe diameter will be increased because of the increased inside pressure.

(B) Pressure wave reflection at the reservoir and propagation toward the valve ($\frac{L}{c} < t < \frac{2L}{c}$)

At time $t = \frac{L}{c}$, the pressure wave will reach the upstream reservoir, and the piezometric head through out the pipe length will be $H_0 + \Delta H$. However, the head on the upstream side of the pipe entrance will be H_0 (since the reservoir level is assumed to remain constant). Since $H_0 + \Delta H > H_0$, the fluid will begin to flow toward the reservoir with velocity V_0 and the head will drop to H_0.

A pressure wave will now propagate toward the valve. In front of this wave (on the valve side) the flow velocity will be zero, pressure head will be $H_0 + \Delta H$ and the pipe will be expanded. Behind the wave (on the reservoir side) the flow velocity will be $-V_0$ (i.e. toward the reservoir), the pressure head will be H_0 and the pipe diameter will be the same as that during the steady state.

(C) Pressure wave reflection at the valve and propagation toward the reservoir $(\frac{2L}{c} < t < \frac{3L}{c})$

The wave reflected from the reservoir will reach the valve at $t = \frac{2L}{c}$. Since the valve is completely closed, it is not possible to maintain a flow velocity of $-V_0$ at the valve. Therefore, the flow velocity instantaneously becomes zero (that is $\Delta V = V_0$) and the pressure head drops to $H_0 - \Delta H$.

Now, this negative pressure wave propagates toward the reservoir. On the front side of the wave, the head is H_0, the flow velocity is $-V_0$, and the pipe diameter is the same as that during the initial steady-state condition; behind the waves however, the pressure head is $H_0 - \Delta H$, flow velocity is zero, and the pipe diameter is reduced.

(4) Pressure wave reflection at the reservoir and propagation toward the valve $(\frac{3L}{c} < t < \frac{4L}{c})$

As the negative wave reaches the upstream reservoir, the pressure head on the reservoir side of the entrance is H_0 and the pressure head on the valve side is $H_0 - \Delta H$. Therefore, the negative pressure wave is now reflected as a positive pressure wave.

On the valve side of this wave, the pressure head is $H_0 - \Delta H$, flow velocity is zero and the pipe diameter is reduced. On the reservoir side of the wave, however, the pressure head is H_0, the flow velocity is V_0 and the pipe diameter is the same as that during the initial steady-state condition. As this wave reaches the valve at $t = \frac{4L}{c}$, we have the same condition at $t = 0$ except that the valve is now closed. Therefore, the above sequence of events starts all over again.

The variation of pressure at valve can be plotted as shown in Fig. 4.2. Fig. 4.2 shows the theoretical period of the pipeline having a time interval of $\frac{4L}{c}$ assuming that the system is frictionless. When the shut-off valve (SOV) at the downstream end is closed, the pressure at the shut-off valve rises immediately and it propagates toward the reservoir. This process continues and the conditions are repeated until the pressure waves are dissipated due to friction in the real physical system.

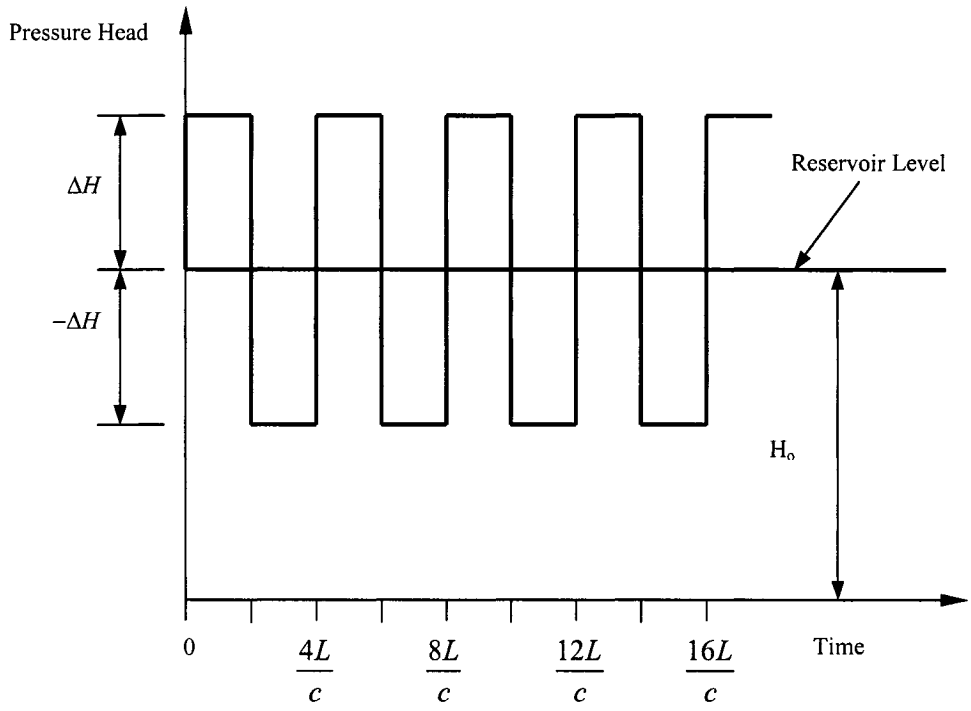

Figure 4.2 Pressure variation at the downstream valve (friction loss is neglected)

4.2 Presentations and Discussions of Experimental Results

4.2.1 Experimental Procedure

A 278 ft-long pipeline with pipe diameter of 2 inches throughout was installed for the experiments. Two shut-off valves were installed at the upstream end and at the downstream end. Before generating the transient flow, the flow rate and line pressure at the downstream end and upstream end were measured for the steady state condition. Both shut-off valves at both ends are then closed simultaneously. A water hammer is therefore produced, generating a positive pressure wave at the downstream end and a negative pressure wave at the upstream end. These two pressure waves propagate toward opposite side separately.

Two transducers were installed at 66.8 ft (upstream pressure transducer) and at 208 ft (downstream pressure transducer) from the upstream end. These transducers measure the pressure fluctuations generated by instantaneous closure of shut-off valves at upstream and downstream ends. To generate different experimental cases with different line pressures and different flow rate, pressure-reducing valve was installed at upstream end. Flow conditions for different flow and pipeline condition are summarized in Table 4.1. Many cases of experiments have been performed in this study and two cases will be shown in this chapter. Line pressures were 120psi with flow rate of 12.5gpm in Case 1 and 100psi with flow rate of 12.0gpm in Case 2 respectively. The speed of pressure wave shown at Table 4.1 is measured by experiment.

Table 4.1 Experimental conditions for Case 1 and Case 2

	Case 1	Case 2
Line Pressure (psi)	120	100
Flow Rate (gpm)	12.5	12.0
Diameter (ft)	0.1667	0.1667
Velocity (fps)	1.275	1.224
Speed of Pressure Wave (fps)	4435	4435
Kinematic Viscosity (ft^2/s)	1.22×10^{-5} ($58^{\circ}F$)	1.22×10^{-5}($58^{\circ}F$)
Reynolds number	17418.38	16721.65
Closing Time of SOV at Downstream (sec)	0.0215	0.0265
Closing Time of SOV at Upstream (sec)	0.031	0.027

Kinematic viscosity and Reynolds number were determined by the measurement of the water temperature and temperature was 58° Fahrenheit. The flow meter was also calibrated using the flow accumulator. In the present study, range of flow rate was restricted to certain range because of size of pipe. Pressure-reducing valve can control line pressure, and range of line pressure was from 60psi to 140psi which was measured at upstream end. Line pressure at the steady state condition was just simply measured by line pressure gauge, which can measure 0 to 200psi. Line pressure at downstream end also was measured in the same manner. It is assumed that velocity is not changing as a steady state before transient flow is generated. Line pressure at the upstream end was very stable when it was measured before transient flow was generated.

Table 4.1 also shows the closing time of shut-off valves at both downstream and upstream ends. Shut-off valve at upstream started closing at 0.701 and completely closed at 0.732. It

takes 0.031 second for Case 1. Shut-off valve at downstream started closing at 0.714 and completely closed at 0.7355. It takes 0.0215 second for Case 1. For Case 2, shut-off valves at both ends started closing at 0.7937 and 0.7982, and were completely closed at 0.8207 and 0.8247 for upstream end and downstream end respectively. It takes 0.027 second and 0.0265 second for upstream and downstream end in Case 2 as shown in Fig. 4.3 and 4.4.

Each closing time for both shut-off valves at downstream and upstream ends was measured experimentally for Case 1 as shown in Fig. 4.3. It is assumed that both shut-off valves at upstream and downstream ends are closed linearly from the beginning to the end as shown in Fig. 4.3. Linear equation for the valve closure of SOV (shut-off valve) at upstream end is $Q = -403.23t + 295.16$ and linear equation for the valve closure of SOV at downstream end is $Q = -581.4t + 427.62$. Each closing time for both shut-off valves at downstream and upstream ends was measured experimentally for Case 2 as shown in Fig. 4.4. It is also assumed that both shut-off valves at upstream and downstream ends are closed linearly from the beginning to the end as shown in Fig. 4.4. Linear equation for the valve closure of SOV at upstream end is $Q = -444.44t + 364.76$ for Case 2 and linear equation for the valve closure of SOV at downstream end is $Q = -452.83t + 373.45$ for Case 2. These linear equations for the valve closure will be used for boundary conditions of the computer simulation.

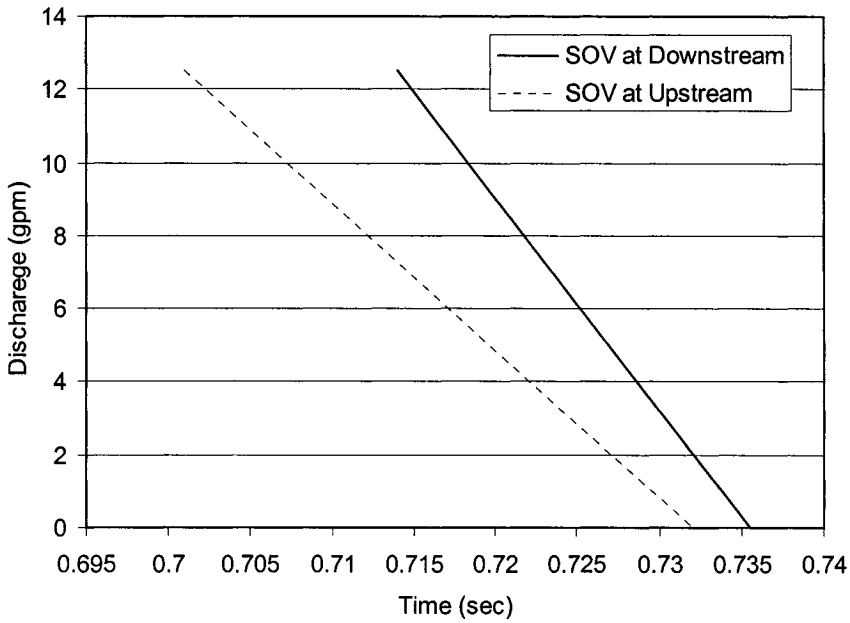

Figure 4.3 Closure of shut-off valves at the both ends of pipeline for Case 1

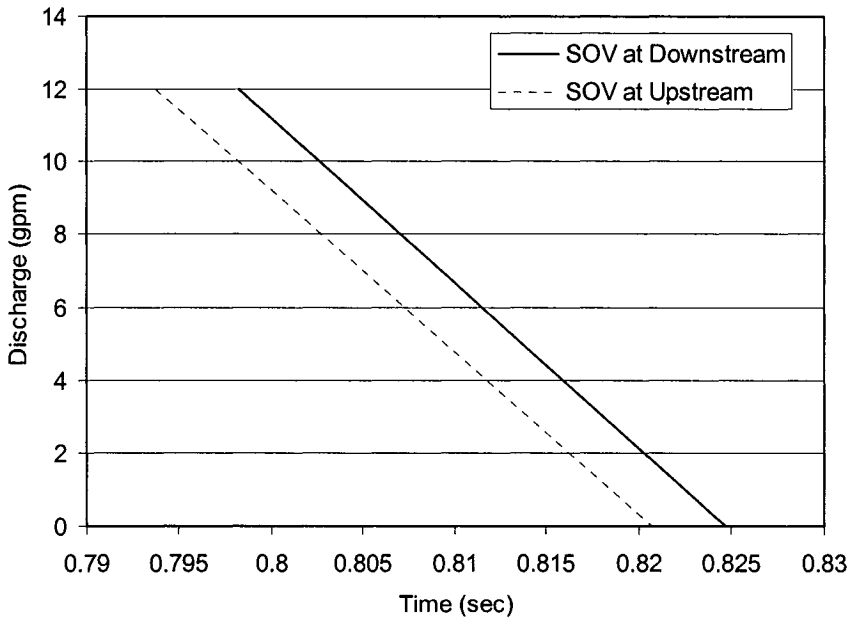

Figure 4.4 Closure of shut-off valves at the both ends of pipeline for Case 2

4.2.2 Experiment for Transient Flow

Fig. 4.5 shows the pressure time history at downstream region (downstream pressure transducer is located at 208ft from the upstream end) as Case 1. When the shut-off valve at the downstream end is closed, pressure at the downstream region rise immediately and it propagates toward the upstream region. This pressure wave goes back to the downstream after it approaches the upstream end that is also closed by shut-off valve. This pressure wave will go back and forth along the pipeline until it is dissipated due to the frictional and minor losses in the system. At the steady state condition, the line pressure is maintained at 120psi and the flow rate before the shut-off valves were closed is maintained at 12.5gpm. Data collection rate is set at 4,000 points per second.

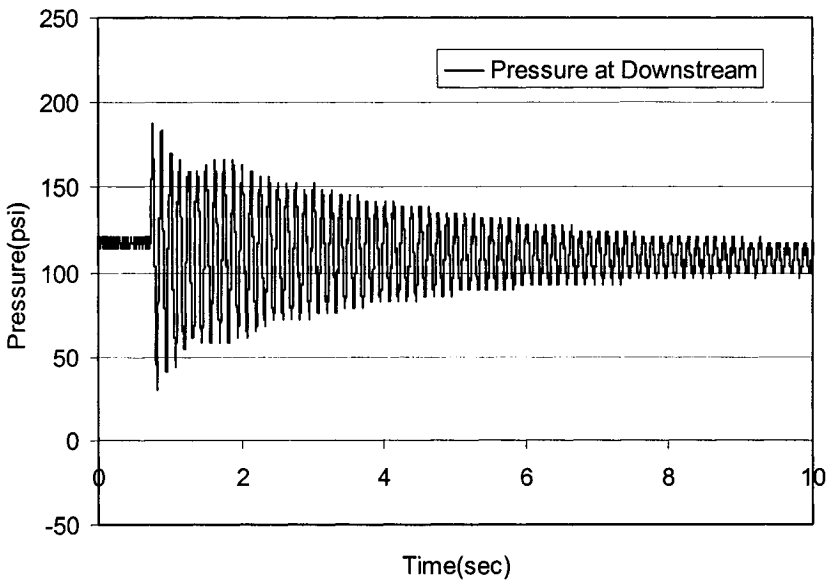

Figure 4.5 Pressure time history at the downstream region (Q=12.5gpm, Case 1)

Fig. 4.6 shows pressure time history at upstream region (upstream pressure transducer is located at 66.8 ft from the upstream end) as Case 1. It is noted when shut-off valve at the downstream end is closed, shut-off valve at the upstream end is also closed simultaneously as shown in Figs. 4.3 and 4.4. From Fig. 4.6, it is seen that as the shut-off valve at the upstream end is closed, pressure at the upstream region goes down immediately and it propagates toward the downstream. This pressure wave goes back to the upstream after it approaches the downstream end that is also closed by shut-off valve at downstream end. The pressure is gradually damped out due to frictional and minor losses.

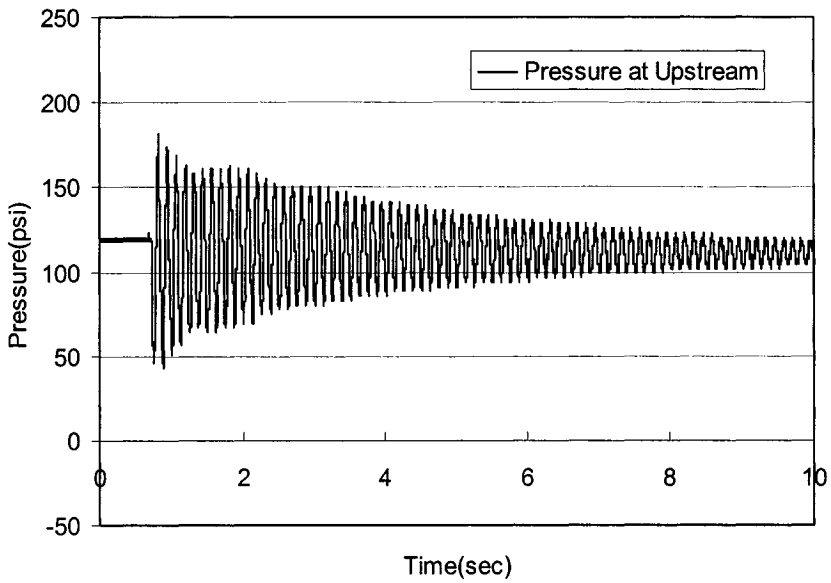

Figure 4.6 Pressure time history at the upstream region (Q=12.5gpm, Case 1)

Fig. 4.7 shows the pressure time history at the downstream region as Case 2. Fig. 4.8 shows the pressure time history at the upstream region as Case 2. Line pressure at the upstream was maintained at 100psi for the steady state condition with flow rate at 12.0gpm in Case 2. As mentioned earlier, the closing of the downstream shut-off valve generates first positive

pressure wave and the closing of the upstream shut-off valve generates first negative pressure wave. These pressure waves will propagate back and forth along the pipeline until it is dissipated due to head losses.

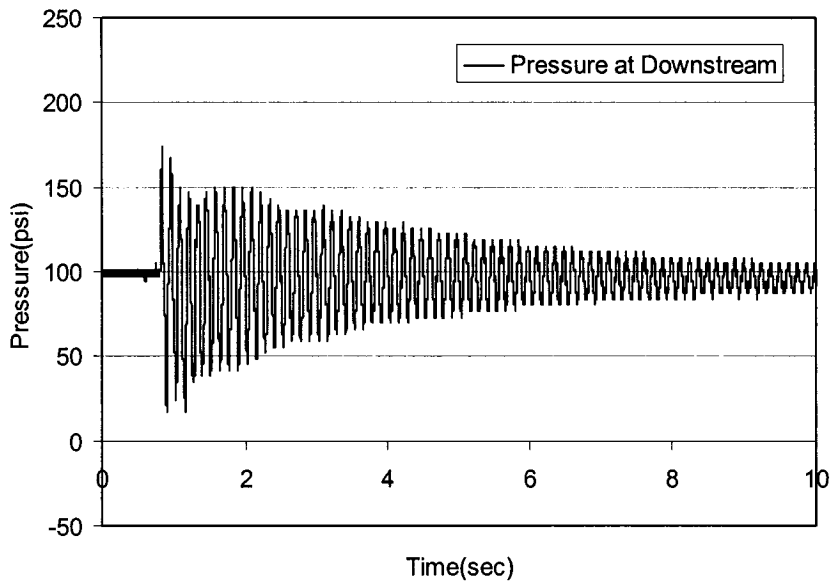

Figure 4.7 Pressure time history at the downstream region (Q = 12.0gpm, Case 2)

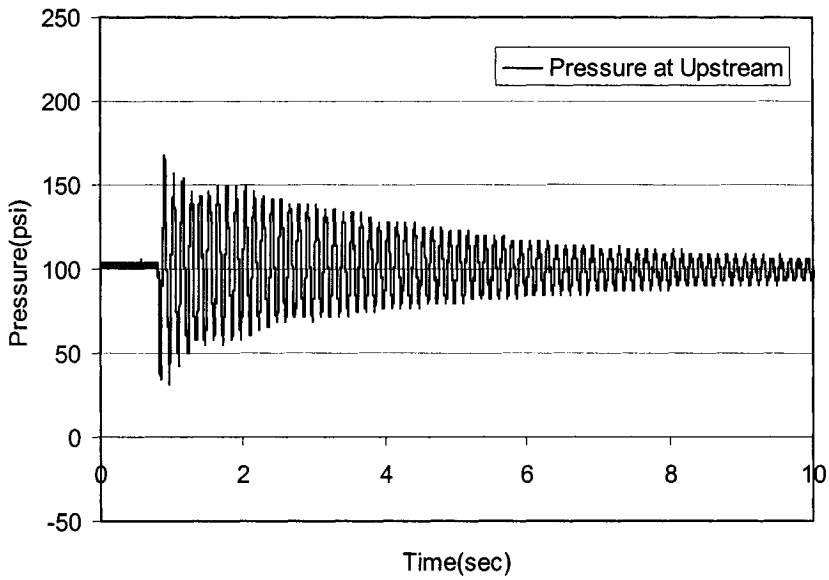

Figure 4.8 Pressure time history at the upstream region (Q = 12.0gpm, Case 2)

It is revealing that this experimental data has 8 Hz of frequency for both Case 1 and Case 2 in this piping system. The period of the pressure wave in this experimental system was 0.125 second using $T = \frac{1}{f}$. The period of the pressure wave in this experimental system can be used to determine the speed of the pressure wave in this experimental setup. The speed of the pressure wave in this experimental system is determined to be 4435 ft/sec for both Case 1 and Case 2.

4.2.3 Experiment with Backflow Prevention Assembly

This experiment shows the effects of the water hammer on backflow prevention assembly, particularly double check valve backflow prevention assembly (DC), which is included in the present experimental setup. In distribution system, check valves in the backflow prevention assembly could be the first recipients of the water hammer as transients are produced by quickly closing valves or pumps on the downstream side of the valves. The results could damage the check valves particularly the second check valve which meets the initial impact of the water hammer against the backflow prevention assembly.

In this section, experiments for backflow prevention assembly, which is installed in the middle of the pipeline will be discussed. A backflow prevention assembly was installed at 48.5ft away from the upstream pressure transducer. Therefore, the distance from the upstream end to the backflow prevention assembly is 115.3ft. The distance from the backflow prevention assembly to the downstream pressure transducer is 92.7ft. And the distance from the downstream end to the backflow prevention assembly is 162.7ft as shown in Table 4.2. For this series of experiments, first check in the backflow prevention assembly has been taken out to simplify and to observe the phenomena of single second check against the water hammer. Thus, only one check valve was installed inside of the backflow prevention assembly for this experiment.

Table 4.2 Length of the each section at piping system

Section	Length (ft)
Upstream end to upstream pressure transducer	66.8
Upstream pressure transducer to backflow prevention assembly	48.5
Backflow prevention assembly to downstream pressure transducer	92.7
Downstream pressure transducer to downstream end	70.0
Total	278.0

The total length of the pipe is 278 ft, pipe diameter is 2 inches, and initial pressure of the upstream end was maintained at 120psi and 100psi for both Case 1 and Case 2 as shown in Table 4.1. The water hammer was created by quickly closing the valves at the downstream end and upstream end simultaneously.

Figs. 4.9 and 4.10 show the pressure time histories at the downstream region and upstream region respectively in the system involving backflow prevention assembly. Fig. 4.11 shows the pressure time histories at the both upstream and downstream regions in the 0.2-second duration from 2.8 to 3.0 seconds. The pressure at the upstream pressure transducer (upstream region) responds at 2.903 seconds and the pressure at the downstream pressure transducer (downstream region) responds at about 2.904 second since the length from the backflow prevention assembly to the downstream pressure transducer is 44.2 ft longer than the length from the backflow prevention assembly to the upstream pressure transducer. Ranges of the differences between the maximum pressure head and minimum pressure head for Case 1 are about 95psi at the downstream region and 60psi at the upstream region.

Without a backflow prevention assembly, ranges of the differences between the maximum pressure head and minimum pressure head are about 160psi at the downstream region and 135psi at the upstream region as previously shown in Figs. 4.5 and 4.6.

Figs. 4.12 and 4.13 show the pressure time histories at the downstream region and upstream region respectively in the system involving backflow prevention assembly. Fig. 4.14 shows the pressure time histories at both regions of upstream and downstream in duration of 0.2 second. The differences between the maximum pressure head and minimum pressure head are about 95psi in the downstream region and 50psi in the upstream region. Without the backflow prevention assembly, the differences between the maximum pressure and minimum pressure are about 150psi at the downstream region and 140psi at the upstream region for Case 2 as previously shown in Fig. 4.7 to 4.8.

The results from the experimental Case 1 and Case 2 show that backflow prevention assembly serves as a damper to the water hammer created by the hydraulic transients. Fluctuation of the pressure at the system having a backflow prevention assembly is damped out relatively faster than that for the system without a backflow prevention assembly when one compares the results of Figs. 4.5 to 4.8 with the results of Figs. 4.9 to 4.14. It also appears that the head losses are significantly increased when the check valve inside of the backflow prevention assembly is closing.

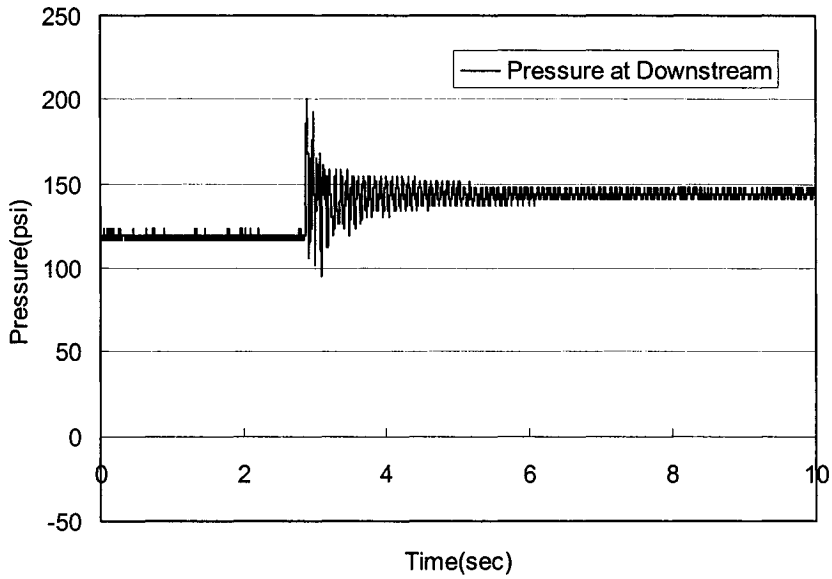

Figure 4.9 Pressure time history at the downstream region (Case 1: $0 \leq t \leq 10$ sec)

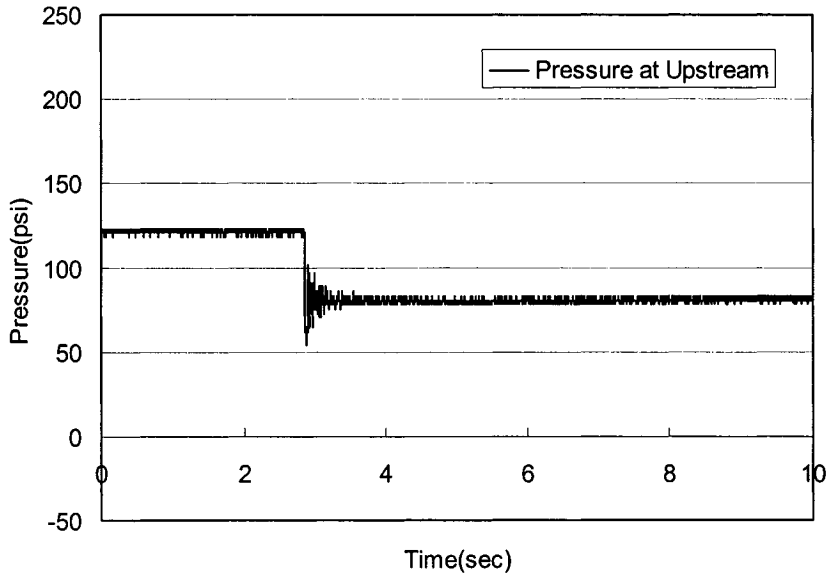

Figure 4.10 Pressure time history at the upstream region (Case 1: $0 \leq t \leq 10$ sec)

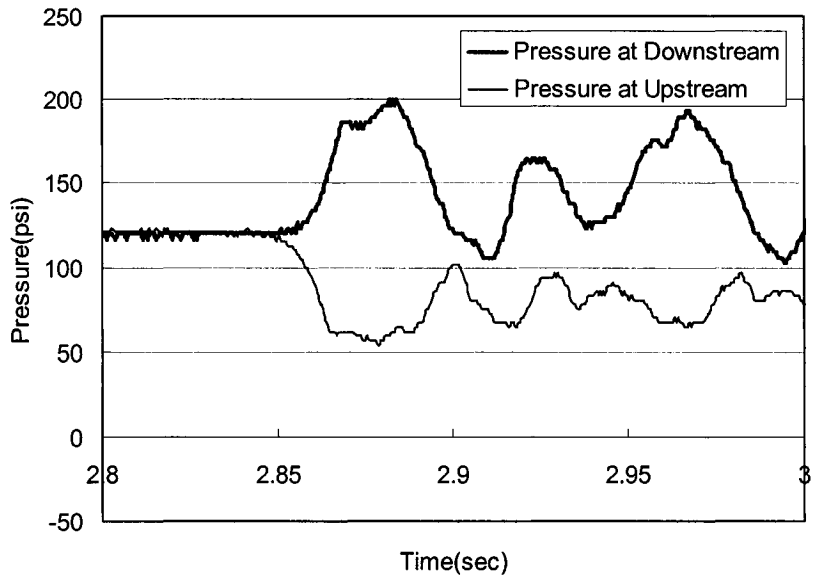

Figure 4.11 Pressure time history at the upstream and downstream region (Case 1: $2.8 \leq t \leq 3.0$ sec)

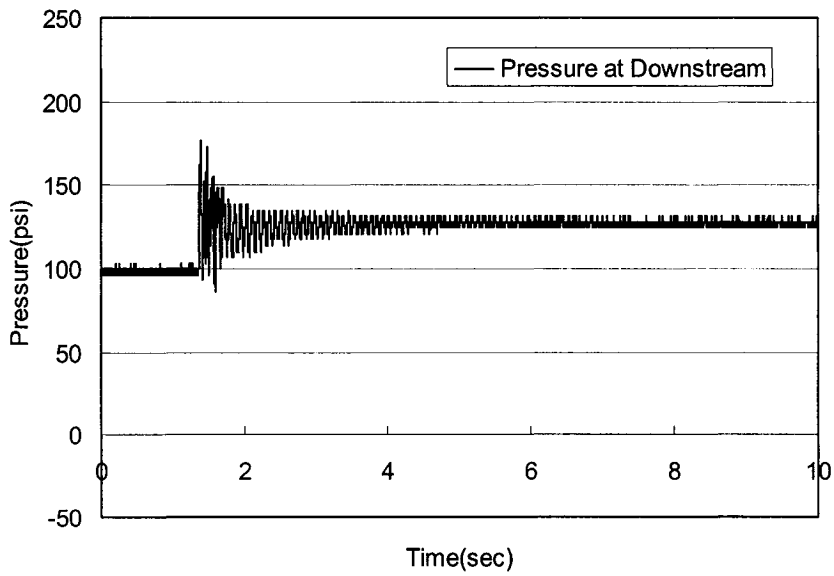

Figure 4.12 Pressure time history at the downstream region (Case 2: $0 \leq t \leq 10$ sec)

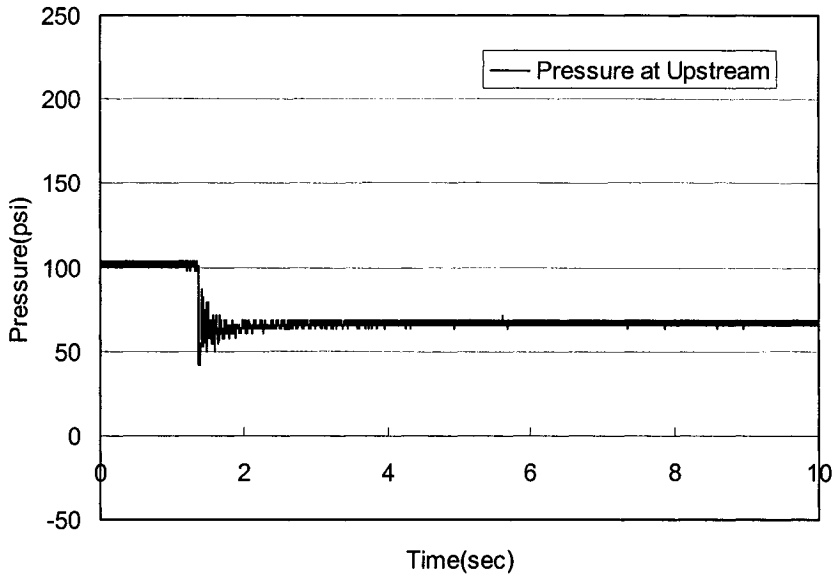

Figure 4.13 Pressure time history at the upstream region (Case 2: $0 \leq t \leq 10$ sec)

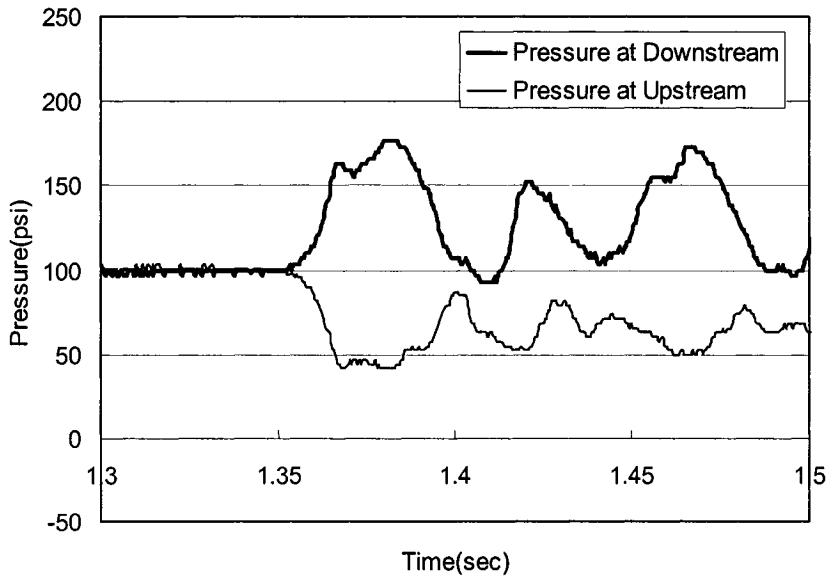

Figure 4.14 Pressure time history at the upstream and downstream region (Case 2: $1.3 \leq t \leq 1.5$ sec)

4.3 Experimental and Modeling Results using the Method of Characteristics

The development of a computer model using the method of characteristics has been discussed in Section 2.2. The model results will now be compared with the experimental data obtained for the present study. Two experimental cases will be presented in order to compare with the experimental data. Case 1 has the line pressure of 120psi with the flow rate at 12.5gpm. Case 2 has the line pressure of 100psi with the flow rate at 12.0gpm. Line pressure and flow rate have been measured at upstream end before the transient was created. The two shut-off valves were manually closed simultaneously as shown in Figs. 4.3 and 4.4.

As shown in Figs. 3.2 and 3.3, the present experimental set up encounters significant minor losses, which are greater than the frictional head loss at certain range of Reynolds number. It is obvious that minor loss is not minor in the present experimental system for the range of Reynolds number from 4,000 to 40,000. The experiments for transient flow have been performed in the range of 4,000 to 40,000. Reynolds numbers was 17,418 for the Case 1 and 16,721 for the Case 2 in the present study. To compare the frictional head loss with the minor head losses, total head losses have been measured in the steady state condition as presented in Fig. 3.3.

When computer simulations for transient flow are performed numerically, if only Darcy-Weisbach frictional coefficient is used to represent the head loss then the equivalent value of "f" must be significantly greater. To overcome the over/underestimation of fluctuation of pressure in computer simulation, new coefficient is needed to accurately estimate the loss coefficient of transient flow instead of only using Darcy-Weisbach coefficient "f". Therefore, equivalent head loss coefficient C_L will be introduced in this chapter. C_L is the combined head loss coefficient that includes various coefficients of head

losses such as coefficient for friction and minor losses. After careful estimations for the piping system, C_L will be fixed. Results of the numerical analysis were calibrated using the experimental data. Equivalent head loss coefficient C_L for this piping system was 0.3. This value is almost more than 7 times larger than Darcy-Weisbach frictional coefficient in Moody's diagram. It is noted that the other significant effect of the head loss in this system might be due to the closing of shut-off valves at both the upstream and the downstream ends. During the process of closing the shut-off valves at the upstream and downstream end, significant pressure loss is encountered because of flow separation from the boundary of shut-off valve. As shown in Fig. 3.6, head loss is even bigger when the angle is small, which means that the velocity of flow is higher because the opened area of ball valve is small. For the computer model, the grid size $\Delta x = 2.2175$ (feet) and time increment $\Delta t = 0.0005$ (sec) as shown in Table 4.3. The Courant stability criterion is satisfied using the Δx and Δt as noted. Two boundary conditions for the upstream end and the downstream end are needed. It is assumed that the hydraulic head for the upstream end is known as a constant head, and the flow rate for the downstream end is constant until the transient condition is generated.

Table 4.3 Parameters used for computer simulation using the method of characteristics

Δx (ft)	2.2175
Δt (second)	0.0005
Number of Nodes	127
C_L	0.3
Speed of Pressure Wave (fps)	4435
Duration of Computation (second)	10

4.3.1 Simulation Case1

Fig. 4.15 shows the computer model results compared with the experimental data at the downstream region for Simulation Case 1. Thin line shows the results using the method of characteristics and thick line shows the experimental data. Line pressure at the upstream end was maintained at 120psi and flow rate was 12.5gpm before the transient was generated. Duration of Simulation Case 1 is 10 seconds as shown in Fig. 4.15. The model results using the method of characteristics agree well with experimental data using equivalent head loss coefficient C_L in dynamic equation. To show more clearly the model results when compared with experiments, Fig. 4.16 shows the pressure time history for the first 2 seconds in Case 1. It is clear that result using the method of characteristics and experimental data agree well. It should be noted that downstream pressure transducer is placed at 208ft from the upstream end which is located at 70ft away from the downstream end. Therefore, the downstream pressure transducer is placed at downstream area; it will be affected first by the valve closure at the downstream end. If both shut-off valves at downstream end as well as upstream end are closed simultaneously, downstream region of the piping system will be affected by the valve closure at downstream end and the upstream region will be affected by the valve closure at upstream end instantaneously. After the instantaneous valve closure at the downstream end, pressure at the downstream region goes up immediately at 0.701 second and it has peak point at 0.73 second as shown in Fig. 4.16. The speed of pressure wave was determined to be 4435 ft/sec. The wave period of the pressure wave at the downstream region for the Case 1 was 0.125 second. Figs. 4.17, 4.18, 4.19, and 4.20 show the pressure time history at the downstream region in Case 1 with different duration of time: 2 to 4 second, 4 to 6 second, 6 to 8 second, and 8 to 10 second respectively. These are

presented so that the pressure time history can be clearly shown when compared with the experiments.

Fig. 4.21 shows the pressure time history at the upstream region in Case 1. Thin line shows the result using the method of characteristics and thick line shows experimental data. Again, the result of the computer simulation agrees well with experimental data as shown in Fig. 4.21. These two results were measured and calculated at the upstream pressure transducer which is 66.8ft away from the upstream end. Shut-off valve at the upstream end was completely closed at 0.732 second while shut-off valve at the downstream end was closed at 0.735 second. After instantaneous valve closure at the upstream end, pressure at the upstream region drops immediately at 0.701 second and it reaches the peak value at 0.732 second as shown in Fig. 4.22. Speed of the pressure wave is determined to be 4435 ft/sec and the period of the pressure wave at the upstream region for Case 1 is 0.125 second. To show more clearly the comparison of model results and the experimental data, Figs. 4.23, 4.24, 4.25, and 4.26 show the pressure time histories at the upstream region in Case 1 with different time duration: 2 to 4 second, 4 to 6 second, 6 to 8 second, and 8 to 10 second respectively.

4.3.2 Simulation Case 2

Fig. 4.27 shows the comparison of simulation with experimental data at the downstream region for Simulation Case 2. Thin line shows the results of the method of characteristics and thick line shows the experimental data. For the experiment, the line pressure at the upstream end was maintained at 100psi and flow rate was 12.0gpm before the transient was created. Duration of simulation was 10 seconds for Case 2 as shown in Fig. 4.27. Shut-off valves were closed manually at the upstream and downstream end with exactly same manner

as in Simulation Case 1. After instantaneous valve closure at the downstream end, pressure at the downstream region rise immediately at 0.798 second and it reached the peak value at 0.824 second as shown in Fig. 4.28. The results of the computer simulation agree well with the experimental data as seen from Figs. 4.27 and 4.28. Figs. 4.29, 4.30, 4.31, and 4.32 show the pressure time histories at the downstream region in Simulation Case 2 with different time durations: 2 to 4 second, 4 to 6 second, and 8 to 10 second respectively.

Fig. 4.33 shows the results of calculation and the experimental data measured at the upstream region for Simulation Case 2. Thin line represents shows the results of the method of characteristics and thick line shows the experimental data. Again the result of the computer simulation agrees well with experimental data as shown in Fig. 4.33. Shut-off valve at the upstream end was completely closed at 0.8207 second while shut-off valve at the downstream end was closed at 0.8247 second. After instantaneous valve closure at the upstream end, pressure at the upstream region drops immediately at 0.793 second and it reaches peak value at 0.82 second as shown in Fig. 4.34. The speed of the pressure wave was 4435 ft/sec and the wave period of the pressure wave at the upstream region for Simulation Case 2 was 0.125 second. Figs. 4.35, 4.36, 4.37, and 4.38 show the pressure time histories at the upstream region in Simulation Case 2 with different time durations: 2 to 4 second, 4 to 6 second, and 8 to 10 second respectively.

In both Case 1 and Case 2, it is observed that the amplitude of oscillating wave using the method of characteristics is slightly smaller than the amplitude of oscillation recorded for the experimental data in the early time period ($0 < t < 6\,\text{sec}$). It is also observed that the experimental data showed that the damping rate of the pressure wave was slightly larger at the larger time ($6\,\text{sec} < t < 10\,\text{sec}$).

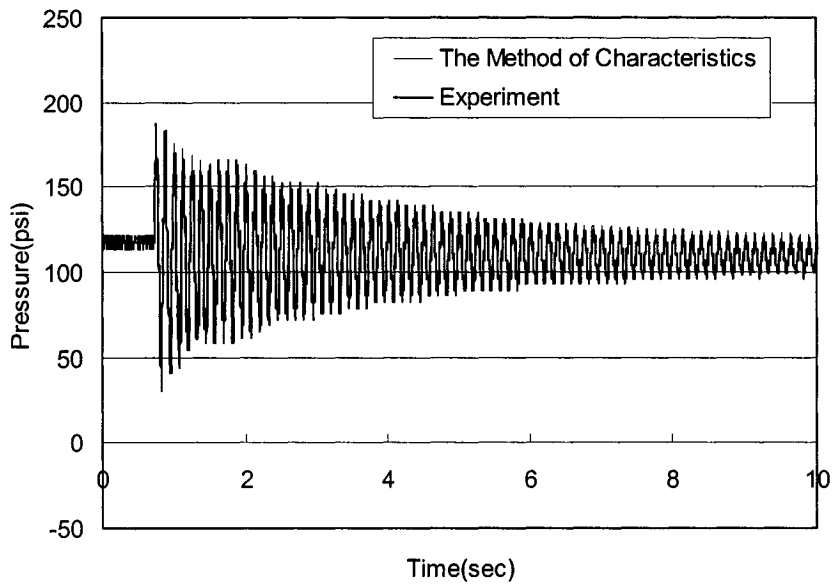

Figure 4.15 Pressure time history at the downstream region (Case 1: $0 \leq t \leq 10$ sec)

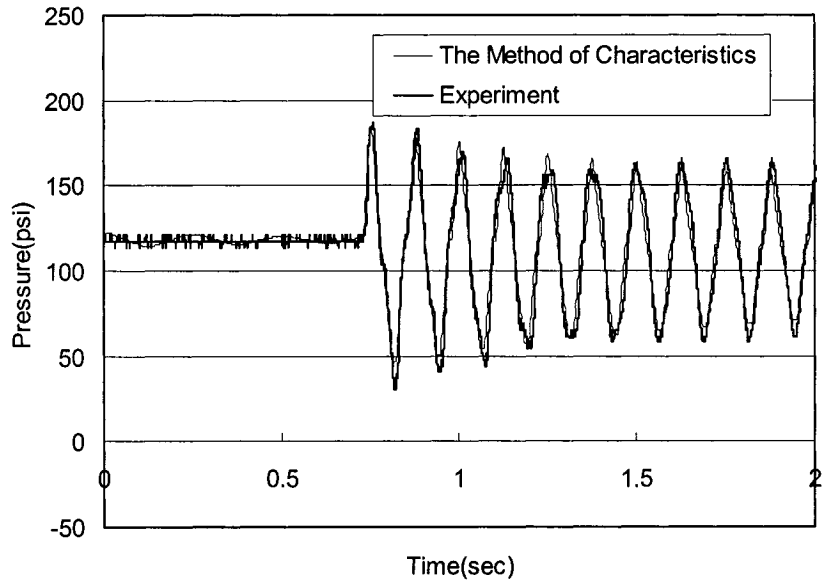

Figure 4.16 Pressure time history at the downstream region (Case 1: $0 \leq t \leq 2$ sec)

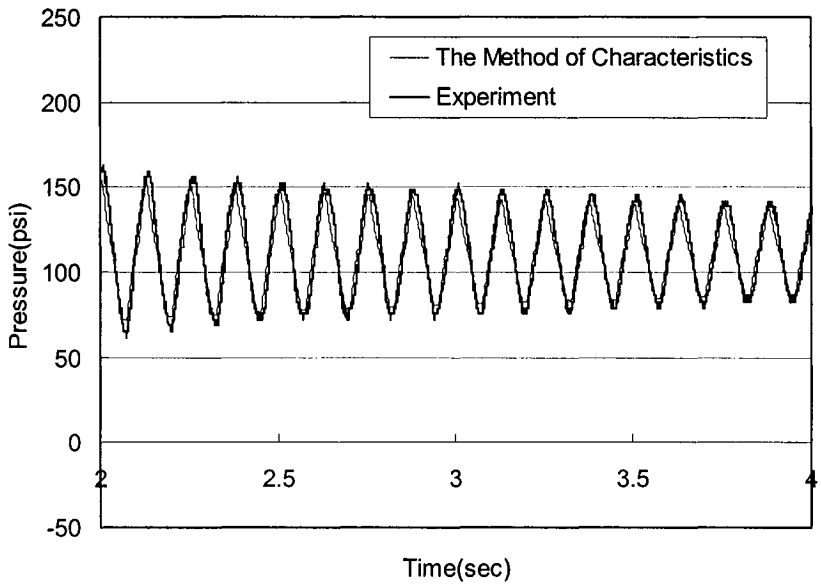

Figure 4.17 Pressure time history at the downstream region (Case 1: $2 \leq t \leq 4$ sec)

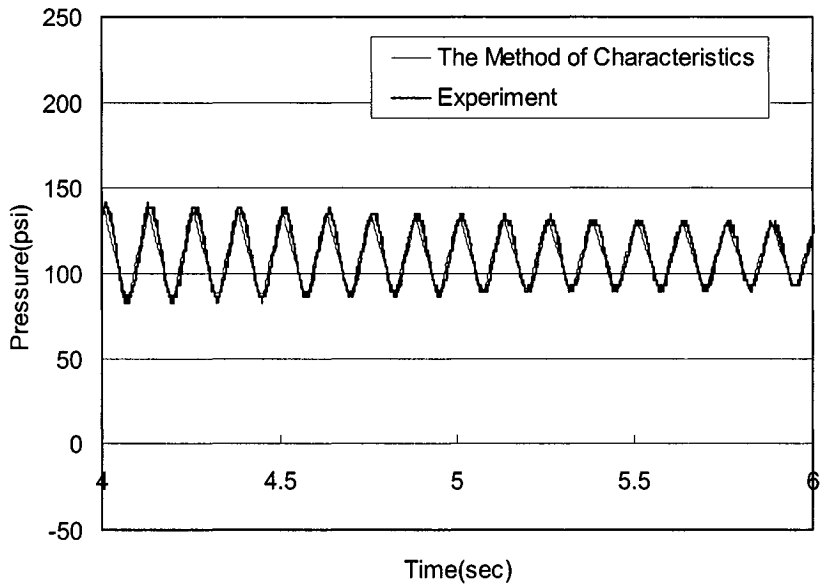

Figure 4.18 Pressure time history at the downstream region (Case 1: $4 \leq t \leq 6$ sec)

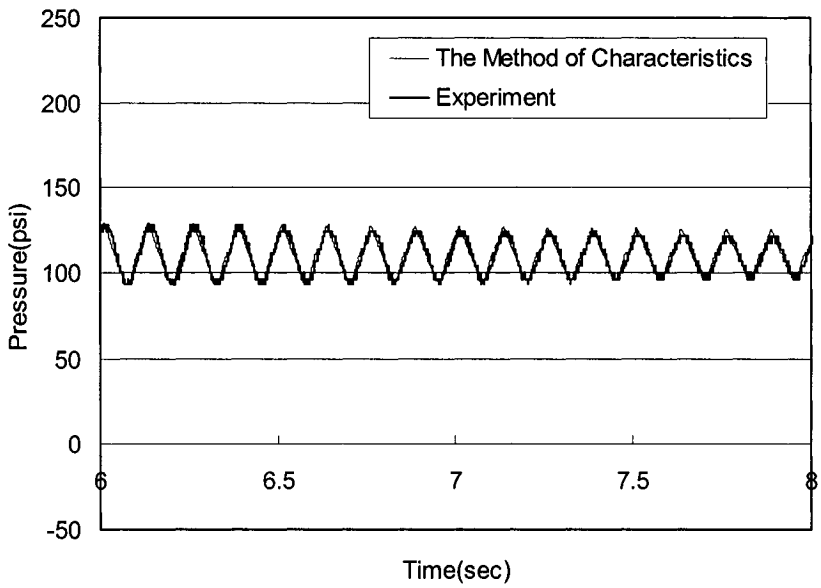

Figure 4.19 Pressure time history at the downstream region (Case 1: $6 \leq t \leq 8$ sec)

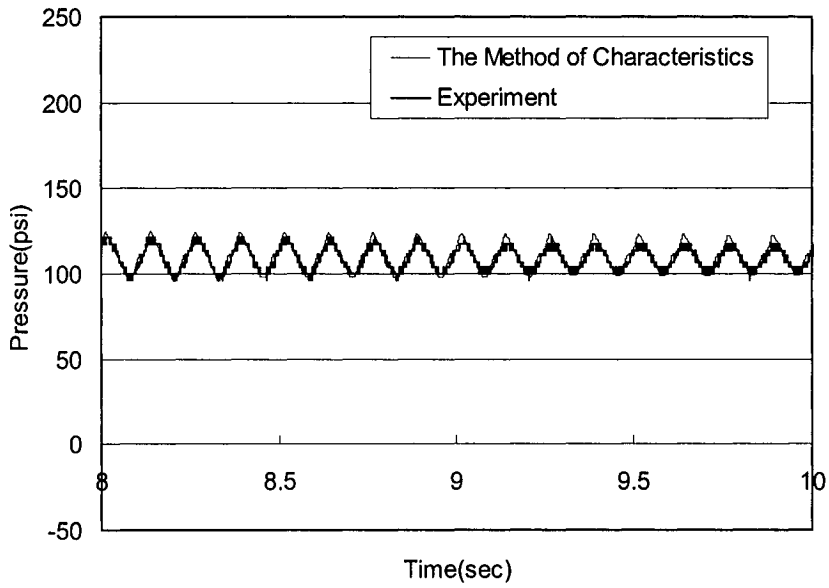

Figure 4.20 Pressure time history at the downstream region (Case 1: $8 \leq t \leq 10$ sec)

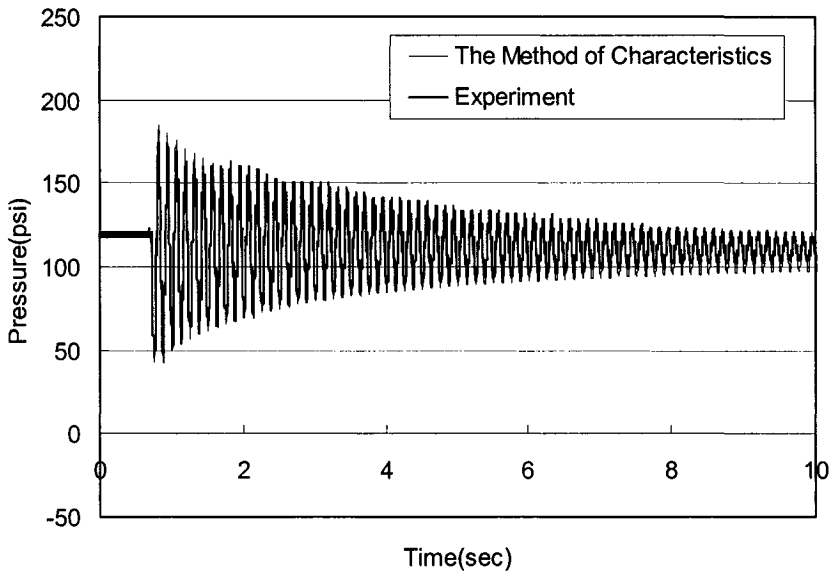

Figure 4.21 Pressure time history at the upstream region (Case 1: $0 \leq t \leq 10$ sec)

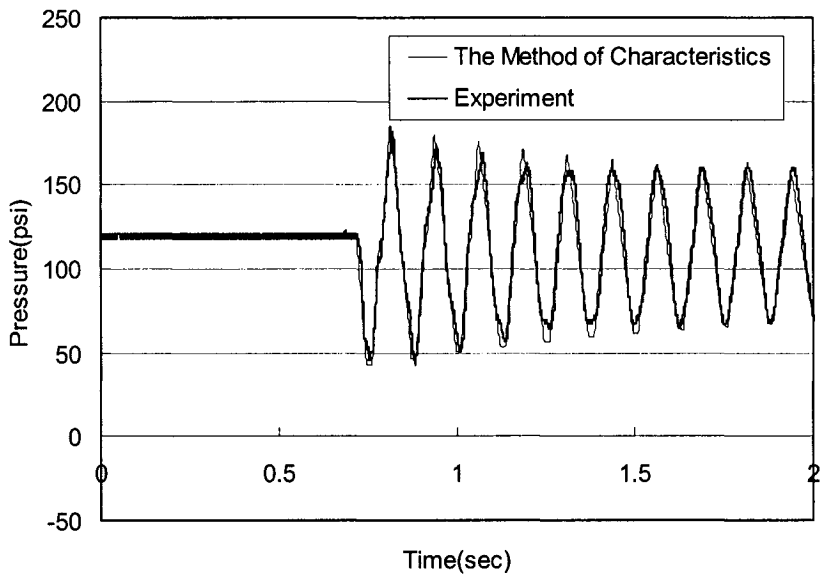

Figure 4.22 Pressure time history at the upstream region (Case 1: $0 \leq t \leq 2$ sec)

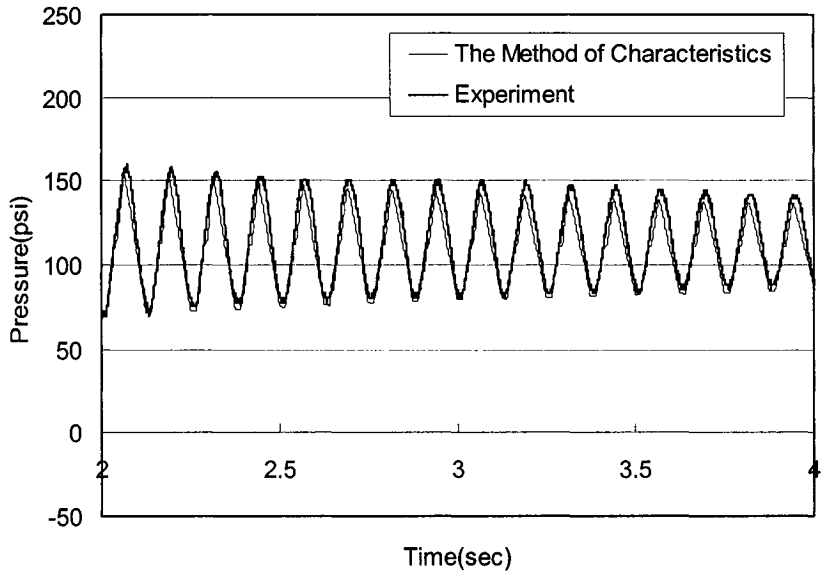

Figure 4.23 Pressure time history at the upstream region (Case 1: $2 \leq t \leq 4$ sec)

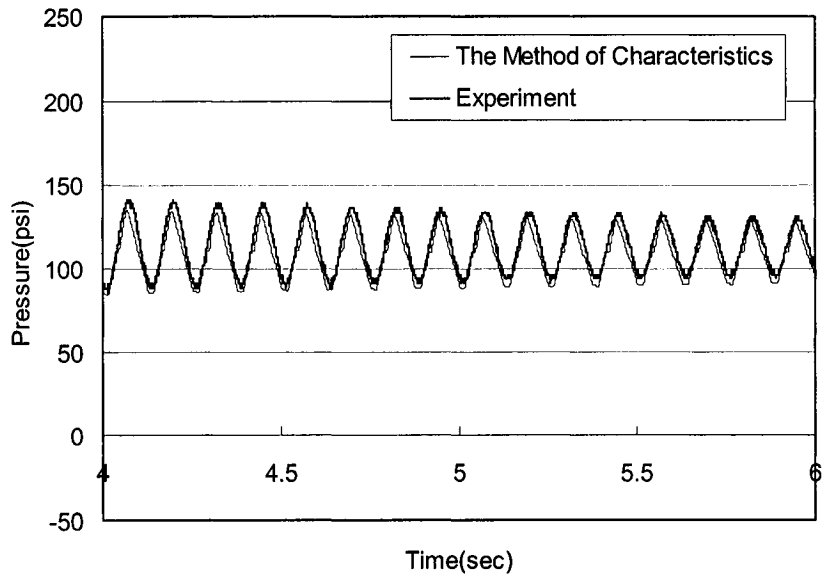

Figure 4.24 Pressure time history at the upstream region (Case 1: $4 \leq t \leq 6$ sec)

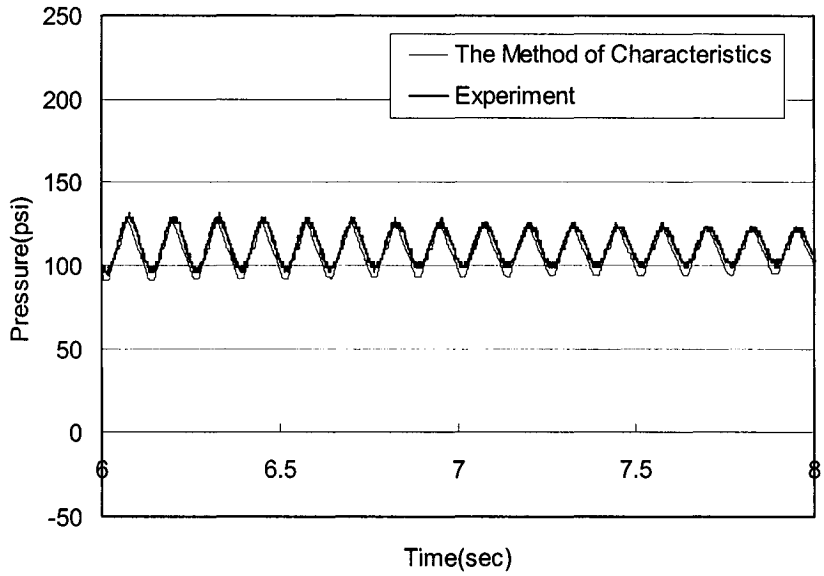

Figure 4.25 Pressure time history at the upstream region (Case 1: $6 \leq t \leq 8$ sec)

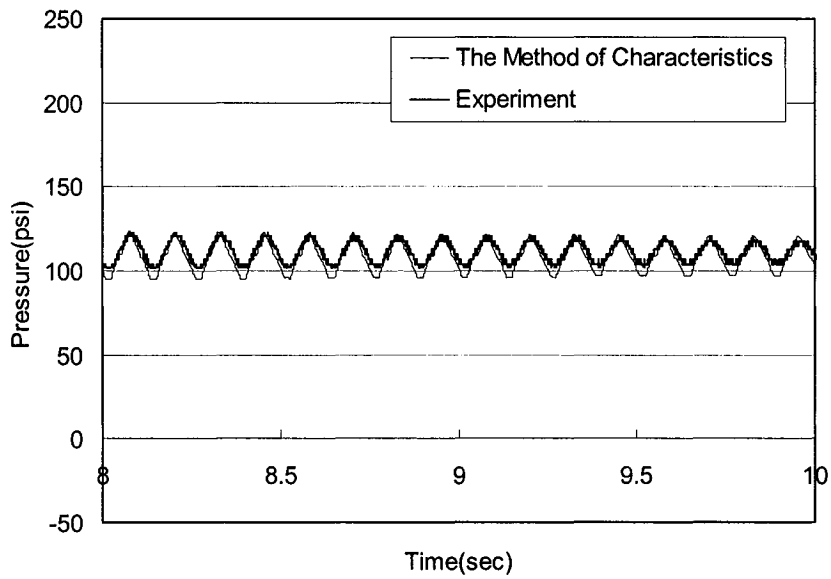

Figure 4.26 Pressure time history at the upstream region (Case 1: $8 \leq t \leq 10$ sec)

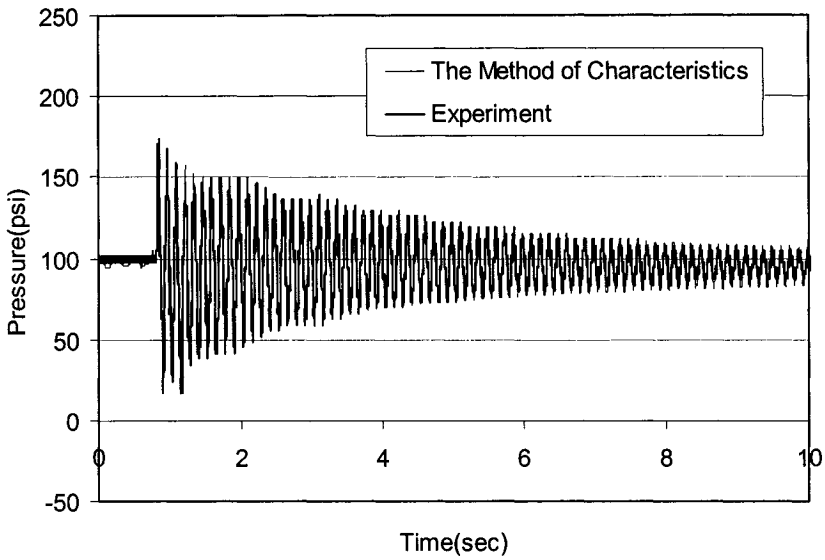

Figure 4.27 Pressure time history at the downstream region (Case 2: $0 \leq t \leq 10$ sec)

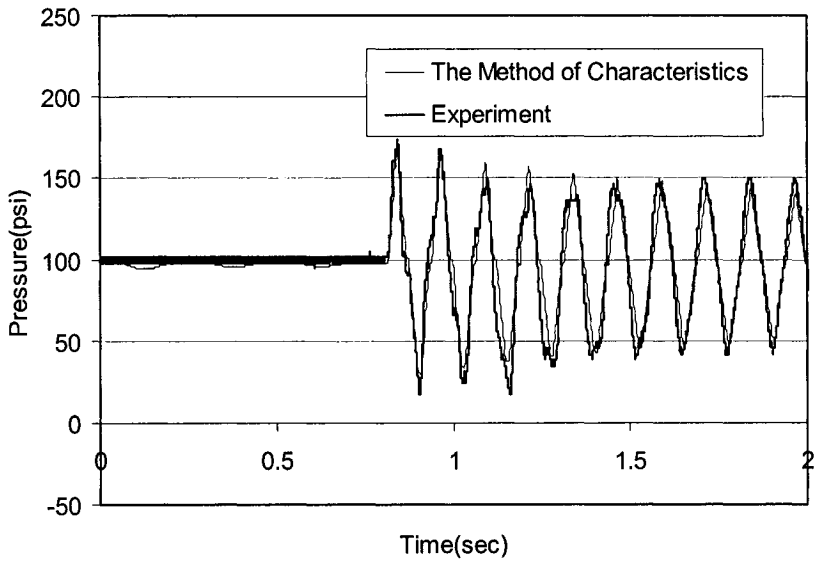

Figure 4.28 Pressure time history at the downstream region (Case 2: $0 \leq t \leq 2$ sec)

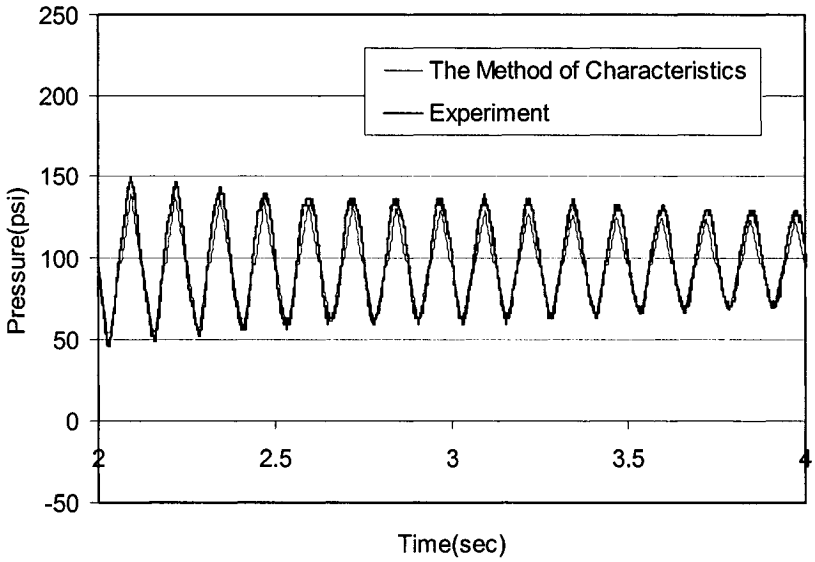

Figure 4.29 Pressure time history at the downstream region (Case 2: $2 \leq t \leq 4$ sec)

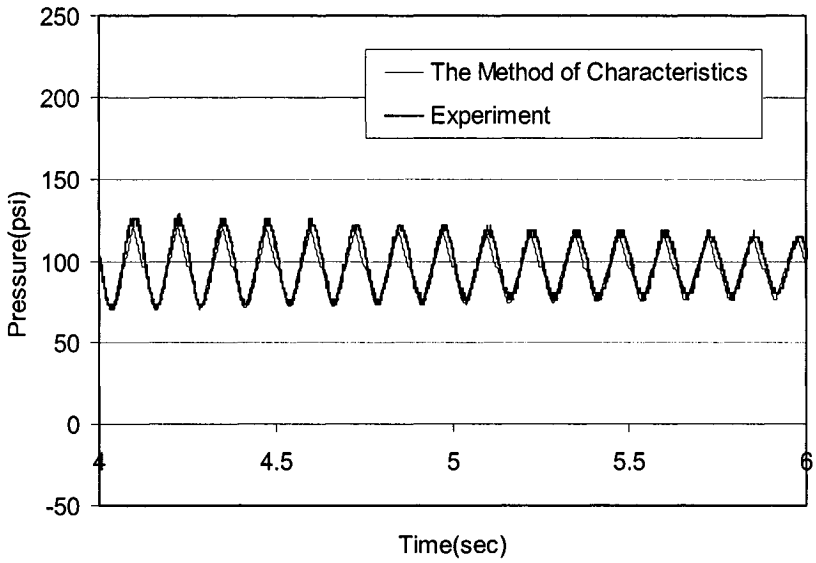

Figure 4.30 Pressure time history at the downstream region (Case 2: $4 \leq t \leq 6$ sec)

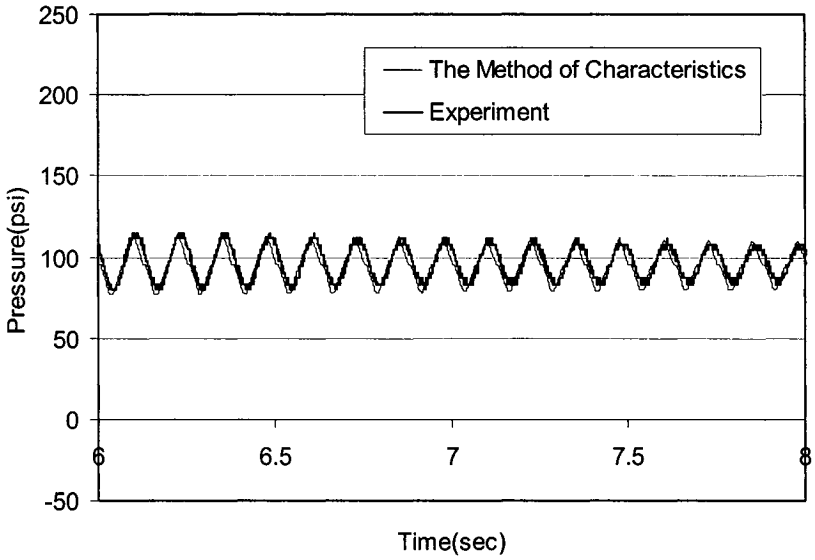

Figure 4.31 Pressure time history at the downstream region (Case 2: $6 \leq t \leq 8$ sec)

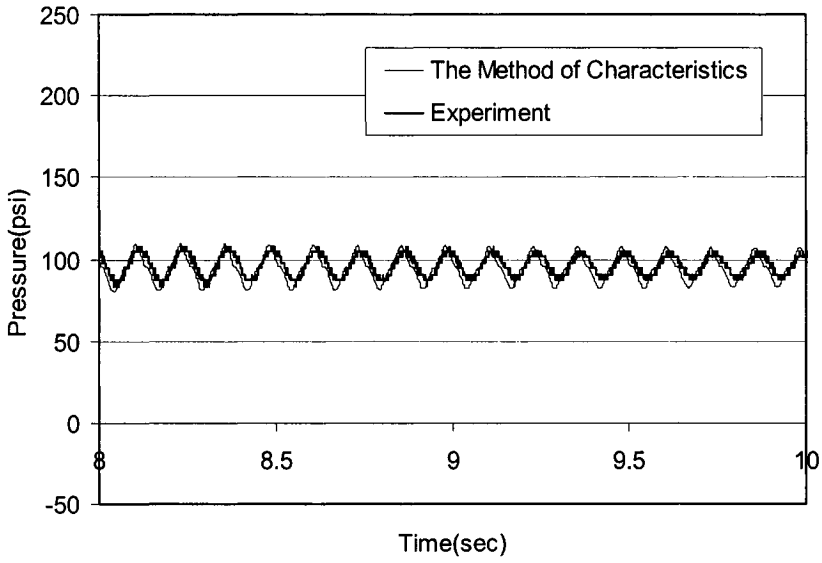

Figure 4.32 Pressure time history at the downstream region (Case 2: $8 \leq t \leq 10$ sec)

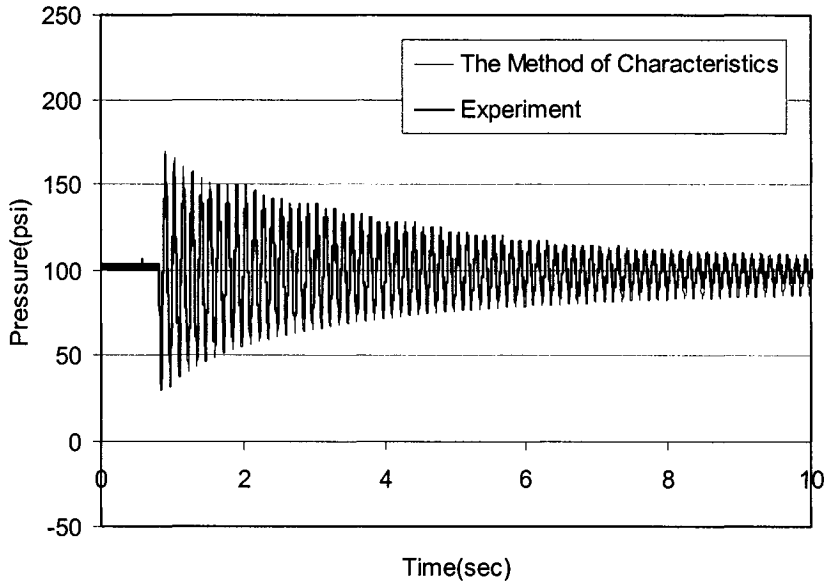

Figure 4.33 Pressure time history at the upstream region (Case 2: $0 \leq t \leq 10$ sec)

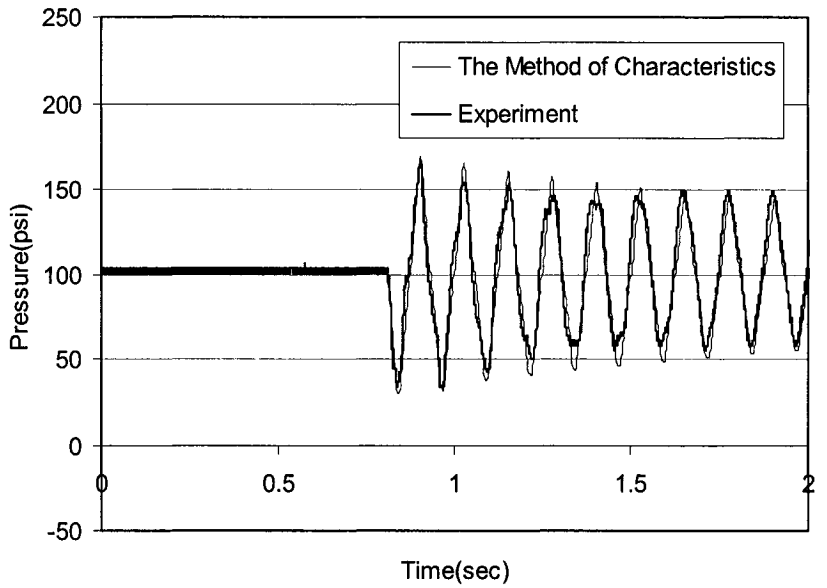

Figure 4.34 Pressure time history at the upstream region (Case 2: $0 \leq t \leq 2$ sec)

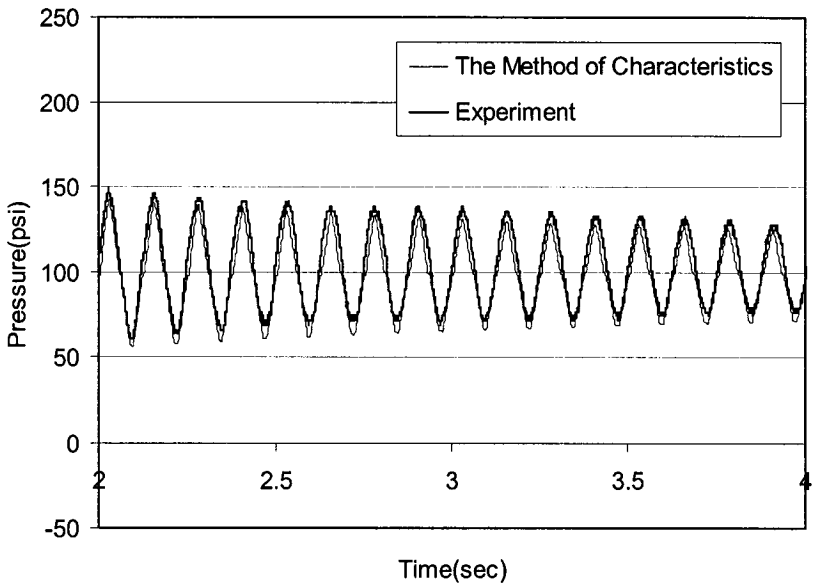

Figure 4.35 Pressure time history at the upstream region (Case 2: $2 \leq t \leq 4$ sec)

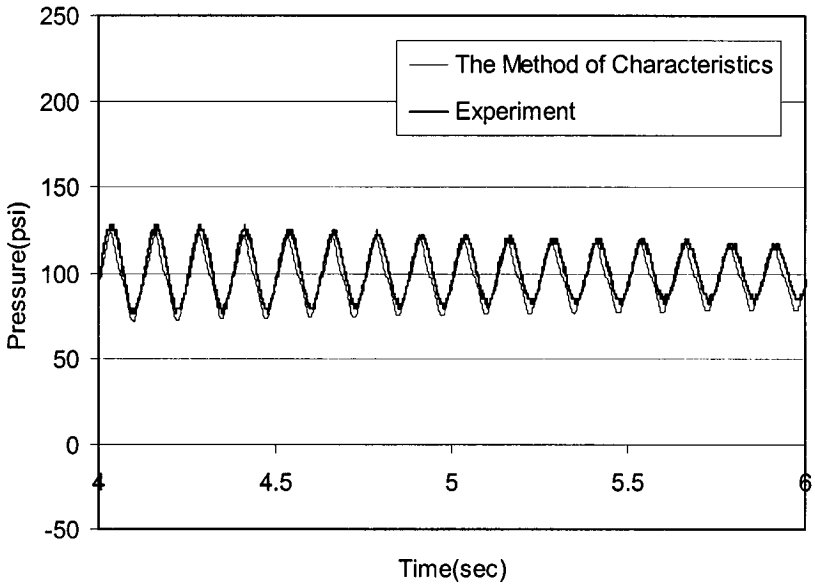

Figure 4.36 Pressure time history at the upstream region (Case 2: $4 \leq t \leq 6$ sec)

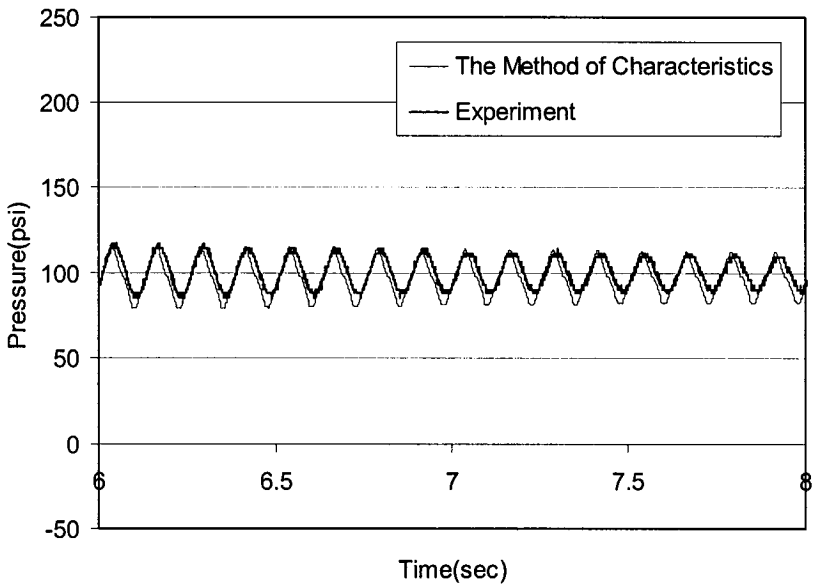

Figure 4.37 Pressure time history at the upstream region (Case 2: $6 \leq t \leq 8$ sec)

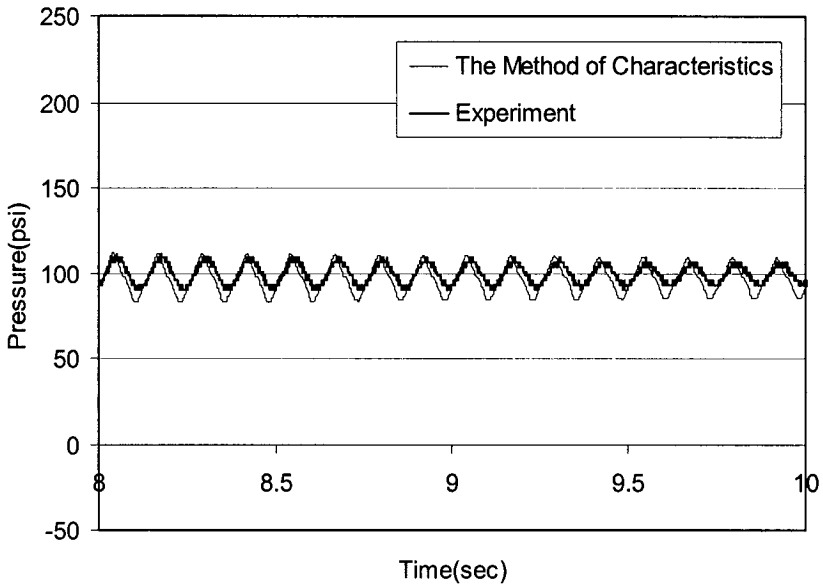

Figure 4.38 Pressure time history at the upstream region (Case 2: $8 \leq t \leq 10$ sec)

4.4 Experimental and Modeling Results using the Two-Dimensional Method

The development of a computer model using the two-dimensional method was previously discussed in Section 2.3. Results of computer simulation using the two-dimensional method will now be presented in this section and compared with the experimental data. Two experimental cases have been presented in Section 4.2. These same experimental data will also be used to compare with the modeling results using the two-dimensional method.

Using the two-dimensional method, Prandtl mixing length theory is used to estimate the shear stress τ . Mixing length relation should be approximated using appropriate κ experimentally. The experimentally determined κ has the role of the damper such as equivalent head loss coefficient C_L in the method of characteristics. If κ is bigger, then oscillation of pressure in the system will be damped out faster, if κ is smaller then oscillation of pressure will be damped out slower. Before computer simulation is started, κ should be estimated carefully. The value of κ is determined to be 0.22 for the current experimental system in this study. Table 4.4 shows the parameters used for computer simulation using the two-dimensional method. For the computer model, the grid size Δx = 2.2175 (feet) and the time increment Δt = 0.0005 (sec) as shown in Table 4.4. The Courant stability criterion is satisfied using the Δx and Δt as noted. The cross sectional area has been divided into 19 equal increment of ΔA for the whole piping system. Therefore, ΔA is 0.001148 ft^2 for the axial grid. Water density was 1.937 $slug/ft^3$ for the present analysis. Two boundary conditions for the upstream end and the downstream end are needed. It is assumed

that the hydraulic head for the upstream end is known as a constant head, and the flow rate for the downstream end is constant until the transient condition is generated.

Table 4.4 Parameters used for computer simulation using the two-dimensional method

Δx (ft)	2.2175
Δt (second)	0.0005
ΔA (ft^2)	0.001148
Number of Longitudinal Nodes	127
Number of Radial Nodes	20
κ	0.22
Speed of Pressure Wave (fps)	4435
Duration of Computation (second)	10

4.4.1 Simulation Case 1

Fig. 4.39 shows the computer model results compared with the experimental data at the downstream region for Simulation Case 1. Thin line shows the result of two-dimensional method and thick line shows the experimental data. The result from the computer simulation using the two-dimensional method agrees well with experimental data as shown in Fig. 4.39. After instantaneous valve closure at the downstream end, pressure at the downstream region rise immediately as shown in Fig. 4.40. Figs. 4.41, 4.42, 4.43, and 4.44 show the pressure time histories at the downstream region with different time durations: 2 to 4 second, 4 to 6 second, 6 to 8 second, and 8 to 10 second respectively. Fig. 4.45 shows the computer model results compared with the experimental data at the upstream region for Simulation Case 1.

Thin line represents the result of two-dimensional method and thick line shows the experimental data. After instantaneous valve closure at the upstream end, pressure at the upstream region drops immediately as shown in Fig. 4.46. Figs. 4.47, 4.48, 4.49, and 4.50 show the pressure time histories at the upstream region with different durations: 2 to 4 second, 4 to 6 second, 6 to 8 second, and 8 to 10 second respectively.

4.4.2 Simulation Case 2

Figs. 4.51 and 4.57 show the pressure time histories at the downstream region and the upstream region respectively. After instantaneous valve closure at the upstream end and the downstream end, the initial pressure will rise at the downstream region and drop at the upstream region. Results of the computer simulation also agree well with experimental data as shown in Figs. 4.51 and 4.57. Fig. 4.52, 4.53, 4.54, 4.55, and 4.56 show the pressure time histories at the downstream region with different duration: 0 to 2 second, 2 to 4 second, 4 to 6 second, 6 to 8 second, and 8 to 10 second. These plots allow a more detailed comparison for the numerical results and experimental data. Similarly, Figs. 4.58, 4.59, 4.60, 4.61, and 4.62 show the pressure time histories at the upstream region with different durations: 0 to 2 second, 2 to 4 second, 4 to 6 second, 6 to 8 second, and 8 to 10 second respectively. In both Simulation Case 1 and Case 2, it is observed that the amplitude of oscillation of the two-dimensional method is slightly higher than the amplitude of oscillation of the experimental data in the beginning of the total 10-second duration as shown in Figs. 4.51 and 4.57. It is also observed that the amplitude of oscillation using the two-dimensional method damped out faster than the experimental data as time increases.

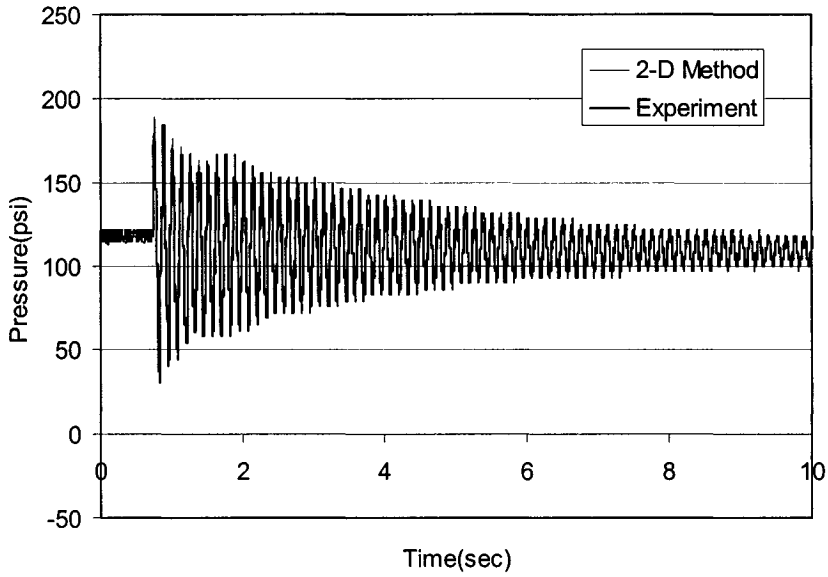

Figure 4.39 Pressure time history at the downstream region (Case 1: $0 \leq t \leq 10$ sec)

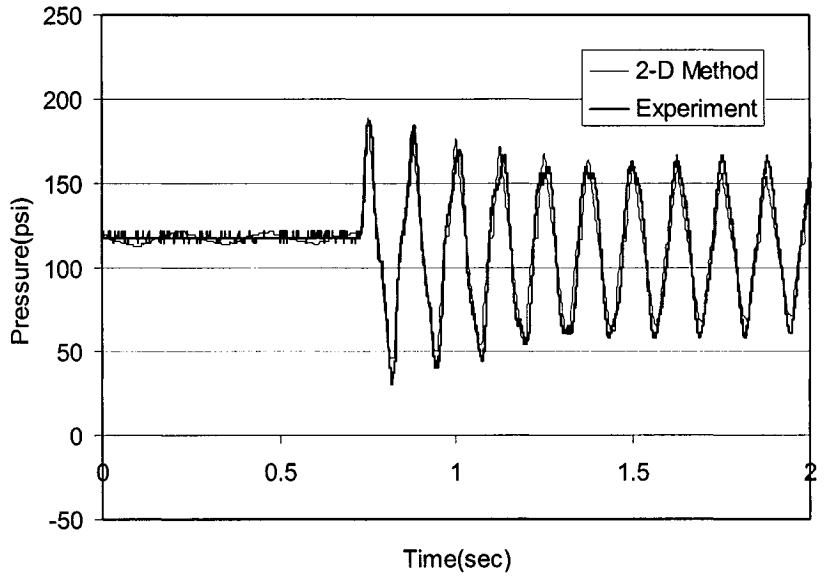

Figure 4.40 Pressure time history at the downstream region (Case 1: $0 \leq t \leq 2$ sec)

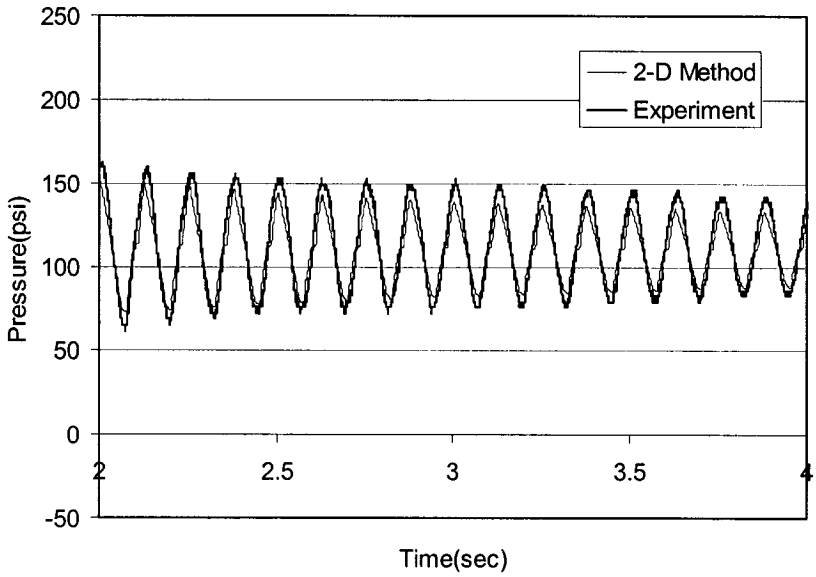

Figure 4.41 Pressure time history at the downstream region (Case 1: $2 \leq t \leq 4$ sec)

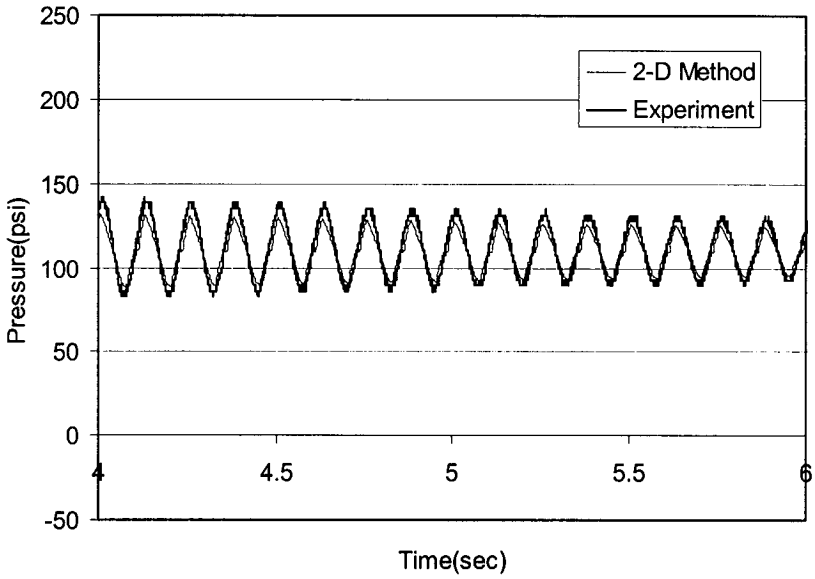

Figure 4.42 Pressure time history at the downstream region (Case 1: $4 \leq t \leq 6$ sec)

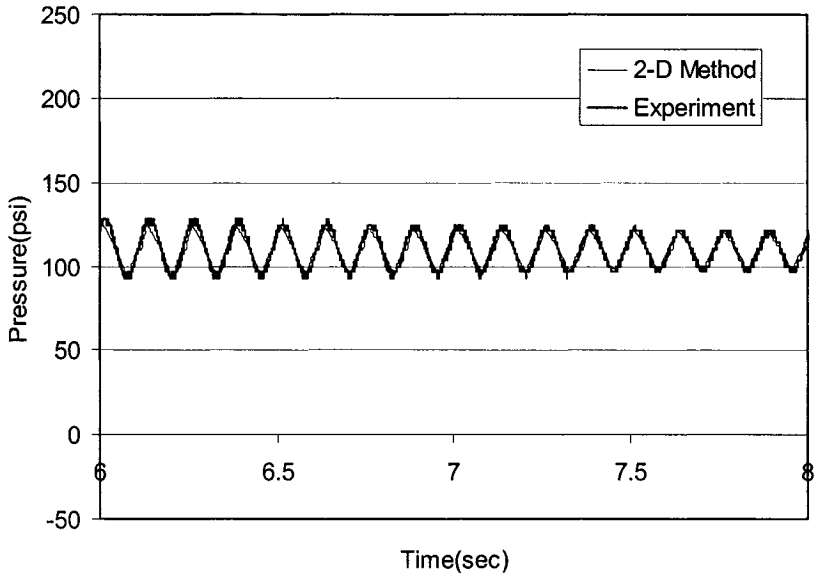

Figure 4.43 Pressure time history at the downstream region (Case 1: $6 \leq t \leq 8$ sec)

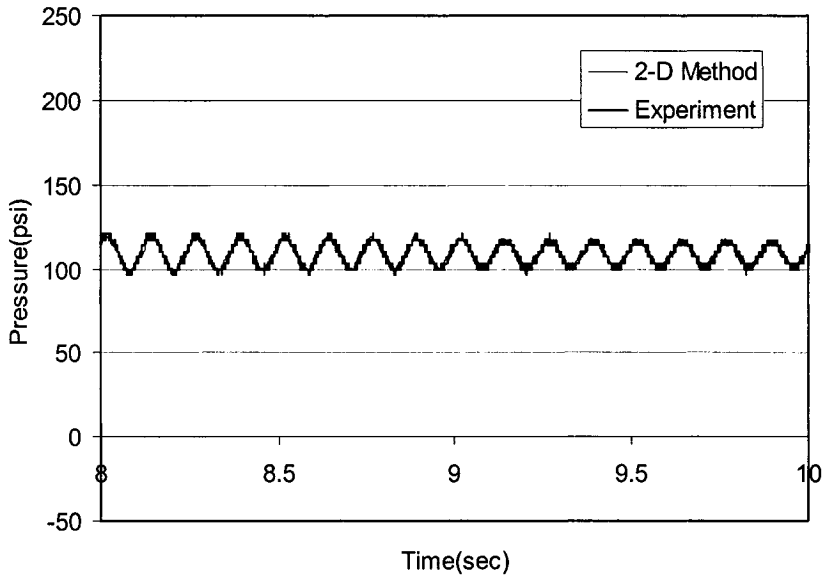

Figure 4.44 Pressure time history at the downstream region (Case 1: $8 \leq t \leq 10$ sec)

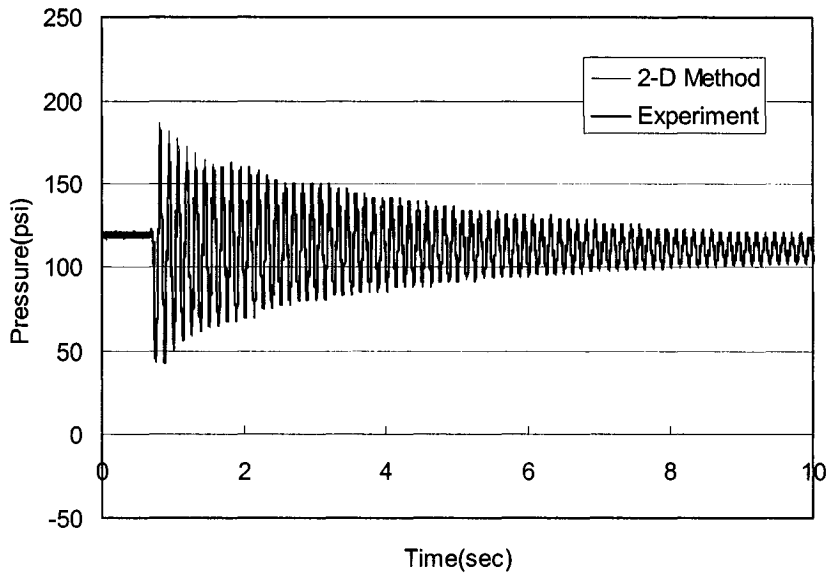

Figure 4.45 Pressure time history at the upstream region (Case 1: $0 \leq t \leq 10$ sec)

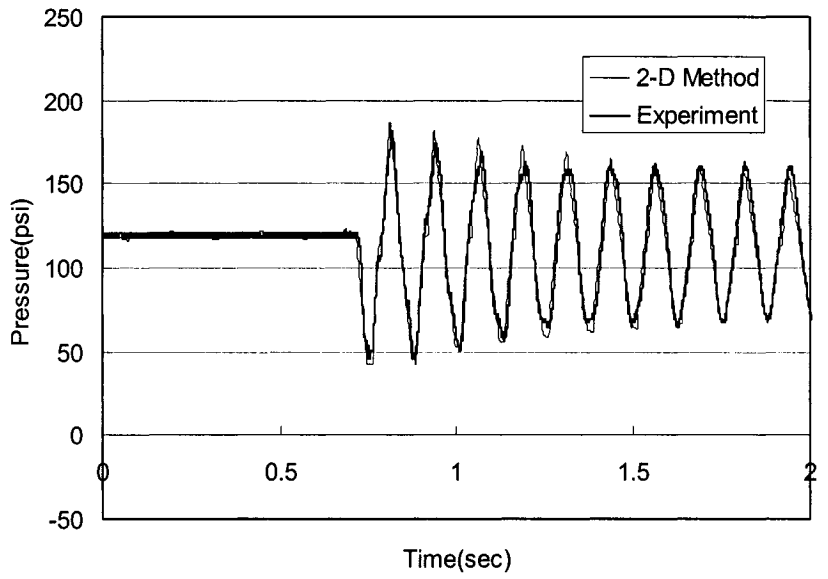

Figure 4.46 Pressure time history at the upstream region (Case 1: $0 \leq t \leq 2$ sec)

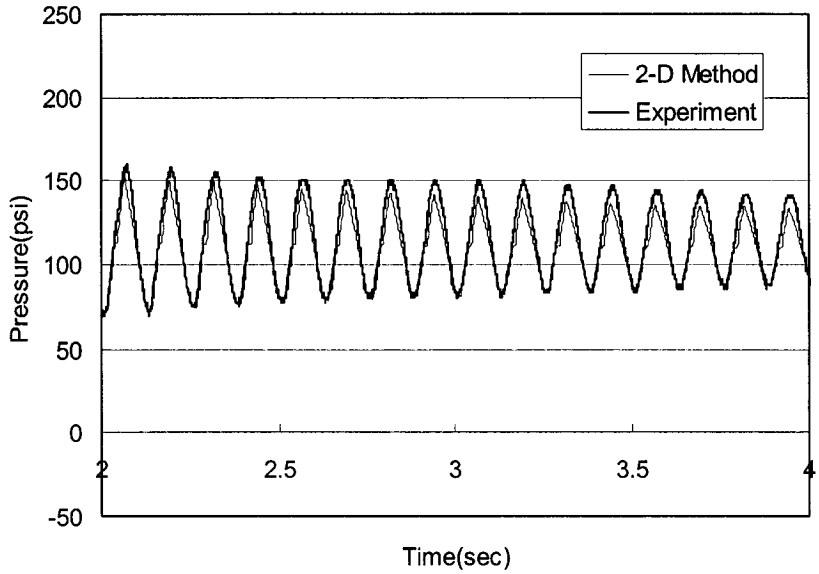

Figure 4.47 Pressure time history at the upstream region (Case 1: $2 \leq t \leq 4$ sec)

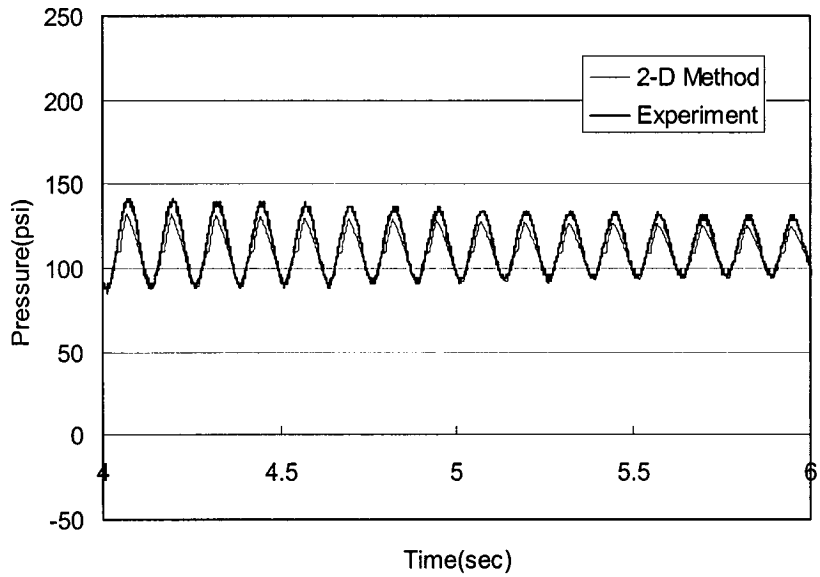

Figure 4.48 Pressure time history at the upstream region (Case 1: $4 \leq t \leq 6$ sec)

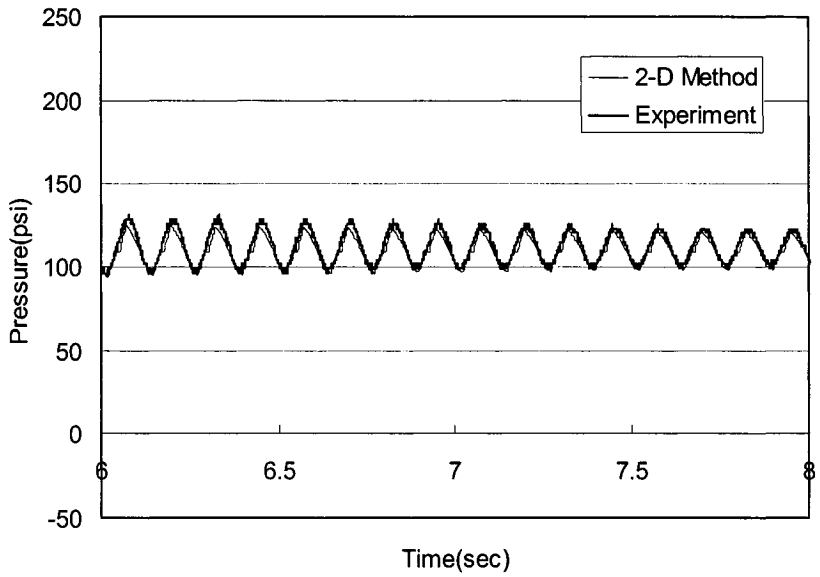

Figure 4.49 Pressure time history at the upstream region (Case 1: $6 \leq t \leq 8$ sec)

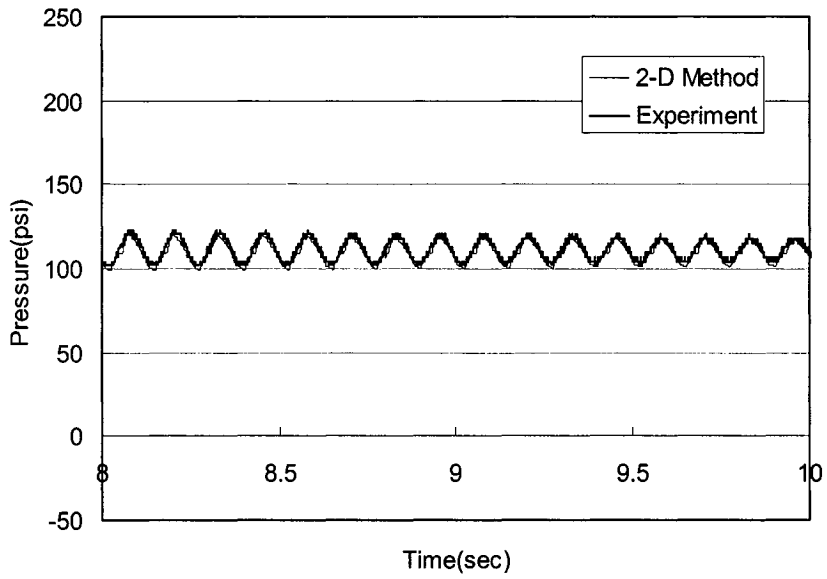

Figure 4.50 Pressure time history at the upstream region (Case 1: $8 \leq t \leq 10$ sec)

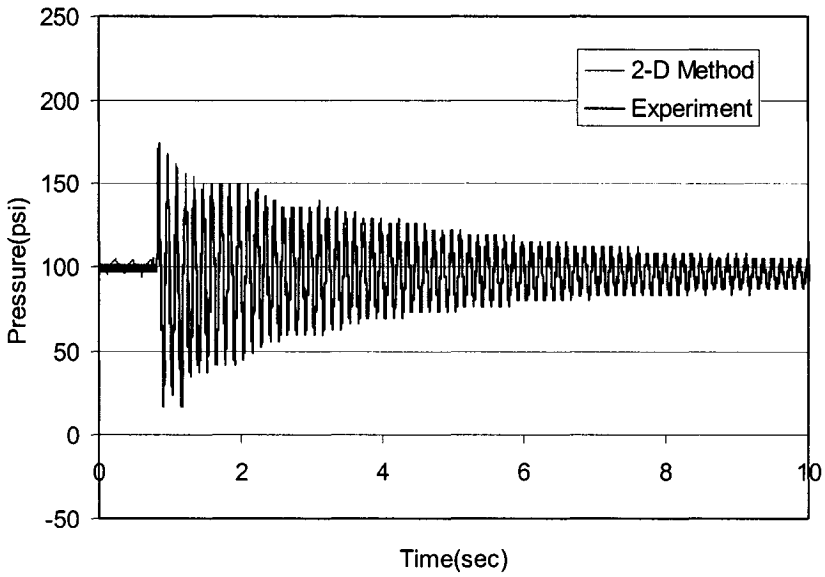

Figure 4.51 Pressure time history at the downstream region (Case 2: $0 \leq t \leq 10$ sec)

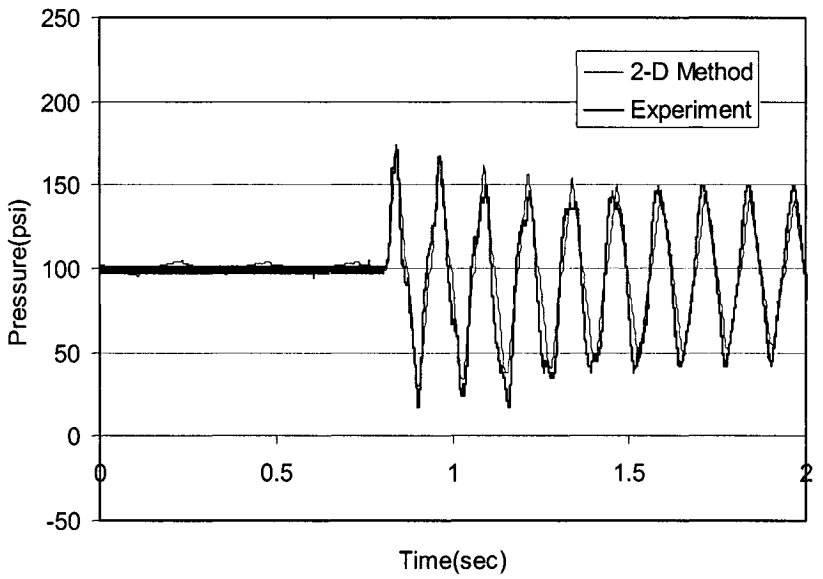

Figure 4.52 Pressure time history at the downstream region (Case 2: $0 \leq t \leq 2$ sec)

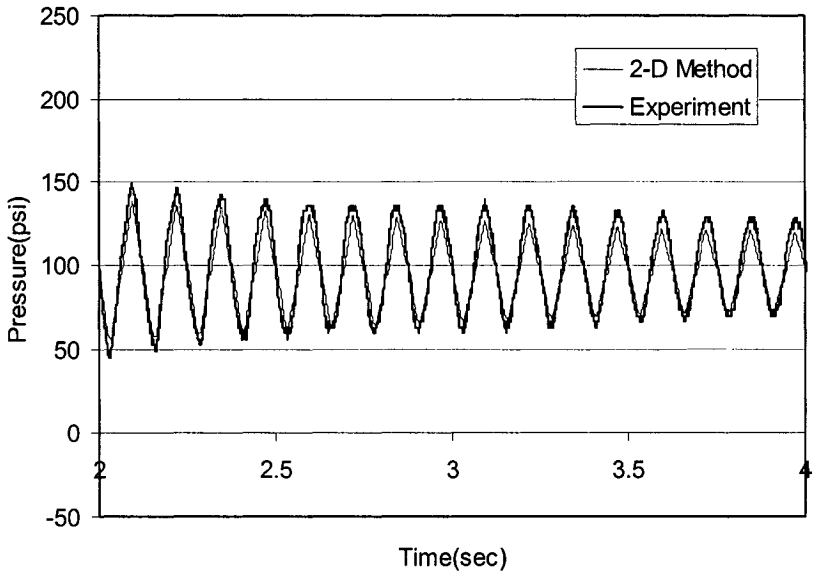

Figure 4.53 Pressure time history at the downstream region (Case 2: $2 \leq t \leq 4$ sec)

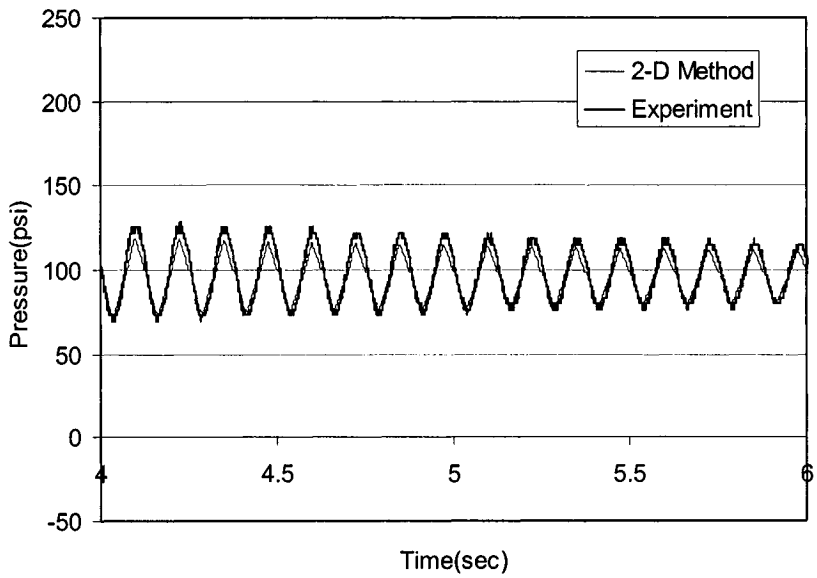

Figure 4.54 Pressure time history at the downstream region (Case 2: $4 \leq t \leq 6$ sec)

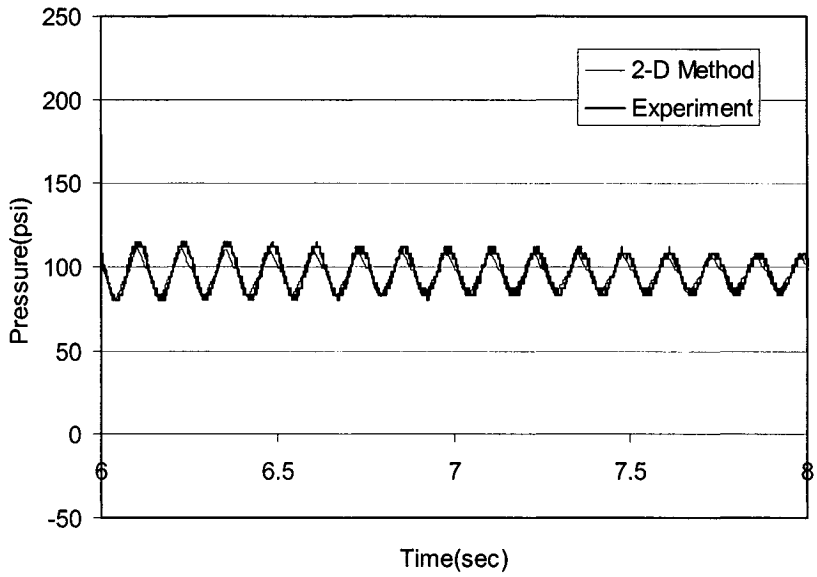

Figure 4.55 Pressure time history at the downstream region (Case 2: $6 \leq t \leq 8$ sec)

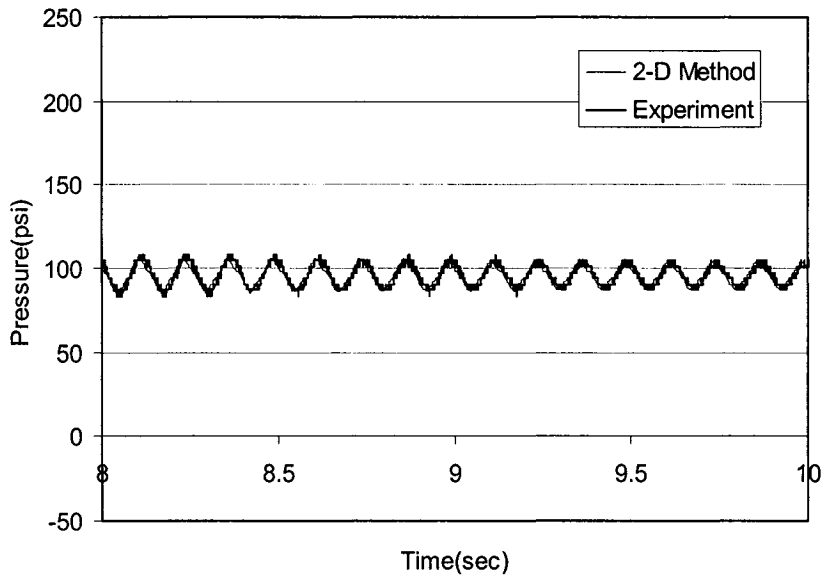

Figure 4.56 Pressure time history at the downstream region (Case 2: $8 \leq t \leq 10$ sec)

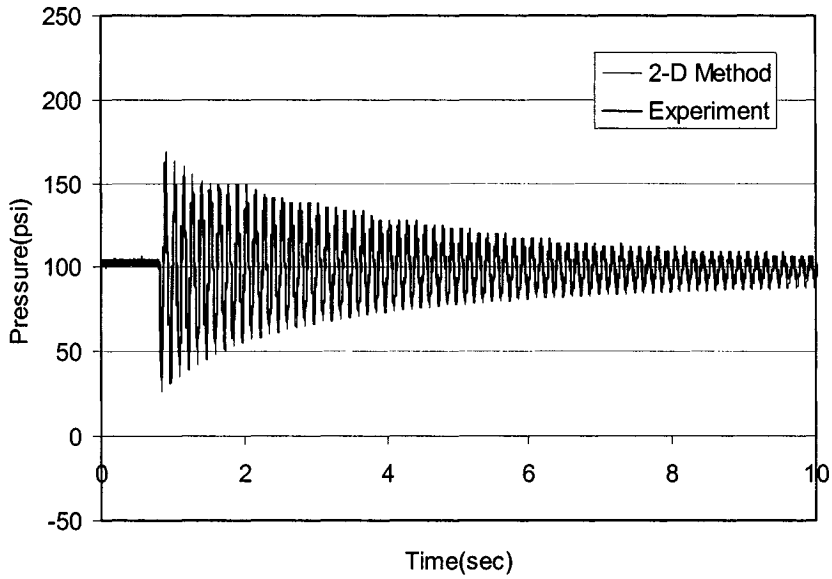

Figure 4.57 Pressure time history at the upstream region (Case 2: $0 \leq t \leq 10$ sec)

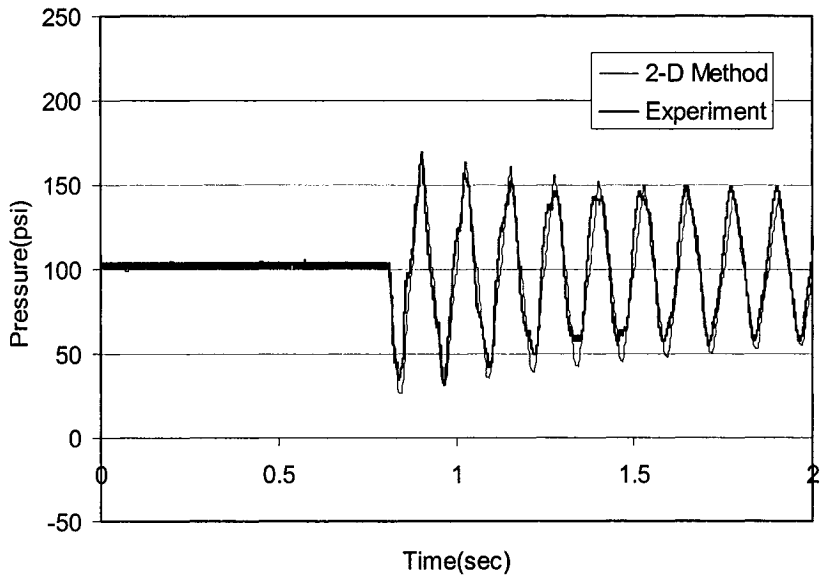

Figure 4.58 Pressure time history at the upstream region (Case 2: $0 \leq t \leq 2$ sec)

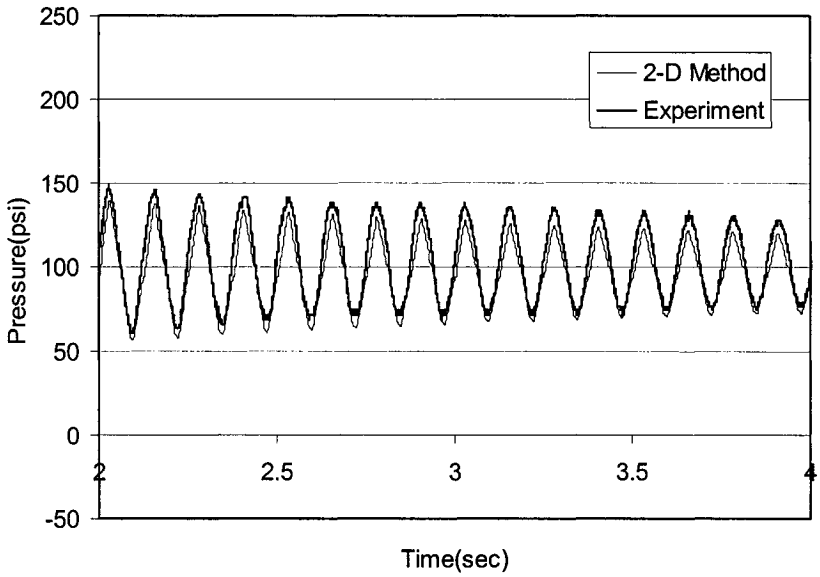

Figure 4.59 Pressure time history at the upstream region (Case 2: $2 \leq t \leq 4$ sec)

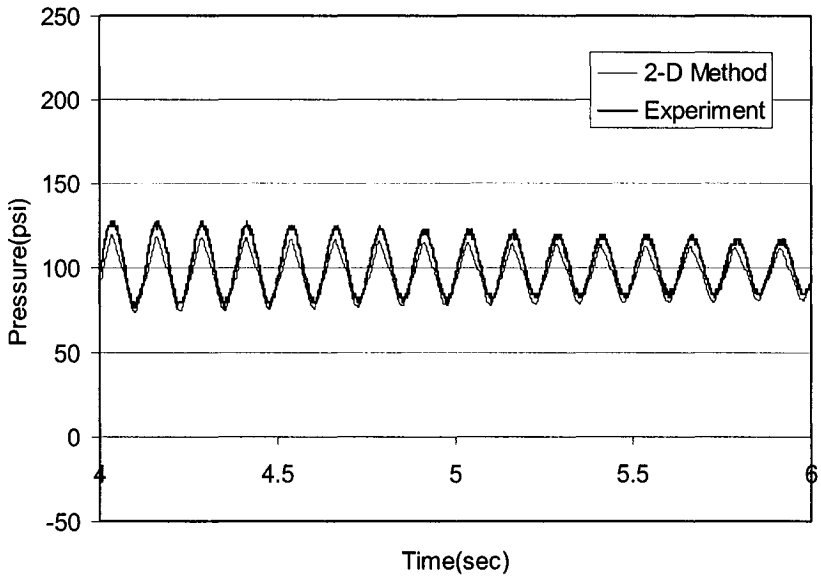

Figure 4.60 Pressure time history at the upstream region (Case 2: $4 \leq t \leq 6$ sec)

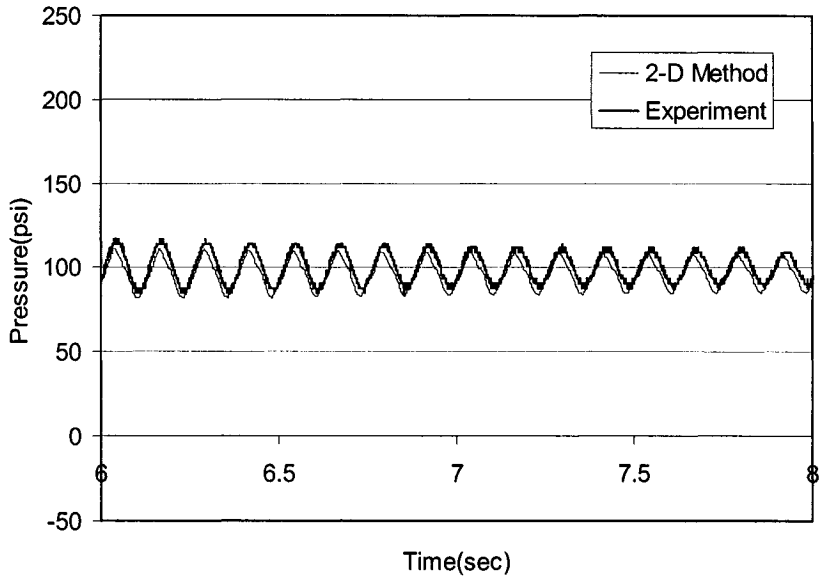

Figure 4.61 Pressure time history at the upstream region (Case 2: $6 \leq t \leq 8$ sec)

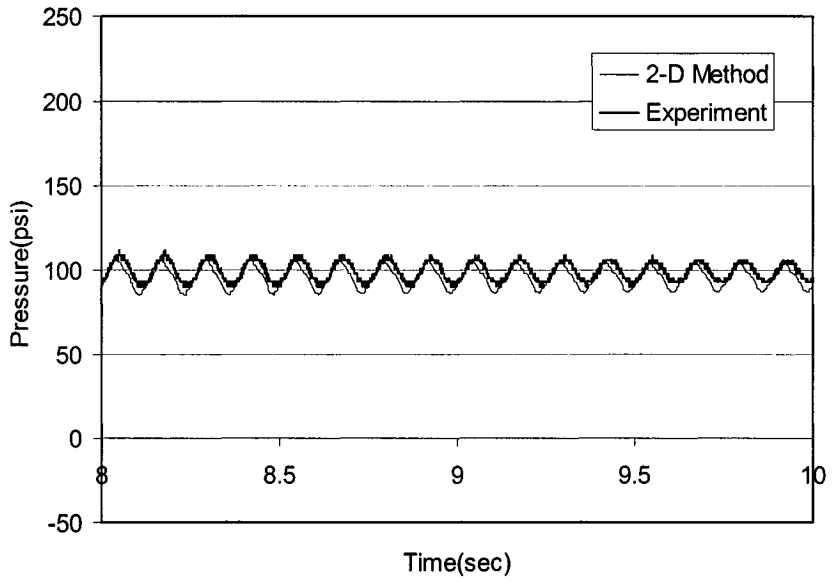

Figure 4.62 Pressure time history at the upstream region (Case 2: $8 \leq t \leq 10$ sec)

4.5 Experimental and Modeling Results using the Implicit Method

Computer model using the implicit method as discussed in Section 2.4 has also been developed for the present study. The model results will be compared with the experimental data obtained for the present study. The results of the two simulation cases using the implicit method will be compared to the experimental data as it is discussed in the previous sections. Experimental data for the Cases 1 and 2 are the same as that discussed in Sections 4.3 and 4.4.

The method of characteristics and the two-dimensional method are the explicit method of the finite difference analysis. The implicit method calculates the pressure and the flow rate at the nodes implicitly while another two methods have been simulating transient flow as a direct calculation in finite difference schemes. Explicit method such as the method of characteristics and two-dimensional method could be more convenient because of the running time in the simulation. But the results of the implicit method are usually better than other methods in the accuracy of computation.

Table 4.5 shows the parameters used for computer simulation using the implicit method. Grid size $\Delta x = 2.2175$ (feet) and time increment $\Delta t = 0.0005$ (second). Therefore, the Courant stability condition is satisfied using the Δx and Δt as noted. Δx is 2.2175 feet and length of the pipeline is 278 feet, thus the pipeline would have 126 segments. For the present study, implicit method will have 127 nodes. 2n+2 (n = 126) equations are needed for the complete solution in implicit method.

Table 4.5 Parameters used for computer simulation using the implicit method

Δx (ft)	2.2175
Δt (second)	0.0005
Number of Grids	127
C_L	0.3
Speed of Pressure Wave (fps)	4435
Duration of Computation (second)	10

The hydraulic head and flow rate need to be defined. Therefore, each node has 2 unknowns for the entire nodes in this piping system as it were discussed in Section 2.4. Total number of equations for the present simulation would be 254 equations for the 254 unknowns, which will be computed simultaneously. Two boundary conditions for the upstream and downstream ends are needed. It is assumed that the hydraulic head for the upstream end is known as a constant head, and the flow rate for the downstream end is constant until the transient condition is generated. The equivalent head loss coefficient C_L is used again for the head loss coefficient as same number as it is discussed in Section 4.3.

4.5.1 Simulation Case1

Fig. 4.63 shows the pressure time history at the downstream region for Simulation Case 1. Thin line presents the simulation result using the implicit method and thick line shows the experimental data. Line pressure at the upstream end is maintained at 120psi with flow rate at 12.5gpm before the transient condition was created. Again the model results using the implicit method agree well with experimental data using equivalent head loss coefficient C_L.

Fig. 4. 64 shows the pressure time history for the first 2 seconds in Simulation Case 1. After instantaneous valve closure at the downstream end, pressure at the downstream region is increased immediately at 0.701 second and it reaches the peak value at 0.73 second as shown in Fig. 4.64. The speed of pressure wave was measured as 4435ft/sec. This is the same as discussed earlier. The wave period of the pressure wave at the downstream region for the Case 1 was 0.125 second. Figs. 4.65, 4.66, 4.67, and 4.68 show the pressure time histories at the downstream region in Case 1 with different time durations: 2 to 4 second, 4 to 6 second, 6 to 8 second, and 8 to 10 second respectively. This allows for a closer examination of the computer model results and experiments.

Fig. 4.69 shows the pressure time history at the upstream region for Simulation Case 1. Thin line presents the modeling result using the implicit method and thick line shows the experimental data. The result of the computer simulation agrees well with experimental data as shown in Fig. 4.69. These two results were measured and calculated at the upstream pressure transducer which is located 66.8ft away from the upstream end. Shut-off valve at the upstream end was completely closed at 0.732 second while shut-off valve at the downstream end was closed at 0.735 second. After instantaneous valve closure at the upstream end, pressure at the upstream region drops immediately at 0.701 second and it reaches peak value at 0.732 second as shown in Figs. 4.70. Fig. 4.71, 4.72, 4.73, and 4.74 show the pressure time histories at the upstream region for Simulation Case 1 with different time durations: 2 to 4 second, 4 to 6 second, 6 to 8 second, and 8 to 10 second respectively. The speed of the pressure wave was determined to be 4435 ft/sec and the wave period of the pressure wave at the upstream region for Case 1 was 0.125 second.

4.5.2 Simulation Case 2

Figs. 4.75 and 4.81 show the curves of pressure time histories at the downstream region and upstream region respectively. After instantaneous valve closure at the upstream and downstream end, pressure is increased immediately at the downstream region and drops at the upstream region. Results of the computation using the implicit method agree well with the experimental data as shown in Figs. 4.75 and 4.81. Figs. 4.76, 4.77, 4.78, 4.79, and 4.80 show the pressure time histories at the downstream region with different time durations: 0 to 2 second, 2 to 4 second, 4 to 6 second, 6 to 8 second, and 8 to 10 second. Figs. 4.82, 4.83, 4.84, 4.85, and 4.86 show the pressure time histories at the upstream region with different time durations: 0 to 2 second, 2 to 4 second, 4 to 6 second, 6 to 8 second, and 8 to 10 second respectively. In both Simulation Case 1 and Case 2, it is observed that amplitude of the oscillating pressure wave using the implicit method is slightly smaller than that for the experimental data in the beginning of the duration as shown in figures. It is also observed that the predicted pressure wave of implicit method is slightly larger than the oscillation of the experimental data in the latter half of the duration of 10 seconds as shown in Figs. 4.63, 4.69, 4.75, and 4.81. Speed of the pressure wave was same as 4435 ft/sec and period of the pressure wave at the upstream region for Case 2 was 0.125 second.

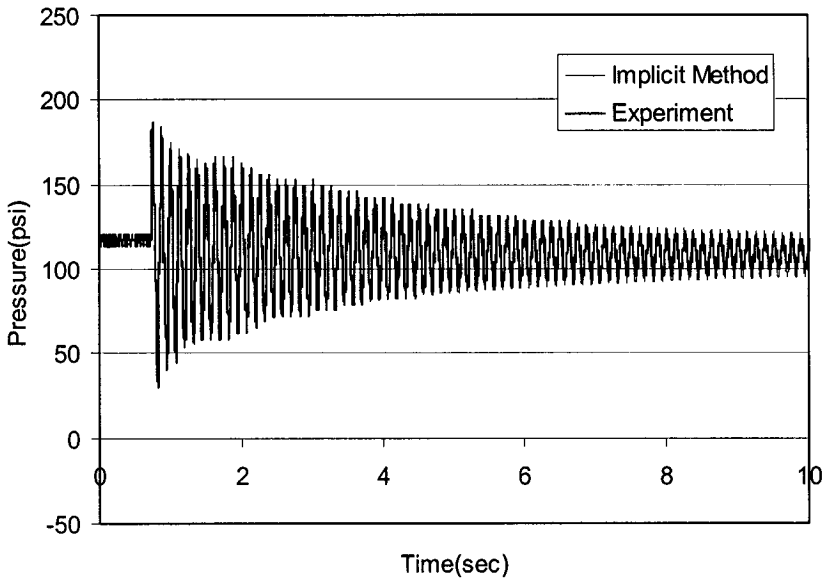

Figure 4.63 Pressure time history at the downstream region (Case 1: $0 \leq t \leq 10$ sec)

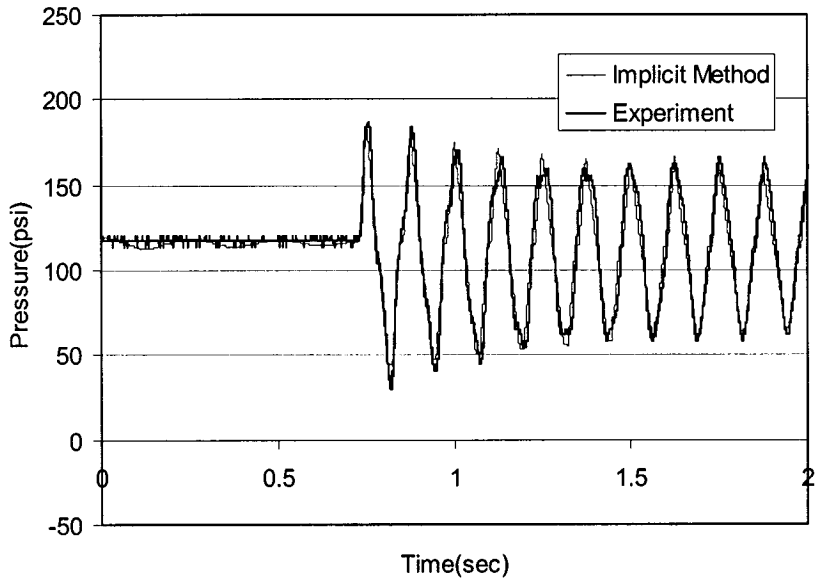

Figure 4.64 Pressure time history at the downstream region (Case 1: $0 \leq t \leq 2$ sec)

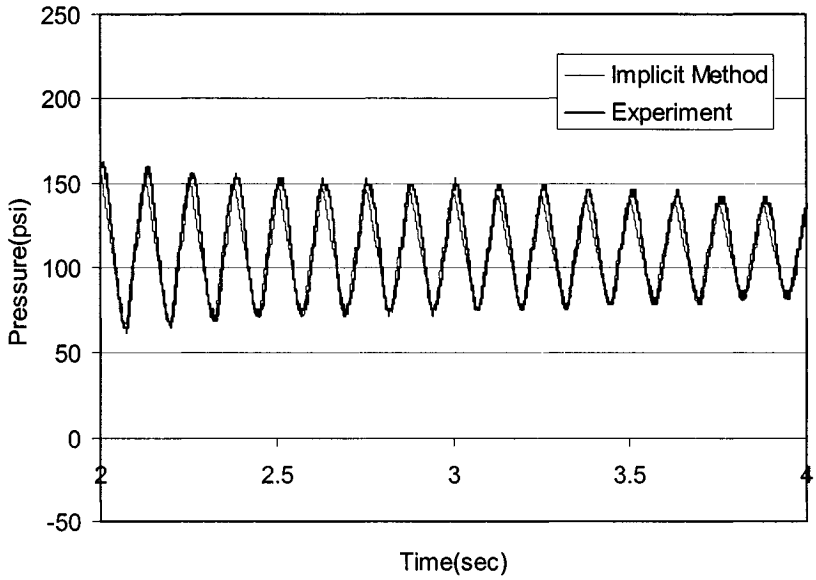

Figure 4.65 Pressure time history at the downstream region (Case 1: $2 \leq t \leq 4$ sec)

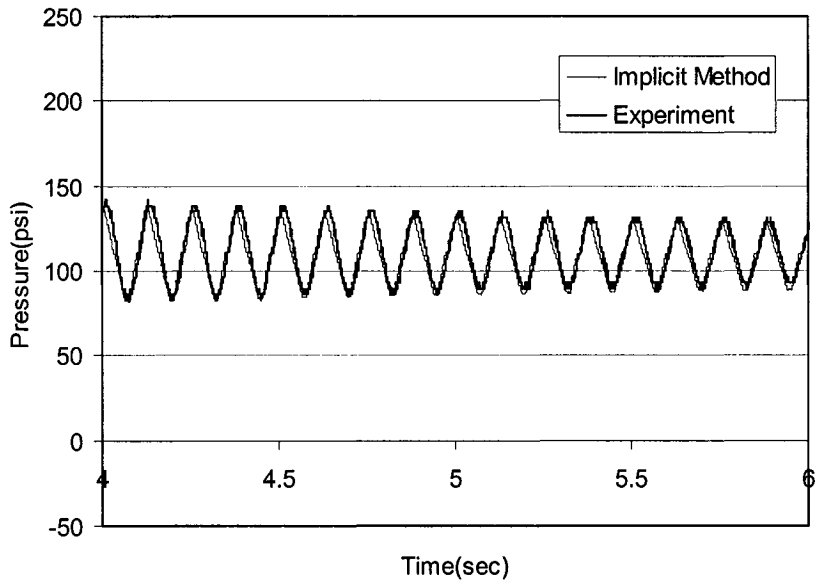

Figure 4.66 Pressure time history at the downstream region (Case 1: $4 \leq t \leq 6$ sec)

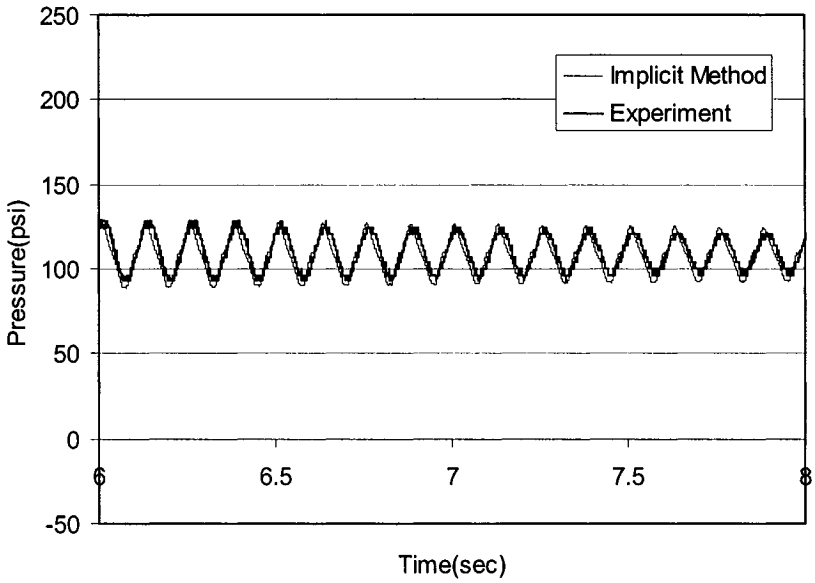

Figure 4.67 Pressure time history at the downstream region (Case 1: $6 \leq t \leq 8$ sec)

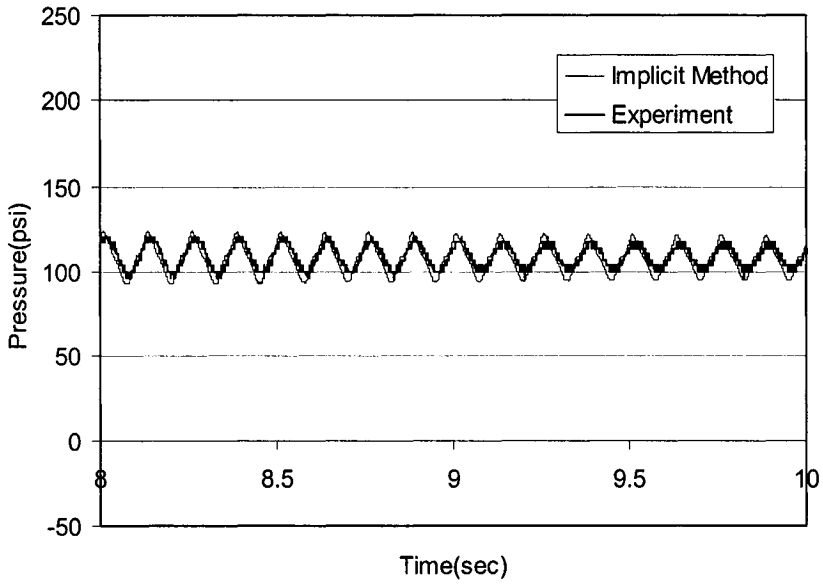

Figure 4.68 Pressure time history at the downstream region (Case 1: $8 \leq t \leq 10$ sec)

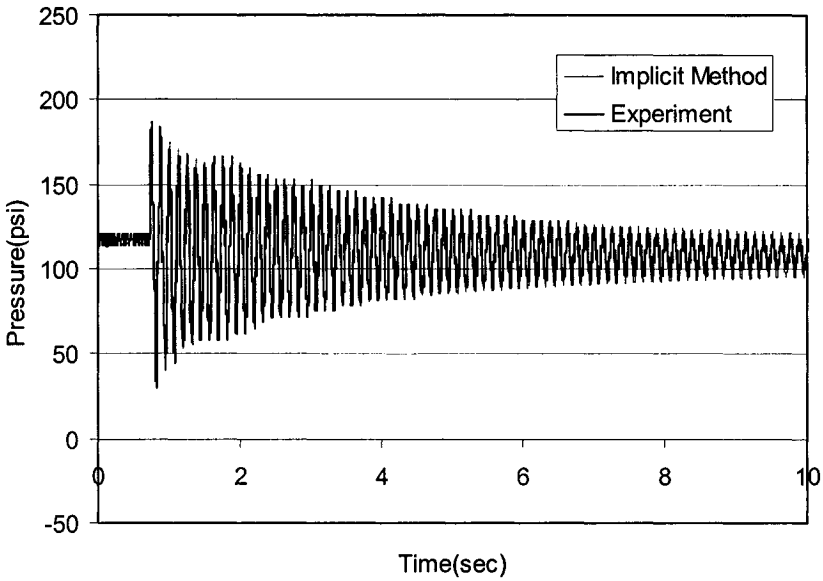

Figure 4.69 Pressure time history at the upstream region (Case 1: $0 \leq t \leq 10$ sec)

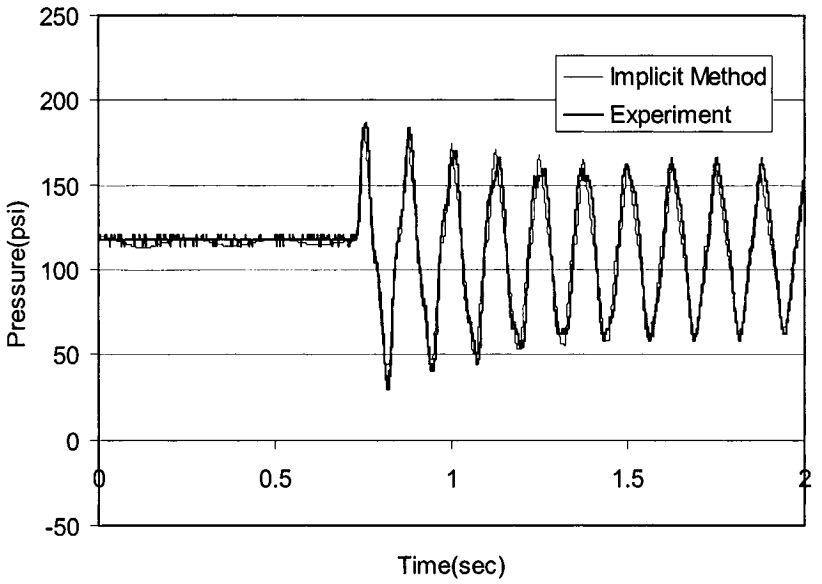

Figure 4.70 Pressure time history at the upstream region (Case 1: $0 \leq t \leq 2$ sec)

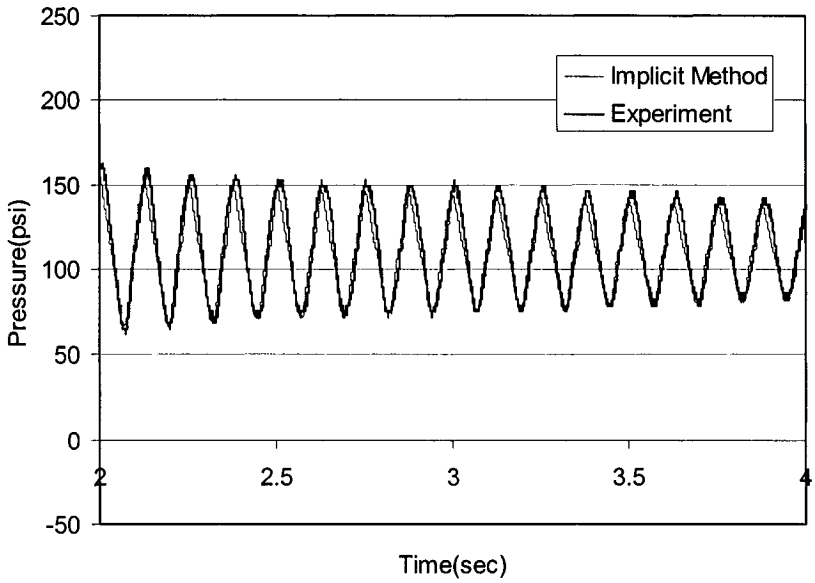

Figure 4.71 Pressure time history at the upstream region (Case 1: $2 \leq t \leq 4$ sec)

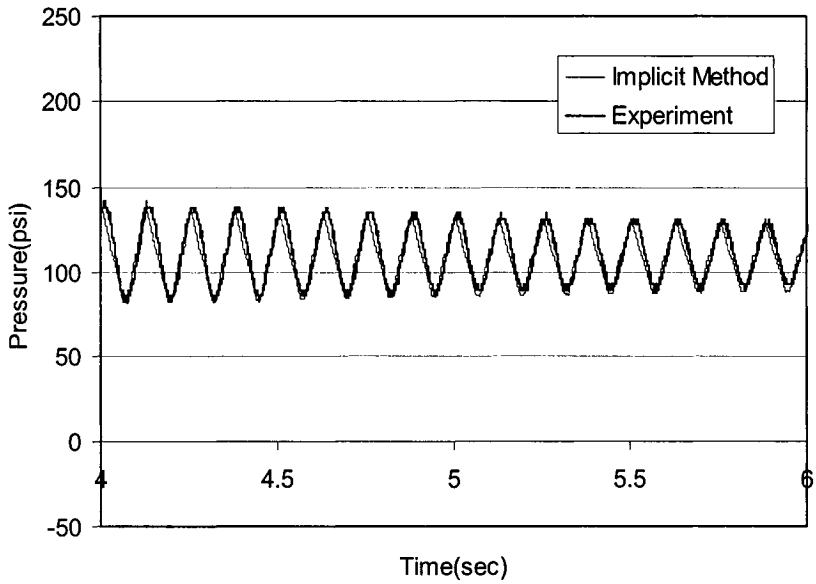

Figure 4.72 Pressure time history at the upstream region (Case 1: $4 \leq t \leq 6$ sec)

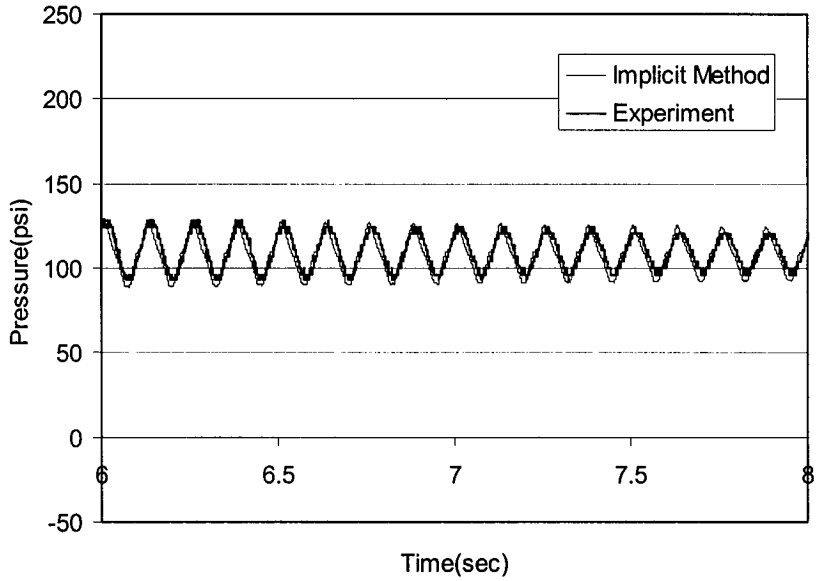

Figure 4.73 Pressure time history at the upstream region (Case 1: $6 \leq t \leq 8$ sec)

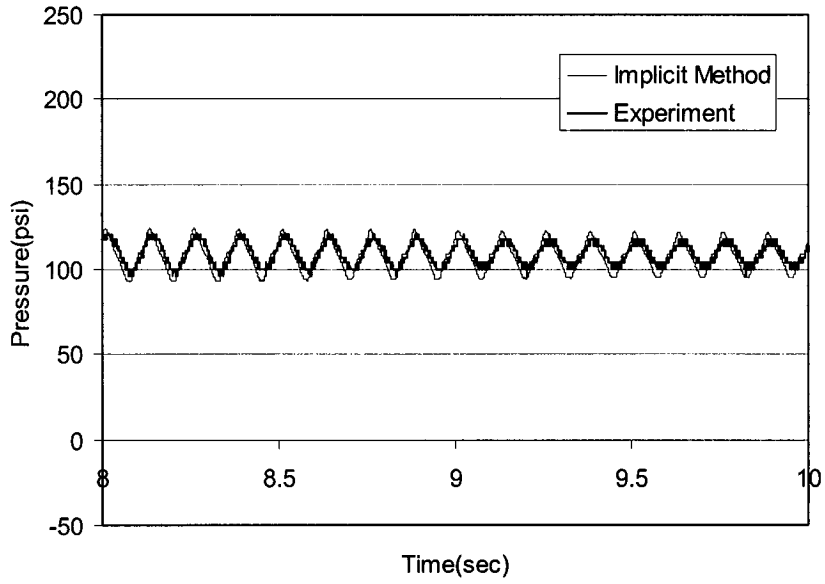

Figure 4.74 Pressure time history at the upstream region (Case 1: $8 \leq t \leq 10$ sec)

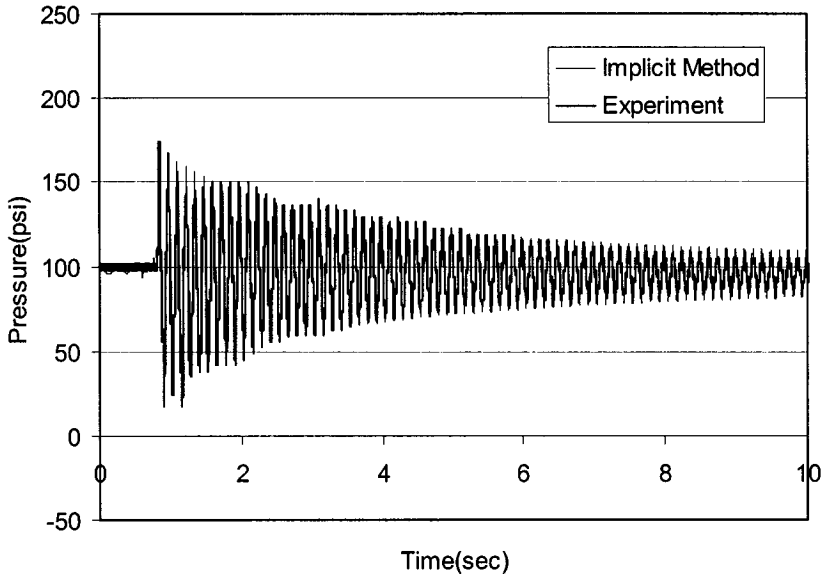

Figure 4.75 Pressure time history at the downstream region (Case 2: $0 \leq t \leq 10$ sec)

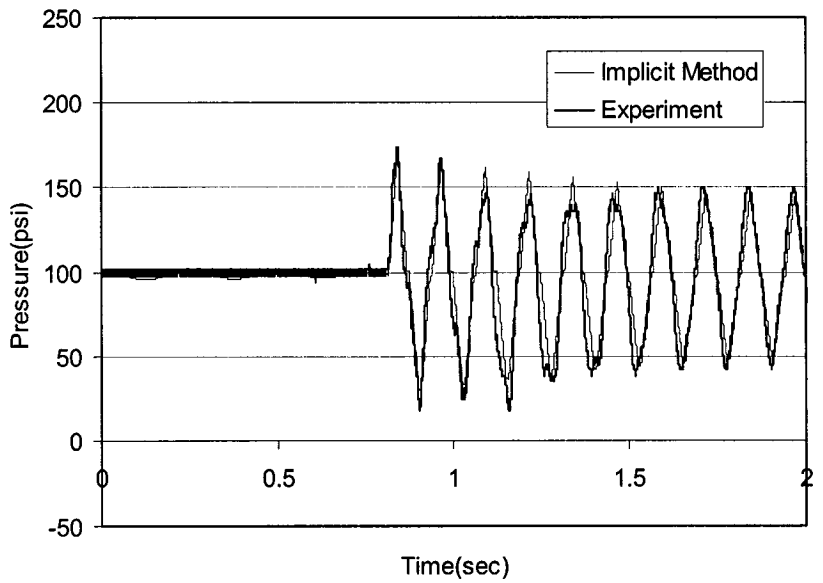

Figure 4.76 Pressure time history at the downstream region (Case 2: $0 \leq t \leq 2$ sec)

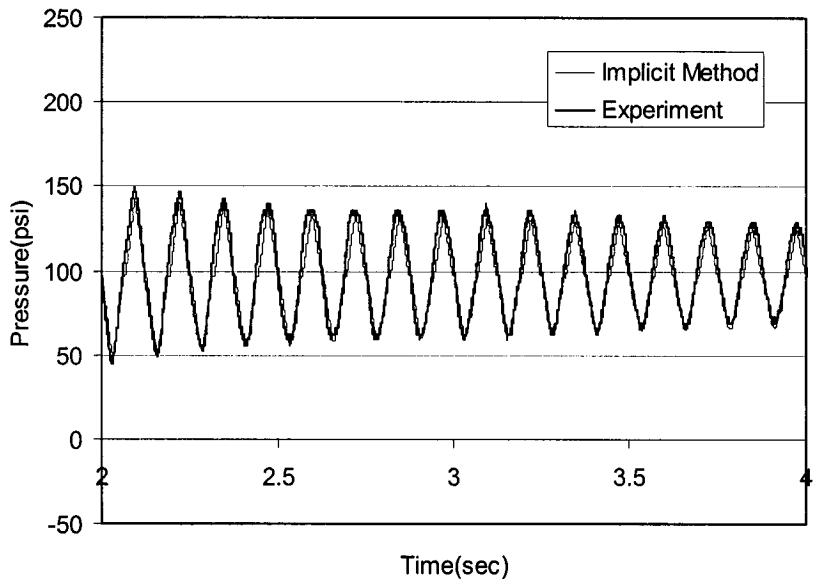

Figure 4.77 Pressure time history at the downstream region (Case 2: $2 \leq t \leq 4$ sec)

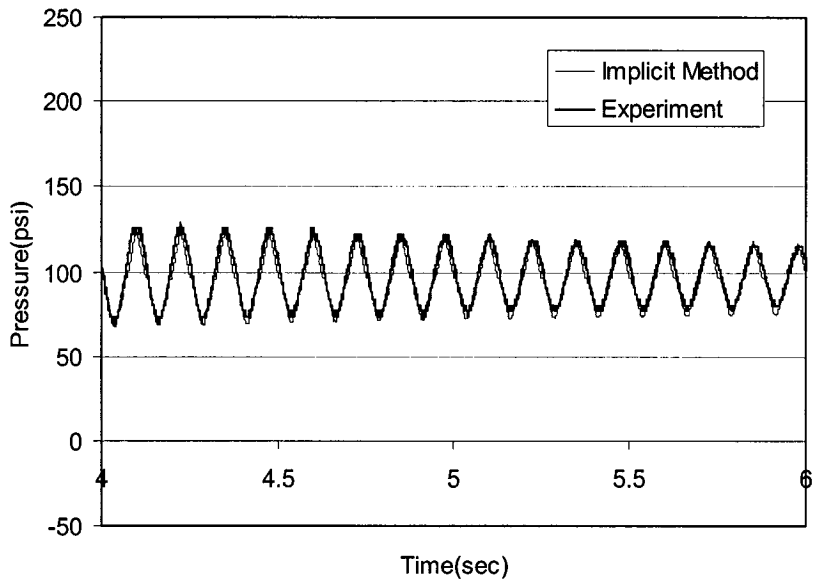

Figure 4.78 Pressure time history at the downstream region (Case 2: $4 \leq t \leq 6$ sec)

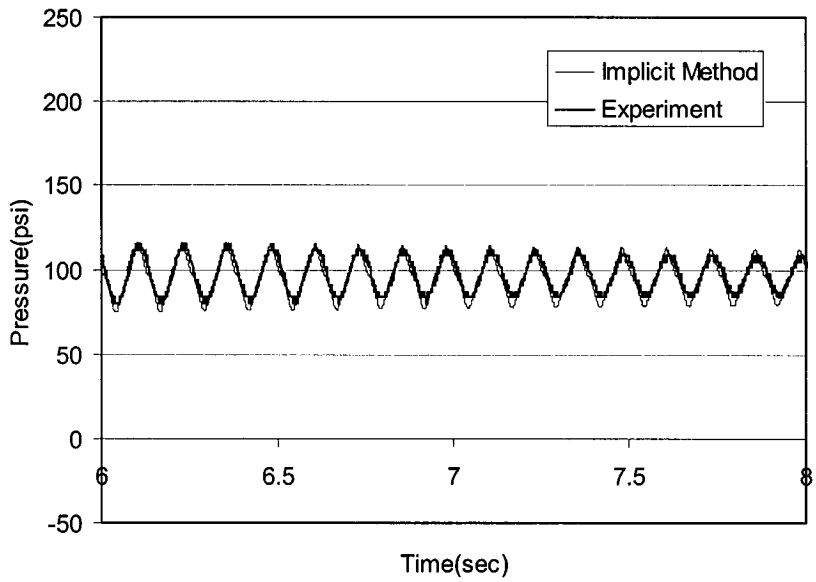

Figure 4.79 Pressure time history at the downstream region (Case 2: $6 \leq t \leq 8$ sec)

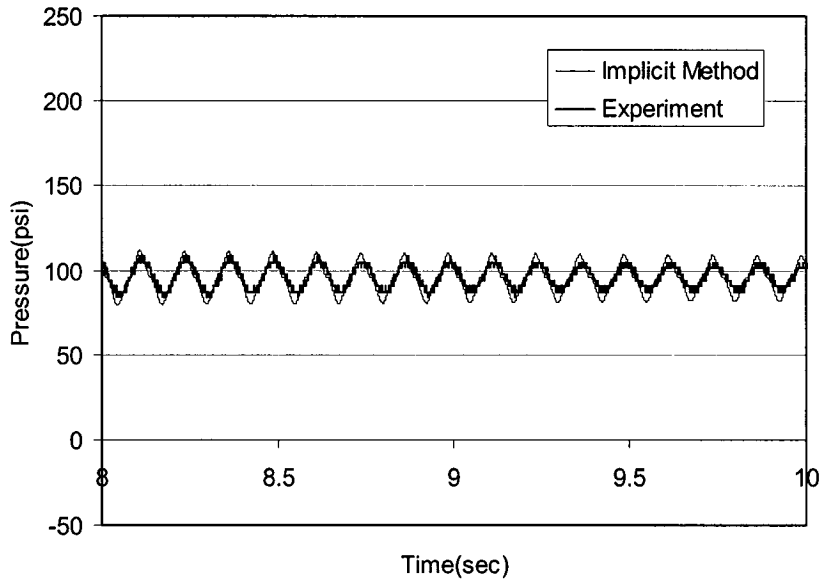

Figure 4.80 Pressure time history at the downstream region (Case 2: $8 \leq t \leq 10$ sec)

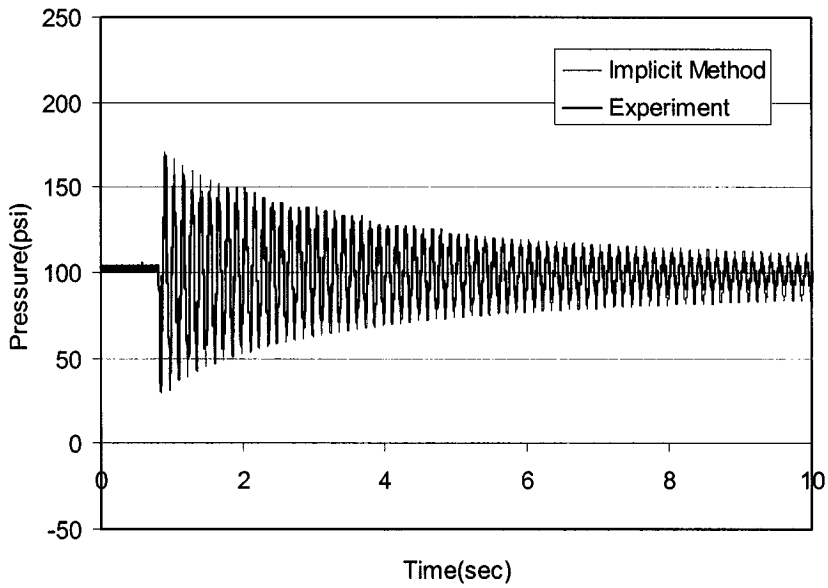

Figure 4.81 Pressure time history at the upstream region (Case 2: $0 \leq t \leq 10$ sec)

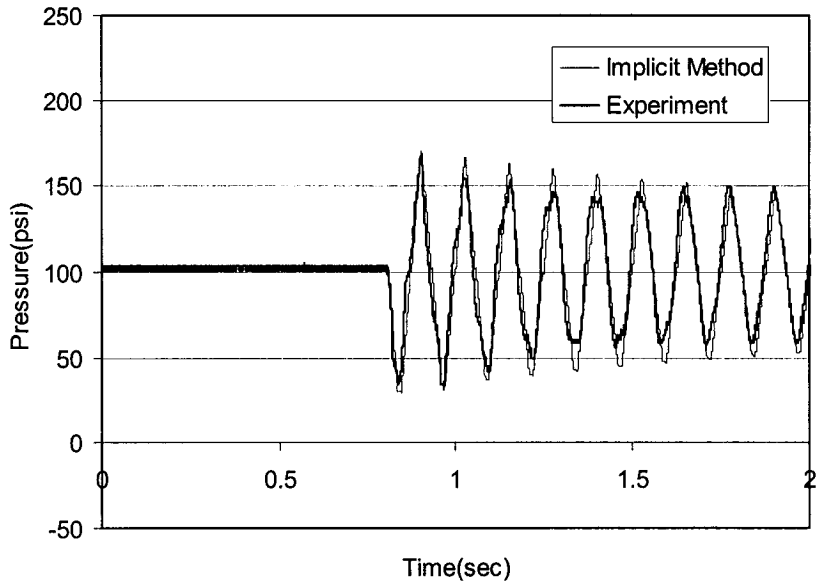

Figure 4.82 Pressure time history at the upstream region (Case 2: $0 \leq t \leq 2$ sec)

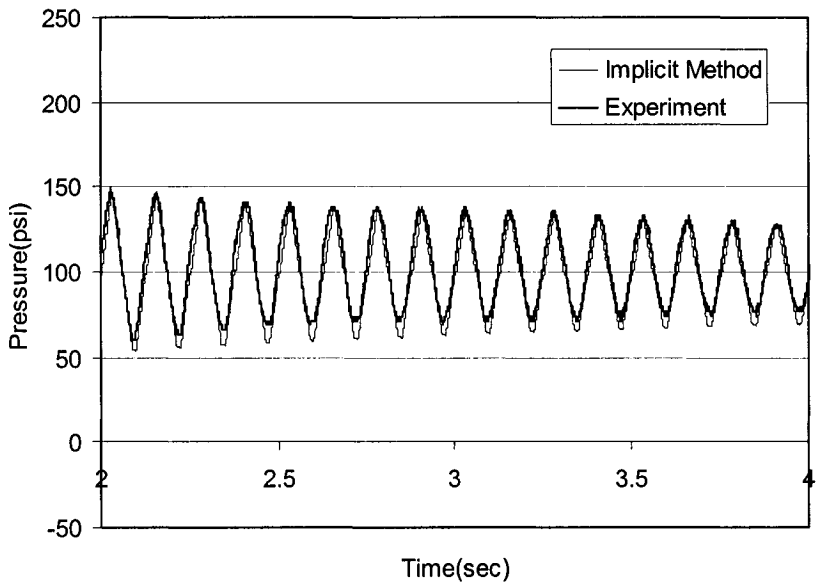

Figure 4.83 Pressure time history at the upstream region (Case 2: $2 \leq t \leq 4$ sec)

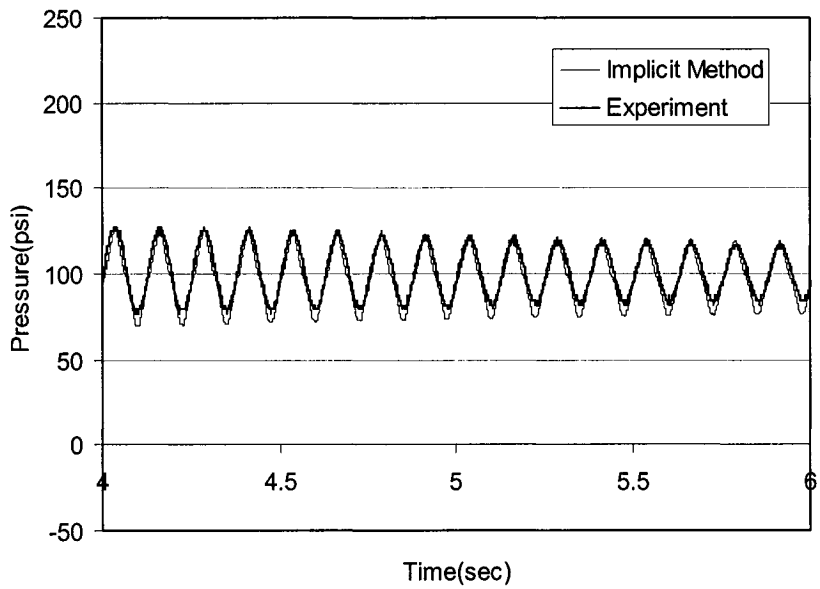

Figure 4.84 Pressure time history at the upstream region (Case 2: $4 \leq t \leq 6$ sec)

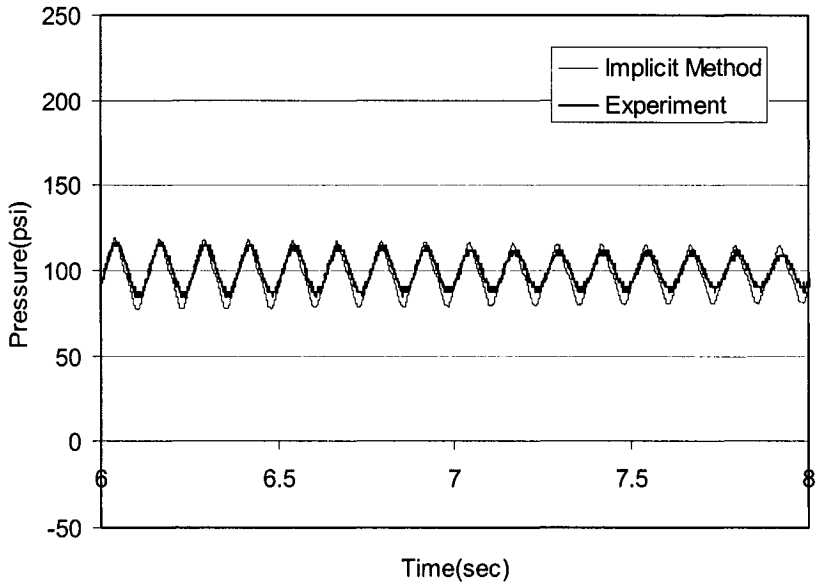

Figure 4.85 Pressure time history at the upstream region (Case 2: $6 \leq t \leq 8$ sec)

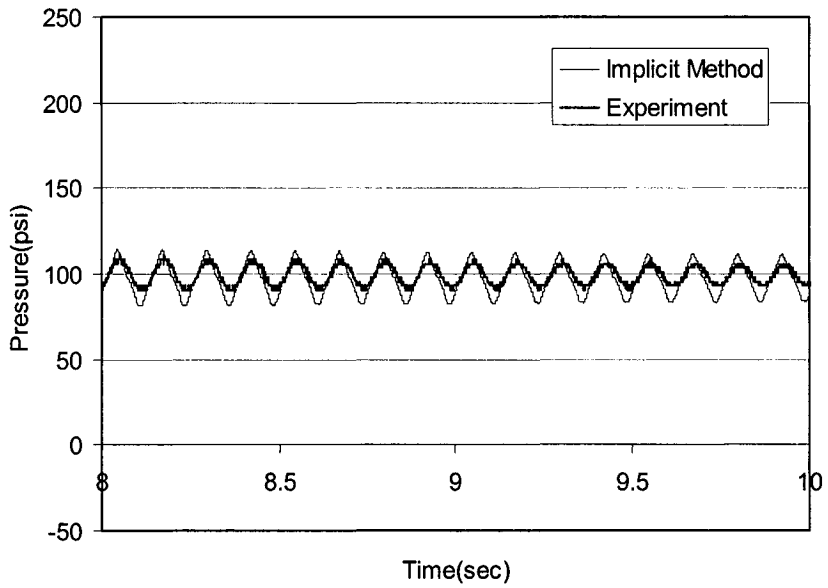

Figure 4.86 Pressure time history at the upstream region (Case 2: $8 \leq t \leq 10$ sec)

4.6 Case Study

For a given piping system, if the pressure head or the flow rate at certain points within the system experience sudden change, the flow and pressure head at various junctions can be expected to be significantly altered as a function of time. Several cases of the transient flow problem will be presented in this section. Results of the simulation for the simple looped network, small city model, small city model with backflow prevention assembly, small city model with surge tank, medium sized city network, and large sized city network will be presented and discussed. For the computer model simulation, the method of characteristics is used.

4.6.1 Simulation of the Simple Looped Network

Fig. 4.87 shows the simple looped network, which was used by Karney and McInnis (1990) with the piping characteristics shown in Table 4.6. This simple looped network has four pipes and four junctions. With the two reservoirs and a downstream valve system, an instantaneous valve closure can cause the pressure to rise at the valve. Fig. 4.88 shows the predicted variation in pressure head at the valve for a looped network described in Fig. 4.87. The result obtained by Karney and McInnis is shown in thick black line while the results of present simulation is shown in thin black line. Comparing these curves, it is clear that the present results agree well with Karney's result. They are identical to Karney's results for the first 50 seconds. It should be noted that Karney's result stopped at the first 50 seconds while the present model results being continued to the first 100 seconds.

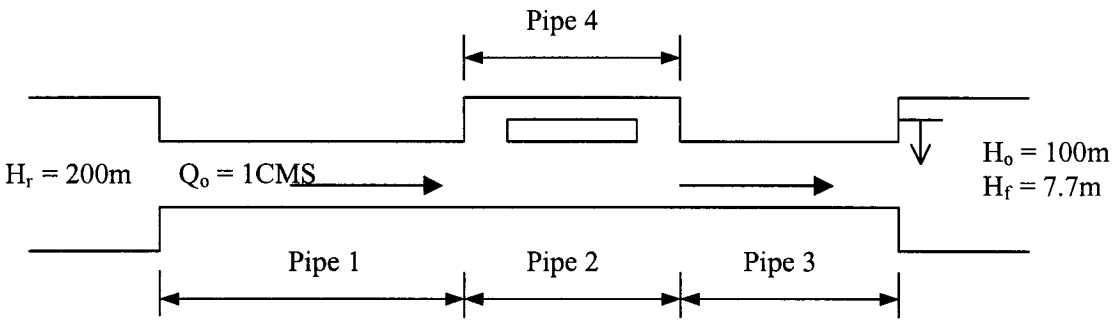

Figure 4.87 Simple looped network

Table 4.6 Simple looped network

	Pipe 1	Pipe 2	Pipe 3	Pipe4
Length (m)	2,000	1,000	1,000	1,000
Diameter (mm)	1,000	1,000	1,000	1,000
Wave Speed (m/sec)	1,000	1,000	1,000	1,000
Friction Loss Coefficient	0.026	0.026	0.026	0.03
Discharge (m^3/sec)	1.0	0.79	1.0	0.21

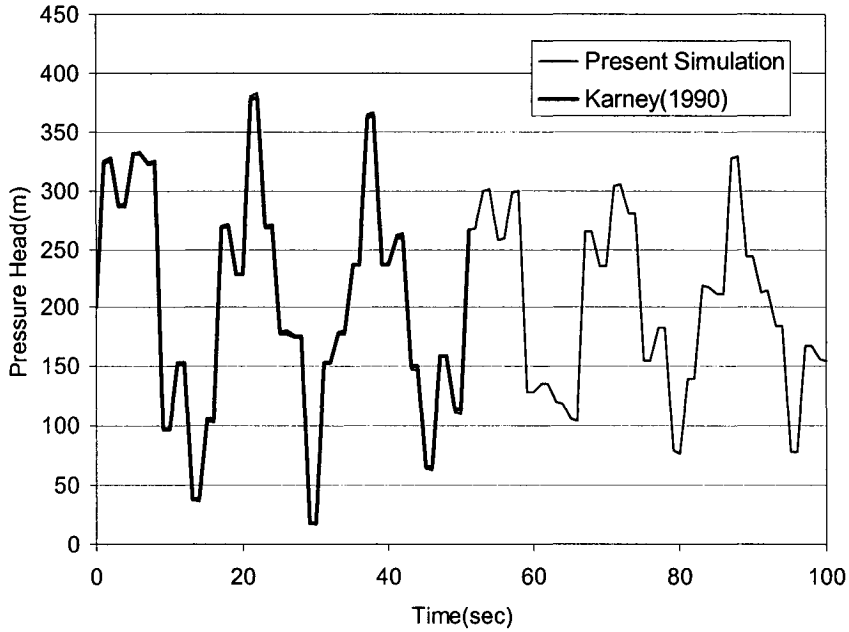

Figure 4.88 Comparison of the predicted variation in pressure head at the valve for a looped network

4.6.2 Small City Model

As part of the present study, the unsteady piping network analysis is performed for a small model city. For the small city network, a simple pipe network was used. A sketch of the pipe network is shown in Fig. 4.89. This simple network has ten pipes, seven junctions, and two reservoirs. The demands at the Junctions #3, #4, #5, #8, and #9 are 3cfs, 2cfs, 4cfs, 2cfs, and 1cfs respectively.

Table 4.7 provides the junction report showing the demand and hydraulic grades at the seven junctions. Table 4.8 shows the steady state solution of the computed discharge in each of the ten pipes.

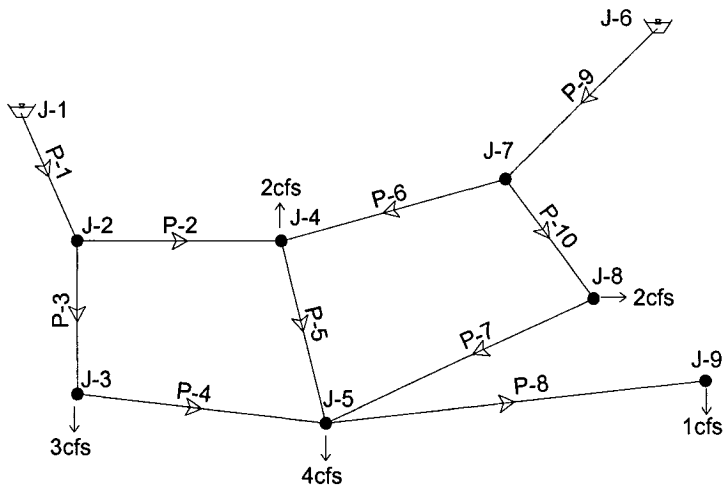

Figure 4.89 Sketch for Small City Network 1

Table 4.7 Small city junction report 1

Label	Elevation (ft)	Demand (cfs)	Calculated Hydraulic Grade (ft)
J-1	1400.0	0.0	1480.00
J-2	1300.0	0.0	1470.34
J-3	1290.0	3.0	1461.84
J-4	1310.0	2.0	1464.14
J-5	1280.0	4.0	1458.42
J-6	1400.0	0.0	1480.00
J-7	1320.0	0.0	1467.62
J-8	1310.0	2.0	1459.00
J-9	1260.0	1.0	1450.72

Table 4.8 Small city pipe report 1

Label	Length (ft)	Diameter (in)	Material	Discharge (cfs)	Pressure Headloss (ft)
P-1	800.0	15.0	Cast iron	8.896	9.66
P-2	1000.0	12.0	Cast iron	3.527	6.20
P-3	600.0	12.0	Cast iron	5.369	8.50
P-4	1200.0	12.0	Cast iron	2.369	3.42
P-5	800.0	10.0	Cast iron	2.346	5.72
P-6	1200.0	8.0	Cast iron	0.818	3.48
P-7	1500.0	8.0	Cast iron	0.284	0.58
P-8	1800.0	8.0	Cast iron	1.000	7.69
P-9	1000.0	10.0	Cast iron	3.103	12.38
P-10	400.0	8.0	Cast iron	2.284	8.62

Fig. 4.90 shows the pipe network modified by the change in demand at Junction #4 and Junction #5. Demand at Junction #5 is linearly decreased from 4cfs to 0cfs within 4 seconds; simultaneously, demand at Junction #4 is linearly increased from 2cfs to 6cfs in this same 4-second period (1cfs=448.43gpm). The junction and the pipe report with the demand change at Junction #4 and Junction #5 are presented in Tables 4.9 and 4.10.

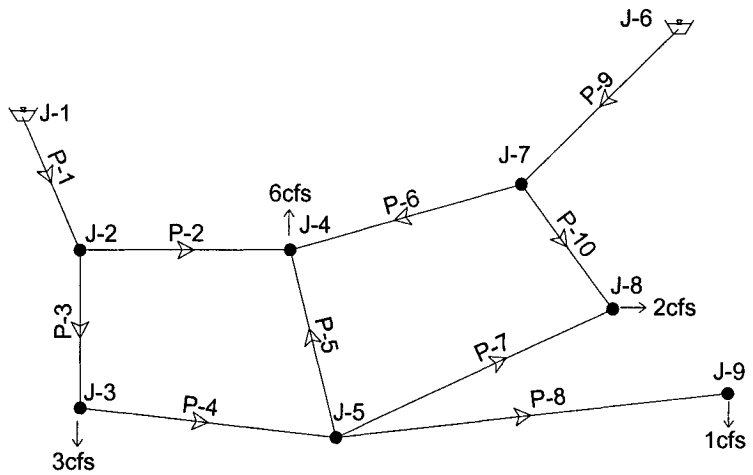

Figure 4.90 Sketch for Small City Network 2

Table 4.9 Small city junction report 2

Label	Elevation (ft)	Demand (cfs)	Calculated Hydraulic Grade (ft)
J-1	1400.0	0.0	1480.00
J-2	1300.0	0.0	1470.25
J-3	1290.0	3.0	1463.67
J-4	1310.0	6.0	1461.39
J-5	1280.0	0.0	1461.85
J-6	1400.0	0.0	1480.00
J-7	1320.0	0.0	1467.96
J-8	1310.0	2.0	1461.80
J-9	1260.0	1.0	1454.16

Table 4.10 Small city pipe report 2

Label	Length (ft)	Diameter (in)	Material	Discharge (cfs)	Pressure Headloss (ft)
P-1	800.0	15.0	Cast iron	8.940	9.75
P-2	1000.0	12.0	Cast iron	4.228	8.85
P-3	600.0	12.0	Cast iron	4.712	6.57
P-4	1200.0	12.0	Cast iron	1.712	1.82
P-5	800.0	10.0	Cast iron	-0.636	0.46
P-6	1200.0	8.0	Cast iron	1.135	6.56
P-7	1500.0	8.0	Cast iron	-0.075	0.05
P-8	1800.0	8.0	Cast iron	1.000	7.69
P-9	1000.0	10.0	Cast iron	3.060	12.04
P-10	400.0	8.0	Cast iron	1.925	6.15

Due to these changes of demand, the flow direction at Pipe #5 and Pipe #7 are changed into the opposite direction as shown in the time dependent discharge curve in Fig. 4.91. From Fig. 4.91, it is seen that the flow direction is reversed in Pipe #5 after 3.2 seconds and in Pipe #7 after 2.5 seconds, before the complete implementation of the change in demand at Junction #4 and Junction #5. Figs. 4.92 and 4.93 show the transient pressure head fluctuation at Junction #4, #5, and #8 as a function of time after the implementation of the change in demand at Junction #4 and Junction #5 is accomplished in 4 seconds. It is noted that the

pressure head at Junction #5 is significantly increased and that the pressure head at Junction #4 is significantly decreased with many cycles of oscillations. In order to detect the effect of different valve open/closure rate on the transient pressure fluctuations, computer simulation is also performed for the network shown in Fig. 4.90 with the changing demands accomplished in 2 seconds. The corresponding results are shown in Figs. 4.94, 4.95, and 4.96 (correspond to Figs. 4.91, 4.92, and 4.93 for 4 second open/closure time). By comparing Figs. 4.91, 4.92, and 4.93 with Figs. 4.94, 4.95, and 4.96, it is very clear that the rapid change of the demand at Junction #4 and Junction #5 produces larger fluctuations of the flow rate and pressure heads. In Figs. 4.97 and 4.98, the effect of 2-second open/closure time is further compared with 4-second open/closure time. In each of these two figures, the 2-second open/closure time causes greater magnitude of the transient fluctuation. As can be expected, the range of peak to trough is significantly increased when the change of demand is accomplished in 2 seconds as compared to those in 4 seconds.

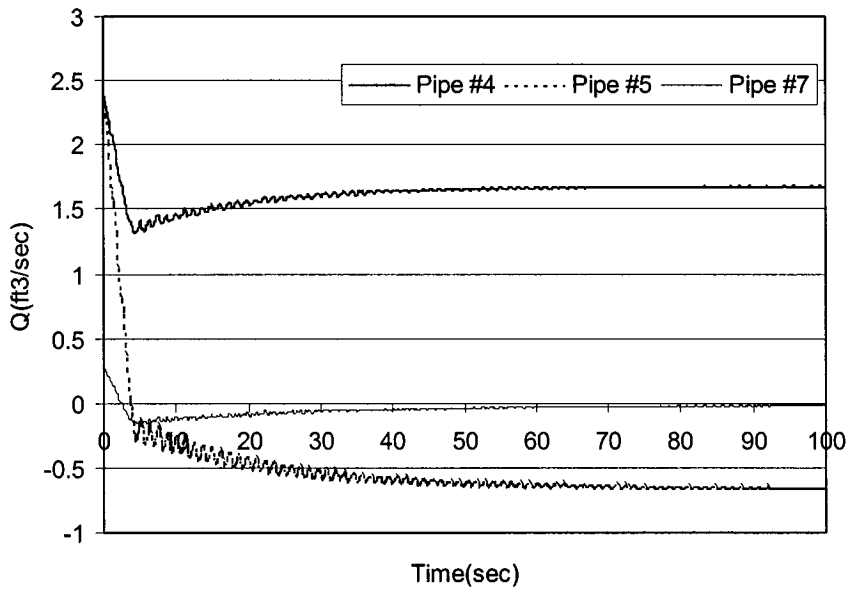

Figure 4.91 Transient flow rate at Pipe #4, #5, and #7 when the change of demand is implemented within 4 seconds

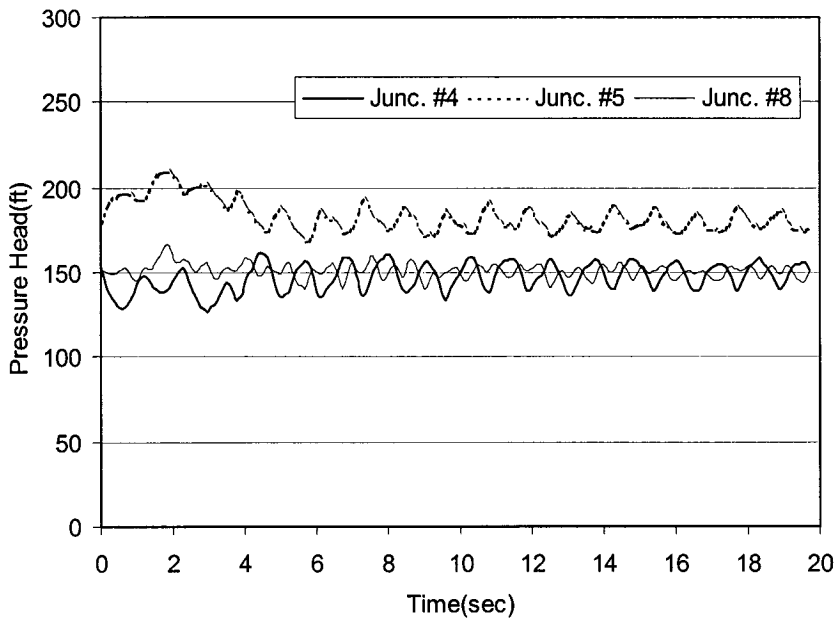

Figure 4.92 Transient pressure fluctuation at Junction #4, #5, and #8 after the change in demand is implemented in 4 seconds

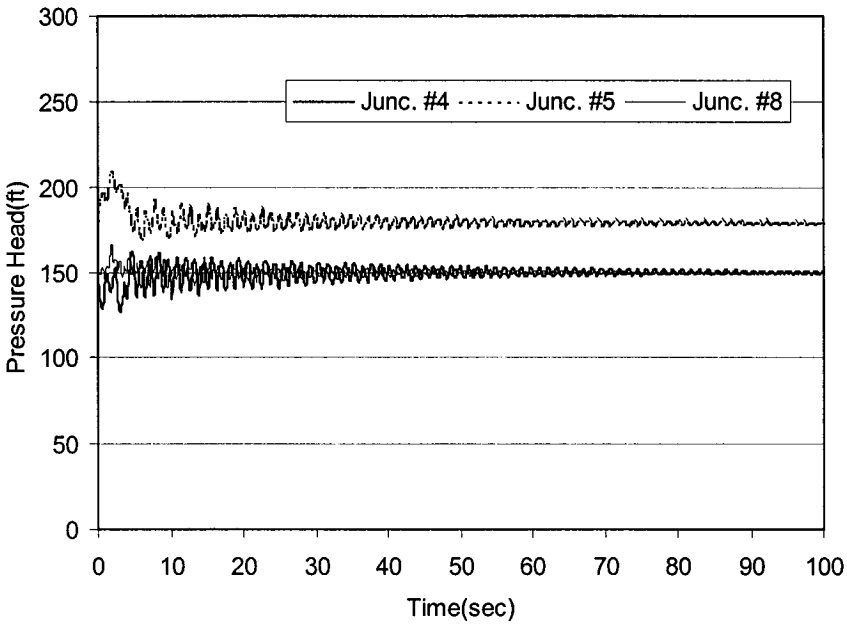

Figure 4.93 Transient pressure fluctuation at Junction #4, #5, and #8 for the first 100 seconds after the change in demand is implemented in 4 seconds

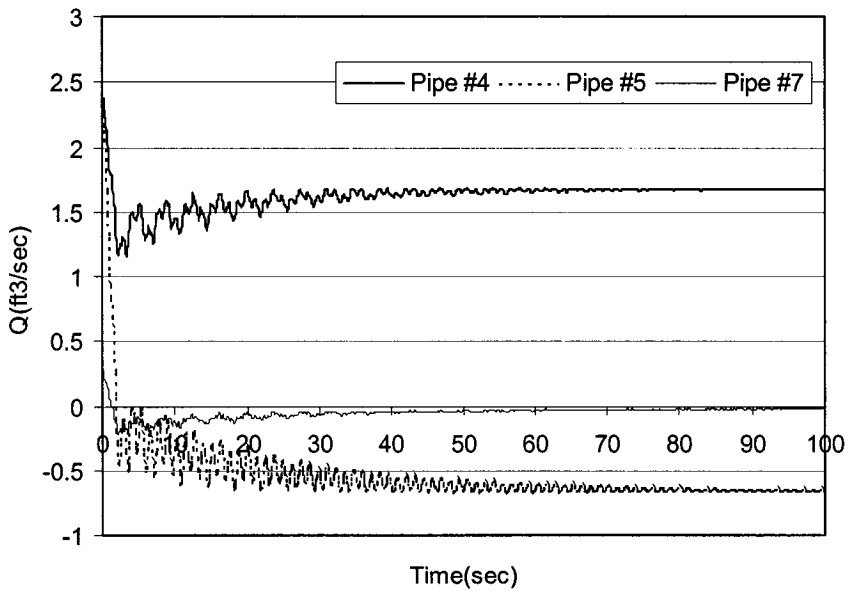

Figure 4.94 Transient flow rate at Pipe #4, #5, and #7 when the change of demand is implemented within 2 seconds

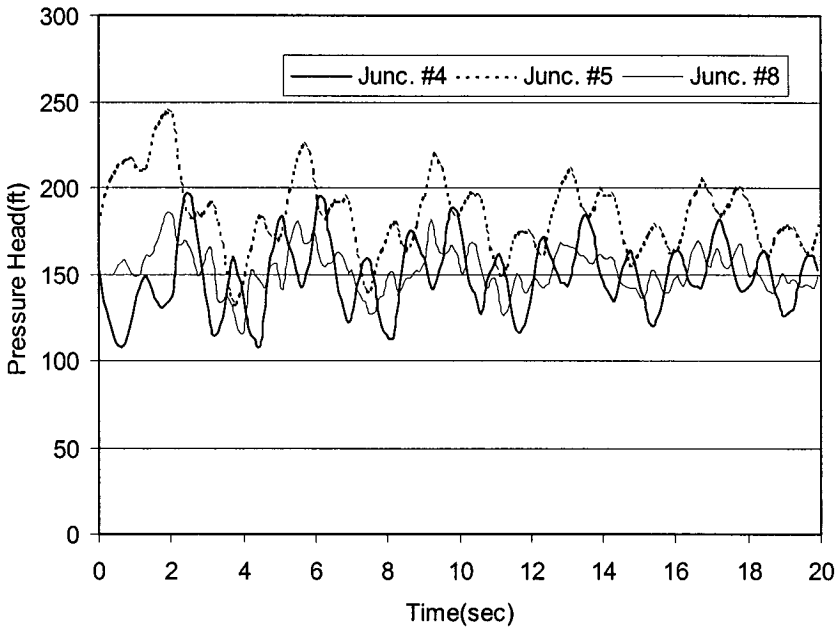

Figure 4.95 Transient pressure fluctuation at Junction #4, #5, and #8 after the change in demand is implemented in 2 seconds

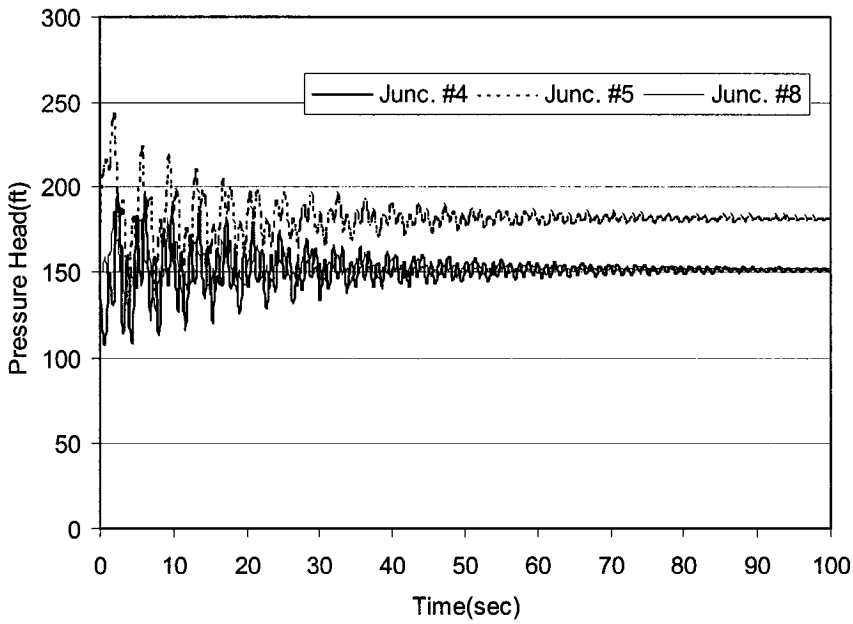

Figure 4.96 Transient pressure fluctuation at Junction #4, #5, and #8 for the first 100 seconds after the change in demand is implemented in 2 seconds

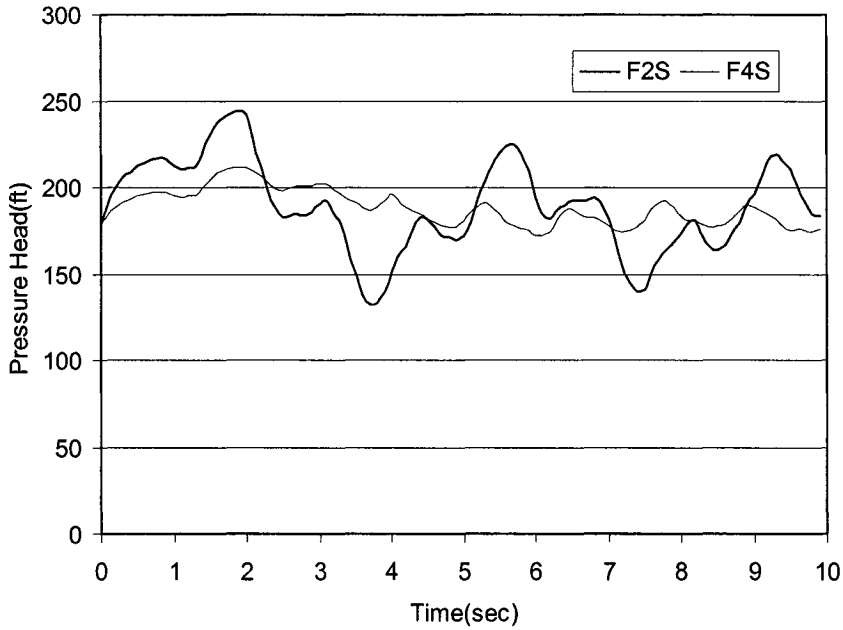

Figure 4.97 Comparison of pressure head fluctuation at Junction #5 showing the effect of different valve open/closure time (2sec vs. 4sec)

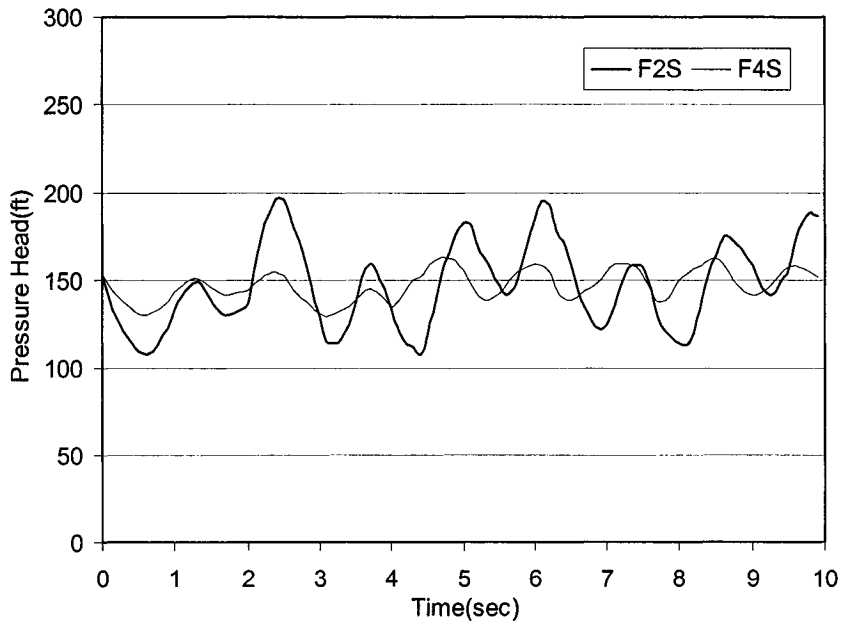

Figure 4.98 Comparison of pressure head fluctuation at Junction #4 showing the effect of different valve open/closure time (2sec vs. 4sec)

4.6.3 Small City Model with Backflow Prevention Assembly

Small city model with different demands has been presented in previous section. In this section, backflow prevention assembly will be added to some pipes in the small city piping network. A sketch of the pipe network is shown in Fig. 4.99. This small city network has ten pipes, seven junctions, two reservoirs, and two Reduced Pressure Principle Backflow Prevention Assembly (RP) placed between Junction #4 & #5 and Junction #5 & 8. This RP Backflow prevention assembly, which is called just RP, actually is consisted of two check valves and one pressure release valve between the check valves. Pipe network is modified by the change in demand at Junction #4 and Junction #5 and the change in hydraulic head at Reservoir #1. Demand at Junction #4 is linearly increased 2cfs to 6cfs within 4 seconds: simultaneously, demand at Junction #5 is linearly decreased from 4cfs to 0cfs within 4 seconds. Hydraulic head at Reservoir #1 is linearly decreased from 1480ft to 1430ft within 50 seconds.

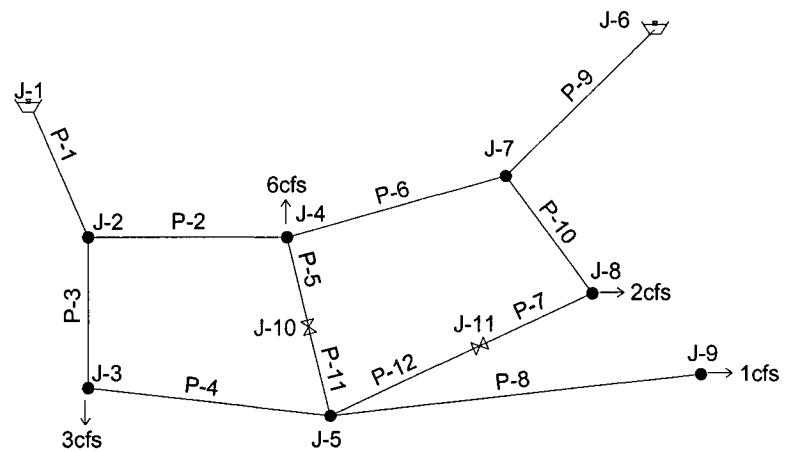

Figure 4.99 Sketch for small city network with two backflow prevention assemblies

Because of these changes of demand and hydraulic head of Reservoir #1, flow direction of Pipe #5 is changed and flow direction of Pipe #7 is changed instantly for several seconds as shown in the time dependent discharge curve presented in Fig. 4.100. From Fig. 4.100, it is seen that the flow direction is reversed in Pipe #5 after 3.7 seconds and in Pipe #7 from 2.9 second to 10.7 second. Fig. 4.101 shows the transient pressure head fluctuation at Junction #4, #5, and #8 as a function of time after the implementations of the change in demand at Junction #4 and Junction #5 and hydraulic head of Reservoir #1 are accomplished. Because the hydraulic head of Reservoir #1 decreases significantly, pressure head at all junctions slowly goes down as shown in Fig. 4.101. In order to detect backflow in this network, two backflow prevention assemblies are installed at Pipe #5 and Pipe #7 each as shown in Fig. 4.99. Now it is assumed that first check valve of the each backflow prevention assembly is not working perfectly because small debris of the pipeline clog the check valve. So now, pressure release valve opens and second check valve is working at the same time. From Fig. 4.102, it is seen that flow of Pipe #5 is blocked, and flow of Pipe #7 continues to flow all the times, but flow of Pipe #4 is reversed now. It is due to the check valve of the backflow prevention assembly. Fig. 4.103 shows pressure head fluctuation, which is different from that shown in Fig. 4.101 due to check valve of backflow prevention assembly.

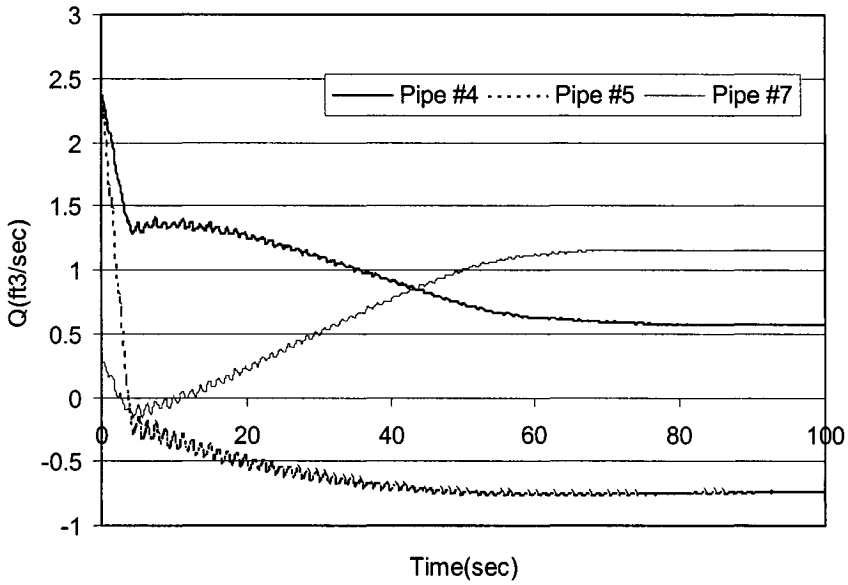

Figure 4.100 Transient flow rate with the changing demand of Junction #4, #5, and the changing hydraulic head of Reservoir #1

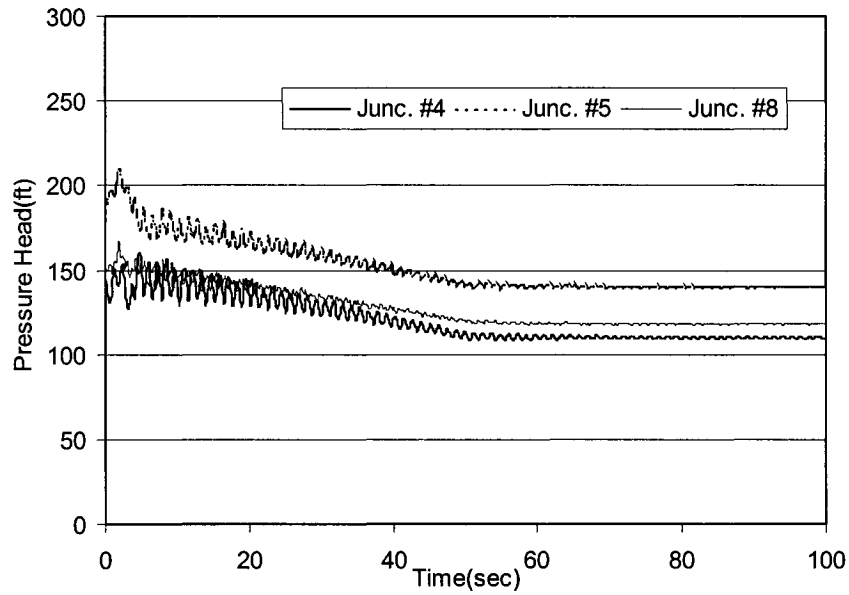

Figure 4.101 Transient pressure fluctuation at Junction #4, #5, and #8 with the changing demand of Junction #4, #5, and the changing hydraulic head of Reservoir #1

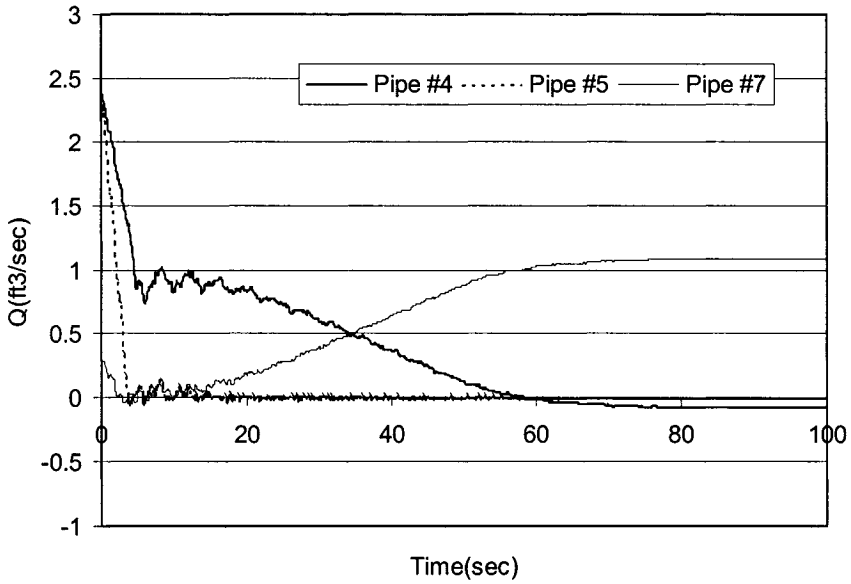

Figure 4.102 Transient flow rate with the changing demand of Junction #4, #5, and the changing hydraulic head of Reservoir #1 (Pipe #5 and #7 has RP)

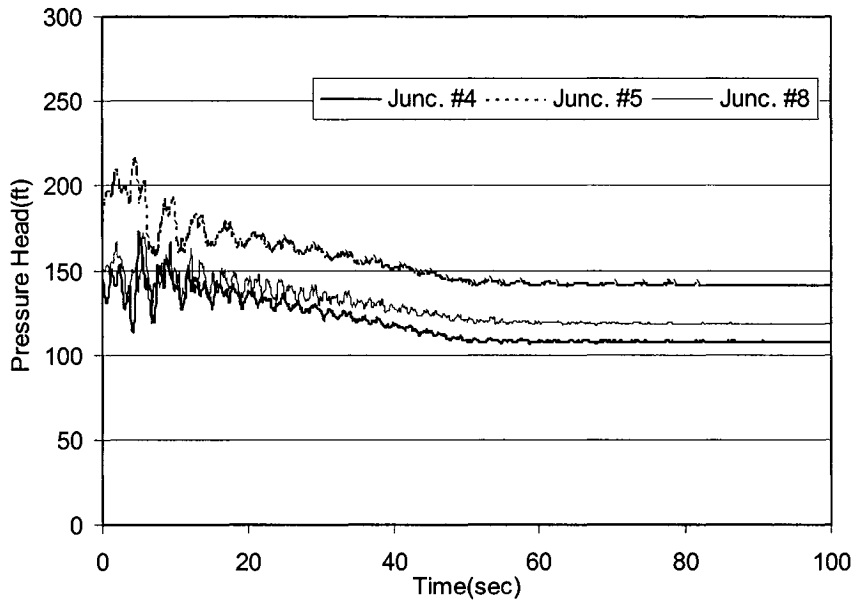

Figure 4.103 Transient pressure fluctuation at Junction #4, #5, and #8 with the changing demand in Junction #4, #5, and the changing hydraulic head of Reservoir #1 (Pipe #5 and #7 has RP)

After one more backflow prevention assembly is installed between Junction #3 and Junction #5 as shown in Fig. 4.104, it is seen that flow direction of Pipe #4 is not reversed anymore as that shown in Fig. 4.105. Fig. 4.106 shows pressure head fluctuations after three backflow prevention assemblies are installed in the pipe network.

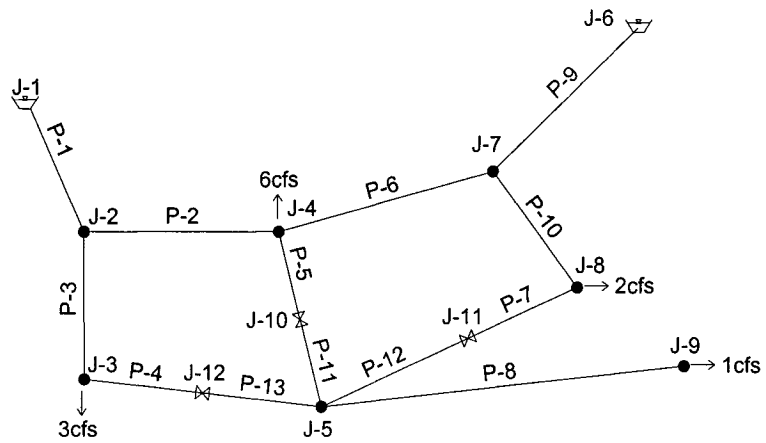

Figure 4.104 Sketch for small city network with three backflow prevention assemblies

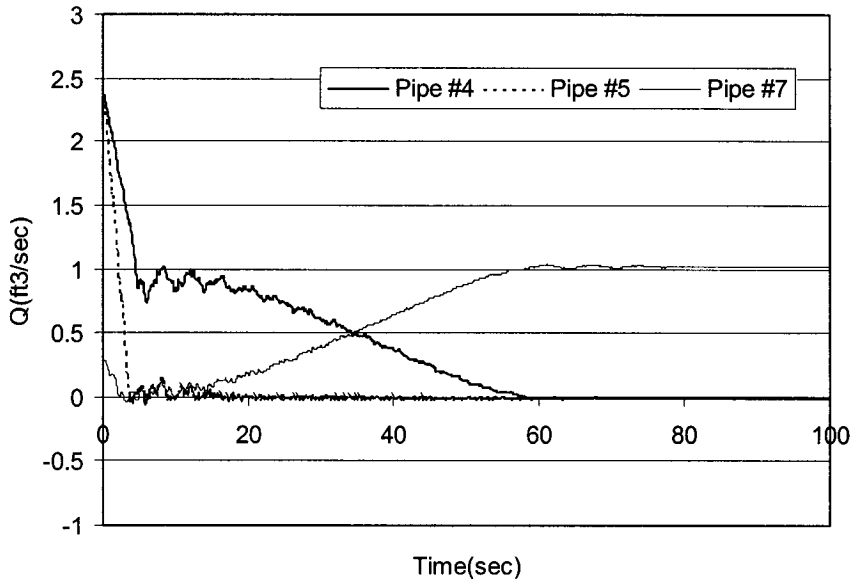

Figure 4.105 Transient flow rate with the changing demand of Junction #4, #5, and the changing hydraulic head of Reservoir #1 (Pipe #4, #5, and #7 has RP)

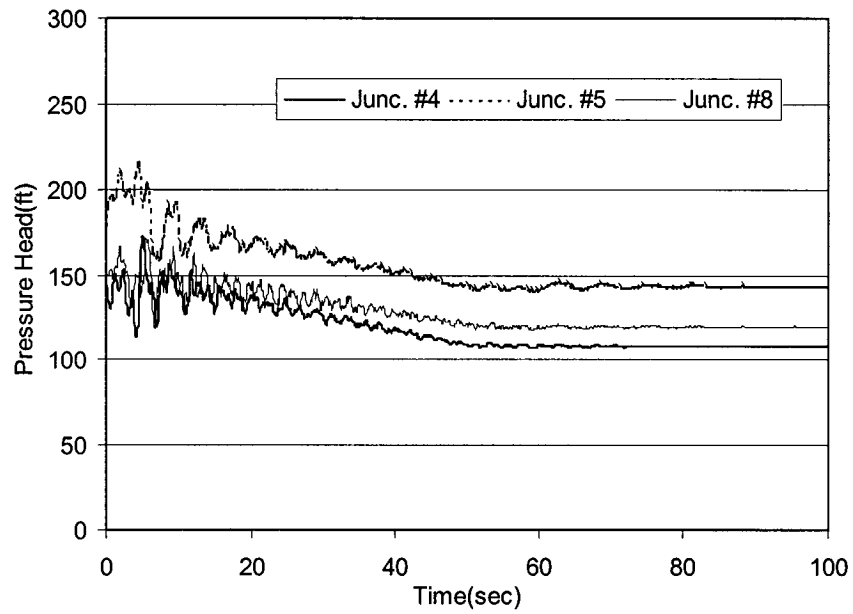

Figure 4.106 Transient pressure fluctuation at Junction #4, #5, and #8 with the changing demand of Junction #4, #5, and the changing hydraulic head of Reservoir #1 (Pipe #4, #5, and #7 has RP)

4.6.4 Small City Model with Surge Tank

To simulate the effect of surge tank installed in the system, this small city pipe network has ten pipes, seven junctions, two reservoirs, and one surge tank. There are two kinds of surge tank. One is the one-way surge tank that only responds when the pressure goes lower than certain pressure limit. The other is the two-way surge tank that responds when the pressures goes higher or lower than certain pressure point.

In this research, both kinds of surge tank are simulated. Surge tank is installed in the middle of the Pipe #9. A sketch of the pipe network is shown in Fig. 4.107. This surge tank is placed 1400ft elevation and height of surge tank is 70ft, area of surge tank is $60ft^2$, area of the orifice is $0.2ft^2$ and orifice coefficient is 0.70.

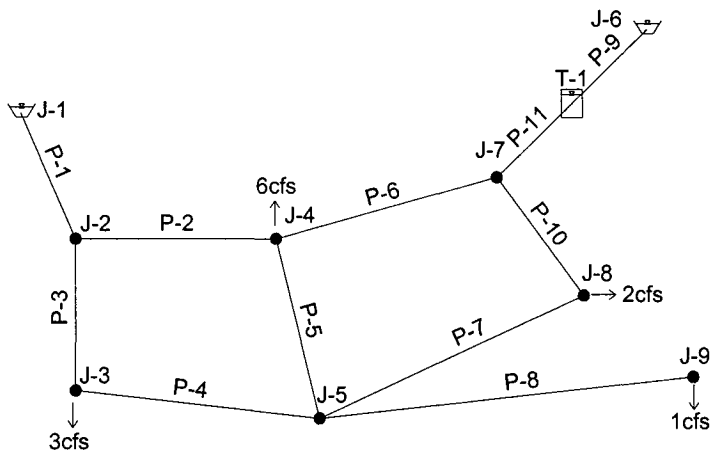

Figure 4.107 Sketch for small city network with a surge tank

Changing the hydraulic head of Reservoir #2 modifies pipe network. The hydraulic head of Reservoir #2 is changed like a sine wave for 32 seconds as shown Fig. 4.108. Because of this pressure wave of the Reservoir #2, pressure of the whole pipe network is responding

instantaneously. Fig. 4.108 shows the pressure fluctuation of Junction #4 and #5 with one-way surge tank. Fig. 4.109 also shows the pressure fluctuation of Junction #4 and #5 with two-way surge tank.

Fig. 4.110 shows the transient head fluctuation of one-way surge tank and two-way surge tank with the changing of the hydraulic head of Reservoir #2. The head of one-way surge tank only goes down, but the head of two-way surge tank goes up and down because two-way surge tank could release and also absorb the fluctuating pressures. For simulation shown in Fig. 4.110, one-way surge tank released $60ft^3$ of water since the head of one-way surge tank goes down 1ft and area of one-way surge tank is $60ft^2$.

Fig. 4.111 shows transient flow rate of Pipe #9, #11 and released from one-way surge tank. When the surge tank is installed in the middle of the Pipe #9, Pipe #9 is divided into Pipe #9 and Pipe #11 as shown Fig. 4.107. At the certain point of Fig. 4.111, flow rate of the Pipe #11 should be the same with that of the Pipe #9 added by the flow rate released from the surge tank. So continuity must be satisfied. Negative sign of flow rate means reverse flow. Fig. 4.112 shows transient flow rate of Pipe #9, #11 and released from two-way surge tank. After 40 seconds later, two-way surge tank is still releasing water, and the difference between flow rate of Pipe #9 and #11 should be the same amount of the flow rate released by two-way surge tank. At this time, the flow rate of two-way surge tank goes to the negative values and positive values. That means two-way surge tank could release the certain pressure and also absorb it. Fig. 4.113 shows how much surge tank could reduce the pressures. In this case, it is clear that two-way surge tank damp out the pressures very much but one-way surge tank appears to be not very effective. One-way surge tank is good enough when the pipe network needs to prevent column separation only which could be happening when power failure occurs in pump station. But if the pipe network requires energy

dissipation too, then two-way surge tank should be installed. Fig. 4.114 shows the simulation results for different cases. Now, the hydraulic head of Reservoir #2 is fluctuating quickly for 2 seconds as shown Fig. 4.114. In this case, obviously both one-way surge tank and two-way surge tank are effective in damping out the pressure. Fig. 4.115 shows the transient head fluctuation of one-way surge tank and two-way surge tank with changes of the hydraulic head in Reservoir #2. And Figs. 4.116 and Fig. 4.117 show the transient flow rate of Pipe #9, #11 and released from one-way surge tank and two-way surge tank with changes in the head of Reservoir #2. When the pipe network and external energy dissipaters are designed, they should be simulated with many possible scenarios.

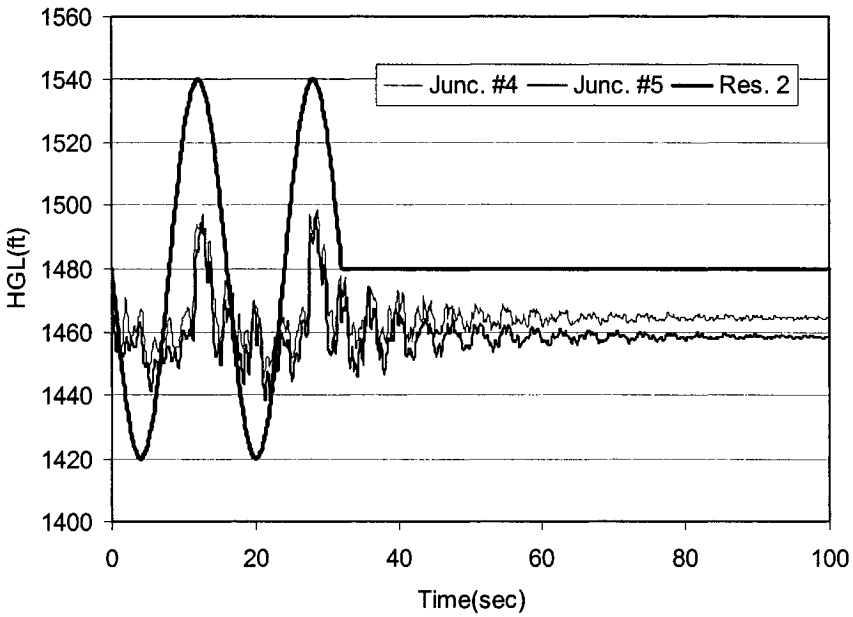

Figure 4.108 Hydraulic head fluctuation at Junction #4 and #5 with the changing hydraulic head of Reservoir #2 (System has one-way surge tank)

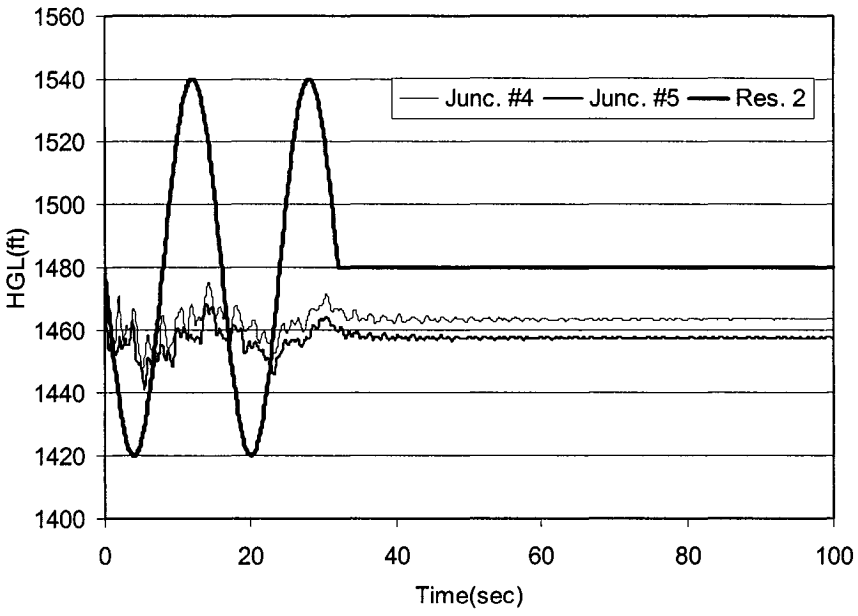

Figure 4.109 Hydraulic head fluctuation at Junction #4 and #5 with the changing hydraulic head of Reservoir #2 (System has two-way surge tank)

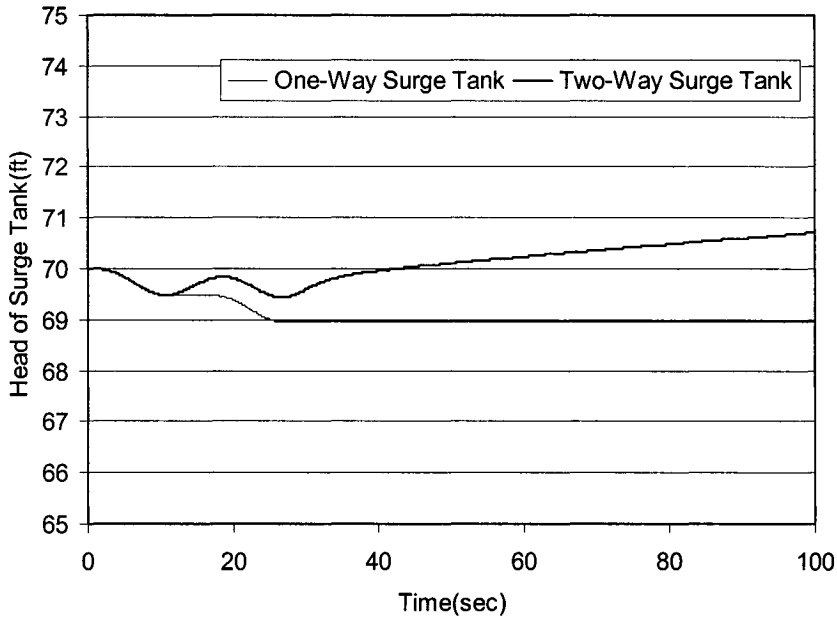

Figure 4.110 Hydraulic head fluctuation of one-way surge tank and two-way surge tank with the changing hydraulic head of Reservoir #2

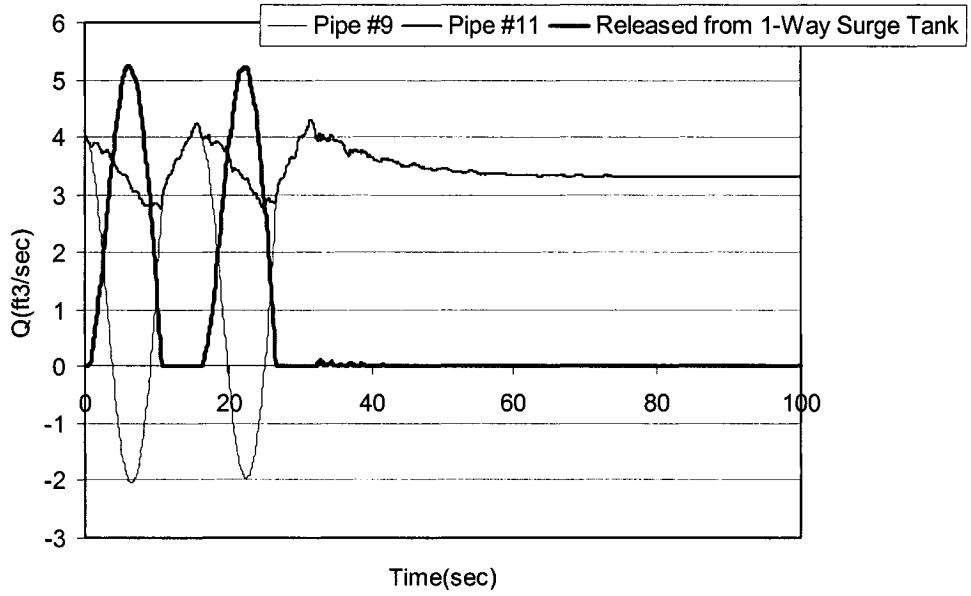

Figure 4.111 Transient flow rate with the changing hydraulic head of Reservoir #2 (System has one-way surge tank)

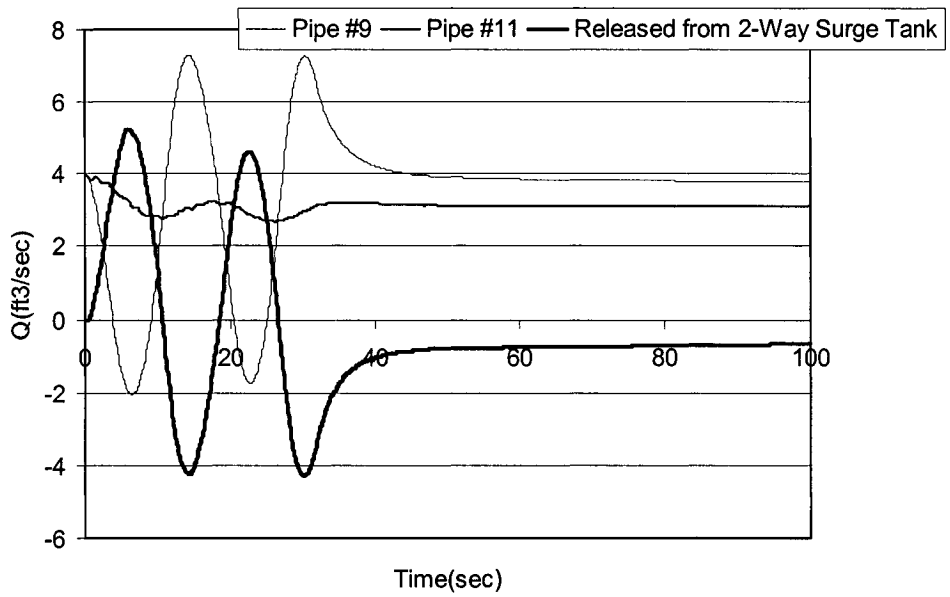

Figure 4.112 Transient flow rate with the changing hydraulic head of Reservoir #2 (System has two-way surge tank)

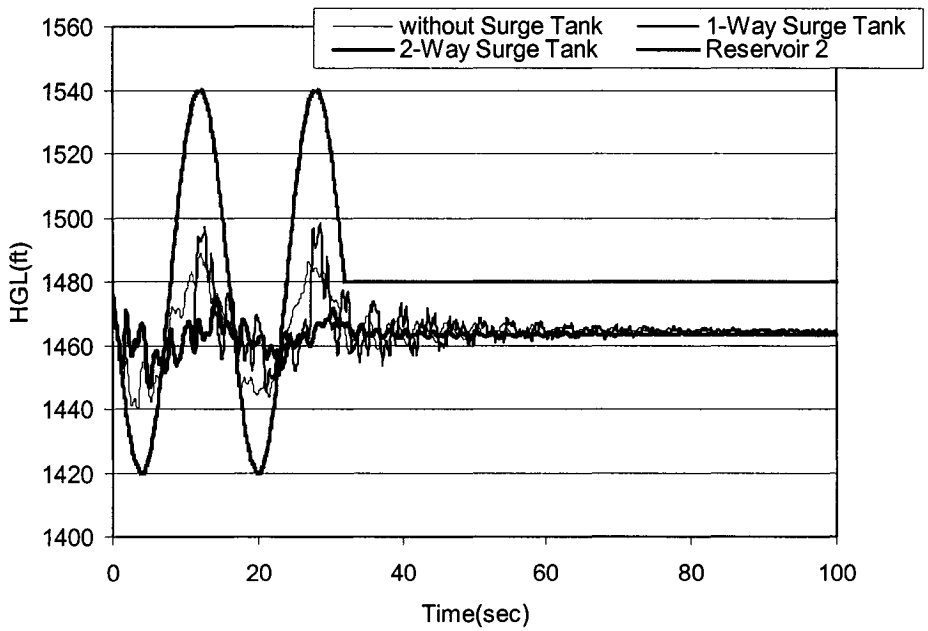

Figure 4.113 Comparison of hydraulic head fluctuation at Junction #4 showing the effect of surge tank with the changing hydraulic head of Reservoir #1

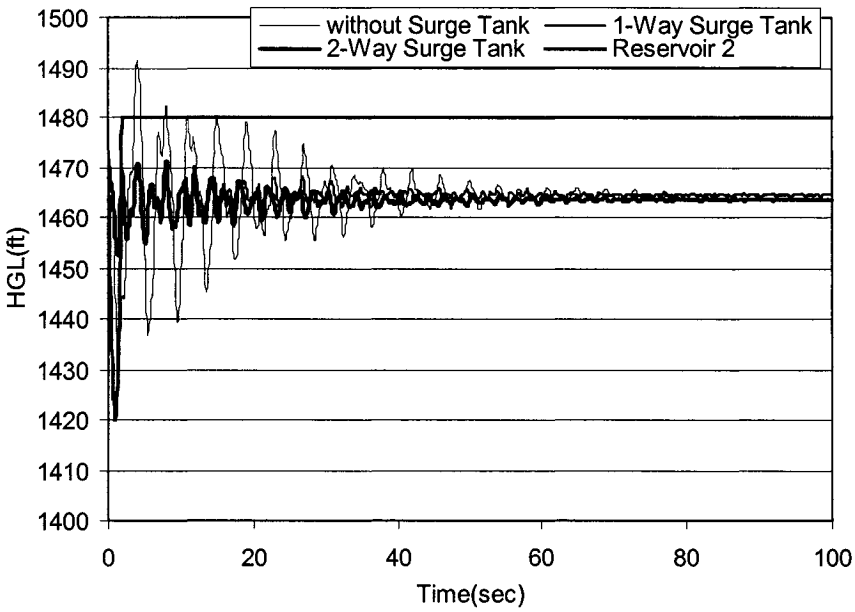

Figure 4.114 Comparison of hydraulic head fluctuation at Junction #4 showing the effect of surge tank with the changing hydraulic head of Reservoir #2

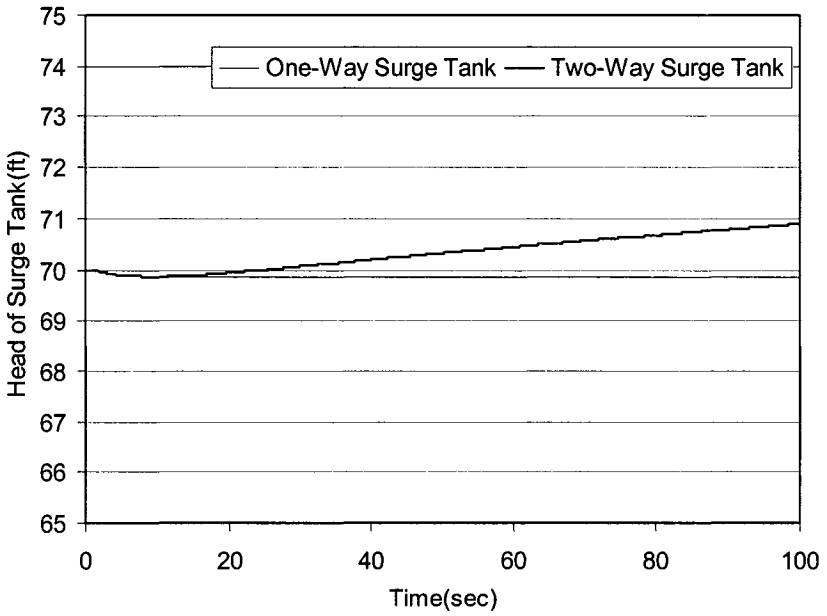

Figure 4.115 Hydraulic head fluctuation of one-way surge tank and two-way surge tank with the changing hydraulic head of Reservoir #2

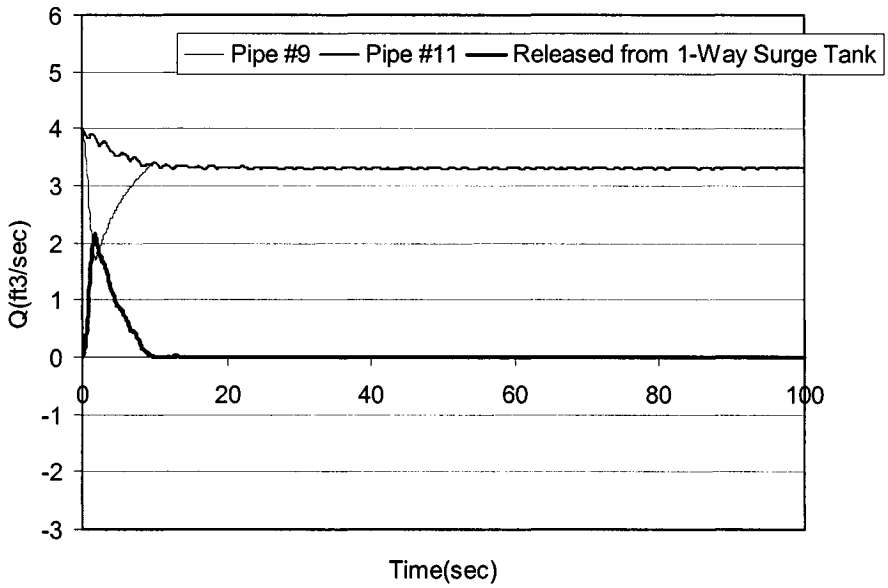

Figure 4.116 Transient flow rate with the changing hydraulic head of Reservoir #2 (System has one-way surge tank)

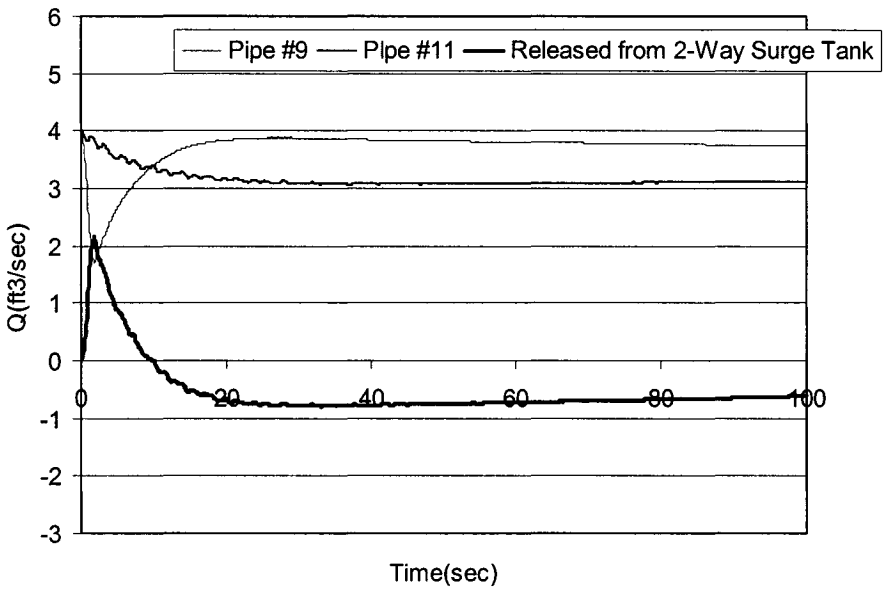

Figure 4.117 Transient flow rate with the changing hydraulic head of Reservoir #2 (System has two-way surge tank)

4.6.5 Model City B (Medium Sized City Network System)

The medium sized city network system chosen for present study consists 252 junctions and 371 pipes. Two pump stations and a reservoir supply 36cfs of flow rate the piping network. Most of the junctions are demands that take flow from the system. Three different simulation conditions are conducted for the present study. Portion of the piping network is shown in Fig. 4.118.

(1) Simulation No. 1 (Model City B)

For the transient flow, it is assumed that a hydrant at Junction #201 opened in two seconds creating a sudden demand of 1121gpm at this location. Figs. 4.118 and 4.119 show the schematics of the part of the system in the immediate vicinity of Junction #201 before and after the hydrant at Junction #201 opens.

The transient flows generated by the opening of the hydrant at Junction #201 are quite dramatic as shown in Fig. 4.120. It shows that the pressure head time history at three Junctions: Junction #125, #200, and #10. The location of Junction #200 is approximately 1200ft from the hydrant. In reviewing Fig. 4.120, it is seen that the pressure head at Junction #200 initially drops 80ft, from 140ft to 60ft, and subsequently drops down to 20ft level. At Junction #125 (which is located near the upper right corner in Fig. 4.118), the magnitude of the pressure drop is smaller but still quite dramatic, dropping from around 180ft to 120ft before it recovers gradually.

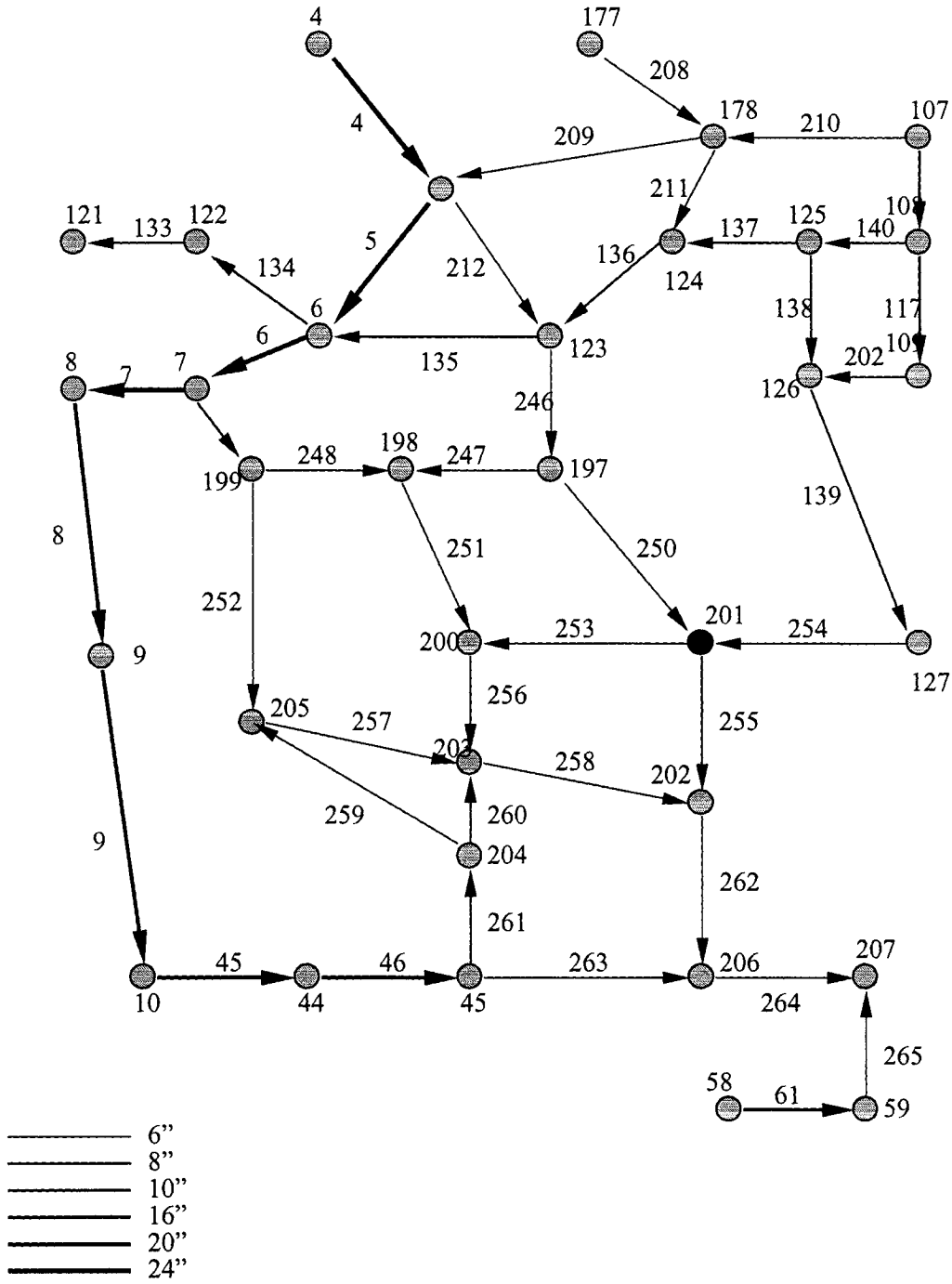

Figure 4.118 Schematic of junctions and pipes in the vicinity of Junction #201 before hydrant opens (Model City B)

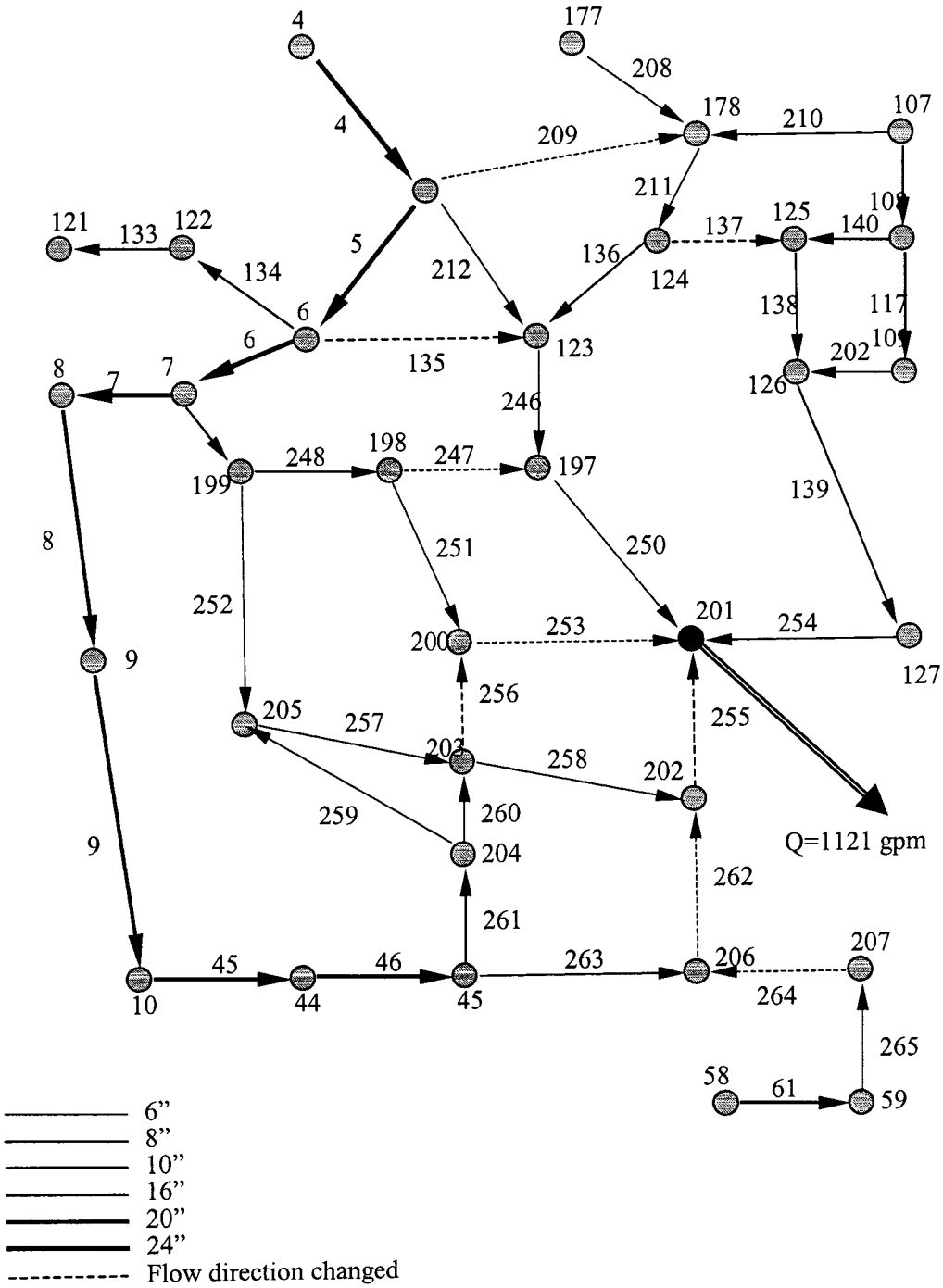

Figure 4.119 Schematic of junctions and pipes in the vicinity of Junction #201 after hydrant opens (Model City B)

At Junction #10 (located near the lower left corner shown in Fig. 4.118) which is fairly well isolated from the hydrant location, a gradually pressure drop of approximately 20ft is experienced. From Fig. 4.120, it is seen that the pressure changes are more immediate and the most dramatic for location closer to the location of the opening hydrant. At location further away, the transient conditions are felt at a later time and less dramatic. These results clearly indicate that a sudden change of demand, such as the opening of a fire hydrant, can have significant effect on the flow and pressure in distribution system. Cross-connection control becomes more important for safe guarding the potable water in the distribution system whenever such sudden demand change may occur. Sudden pressure drop of such magnitude can cause backflows and if cross-connection exists it can certainly create undesirable consequences, capable of compromising the integrity of the potable water system. Similar results of pressure at Junction #6, #205, and #203 are presented in Fig. 4.121. The pressure drops at Junction #205 and #203 are quite drastic as they are located closer to the open hydrant location. The pressure drop at Junction #6 (which is located further away from Junction #201) is noticeable but not quite drastic. The dramatic changes in flows at some of the pipes caused by the opening of hydrant at Junction #201 are shown in Figs. 4.122 and 4.123. From Fig. 4.122, it is seen that the flow in Pipe #253 (connecting Junction #200 and #201) reverses very dramatically almost immediately after the hydrant begins to open. In examining Fig. 4.123, it is seen that the flow at Pipe #46 (located near the lower left corner in Fig. 4.118) increases dramatically in order to meet the sudden change in demand at Junction #201.

(2) Simulation No. 2 (Model City B)

In order to examine the effect of changes in ground elevation on the transient pressure in the pipes and junctions, Simulation No. 2 of Model City B was performed. Simulation No. 2 is performed with a minor modification of ground elevation at three locations (as compared to Simulation No. 1) as shown in Table 4.11.

Table 4.11 Ground elevation at three different locations

Junction No.	Ground Elevation (ft) at Simulation no. 1	Ground Elevation (ft) at Simulation no. 2
198	96.0	110.9
201	96.4	90.4
203	96.9	110.0

Thus, the difference between Simulation No. 1 and Simulation No. 2 is that the ground elevation at the neighboring area of hydrant at Junction #201 is modified. All other conditions remain the same.

Fig. 4.124 shows the transient pressure fluctuation at Junction #125, #200, and #10 for Simulation No. 2. The total pressure head drop is more than 120ft; moreover, the low pressure at the trough point is at the undesirable -20ft (pulling a vacuum). By comparing Fig. 4.124 with Fig. 4.120, one finds that the general pattern of the pressure fluctuation at the three respective locations is quite similar. The absolute value at Junction #200 is different and that the negative pressure exists for Simulation No. 2 (Fig. 4.124) but not for Simulation No. 1. This demonstrates that variations on ground level can produce negative pressure below atmospheric pressure when drastic demand change at certain location occurs.

Fig. 4.125 presents the transient pressure fluctuation at Junction #6, #205, and #203 (Model City B, Simulation No. 2). The dramatic changes in pressure head are evident for Junction #205 and #203 although, at the low pressure point the pressure heads at both locations are still positive. By comparing the results in Fig. 4.125 with that in Fig. 4.121, one sees that the general pressure pattern is quite similar in each of the respective three locations but the absolute value is different.

Fig. 4.126 shows the transient flow rate at Pipe #253 and #137. Flow at Pipe #253 reverses quickly to meet the change in demand as a result of the hydrant opening at Junction #201. Again the general pattern is similar to that shown in Fig. 4.122. A similar curve for Pipe #46, #209, and #264 is shown in Fig. 4.127 showing similar trend as that presented in Fig. 4.123. The result of Simulation No. 2 (allowing more variation of ground elevations) shows that the transient pressure can reach the undesirable negative pressure range easily when the hydrant opens suddenly. Such undesirable low-pressure condition can cause back flow and backsiphonage, thus, worsen the cross-connection problems.

(3) Simulation No. 3 (Model City B)

Another simulation for Model City B is conducted for Simulation No. 3. In this simulation, the hydrant at Junction #201 is assumed to open in 5 seconds. Thus, the only difference between Simulation No. 2 and Simulation No. 3 is that in Simulation No. 2 the hydrant opens in 2 seconds, but in the Simulation No. 3 hydrant opens in 5 seconds. This simulation is to ascertain the effect of slower opening of the hydrant. Fig. 4.128 presents the pressure fluctuation at Junction #125, #200, and #10 when the hydrant at Junction #201 opens in 5 seconds. From Fig. 4.128, it is seen that the pressure drop at Junction #200 is somewhat

lessen and that the low pressure point does not reach the negative value when compares with Fig. 4.124. Fig. 4.129 shows the pressure at Junction #6, #205, and #203. Again, the low pressure point does not reach the level shown in Fig. 4.125 confirming the slower hydrant-opening rate does lessen the dramatic pressure drop even though the general pattern is quite similar. Figs. 4.130 and 4.131 show the discharge rate at five pipes when the hydrant opens in 5 seconds. Results shown in these figures confirm that the slower hydrant-opening rate will lessen the impact of hydraulic transient (pressure and discharge) caused by the sudden changes in demand such as opening the hydrant.

Comparison of pressure head fluctuation at three junctions: Junction #200, #205, and #202 for different hydrant opening rate (2 sec. vs. 5 sec.) are presented in Figs. 4.132, 4.133, and 4.134 respectively. By reviewing these results, it is clear that when hydrant opens in 5 seconds the resulting transient flow at the vicinity of the open hydrant will cause a larger reduction in pressure. In some situation, such as that at Junction #200, negative pressure is evident.

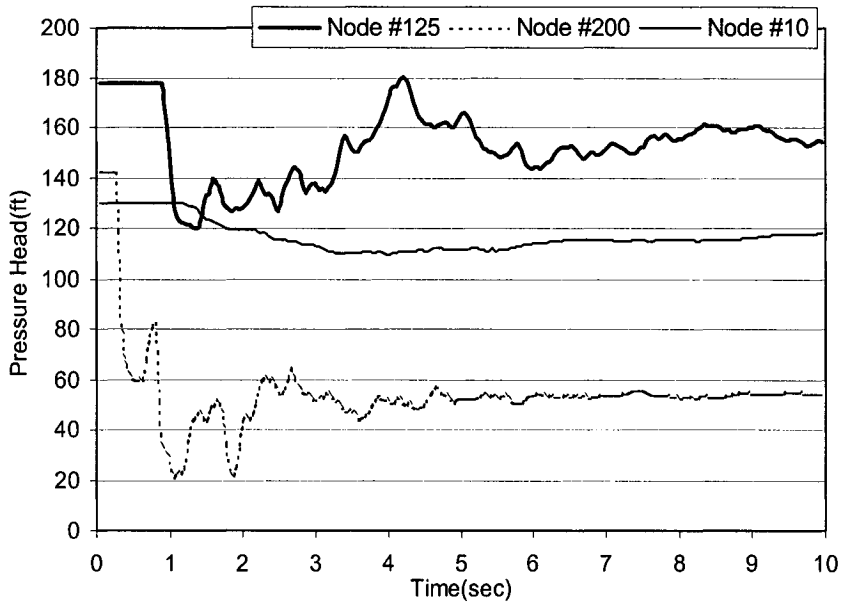

Figure 4.120 Transient pressure fluctuation at Junction #125, #200, and #10 (Model City B, Simulation No. 1)

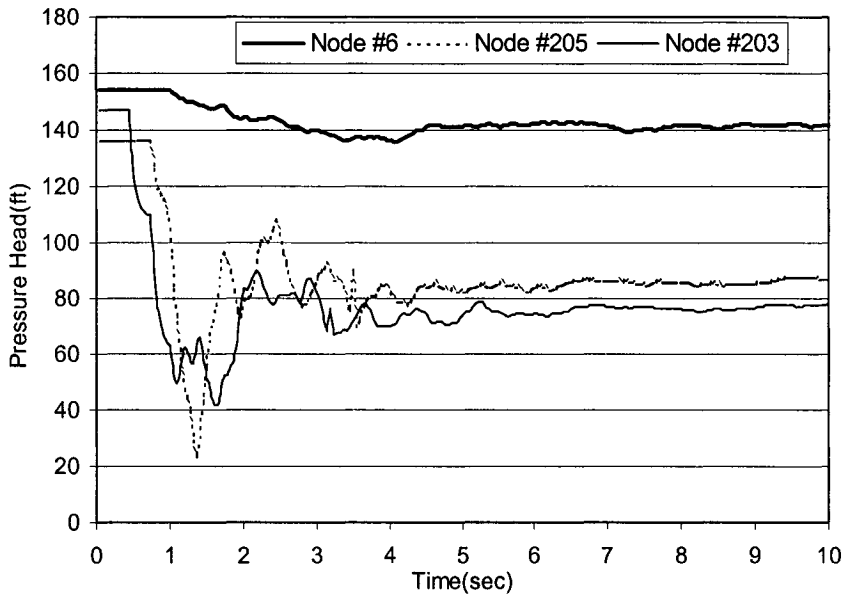

Figure 4.121 Transient pressure fluctuation at Junction #6, #205, and #203 (Model City B, Simulation No. 1)

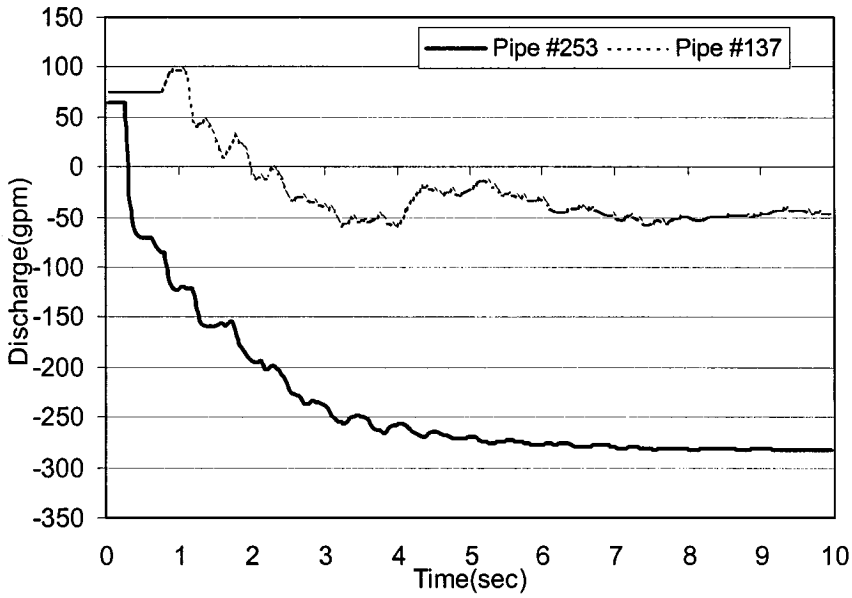

Figure 4.122 Transient flow rate at Pipe #253 and #137 (Model City B, Simulation No. 1)

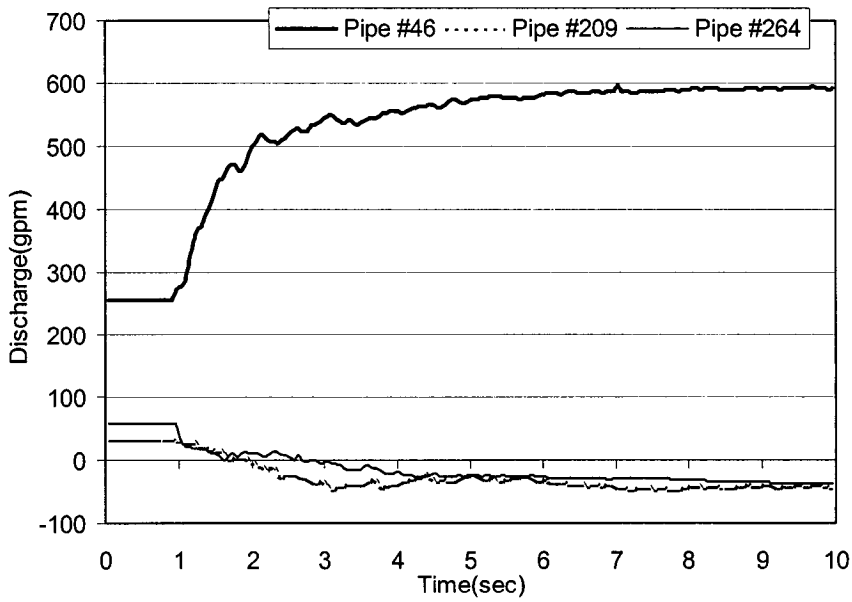

Figure 4.123 Transient flow rate at Pipe #46, #209, and #264 (Model City B, Simulation No. 1)

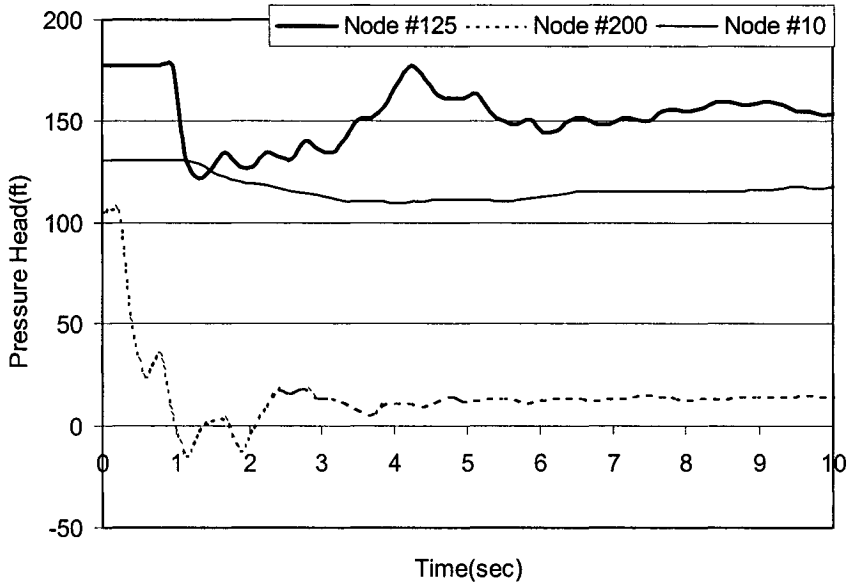

Figure 4.124 Transient pressure fluctuation at Junction #125, #200, and #10 (Model City B, Simulation No. 2, hydrant opens in 2 seconds)

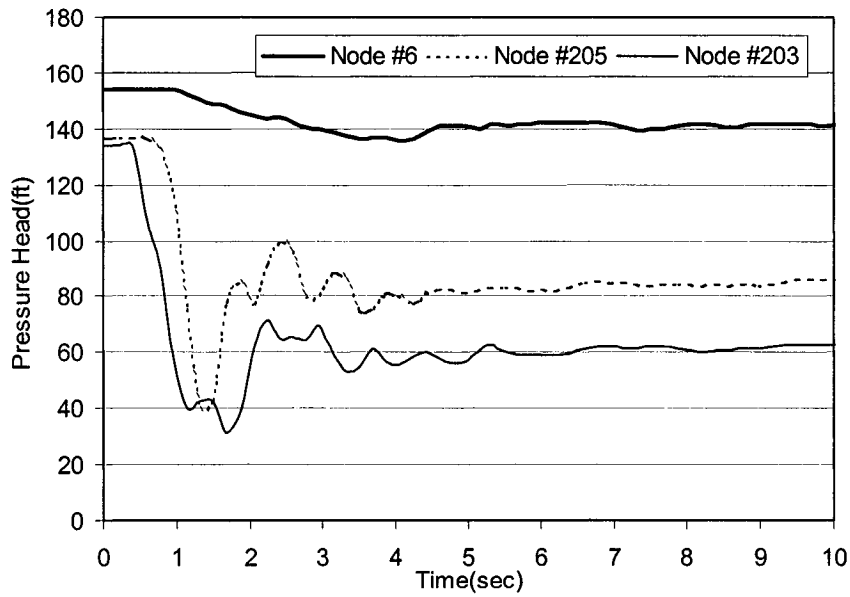

Figure 4.125 Transient pressure fluctuation at Junction #6, #205, and #203 (Model City B, Simulation No. 2, hydrant opens in 2 seconds)

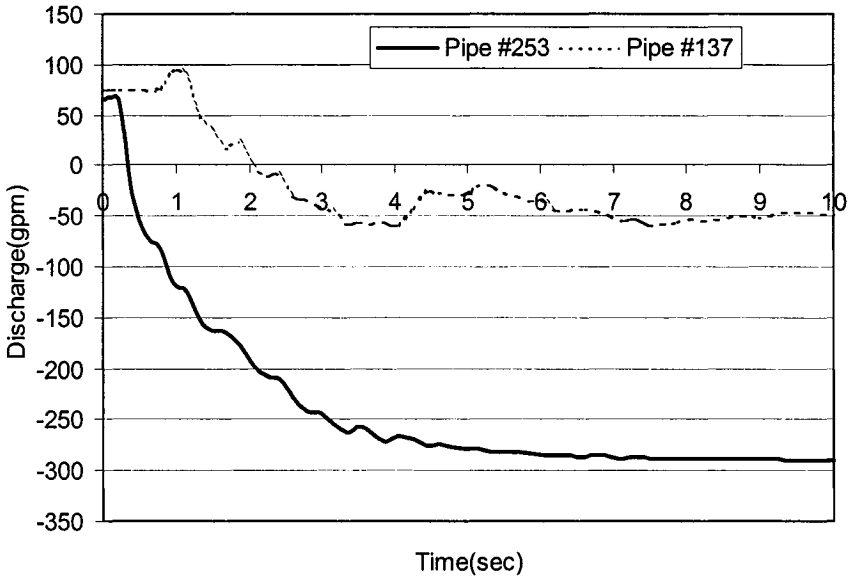

Figure 4.126 Transient flow rate at Pipe #253 and #137 (Model City B, Simulation No. 2, hydrant opens in 2 seconds)

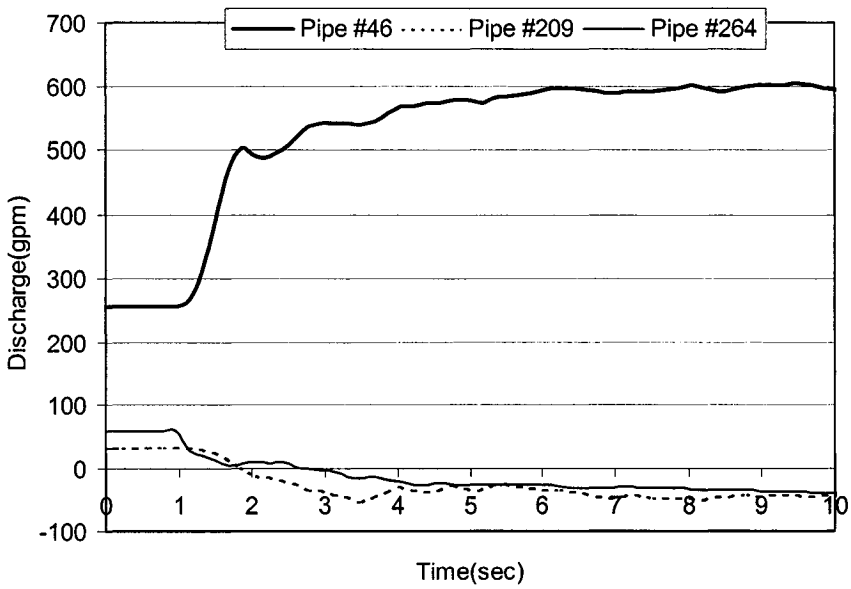

Figure 4.127 Transient flow rate at Pipe #46, #209, and #264 (Model City B, Simulation No. 2, hydrant opens in 2 seconds)

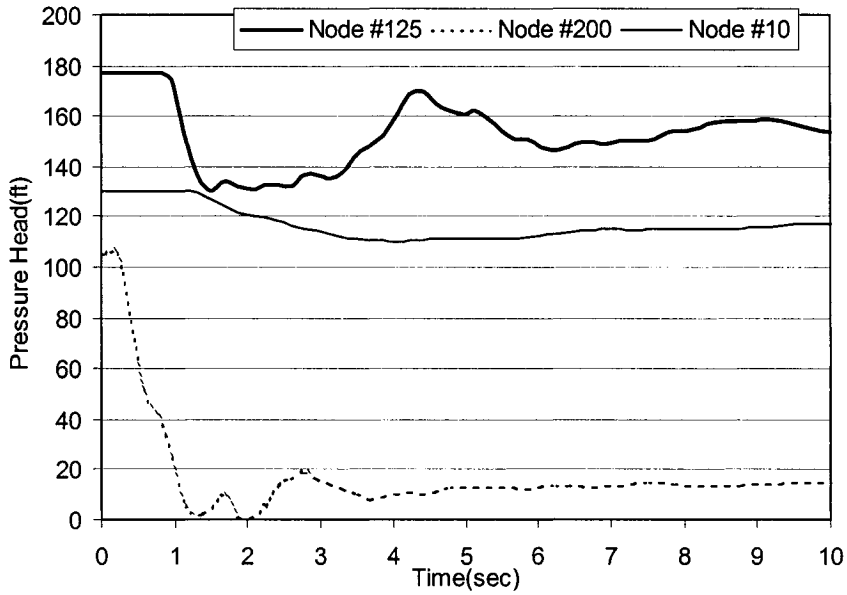

Figure 4.128 Transient pressure fluctuation at Junction #125, #200, and #10 (Model City B, Simulation No. 3, hydrant opens in 5 seconds)

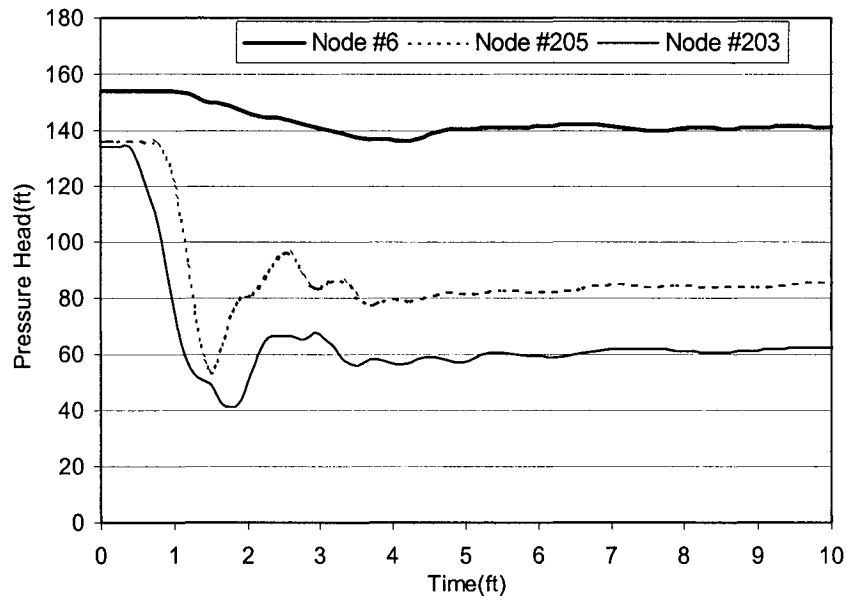

Figure 4.129 Transient pressure fluctuation at Junction #6, #205, and #203 (Model City B, Simulation No. 3, hydrant opens in 5 seconds)

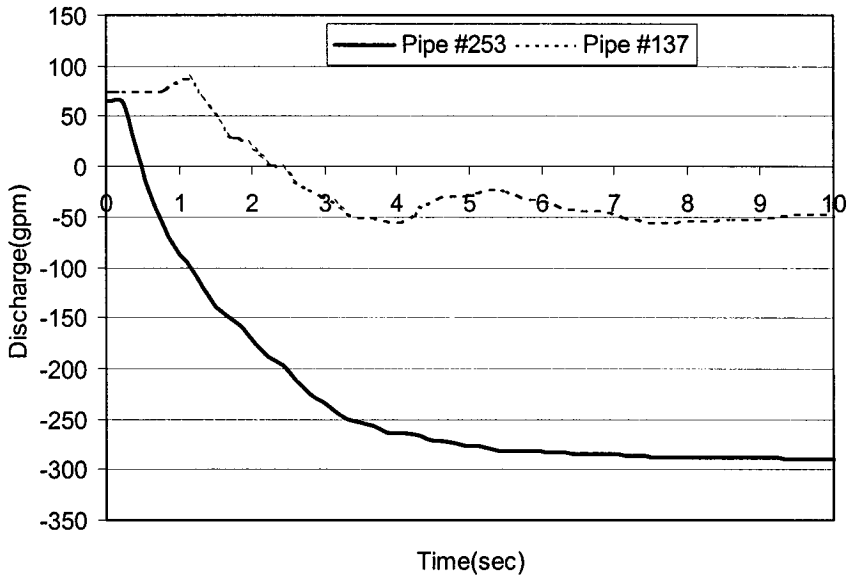

Figure 4.130 Transient flow rate at Pipe #253 and #137 (Model City B, Simulation No. 3, hydrant opens in 5 seconds)

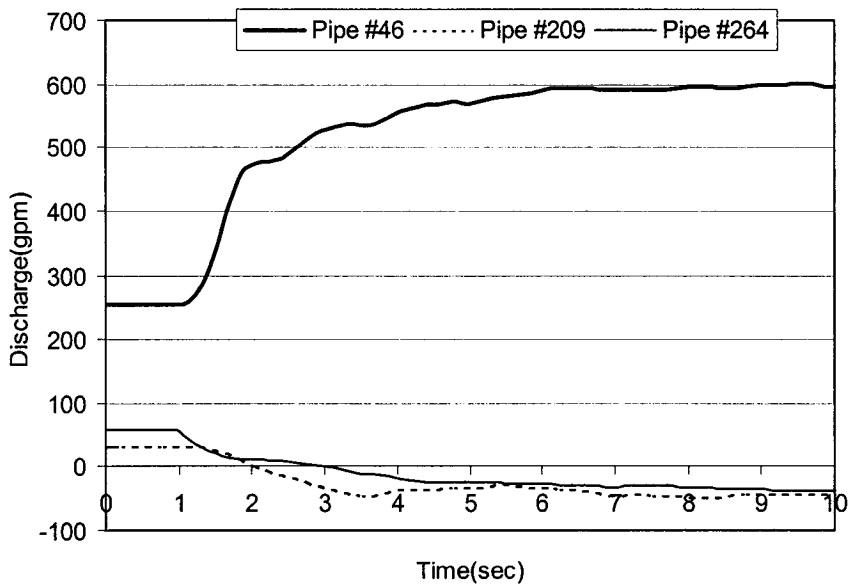

Figure 4.131 Transient flow rate at Pipe #46, #209, and #264 (Model City B, Simulation No. 3, hydrant opens in 5 seconds)

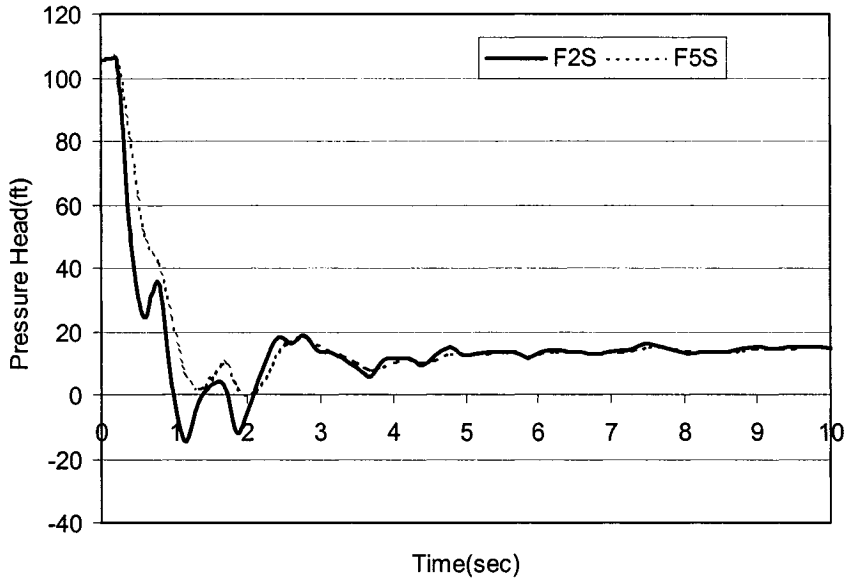

Figure 4.132 Comparison of pressure head at Junction #200 for different hydrant opening rate (2sec vs. 5sec)

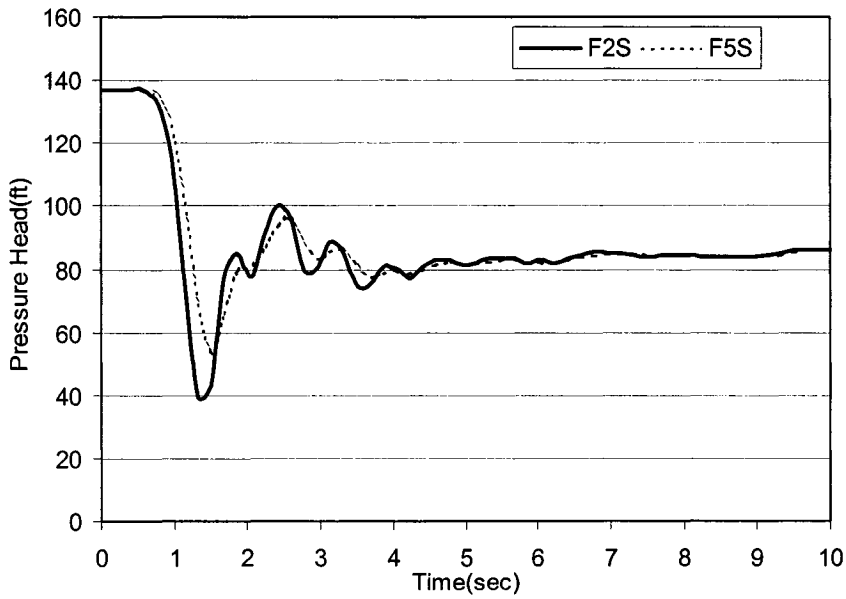

Figure 4.133 Comparison of pressure head at Junction #205 for different hydrant opening rate (2sec vs. 5sec)

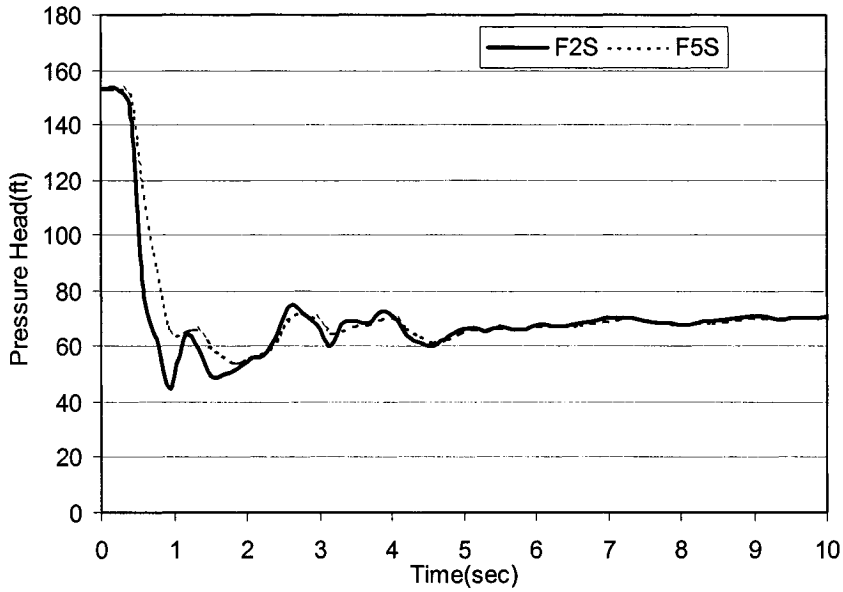

Figure 4.134 Comparison of pressure head at Junction #202 for different hydrant opening rate (2sec vs. 5sec)

4.6.6 Model City A (Large Sized City Network System)

The large sized city network system chosen for present study consists of 231 junctions and 321 pipes. A pump station located at a water treatment plant that delivers 236cfs to meet the system demands and six storage reservoirs supplies and regulates the flow in the system. Most of the junctions identified in the system are demands that take flow from the system. Figs. 4.135 and 4.136 show the schematics of a part of the system in the immediate vicinity of Junction #181 before and after the hydrant at Junction #181 opens. This large network system is larger than the medium-sized system (Model City B). Pipes in this system are bigger and distance between Junctions (pipe length) is longer.

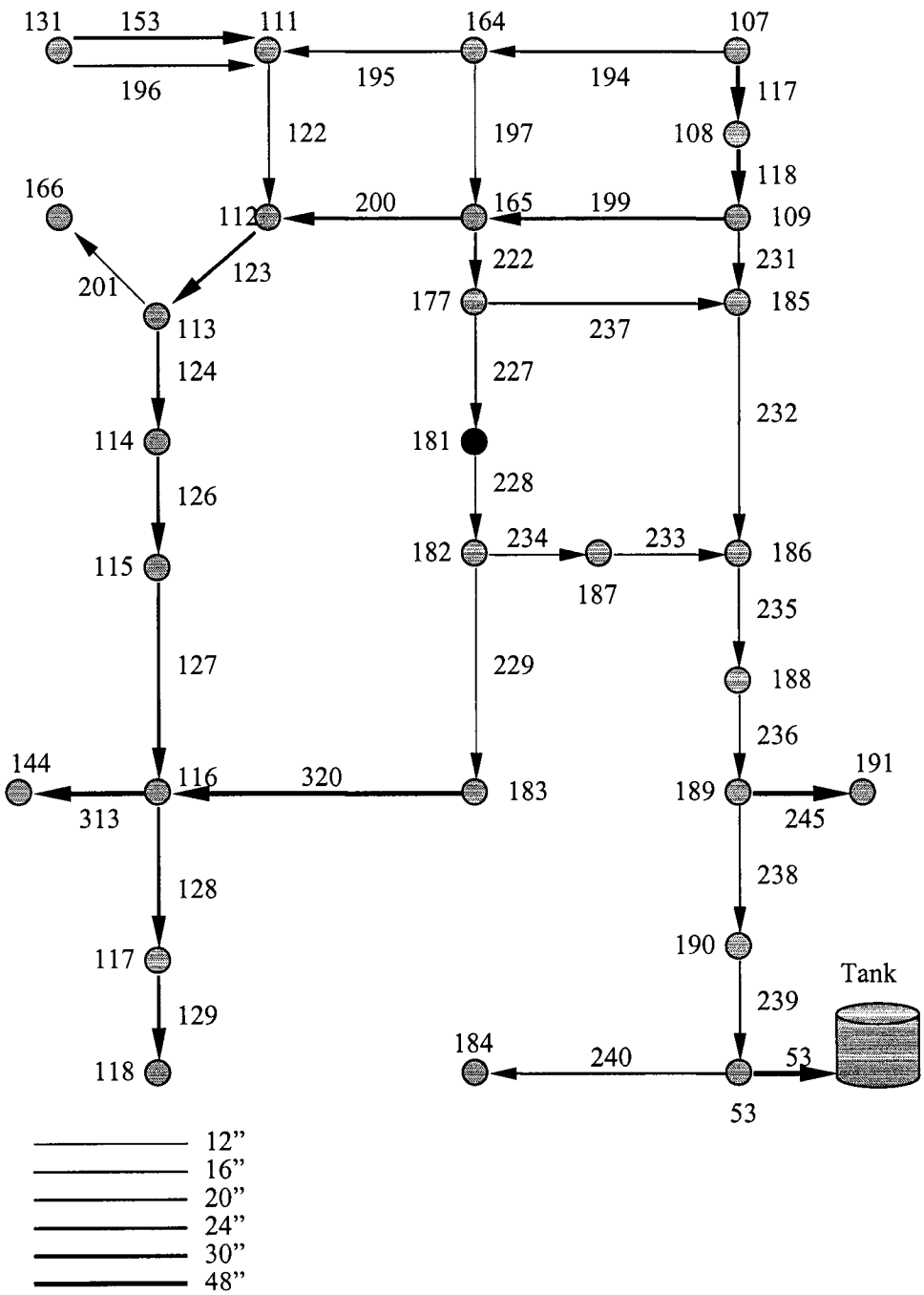

Figure 4.135 Schematic of junctions and pipes in the vicinity of Junction #181 before hydrant opens (Model City A)

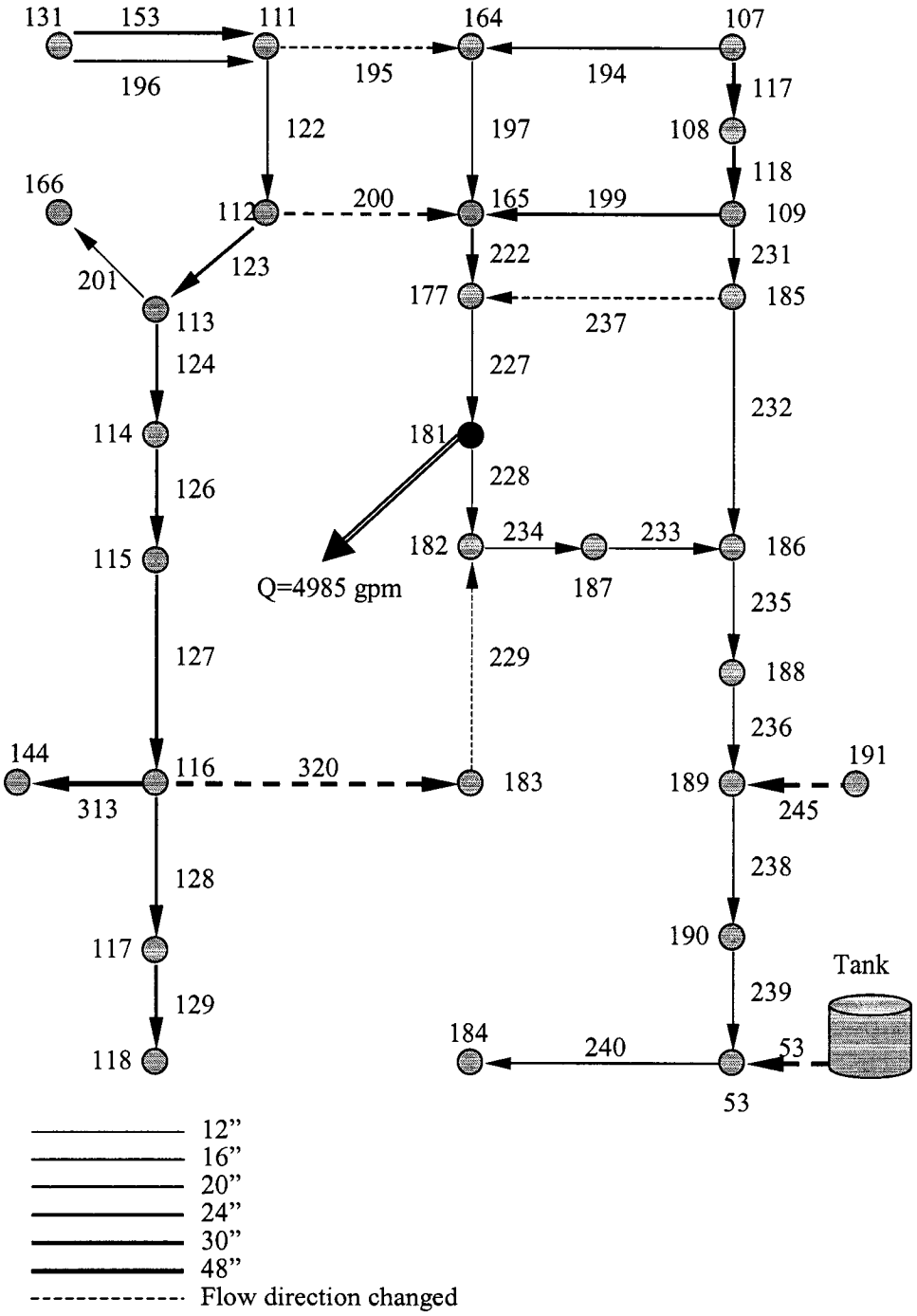

Figure 4.136 Schematic of junctions and pipes in the vicinity of Junction #181 after hydrant opens (Model City A)

(1) Simulation No. 1 (Model City A)

For the transient analysis, it was assumed that a hydrant at Junction #181 opened in 2 seconds (Simulation No. 1), creating a sudden demand of 4985gpm at this location. Because of the large-sized pipelines in this model, the flow was limited to this amount instead of assuming a full capacity opening which would result in flows in excess of 11,000gpm. The sudden demand caused by the opening of hydrant at Junction #181 caused many flow reversals in the system. The dash lines in Fig. 4.136 for those junctions contained in Fig. 4.135 indicate the pipes experiencing the flow reversal. Some of these flow reversal occur at location quite a distance from Junction #181. From Fig. 4.136, it is seen that one of the pipeline flow reversals occurs on the line to a reservoir and another occurs in a 48-inch diameter pipe. Four different simulation runs are conducted for this large network system (Model City A). The results indicated in Fig. 4.136 are from Simulation No. 1. The hydrant opens at Junction #181 is completed in 2 seconds with the flow at 4985gpm. Fig. 4.137 presents the transient pressure fluctuation at Junction #177, #111, and #116 showing the transient effect at locations with different distances from the open hydrant. At Junction #177, located 600ft from the hydrant, the computed pressure will drop below atmospheric pressure for a brief instant with an overall pressure drop of 125ft. At Junction #111, some distance away from the hydrant location, the pressure fluctuation is less dramatic, as would be expected, but are still significant. At Junction #116, further away from the hydrant location the magnitude of fluctuating pressure is smaller, but cannot be ignored. These pressure fluctuations clearly indicate that a sudden demand, such as the opening of a fire hydrant, can have far reaching effects on the distribution system, similar to the case with medium sized system discussed in the previous section. Transient pressure fluctuation at three other

locations, Junction #190, #182, and #107 is presented in Fig. 4.138. The pressure at Junction #182 is expected to drop over 90ft although it does not drop below atmospheric pressure. The locations in these figures are chosen with different distance from the open hydrant, which can be clearly shown. The transient flow rate at Pipe #237, #195, and #320 is presented in Fig. 4.139. It is seen that in all of these three pipes there are flow reversal due to the open hydrant at Junction #181. The flow rate fluctuation at three other pipes (Pipe #201, #233, and #245) is shown in Fig. 4.140 showing the varying degree of impact on the flow rate depending on the distance away from the open hydrant location.

(2) Simulation No. 2 (Model City A)

For Simulation No. 2 in Model City A (Large Sized System), the elevation at Junction #177 is raised by 20ft to 750ft. All other parameters are the same as in Simulation No. 1: The hydrant opening time is also assumed to be two seconds. The pressure fluctuation at Junction #177, #111, and #116 is presented in Fig. 4.141. The low pressure point at Junction #177 clearly drops below atmospheric pressure, until it gradually recovers after three second. Thus, the results clearly show that the pressure drops at locations close to the open hydrant are very dramatic. Whether it will drop below atmospheric pressure (pulling vacuum) will certainly depend on the elevation of the junction. Sudden drop of pressure, especially dropping below atmospheric pressure will be a serious problem if direct or in-direct cross-connection exists. The example shown so far does indicate the real potential for adverse effect. Pressure fluctuation at three other locations (Junction #190, #182, and #107) is shown in Fig. 4.142. The flow rate fluctuations at six pipelines are presented in Figs. 4.143 and 4.144. The impact on Pipe #237 is quite dramatic as can be seen in Fig. 4.143. Before the

transient analysis begins, the discharge of nearly +700gpm is flowing in Pipe #237. As soon as the hydrant open for 2 seconds, the flow in Pipe #237 quickly reverse and reaches a level of –200gpm before the oscillations set in for many cycles. Flows in Pipe #320 experiences similar pattern as well.

(3) Simulation No. 3 (Model City A)

Changing the hydrant opening time from 2 seconds to 5 seconds performs this simulation. Thus, the only difference between Simulation No. 3 and Simulation No. 2 is the hydrant opening time. The four corresponding curves on pressures and flow rates are presented in Figs. 4.145 to 4.148. Looking at Fig. 4.145, the drop in pressure at Junction #177 is not as rapid as that shown in Fig. 4.141, the low pressure point is just barely touching the atmospheric pressure. Therefore, by increasing the hydrant opening time, it goes a long way to lessen the impact of the resulting hydraulic transients caused by the changing in demands at the certain junctions. The same observation can also be made by comparing Fig. 4.146 with 4.142, Fig. 4.147 with 4.143, and Fig. 4.148 with Fig. 4.144. The longer hydrant opening time will greatly lessen the impact of the sudden change in pressure and flow.

(4) Simulation No. 4 (Model City A)

This simulation is performed by raising the water level 60ft from 817ft to 877ft at the reservoir of tank 52. Elevation at Junction #177 is set at 750ft (the same as in Simulation No. 2) and the hydrant opens in 2 seconds. Thus, the only difference between Simulation No. 4 and Simulation No. 2 is that the water level at reservoir is raised by 60ft. The corresponding curves for pressure and flow rate are presented in Figs. 4.149 to 4.151. Looking at Fig. 4.149,

it is seen that the pressure drop at Junction #177 does not reach the low point shown in Fig. 4.141, even though it also drops below atmospheric pressure. From Fig. 4.150, the total pressure drop at Junction #182 is approximately 100ft, but because the initial value is now at 120ft, the low pressure point is at 20ft, not as low as that shown in Fig. 4.142 (which is approximately 8ft). Similar impact can also be seen in Fig. 4.151 when one compares the flow rate time history with those shown in Fig. 4.143. Thus, the higher reservoir water level, the less possibility of developing a vacuum conditions at low pressure point.

From the results presented earlier, it is noted that slower opening rate of hydrant will lessen the impact of the drastic hydraulic transient phenomena. In order to demonstrate this more clearly, the results on pressure drop in some key locations are presented for direct comparison. Fig. 4.152 presents the comparison of pressure head at Junction #177 for two different hydrant opening rate: 2sec vs. 5sec. From the curves presented, it is clearly seen that for the case of 2 seconds hydrant opening the initial pressure drop occurs swiftly to the level below the atmospheric pressure. For the 5 second opening, the pressure drop is more moderate and it stops near the atmospheric pressure level. Again, this sharp and drastic pressure drop can induce backflow and bring about serious cross-connection related problem into a water distribution system. Similar comparison of pressure drop is presented in Fig. 4.153 for Junction #182. Again, the initial pressure drop at Junction #182 is drastic and swift for 2-second hydrant opening while the drop in 5–second opening is more moderate. The impact on raising the water level at the reservoir is shown in Fig. 4.154 for Junction #177. The solid black line shows the result of pressure history at Junction #177 when the open hydrant is accomplished in 2 seconds. The dashed line shows the result of raising the reservoir water level by 60ft, with the same 2-second opening time for the hydrant. It is seen, from these two curves, that the pressure history follows the same pattern with the elevated

water level contributing to uniform increase in the pressure level at Junction #177. Fig. 4.155 shows the similar comparison at Junction #182. Again, the elevated water level at Tank 52 contributes to the general increase in the pressure level and that the same trend is followed for both cases.

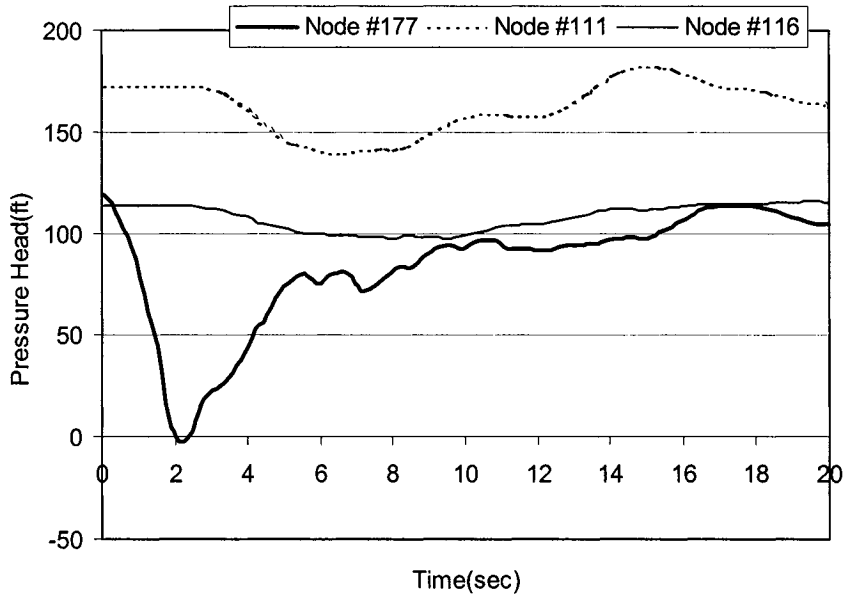

Figure 4.137 Transient pressure fluctuation at Junction #177, #111, and #116 (Model City A, Simulation No. 1, hydrant opens in 2 seconds)

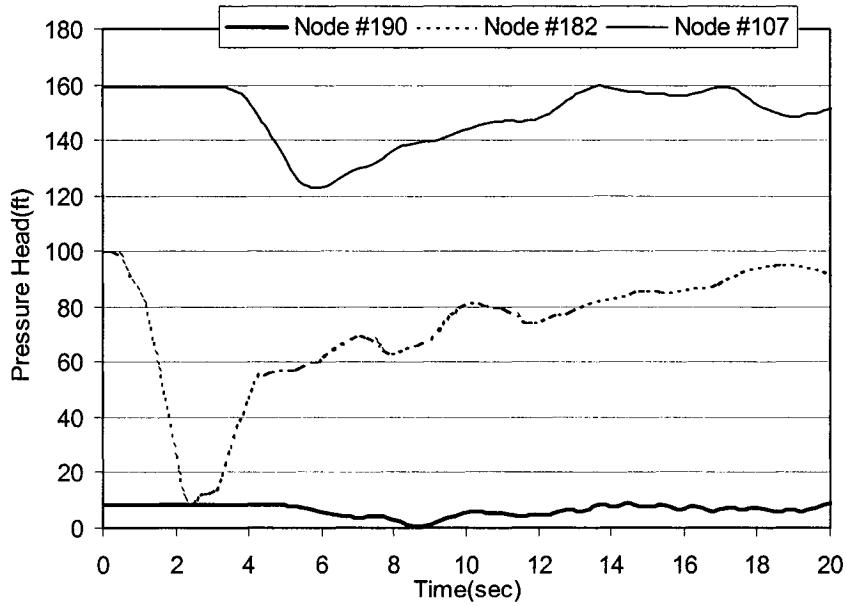

Figure 4.138 Transient pressure fluctuation at Junction #190, #182, and #107 (Model City A, Simulation No. 1, hydrant opens in 2 seconds)

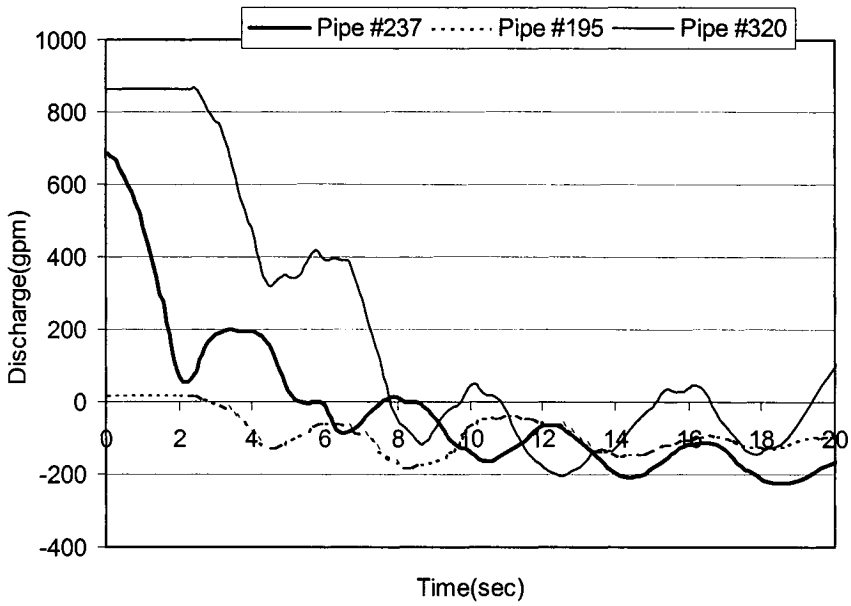

Figure 4.139 Transient flow rate at Pipe #237, #195, and #320 (Model City A, Simulation No. 1, hydrant opens in 2 seconds)

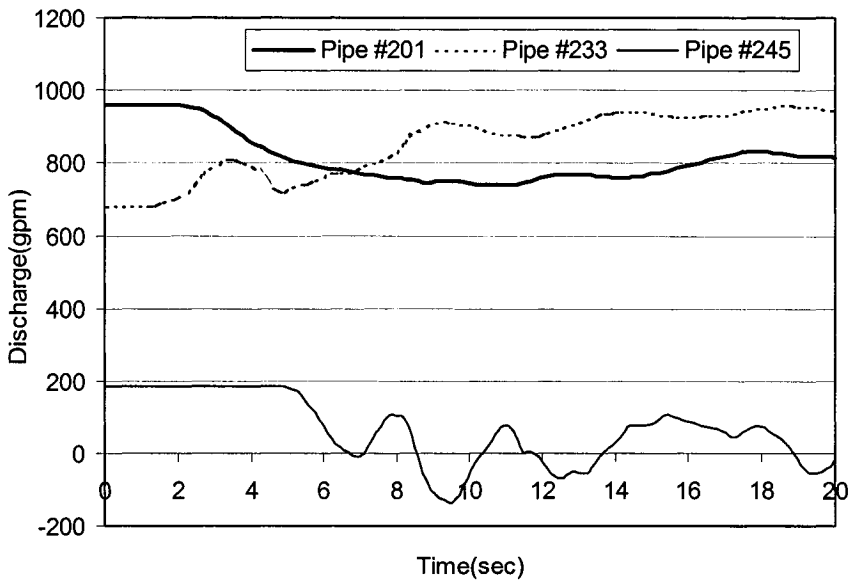

Figure 4.140 Transient flow rate at Pipe #201, #233, and #245 (Model City A, Simulation No. 1, hydrant opens in 2 seconds)

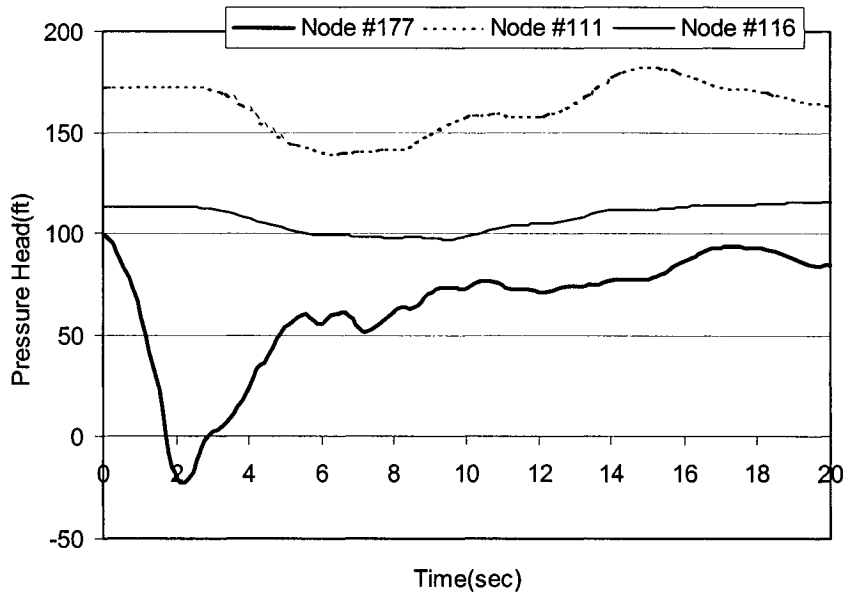

Figure 4.141 Transient pressure fluctuation at Junction #177, #111, and #116 (Model City A, Simulation No. 2, hydrant opens in 2 seconds)

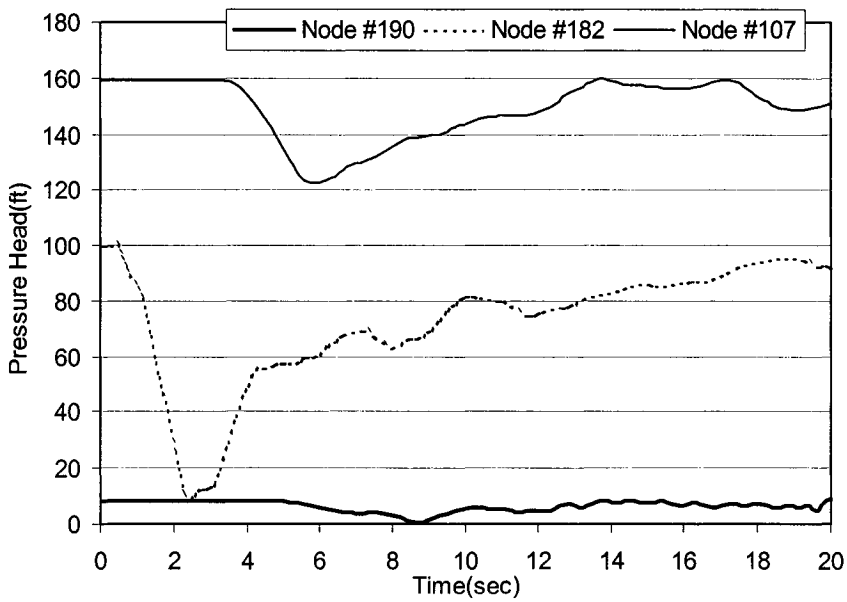

Figure 4.142 Transient pressure fluctuation at Junction #190, #182, and #107 (Model City A, Simulation No. 2, hydrant opens in 2 seconds)

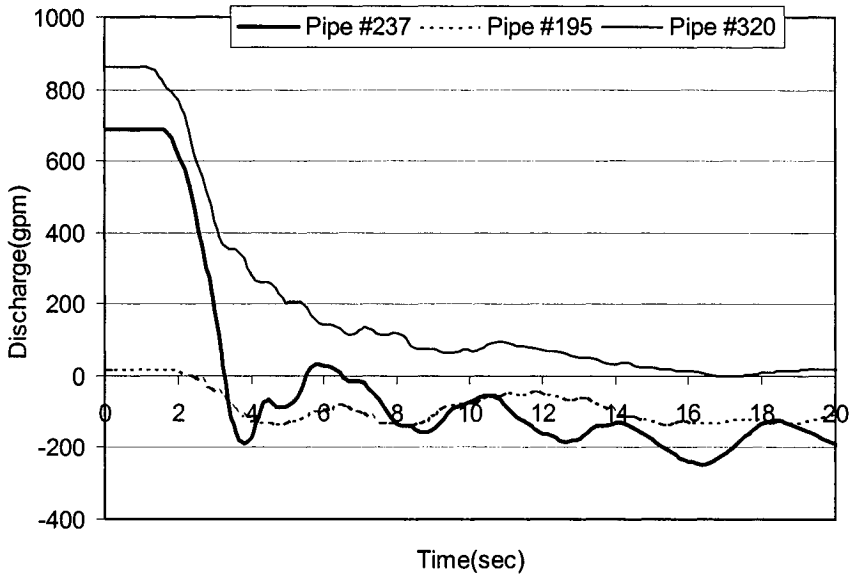

Figure 4.143 Transient flow rate at Pipe #237, #195, and #320 (Model City A, Simulation No. 2, hydrant opens in 2 seconds)

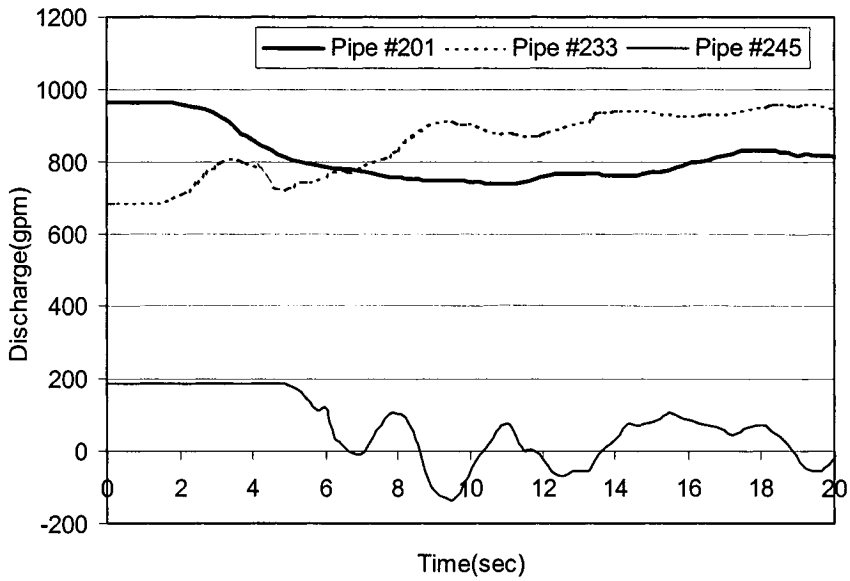

Figure 4.144 Transient flow rate at Pipe #201, #233, and #245 (Model City A, Simulation No. 2, hydrant opens in 2 seconds)

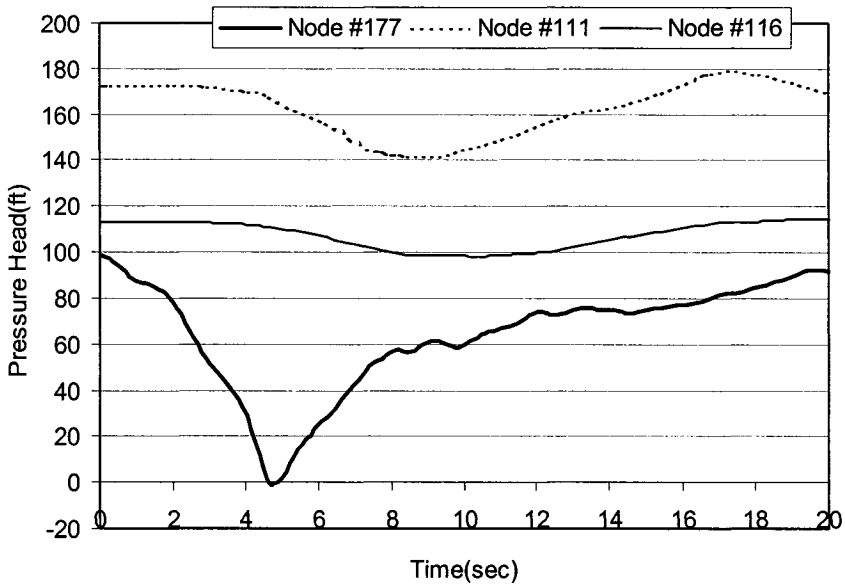

Figure 4.145 Transient pressure fluctuation at Junction #177, #111, and #116 (Model City A, Simulation No. 3, hydrant opens in 5 seconds)

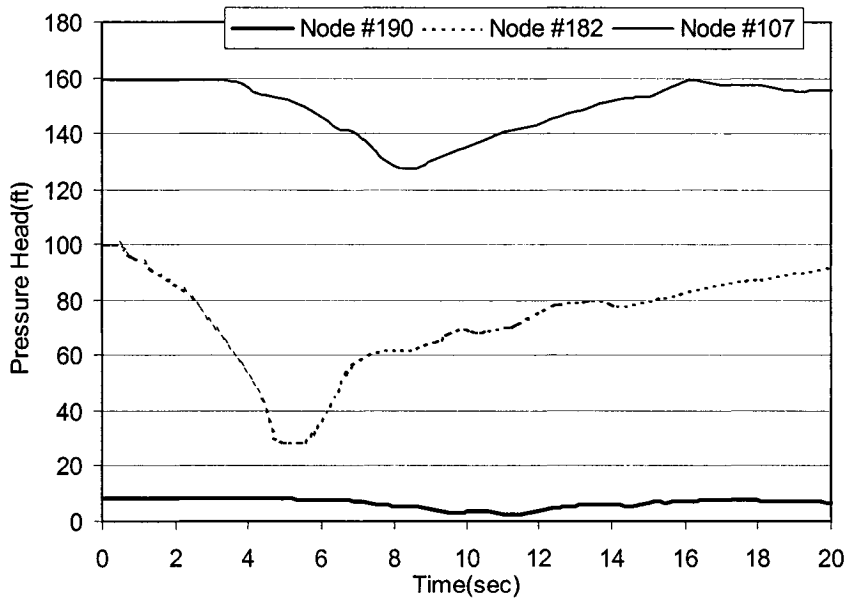

Figure 4.146 Transient pressure fluctuation at Junction #190, #182, and #107 (Model City A, Simulation No. 3, hydrant opens in 5 seconds)

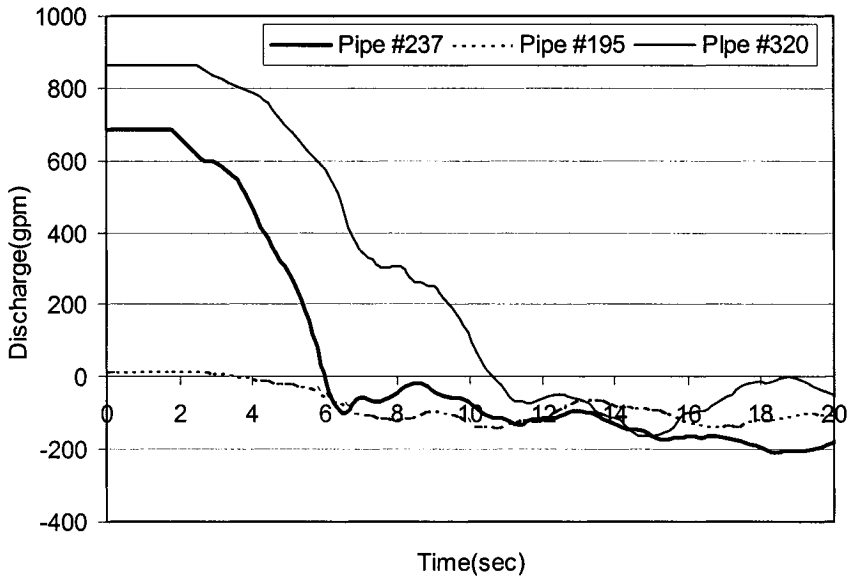

Figure 4.147 Transient flow rate at Pipe #237, #195, and #320 (Model City A, Simulation No. 3, hydrant opens in 5 seconds)

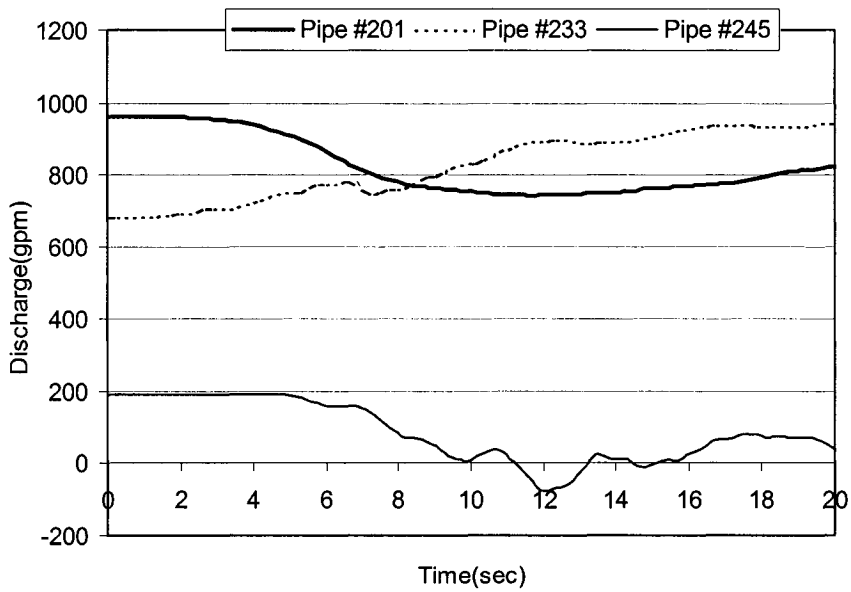

Figure 4.148 Transient flow rate at Pipe #201, #233, and #245 (Model City A, Simulation No. 3, hydrant opens in 5 seconds)

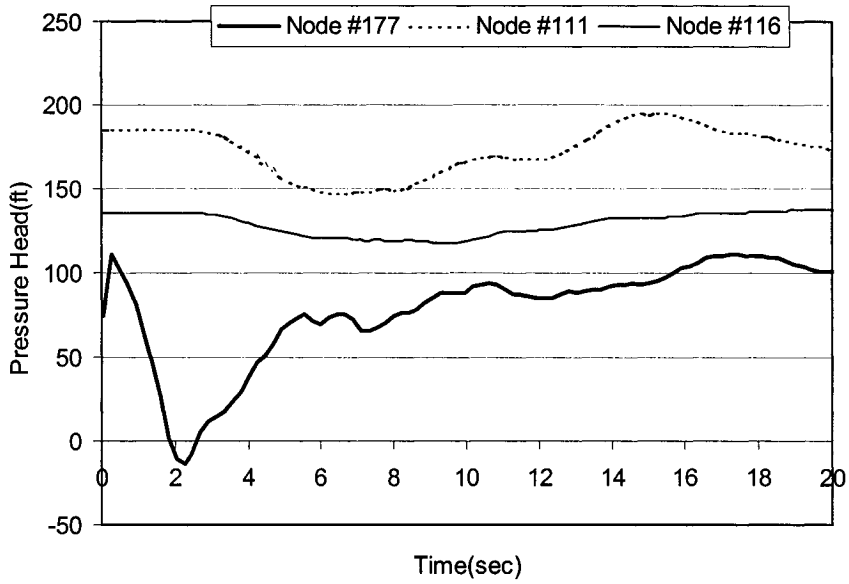

Figure 4.149 Transient pressure fluctuation at Junction #177, #111, and #116 (Model City A, Simulation No. 4, hydrant opens in 2 seconds)

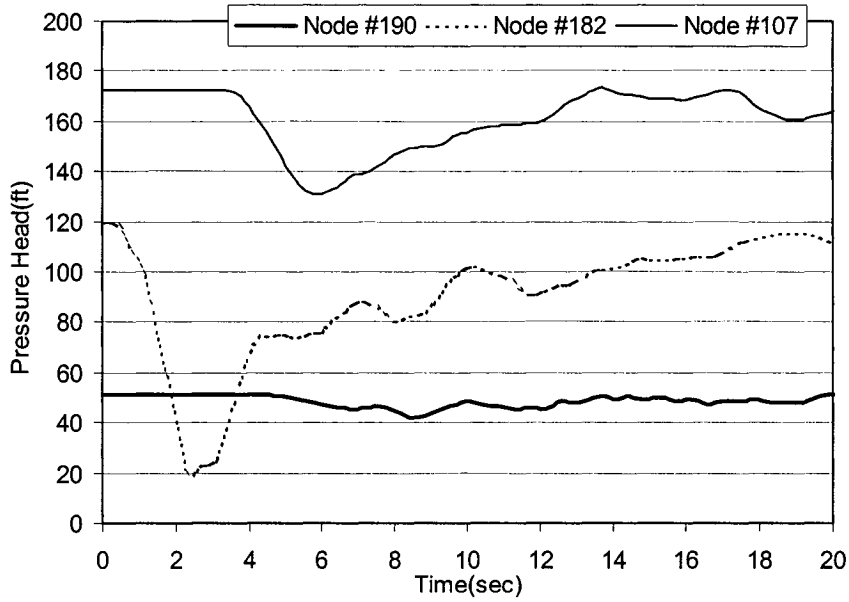

Figure 4.150 Transient pressure fluctuation at Junction #190, #182, and #107 (Model City A, Simulation No. 4, hydrant opens in 2 seconds)

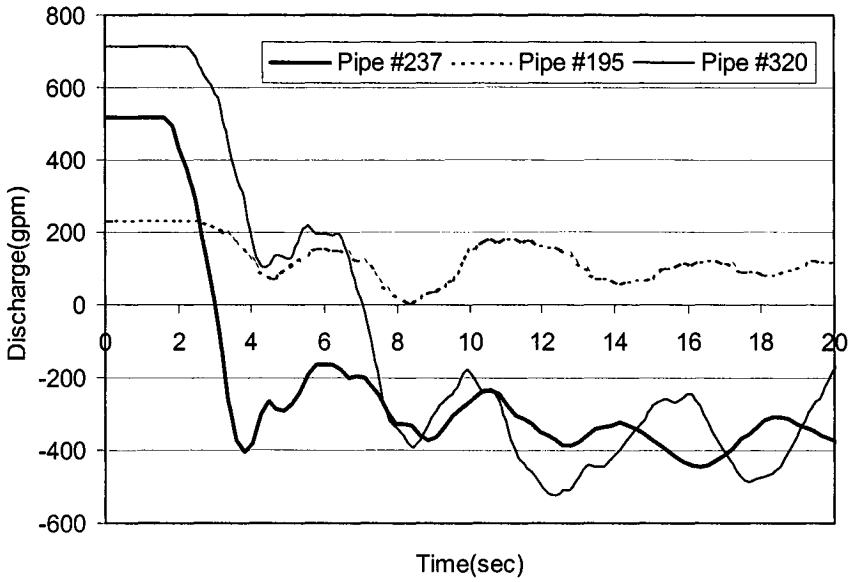

Figure 4.151 Transient flow rate at Pipe #237, #195, and #320 (Model City A, Simulation No. 4, hydrant opens in 2 seconds)

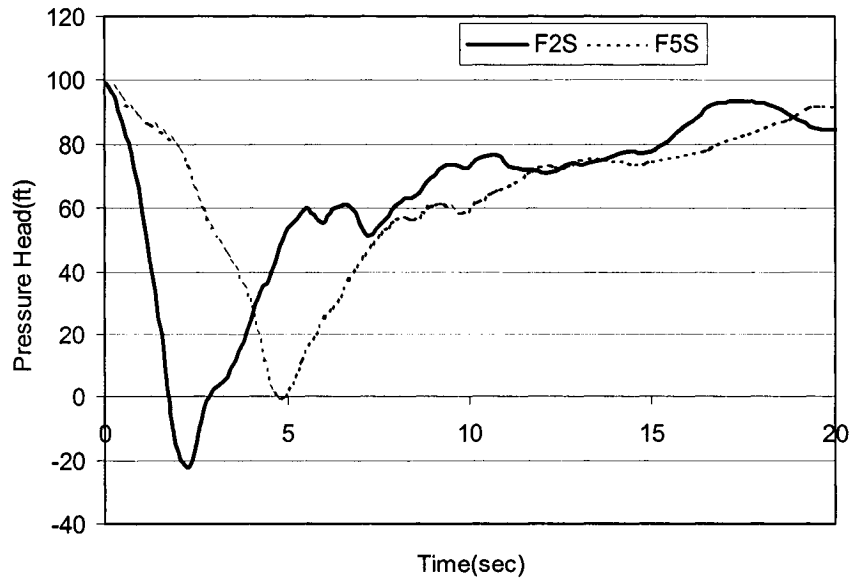

Figure 4.152 Comparison of pressure head at Junction #177 for different hydrant opening rate (Model City A, 2sec vs. 5sec)

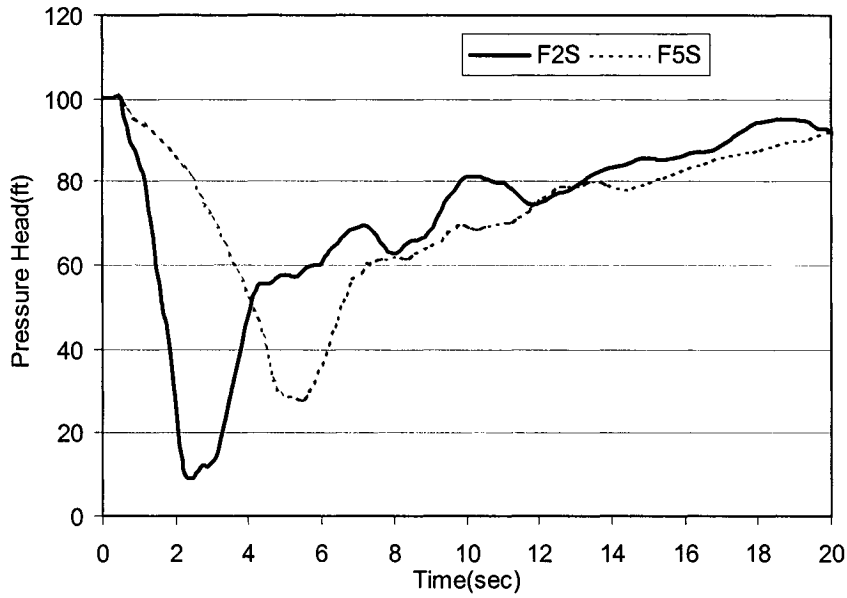

Figure 4.153 Comparison of pressure head at Junction #182 for different hydrant opening rate (Model City A, 2sec vs. 5sec)

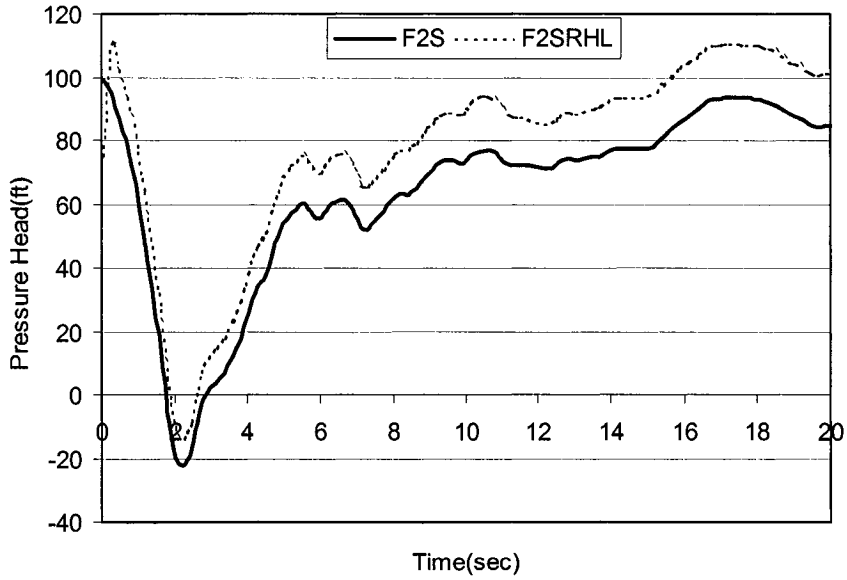

Figure 4.154 Comparison of pressure head at Junction #177 for different reservoir water level (Model City A)

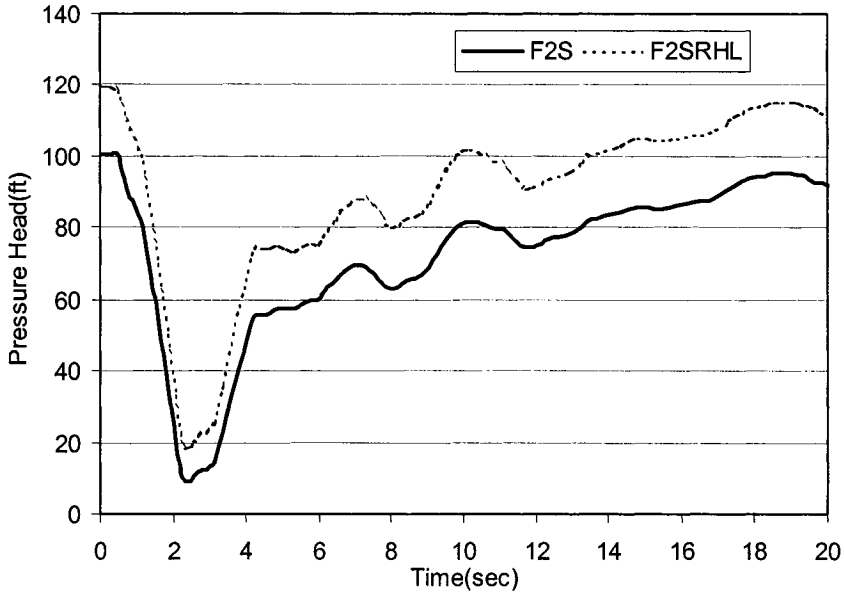

Figure 4.155 Comparison of pressure head at Junction #182 for different reservoir water level (Model City A)

4.7 Discussion

4.7.1 Discussion for the Computations according to the Experiment

Case 1 and Case 2

Table 4.12 shows the RMS errors for the results of three different computations comparing with experimental data. RMS errors for the two different durations of computations, such as duration of 10-second and duration of 2-second, have been calculated for Case 1 as shown in Table 4.12. All three types of computation have good agreement with experimental data. In the duration of 10-second, two-dimensional model has the smallest RMS error. The smallest value for the RMS error in the duration of 10-second was 5.68 at the upstream region. The smallest value for the RMS error in the duration of 2-second was 4.70, which is computed by two-dimensional model at the upstream region.

Table 4.12 RMS errors for the results of computations (Case 1)

Method of Computation	Place of Transducer	RMS Error (psi)	
		Duration of 2sec	Duration of 10sec
The Method of characteristics	Upstream	5.47	9.72
	Downstream	6.03	9.27
Two-Dimensional Model	Upstream	4.70	5.68
	Downstream	5.90	6.35
Implicit Method	Upstream	5.07	7.71
	Downstream	5.59	7.19

Table 4.13 shows the RMS error for the results of three different types of computations comparing with experimental data for Case 2. The smallest value of RMS error was 6.00, which is computed by the method of characteristics at the upstream region in duration of 2 second. In duration of 2 second, the method of characteristics has the smallest value of RMS error in the both upstream and downstream regions for Case 2. All three types of computation have the smaller value of RMS error in the duration of 2 second for both Case 1 and Case 2 which means the results of the beginning in the computation have better agreement than the results of the latter half of the computation.

Table 4.13 RMS errors for the results of computations (Case 2)

Method of Computation	Place of Transducer	RMS Error (psi)	
		Duration of 2sec	Duration of 10sec
The Method of Characteristics	Upstream	6.54	11.49
	Downstream	6.00	10.05
Two-Dimensional Model	Upstream	7.23	11.26
	Downstream	7.14	9.16
Implicit Method	Upstream	7.59	9.34
	Downstream	6.34	6.91

If smaller size of the grid is used to avoid the shifting the pressure wave at the latter half of the whole time duration in this computation, RMS error will be decreasing. In these calculations, execution time of computation for the implicit method was very much longer than that of another two types of computation because of the size of huge matrix for the each

time step at this time. Therefore, grid size Δx of implicit method could not be decreased at this time and also the grid size of the other two methods was not decreased. Grid size Δx and time increment Δt were used as same values as 2.2175 ft and 0.0005 second respectively in Case 1 and Case 2 for all three types of computation to observe the RMS errors. Therefore, total number of longitudinal segments was 126 and the number of grids was 127 for all three methods.

4.7.2 Discussion for the Case Study

Several cases of numerical simulation for the transient flow in distribution system with the various different scenarios have been performed using the method of characteristics in this research.

The simple looped network having two reservoirs, four pipes, and four junctions has been simulated and result of that is quite well agreed with Karney (1990)'s result. The small city model with ten pipes, seven junctions, and two reservoirs has been simulated changing the demand at the specific junctions. After analyzing the results, it is clearly observed that rapid change of the demand at the junction produces greater fluctuations of the flow rate and pressure heads. In this simulation, 2-second open/closure time causes greater magnitude of the transient fluctuation. Therefore, it is very obvious that operations of the system should be done with very careful caution.

Small city model having backflow prevention assembly has been simulated. Backflow prevention assembly was added to the calculation of the small city model. In this case, effect of head loss for the backflow prevention assembly was neglected. Because of changing the demand at the junctions and changing the hydraulic head of the reservoir, check valve in the

backflow prevention assembly has been opened and closed. Therefore, fluctuations of the results for the simulations having the backflow prevention assembly are more oscillating at the beginning of the simulations. It is demonstrating that backflow prevention assembly is a very important hydraulic device in the distribution system. Distribution system needs to have backflow prevention assembly to prevent the backflow. In the last case of the simulation of case study, small city model with surge tank has been simulated. One-Way Surge Tanks are generally used in connection with pumping system and usually designed to prevent column separation. One-Way Surge Tanks are also used to prevent low pressures in the system. And Two-Way Surge Tanks are used for certain points of high and low pressure at the distribution system. Effects of the One-Way Surge Tank and Two-Way Surge tank in the distribution system have been demonstrated. Results of simulation show that if the distribution system needs an energy dissipater then Two-Way Surge Tank should be installed. In certain cases, both One-Way Surge Tank and Two-Way Surge Tank are very much effective for damping out the pressure. When the distribution system and external energy dissipaters are designed, many different cases of simulation should be performed for economical and safe design.

Simulations for the medium sized city network and large sized city network have been performed with various scenarios. The computer modeling provided clear evidence that sudden change in demand can cause drastic pressure drops and flow reversal. This may be due to main breaks, fire hydrant use, or other changes in water demand. The impact of rapid pressure drop and flow reversal could be lessened if the rate of change is decreased. Although this may not be possible in the case of a main break, it is possible in cases of flushing hydrants and other controlled changes in the system. The computer modeling showed that systems with larger elevation differences are more susceptible to the negative

impact of sudden change of water demand in the system. Since the evidence shows that sudden changes in demand can clearly create undesirable conditions within the distribution system, appropriate plans should be made prior to potential disasters. These plans can only be made after a careful study of the response of the system to various assumed scenarios.

CHAPTER 5

CONCLUSIONS

The potable water distribution system is one of the significant hydraulic engineering accomplishments. Through the distribution system, the potable water can be delivered to the water users. Therefore, the water distribution system is the essential link between the water supply source and the water users. However, sudden changes in water demand can create transient flow that could induce many undesirable consequences such as excessive negative pressure or backflows in distribution system. If conditions are changed very rapidly, huge pressures can be generated, and it could be enough magnitude to burst pipes and damage the equipments in pipe systems. Transient flow is enough to cause a failure in the distribution system. Therefore, analysis of transient flow should not be excluded for the design and operational guidance of the distribution system.

The objective of this study has been to develop numerical method that can analyze the transient flow in distribution system. Three different types of computer program for simulating the transient flow in distribution system have been developed in this study. Experiment for transient flow has been conducted to verify some of the computer simulation and to determine the head loss coefficients for the theoretical equations. Many complex hydraulic devices can be represented mathematically. It is shown that many common hydraulic devices can be simplified to an algebraic relation that expresses the physical structure of the pipe system. These developments can have benefits such as a safer system operation, an improved model of the system, or lower maintenance cost.

Detailed conclusions drawn from computer simulations and experiments conducted for the present study are summarized below:

(1) A 278ft-long pipeline has been installed to perform the experiment for transient flow in the laboratory. Frictional head loss and minor head losses at the steady state condition in the piping system have been measured experimentally. In this system, effects of the minor losses were significant in certain range of Reynolds number. To compare the total head loss with the frictional head loss, total head loss coefficient "M" was introduced. Total head loss coefficient "M" was much bigger than the frictional head loss term $f(\frac{L}{D})$ in the range of Reynolds number from 4,000 to 40,000. "M" was almost the same as the frictional head loss term $f(\frac{L}{D})$ in the range of Reynolds number from 60,000 to 100,000. Head loss coefficient k_{Ball} for ball valve was also measured experimentally. Results show that the head loss at ball valve was huge and was not a minor effect. Head loss coefficient k_{DC} for single and double check valve was measured experimentally under various flow velocities. In the range of Reynolds number from 4,000 to 20,000, values of head loss coefficient k_{DC} are significantly high.

(2) Experiments for transient flow have been performed in the lab. The results of the experiments are used to evaluate the coefficients such as head loss coefficient provided by theoretical equations. Results of experiment show that rapidly closing the valve or changing the water demand in the system could cause large fluctuations of the pressure. Fluctuations of the pressure wave propagate along the pipeline and can damage the system. After measuring the pressure-time histories of the water hammer involving with backflow

prevention assembly, it was found that the backflow prevention assembly dampens out the oscillations of pressure in the system. Single check valve reduced 40 % and 36.7 % of the maximum height of pressure wave at downstream region in Case 1 and Case 2 respectively. Furthermore, single check valve reduced 55 % and 64 % of the maximum height of pressure wave at upstream region in Case 1 and Case 2 respectively.

(3) It is found that the head losses in the system are very important for transient flow simulation. Therefore, before performing the computation for transient flow, the head loss coefficient should be carefully determined. If only the frictional head loss coefficient "f" is used for the dynamic equation from the two governing equations, the pressure oscillation will be overestimated and energy decay will be underestimated in the computation. Therefore, the equivalent head loss coefficient C_L for transient flow was introduced and determined by experimentally in the present study. Equivalent head loss coefficient C_L for the present experimental setup was 0.3, which was almost seven times bigger than frictional head loss coefficient for this experimental setup since the minor loss effect was significant and the head loss at a ball valve was large.

(4) The method of characteristics has been developed and applied in this study. Many boundary conditions and hydraulic devices have been defined as a simple form for the numerical analysis. Results of the computation using the method of characteristics with an equivalent head loss coefficient C_L achieved good agreement with experimental results.

(5) The two-dimensional method has been developed to simulate the transient flow in the present study. Damping coefficient "κ" in the equation of mixing length was determined experimentally before the computation for transient flow is performed. "κ" was 0.22 for this experimental setup. The computational results have good agreement with the experimental data.

(6) The implicit method has also been developed to simulate the transient flow in piping system. The governing equations for the implicit method are the same as those for the method of characteristics. Therefore, the equivalent head loss coefficient C_L can be used. Results of the computation using the implicit method show that the accuracy of this method is slightly better than that of the method of characteristics for 10 seconds of time duration in both Cases 1 and 2. However, the implicit method has a problem with the long execution time if the simulation is carried out for longer-term simulation.

(7) Several cases of simulation have been performed to observe the transient effects for distribution system. In order to detect the effect of different valve open/closure rates on the transient pressure fluctuations, computer simulations have been performed for the small city model with changes in demand. In the simulation for the small city model, it was noticed that rapidly changing the demand could significantly increase the pressure head in distribution system. The simulation for the small city model with backflow prevention assembly has been performed in order to understand the effect of the assembly in the system. After conducting the several cases of simulation for the small city model with the assembly, it became obvious that changing the demand or changing the hydraulic head at any position at the system can induce the backflow in the system. Therefore, when the

distribution system is designed, simulations for the whole distribution system need to be conducted to prevent the backflow or any similar type of undesirable flow. So far, installing backflow prevention assembly could be the safest way to prevent the backflow in distribution system.

(8) The simulation for two kinds of surge tanks as hydraulic devices in distribution system has also been performed. From the results of simulation for the surge tanks, it is seen that the two-way surge tank worked very well for reducing excessive high pressure and low pressure or column separation in the distribution system. One-way surge tank, as well as two-way surge tank, was working good enough to prevent the excessive low pressure in certain cases. Therefore, simulations with the different scenarios should be done for the efficient design of surge tank in distribution system.

(9) Results from the computer modeling for the medium sized city and large sized city clearly indicate that sudden changes in the water demand due to hydrant opening caused drastic transient flow conditions resulting in significant pressure loss or flow reversal in a network system of virtually any size. Many examples demonstrate that the loss in pressure could reach below atmospheric pressure. Distribution systems that have greater variance in ground elevation will have even greater possibility of creating sub-atmospheric pressure when drastic pressure reduction occurs. Slower hydrant opening rates significantly reduce the impact of hydraulic transients created. When the distribution system is designed, many different cases of simulation should be performed for economical and safe design.

BIBLIOGRAPHY

1. Allievi, L. (1925). "Theory of Water-Hammer." *Trans. Amer. Soc. Civ. Engrs.*

2. Banks, D. D. & Banks, D. S. (1988). *Industrial Hydraulic Systems.* Prentice Hall, New York, NY.

3. Beitler, S. R. & Lindahl, E. J. (1947). *Hydraulic Machinery.* Irwin-Farnham Publishing Co., Chicago, Illinois.

4. Brunone, B., Golia, U. M., & Greco, M. (1995). "Effects of two-dimensionality on pipe transients modeling." *Journal of Hydraulic Engineering*, ASCE, Vol. 121, No. 12, 906-912.

5. Chaudhry, H. M. (1979). *Applied Hydraulic Transients.* Van Nostrand Reinhold, New York.

6. Chaudhry, M. H., and Hussaini, M. Y. (1985). "Second-order accurate explicit finite-difference schemes for water-hammer analysis." *Journal of Fluids Engineering*, 107(4), 523-529.

7. Coulbeck, B. and Evans, E. (1992). *Pipeline systems.* Kluwer Academic Publishers, Dordrecht, The Netherlands.

8. Fletcher, C. A. J. (1991). *Computational Techniques for Fluid Dynamics.* Springer-Verlag, New York.

9. Foundation for Cross-Connection Control and Hydraulic Research (1993). *Manual of Cross-Connection Control 9th Edition.* University of Southern California.

10. Ghidaoui, M. S. and Karney, B. W. (1994). "Equivalent differential equations in fixed-grid characteristics method." *Journal of Hydraulic Engineering*, ASCE, 115(11), 1159-1175.

11. Ghidaoui, M. S., Karney, B. W., & McInnis, D. A. (1998). "Energy estimates for discretization errors in water-hammer problems." *Journal of Hydraulic Engineering*, ASCE, Vol. 124, No. 4, 384-393.

12. Goldberg, D. E., and Wylie, E. B. (1983). "Characteristics method using time-line interpolations." *Journal of Hydraulic Engineering*, ASCE, 109(5), 670-683.

13. Hino, M., Masaki, S., and Shuji, T. (.1976). "Experiments on transition to turbulence in an oscillatory pipe flow." *Journal of Fluid Mechanics*, 75(2), 193-207.

14. Islam, M. R. & Chaudhry, M. H. (1998). "Modeling of constituent transport in unsteady flows in pipe networks." *Journal of Hydraulic Engineering*, ASCE, 124(11), 1115-1124.

15. Jelev, I. (1989). "The damping of flow and pressure oscillations in water-hammer analysis." *Journal of Hydraulic Engineering*, ASCE, 27(1), 91-114.

16. Karassik, I. J., Krutzsch, W. C., Fraser, W. H., and Messina, J. P. (1986). *Pump Handbook.* McGraw-Hill, New York, NY.

17. Karney, B. W. & McInnis, D. (1990). "Transient analysis of water distribution systems." *J. AWWA*, 82(7), 62-70.

18. Karney, B. W. & Mcinnis, D. (1992). "Efficient calculation of transient flow in simple pipe networks." *Journal of Hydraulic Engineering*, ASCE, 118(7), 1014-1031.

19. Karney, B. W. (1990). "Energy relations in transient closed-conduit flow." *Journal of Hydraulic Engineering*, ASCE, Vol. 116, No. 10, 1180-1196.

20. Karney, B. W., and Ghidaoui, M. S. (1997). "Flexible discretization algorithm for fixed-grid MOC in pipeline systems." *Journal of Hydraulic Engineering*, ASCE, 123(10), 1004-1011.

21. Kerh, T. (1989). "Computer simulation of viscous fluid interaction with a dynamic structural system," *Thesis of doctor of philosophy*, University of Southern California, Los Angeles, CA.

22. Kerh, T., Lee, J. J. and Wellford, L. C. (1997). "Transient fluid-structure interaction in a control valve." *Journal of Fluids Engineering*, ASME, Vol. 119, 354-359.

23. King, H. W., Brater, E. F., Lindell, J. E., and Wei, C. Y. (1996). *Handbook of Hydraulics.* McGraw-Hill, New York.

24. Lai, C. (1988). "Comprehensive method of characteristics models for flow simulation." *Journal of Hydraulic Engineering*, ASCE, Vol. 114, No. 9, 1074-1097.

25. Lal, J. (1956). *Hydraulic Machines.* Metropolitan Book Co., Delhi.

26. Lester, C. B. (1994). *Hydraulics for Pipeliners.* Gulf Publishing Company, Houston, TX.

27. Marchi. E. (1961). "Il moto uniforme delle correnti liquide nei condotti chiusi e aperti." *L'Energia Elettrica*, Milan, Italy, 38(4), 289-301 (in Italian).

28. Mays, L. W. (2000). *Water Distribution Systems Handbooks.* McGraw-Hill, New York.

29. McInnis, D. & Karney, B. W. (1995). "Transients in distribution networks: Field tests and demand models." *Journal of Hydraulic Engineering*, ASCE, Vol. 121, No. 3, 218-231.

30. Merati, P., Macelt, M. J. & Erickson, R. B. (2001). "Flow Investigation Around a V-Sector Ball Valve." *Journal of Fluids Engineering*, ASME, Vol. 123, 662-671.

31. Merati, P., Macelt, M. J. and Erickson, R. B. (2001). "Flow investigation around a V-Sector ball valve." *Journal of Fluids Engineering*, ASME, Vol. 123, 662-672.

32. Mitra, A. K. and Rouleau, W. T. (1985). "Radial and axial variations in transient pressure waves transmitted through liquid transmission lines." Journal of Fluids Engineering" ASME, Vol. 107 105-111.

33. Parmakian, J. (1955). *Water-Hammer Analysis.* Prentice-Hall, Inc., New York.

34. Pezzinga, G. & Scandura, P. (1995). "Unsteady flow in installations with polymeric additional pipe." *Journal of Hydraulic Engineering*, ASCE, Vol. 121, No. 11, 802-811.

35. Pezzinga, G. (1999). "Quasi-2D model for unsteady flow in pipe networks." *Journal of Hydraulic Engineering,* ASCE, 125(7), 676-685.

36. Rich, G. R. (1951). *Hydraulic Transients.* McGraw-Hill Book Company, Inc., New York.

37. Schohl, G. A. (1993). "Improved approximate method for simulating frequency-dependent friction in transient laminar flow." *Journal of Fluids Engineering*, ASME, Vol. 115, 420-424.

38. Shimada, M. (1988). "Time-marching approach for pipe steady flows." *Journal of Hydraulic Engineering*, ASCE, Vol. 114, No. 11, 1301-1320.

39. Silva-Araya, W. F. & Chaudhry, M. H. (1997). "Computation of energy dissipation in transient flow." *Journal of Hydraulic Engineering*, ASCE, Vol. 123, No. 2, 108-115.

40. Simpson, A. R., and Wylie, E. B. (1991). "Large water-hammer pressures for column separation in pipelines." *Journal of Hydraulic Engineering*, ASCE, 117(10), 1310-1316.

41. Stewart, H. L. (1977). *Hydraulic and Pneumatic Power for Production.* Industrial Press Inc., New York, NY.

42. Suo, L. and Wylie, E. B. (1989). "Impulse response method for frequency-dependent pipeline transients." *Journal of Fluids Engineering*, ASME, Vol. 111, 478-482.

43. Trostmann, E. (1996). *Water Hydraulics Controls Technology.* Marcel Dekker Inc., New York, NY.

44. Tullis, J. P. (1989). *Hydraulics of Pipelines.* John Wiley & Sons, New York.

45. van Lookeren Campagne, C., Nicodemus, R., de Bruin, G. J. & Lohse, D., (2002). "A Method for Pressure Calculation in Ball Valve Containing Bubbles." *Journal of Fluids Engineering*, ASME, Vol. 124, 765-771.

46. Vardy, A. E., and Hwang, K. (1991). "A characteristics model of transient friction." *Journal of Hydraulic Research*, 29(5), 669-684.

47. Vardy, A. E., Brown, J., and Hwang, K. (1993). "A weighting function model of transient turbulent pipe friction." *Journal of Hydraulic Research*, 31(4), 533-548.

48. Vardy, A. E., Brown, J. (1995). "Transient, turbulent, smooth pipe friction." *Journal of Hydraulic Research*, 33(4), 435-456.

49. Walski, T. M., Chase, D. V., & Savic, D. A. (2001). *Water Distribution Modeling.* Haestad Press, Waterbury, CT, USA.

50. Watters, G. W. (1979, 1984). *Analysis and Control of Unsteady Flow in Pipelines.* Butterworths, Boston.

51. Wurbs, R. A. & James, W. P (2002). *Water Resources Engineering.* Prentice Hall, Upper Saddle River, NJ.

52. Wylie, B. E. & Streeter, V. L. (1993). *Fluid Transients in Systems.* FEB Press, Ann Arbor, Mich.

53. Wylie, B. E. (1983). "The Microcomputer and pipeline transients." *Journal of Hydraulic Engineering*, ASCE, Vol. 109, No. 12, 1176-1194.

54. Yeaple, F. D. (1966). *Hydraulic and Pneumatic Power and Control.* McGraw-Hill, New York, NY.

55. Zaki, N. M. (1993). "Numerical and experimental investigations of turbulent flows through an obstruction in pressure conduits." Thesis of doctor of philosophy, University of Southern California, Los Angeles, CA.